An Experimental Investigation of Flow and Reaction Processes during Gas Storage and Displacement in Coal

Mojgan Hadi Mosleh

Geoenvironmental Research Centre

Cardiff School of Engineering

Cardiff University

Thesis submitted in candidature for the degree of Doctor of Philosophy at Cardiff University

May 2014

DECLARATION

This work has not previously been accepted in substance for any degree and is not concurrently submitted in candidature for any degree.

Signed …….. (Mojgan Hadi Mosleh) Date ……28/05/2014……..

STATEMENT 1

This thesis is being submitted in partial fulfillment of the requirements for the degree of Doctor of Philosophy (PhD).

Signed …….. (Mojgan Hadi Mosleh) Date ……28/05/2014……..

STATEMENT 2

This thesis is the result of my own independent work/investigation, except where otherwise stated. Other sources are acknowledged by explicit references.

Signed …….. (Mojgan Hadi Mosleh) Date ……28/05/2014……..

STATEMENT 3

I hereby give consent for my thesis, if accepted, to be available for photocopying and for inter-library loan, and for the title and summary to be made available to outside organisations.

Signed …….. (Mojgan Hadi Mosleh) Date ……28/05/2014……..

Acknowledgements

I would like to sincerely thank my supervisors Professor H.R. Thomas and Dr. S. Tripathy for their invaluable guidance, support, comments and suggestions throughout this research. My appreciations also go to Dr. P. Vardon and Dr. M. Turner for their support at the early stages of this work. Additionally, the work undertaken would not have been possible without the financial support of the Seren Project, funded by the Welsh European Funding Office (WEFO).

My friend and colleague, Dr. Lee Hosking, deserves a special appreciation for his contribution towards the final stages of this thesis. He has patiently shared his great knowledge of numerical modelling with me and helped me to understand better the theoretical aspects of this work.

I would like to thank Jerry Sutton and Michael Bulley from GDS Instruments for their invaluable inputs and support during the construction of the laboratory facility. I am also very grateful to many of the technical staff, both in the Engineering department and the Earth Sciences department: Malcolm, Steve, Paul, Len, Harry, Gareth, Carl, Tony and Peter.

I would like to express my gratitude towards all my friends and colleagues at the GRC: Michael, Rob, Talib, Alex, Pauline, Irfan, Danothy, Ram, Shakil, Claire, Hesham, Eleni, Manju, Ben, Jamie, Vasilis, Renato, Alejandro, Siva, Sanjana, Panos, and many others.

Outside of the GRC, special thanks go to my friends Dennis, Freda, Sahand, Ali, Reyhaneh, Saeed, Meysam, Zahra, and Reza, for their continuous encouragement, and for making my stay at Cardiff a memorable time.

A special thanks is given to all my family members for their continual love and support, especially my father and mother, my dearest siblings, Maryam, Majid, Mehdi, and my beloved nieces, Samaneh and Salina. I am also grateful to all my respected in-law family members, for their continuous support and encouragement.

And most of all my best friend and husband, Majid, deserves a very special acknowledgement for his endless love and friendship. I thank him for being patient and supportive in every possible way. So, I dedicate this thesis to him with my deepest gratitude.

Summary

An advanced laboratory facility has been designed, developed and commissioned which offers an extensive capability for detailed study of various aspects of geoenergy problems in fractured rocks. It comprises i) a high pressure manometric sorption apparatus, ii) a high pressure triaxial core flooding system and iii) an ancillary system including pure and mixed gas supply and analysing units. The manometric sorption apparatus is capable of measuring adsorption/desorption isotherms of various gas species on powdered and intact samples. The triaxial core flooding system is capable of measuring the gas flow properties and deformation behaviour of coal samples, up to 0.1m diameter and 0.2m length. Deep underground conditions in terms of pore pressure and confining pressure can be replicated using the high pressure triaxial cell for depths up to 2000m. The laboratory facility has been designed and developed to produce high resolution data for a broad range of gas injection pressures (up to 20MPa) and temperature values (up to 338K). Appropriate pressure transducers and flow meters were selected and have been incorporated into the system following a series of detailed and thorough analyses performed to define and optimise the specifications of the measurement devices.

Anthracite coal samples from the South Wales coalfield (6-ft seam measure) have been characterised and tested.

Equilibrium and kinetic phenomena of the adsorption and desorption of different gases, i.e. nitrogen (N_2), methane (CH_4) and carbon dioxide (CO_2), at injection pressures up to 7MPa have been studied. A series of core flooding experiments have been carried out on samples of 0.07m diameter and 0.12m length, at gas injection pressures up to 5.5MPa and confining pressures up to 6MPa. The absolute and relative permeability of the samples, to different gases and the permeability evolution with changes in the gas pressure and confining stress condition have been studied. The fate of adsorbed CO_2 was studied via a sequential series of N_2 and CH_4 flooding experiments. The storage and displacement of N_2 and CO_2 in a sample saturated with CH_4 at 5MPa pressure was investigated via another series of flooding tests. During the injection of the gases, the composition of the outflow gas was analysed.

Modelling work has been carried out to further investigate the experimental results and processes involved in gas transport and reactions. The numerical model used, includes a theoretical approach for modelling the permeability evolution in coal.

The results of the gas adsorption tests indicated a higher adsorption capacity to CO_2 compared to CH_4 and N_2, i.e. 1.3 and 2.5 times higher, respectively. Also, different hysteresis behaviours were observed during the adsorption and desorption measurements, for the different gases studied. An improved understanding of the controlling mechanisms of gas adsorption rate and the kinetics of the processes has thus been achieved.

From the results of the core flooding experiments, it was found that the permeability evolution of the coal sample to CO_2, due to an increase in gas pressure, exhibited a different pattern compared to the other gases. A considerable reduction above a certain gas pressure value was observed. This was found to be related to coal matrix swelling induced by CO_2 adsorption. The results of following N_2 and CH_4 flooding experiments showed a partial restoration of the initial permeability of the coal sample, indicating the stability of the adsorbed CO_2 in the coal matrix during the period of analysis.

The results of N_2 and CO_2 storage and displacement in coal showed that CO_2 injection into coal was more efficient in terms of total CH_4 recovery, gas displacement ratio, breakthrough time and amount of the gas storage than achieved through N_2 displacements. The effect of swelling on the coal permeability however was found to be considerable.

The application of the experimental results in the adopted theoretical model led to the identification of the major mechanisms controlling the behaviour of coal during gas displacement, together with the influential factors on flow behaviour. The results also highlighted coupled physico-chemical effects during carbon dioxide sequestration in coal.

It is claimed that the work presented in this thesis has provided a new and comprehensive set of high resolution data. Various aspects related to high pressure flow and reaction of various gas species in coal have been studied. A detailed set of benchmarks have been produced that can be used for the development and validation of theoretical models. New insights into several phenomena related to carbon sequestration in coal are thus claimed to have been achieved.

Nomenclature

a	Coefficient related to the non-ideality of gases, equation (3-5)
a_F	Matrix block width, defined in Figure (8.1)
a_M	Matrix pore width, defined in Figure (8.1)
A	Cross-sectional area of the sample
b	Coefficient related to the non-ideality of gases, equation (3-5)
b_F	Fracture width, defined in Figure (8.1)
b_L^j	Inverse Langmuir pressure constant for the j^{th} component
b_M	Sub-matrix block dimension, defined in Figure (8.1)
c_f	Fracture compressibility
c_{f0}	Initial fracture compressibility
c_g^i	Gas concentration
$c_{g\alpha}^i$	Gas concentration of the i^{th} component
C	Sutherland's constant depending on gas species
$C_{c_g c_g F}$	Defined in equation (A-26)
$C_{c_g c_g M}$	Defined in equation (A-31)
$C_{c_g s_g M}$	Defined in equation (A-32)
D_g^{0i}	Reference diffusion coefficient at low gas density, equation (A-10)
D_g^i	Diffusion coefficient
D_{geM}^i	Effective diffusion coefficient, equation (A-20)
$D_{g\alpha}^i$	Diffusion coefficient at higher gas density, equation (A-10)
$D_{K\alpha}^i$	Knudsen diffusion coefficient
E	Young's modulus
f_T	Target function, defined in equation (5-2)
g	Gravitational acceleration
G_s	Specific gravity
h	Depth
$\mathbf{J}_{c_g F}$	Defined in equation (A-28)
$\mathbf{J}_{c_g M}$	Defined in equation (A-34)
$\mathbf{J}_{gAdv\alpha}^i$	Advective component of flux
$\mathbf{J}_{gDifF}^i$	Total diffusion fluxes for fracture continuum
$\mathbf{J}_{gDifM}^i$	Total diffusion fluxes for matrix continuum

$\mathbf{J}^{i}_{gDif\alpha}$	Diffusive component of flux
$\mathbf{J}^{i}_{g\alpha}$	Total flux of the gas component *i*
k	Permeability coefficient
k_0	Permeability of the coal at initial stress condition
$k_{(CO_2)}$	Permeability of the coal to CO_2
k_F	Absolute permeability in the fracture
k_{F0}	Initial absolute permeability in the fracture continuum
k_g	Gas permeability coefficient
$k_{(He)}$	Permeability of the coal to helium
k_M	Absolute permeability in the matrix continuum
k_{M0}	Initial absolute permeability in the matrix continuum
$k_{(N2)}$	Permeability of the coal to N_2
k_r	Relative permeability of the coal sample
$k_{\alpha 0}$	Initial bulk permeability
$k^{L}_{\alpha 0}$	Initial local permeability
$K_{c_g c_g F}$	Defined in equation (A-27)
$K_{c_g c_g M}$	Defined in equation (A-33)
K^{A}_{g}	Gas conductivities in the fracture and matrix continua
$K_{g\alpha}$	Unsaturated gas conductivity of facture and matrix continua
l	Typical thickness of a matrix block or fracture spacing
L	Sample length
m_s	Mass weight of the solid material
n_0	Initial gas adsorption at the beginning of each pressure step at each stage
n_1	Initial amount of free gas in the reference cell
n_2	Amount of free gas in both reference cell and sample cell immediately after connecting the cells
n_3	Amount of free gas at equilibrium state
n^{abs}_{ads}	Absolute adsorption
n^{ex}_{ads}	Excess amount of adsorbed gas
$n^{ex}_{ads(total)}$	Total excess adsorption
n_B	Bulk porosity
n_{B0}	Initial bulk porosity
n_{eq}	Total gas adsorption at equilibrium
n_F	Fracture porosity
n_{F0}	Initial fracture porosity

n_F^L	Local fracture porosity
n_{inj}	Number of moles of the gas in the reference cell
n_L	Langmuir parameter for adsorption capacity
n_L^{abs}	Langmuir absolute adsorption
n_L^i	Langmuir capacity for the component *i*
n_M	Matrix porosity
n_{M0}	Initial matrix porosity
$\overline{n}_{residual(0)}$	Initial residual adsorption at time zero
$\overline{n}_{residual(t)}$	Defined in equation (5-3)
$\overline{n}'_{residual(0)}$	Defined in equation (5-6)
$\overline{n}''_{residual(0)}$	Defined in equation (5-6)
n_t	Gas adsorption amount at time *t*
n_{unads}^{ex}	Amount of the unadsorbed gas
n_α	Porosity of fracture or matrix continua
$n_{\alpha 0}$	Initial bulk porosity
$n_{\alpha 0}^L$	Initial local porosity
P_0	Reference pressure
P_1	Gas pressures in the reference cell
P_2	Gas pressures after connecting the cells
P_3	Gas pressures at equilibrium state
P_c	Confining pressure
P_{down}	Downstream gas pressure
P_{eq}	Pressure of free gas at equilibrium
P_g	Gas pressure
P_L	Langmuir parameter for pressure
P_{ref}	Gas pressure in the reference cell
P_{up}	Upstream gas pressure
Q_0	Volumetric rate of flow at reference pressure
$Q_{c_gF}^{ex}$	Defined in equation (A-29)
$Q_{c_gM}^{ex}$	Defined in equation (A-35)
R	Universal gas constant
$R_{g\alpha}^i$	Sink/source term accounting for geochemical reactions
$s_{g\alpha}^i$	Amount of gas lost/gained due to sorption reactions with the solid phase
$s_{g\infty M}^i$	Adsorbed concentration at equilibrium with the free gas pressure in the matrix continua

$S_{g\alpha}$	Degree of gas saturation
t	Time
T	Gas temperature
T_0	Reference temperature
T_{ave}	Average surface temperature
T_g	Ground temperature
V	Volume of gas injected from calibration cylinder
V_1	Defined in equation (3-3)
V_2	Defined in equation (3-4)
V_3	Defined in equation (3-4)
V_B	Bulk volume of the rock
V_F^P	Volume of the pores in the fractured zone
V_F^T	Total volume of the fractured zone
V_m	Molar volume
V_{RC}	Volume of the reference cell
V_s	Volume of the solid particles of the sample
V_{s0}	Initial volume of the coal sample
V_{SC}	Volume of the sample cell
V_v	Void volume of the sample cell
w_f	Volumetric weighting factor
z	Elevation
Z	Compressibility factor
Z_1	Corresponding gas compressibility factors to P_1
Z_2	Corresponding gas compressibility factors to P_2
Z_3	Corresponding gas compressibility factors to P_3
Z_{eq}	Compressibility factor of the free gas at equilibrium condition
Z_{He}	Compressibility factor of helium
Z_{ref}	Compressibility factor of gas in the reference cell
Z_α	Gas compressibility factor in fracture or matrix continua
α	Coefficient related to the non-ideality of gases
α_f	Rate of fracture compressibility change
η	Stress attenuation coefficient
β	Factor related to the geometry of the matrix blocks
$\Gamma_{g\alpha}^i$	Sink/source term representing the mass exchange of the gas component *i* between the fracture and matrix continua

$\delta_{i\alpha}$	Constrictivity factor for specifying species to account for configurational diffusion
δV_{α}	Incremental volume
ΔV_{oil}	Displaced volume of the silicone oil inside the pump
ε_L^j	Langmuir strain constant for the j^{th} component
ε_s^j	Sorption induced strain for the j^{th} pore gas component
ε_{s0}^j	Initial sorption induced strain for the j^{th} pore gas component in the matrix continuum
ε_v	Total volumetric strain of the coal sample associated with 1MPa pressure increase
$\theta_{g\alpha}$	Volumetric gas content of the fracture network and matrix blocks
λ	Defined in equation (A-2)
μ_g	Gas viscosity
μ_{g0}	Reference viscosity at reference temperature T_0
$\mu_{g\alpha}^0$	Gas mixture viscosity at low pressure
$\mu_{g\alpha}^D$	Further adjustment for dense gases
v	Poisson's ratio
ρ_{ads}	Density of the adsorbed-phase
ρ_{free}	Density of free gas at equilibrium
ρ_{gas}	Density of the free gas at equilibrium condition
$\rho_{g\alpha}$	Higher gas density
ρ_g^0	Low gas density
ρ_g^A	Gas densities in the fracture and matrix continua
ρ_s	Density of the solid
ρ_w	Density of the water
σ_{eff}	Effective stress
σ_{gAdv}	First order mass exchange coefficient for gas advection
σ_{gDif}^i	First order mass exchange coefficient for gas diffusion of the i^{th} component
τ , τ' , τ'' , τ'''	Adsorption rate coefficients
$\tau_{g\alpha}$	Gas tortuosity factor
τ_r^i	Sorption rate
∇	Gradient operator

Contents

Chapter 1- Introduction

1.1. Introduction 1-1
1.2. Carbon sequestration in coal seam- field scale practice 1-5
1.3. Potentials for carbon sequestration in coal in South Wales coalfield 1-7
1.4. Objectives of the research 1-8
1.5. The scopes and limitations 1-9
1.6. Thesis outline 1-10
1.7. References 1-12

Chapter 2- Literature Review

2.1. Introduction 2-1
2.2. A review on the experimental apparatuses 2-2
2.2.1. Apparatuses related to gas sorption measurements 2-2
2.2.2. Apparatuses related to gas flow and permeability measurements 2-5
2.2.3. Apparatuses related to coal swelling/shrinkage measurements 2-7
2.3. Experimental measurement methods 2-9
2.3.1. Gas adsorption/desorption measurement methods 2-10
2.3.2. Gas flow and permeability measurement methods 2-13
2.3.3. Swelling/shrinkage measurement methods 2-15
2.4. The interactions between coal and gases 2-16
2.4.1. Coal sorption capacity to gases 2-17
2.4.2. Effects of the coal rank on sorption properties 2-18
2.4.3. Effects of the moisture content on sorption properties 2-20
2.4.4. Effects of temperature on sorption properties 2-21
2.4.5. Effect of gas pressure on sorption properties 2-22
2.4.6. Effects of sample type and confining pressure on sorption properties 2-23

2.4.7. Effects of coal matrix swelling/shrinkage on sorption properties 2-23
2.5. Gas transport in coal 2-24
2.5.1. Coal permeability to gases 2-24
2.5.2. Effects of the effective stress on coal permeability 2-25
2.5.3. Effects of the gas adsorption/desorption on permeability 2-27
2.6. Gas storage and displacement in coal 2-28
2.7. Theoretical aspects and computational modelling studies 2-32
2.8. Conclusions 2-36
2.9. References 2-38

Chapter 3- Apparatus Design, Construction and Commissioning

3.1. Introduction 3-1
3.2. The manometric sorption apparatus 3-2
3.2.1. Design considerations 3-2
3.2.2. Scenarios and analysis conditions 3-4
3.2.3. Estimations of the gas pressure variations 3-6
3.2.4. Results of analysis 3-10
3.2.5. Concluding remarks on the design considerations 3-18
3.3. The triaxial core flooding system 3-19
3.3.1. Design considerations 3-19
3.3.2. Scenarios and analysis conditions 3-19
3.3.3. Estimation of the range of gas flow rates 3-21
3.3.4. Results of analysis 3-23
3.3.5. Concluding remarks on the design considerations 3-23
3.4. Construction and commissioning 3-26
3.4.1. The adsorption/desorption cell 3-28
3.4.2. Pressure transducers 3-28
3.4.3. Needle valves and tubes 3-29
3.4.4. Water bath and temperature controller 3-31
3.4.5. Volume calibration cylinder 3-31
3.4.6. Vacuum pump 3-32

3.4.7. The triaxial cell 3-33
3.4.8. The loading system 3-35
3.4.9. The confining system 3-35
3.4.10. Temperature control system 3-37
3.4.11. Measurement system 3-38
3.4.12. Gas supplying unit 3-39
3.4.12.1. Gas cylinders 3-40
3.4.12.2. Gas booster 3-40
3.4.12.3. Gas reservoirs 3-41
3.4.13. Gas analysing unit 3-41
3.5. Conclusions 3-43
3.6. References 3-44

Chapter 4- Material and Methods

4.1. Introduction 4-1
4.2. Coal samples and sample preparation methodology 4-2
4.2.1. Preparation of the powdered coal samples 4-2
4.2.2. Preparation of the core samples 4-4
4.3. Coal characterisation tests 4-6
4.3.1. The Proximate analysis 4-6
4.3.2. The Ultimate analysis 4-7
4.3.3. The density and porosity of coal 4-7
4.4. The experimental temperature 4-10
4.5. Adsorption/desorption measurements method 4-11
4.5.1. The helium pycnometry 4-14
4.6. Core flooding tests 4-19
4.6.1. Gas flow measurements 4-22
4.6.2. Calculation of coal permeability to gases 4-26
4.7. Coal swelling and shrinkage measurement 4-26
4.7.1. Compressibility of the silicone oil 4-28
4.8. Conclusions 4-29

4.9. References 4-30

Chapter 5- Gas Adsorption/Desorption Behaviour in Coal

5.1. Introduction 5-1
5.2. The excess adsorption isotherms 5-1
5.3. The absolute adsorption isotherms 5-4
5.4. Gas desorption behaviour 5-10
5.5. The adsorption kinetics 5-13
5.6. Conclusions 5-24
5.7. References 5-26

Chapter 6- Gas Flow Behaviour in Coal

6.1. Introduction 6-1
6.2. He flooding experiment 6-2
6.2.1. Absolute permeability of the coal 6-5
6.2.2. Coal volumetric strains in response to He injection 6-9
6.3. N_2 flooding experiment 6-11
6.3.1. Permeability of the coal to N_2 6-12
6.3.2. Coal volumetric strains in response to N_2 injection 6-16
6.4. CO_2 flooding experiment 6-19
6.4.1. Permeability of the coal to CO_2 6-20
6.4.2. Volumetric strains due to CO_2 injections 6-24
6.5. Fate of the adsorbed CO_2 in coal 6-27
6.5.1. The phase 2 of N_2 flooding experiment 6-29
6.5.2. CH_4 flooding experiment 6-30
6.6. Conclusions 6-32
6.7. References 6-33

Chapter 7- Gas Storage and Displacement in Coal

7.1. Introduction 7-1

7.2. Initial properties of the coal sample 7-3

7.2.1. He flooding experiment 7-3

7.2.2. CH_4 flooding experiment 7-6

7.3. N_2 experiment 7-8

7.4. CO_2 experiment 7-11

7.5. CH_4 recovery 7-13

7.6. CO_2 storage in coal 7-15

7.7. Conclusions 7-17

7.8. References 7-19

Chapter 8- Further Insight into the Permeability Evolution during Gas Flow and Displacement in Coal

8.1. Introduction 8-1

8.2. Permeability evolution model 8-3

8.2.1. Permeability model- background 8-3

8.2.2. Variation of the coal permeability to N_2, CH_4 and CO_2 8-7

8.3. Permeability model application in gas storage/displacement experiments 8-12

8.3.1. Initial and boundary conditions 8-14

8.3.2. Additional material parameters 8-16

8.3.3. Simulations results and discussions 8-17

8.3.3.1. N_2 simulation 8-17

8.3.3.2. CO_2 simulation 8-18

8.4. Conclusions 8-22

8.5. References 8-24

Chapter 8- Conclusions and Suggestions for Further Research

9.1. Introduction 9-1

9.2. Laboratory development 9-1
9.3. Gas sorption behaviour in coal 9-3
9.4. Gas flow behaviour in coal 9-4
9.5. Gas storage and displacement processes in coal 9-5
9.6. Permeability evolution during gas flow and displacement in coal 9-6
9.7. Overall conclusions 9-7
9.8. Suggestions for further research 9-9
9.9. References 9-10

Appendix A- Theoretical formulation of gas transport and reactions A-1

Chapter 1

Introduction

1.1. Introduction

The climate of the Earth is affected by increasing the concentration of greenhouse gases. Carbon dioxide (CO_2) is the main anthropogenic greenhouse gas and its concentration in the atmosphere is increasing continuously. Therefore, many countries have pledged to reduce the emissions of greenhouse gases (Berlin et al., 2007). One option to reduce emissions of carbon dioxide from combustion of fossil fuels to the atmosphere is to capture and store the carbon dioxide in porous rocks in deep geological formations (Orr, 2009).

A number of options for the storage of captured carbon dioxide have been suggested, including sequestration in the oceans (e.g. Israelsson et al., 2010; Adams and Caldeira, 2009), in the geological reservoirs such as oil and gas fields (e.g. Leach et al., 2011; Vega and Kovscek, 2010; Damen et al., 2005), deep saline aquifers (e.g. Yu et al., 2013; Ogawa et al., 2011) and deep coal seams (e.g. Yamazaki et al., 2006; Reeves and Schoeling, 2000).

Among the storage options, the underground storage of carbon dioxide in unmineable coal seams is an appealing way of addressing the increase in the atmospheric concentration of carbon dioxide (White et al., 2005). Sequestration of carbon dioxide in coal seams can be considered as an efficient way of safely sequestering carbon dioxide in an adsorbed state that is expected to be stable for geologically significant periods (White et al., 2003; Smith et al., 2002). In addition, the large ratio of surface area to volume in coal seams allows storage of up to seven times as much gas as the same volume of rock in other natural reservoirs (EIA, 2010). The worldwide carbon dioxide sequestration potential has been estimated at 150Gt of carbon dioxide (Gale and Freund, 2001).

Deep unmineable coal seams can be convenient sinks, because they are widespread and exist in many cases in proximity to fossil-fuel based power stations (White et al., 2005). Many power plants are located near the coal seams, which would reduce the transportation costs. Figure 1.1 shows a schematic diagram of the carbon sequestration process in a coal seam.

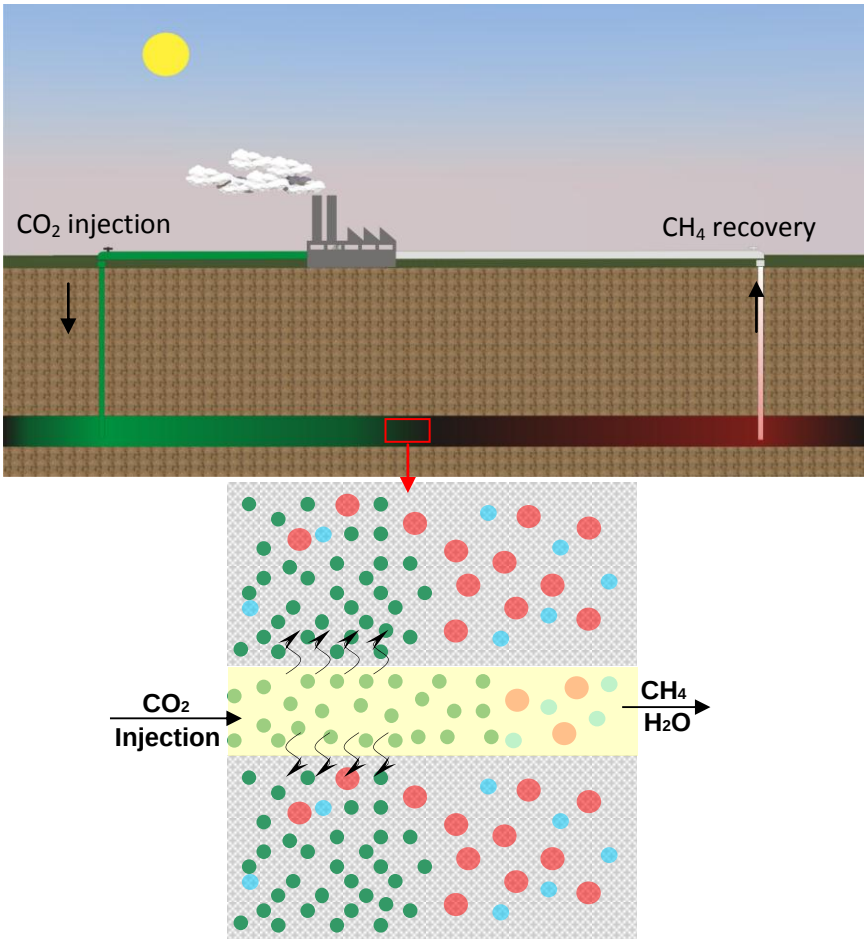

Fig 1.1. Schematic diagram of carbon sequestration in coal seam and methane recovery.

The interaction energy between carbon dioxide and coal is larger than that between methane and coal which means that the adsorption strength of carbon dioxide on coal is stronger than that of methane (Zhang et al., 2011). This may also enhance the production of the coalbed methane (CBM) as a by-product which can be considered as a profit to help offset the expense of the carbon sequestration (Ozdemir et al., 2003).

Coal is a sedimentary rock which is a mixture of organic (C_nH_n) and inorganic chemicals (Ash/mineral matter) formed from gradual compaction and thermal alteration of plant matter (Thomas, 2002). The degree of alteration (or metamorphism) of coal that occurs as a coal matures from peat to anthracite is referred to as rank. The lowest rank of coal is lignite which is generally high in moisture content and volatile matter. As coal rank increases the volatile matter and moisture content generally decreases. The carbon content of coal increases from sub-bituminous, bituminous, semi-anthracite to anthracite

(Speight, 2005). As the organic matter is gradually altered through coalification process, it is compacted to a great extent, so that a 30m thick sequence of lignite may yield just 1m of anthracite (Speight, 2005). During this process methane (CH_4) is produced and accumulates in the coal seam. The trapped methane in the coal seam is then absorbed to micropores on the coal surface or remains within the natural fracture system (cleats).

Several molecular structures of coal have been suggested in the literature. For instance, Marzec (1986) suggested a two-phase structure for coal in which a small amount of components with low molecular weight is trapped within a three-dimensional macromolecular network with covalent cross-links. Jones et al., (1999) suggested a three dimensional structure of randomly oriented small aromatic clusters. Figure 1.2 presents a micro-structure model for anthracite coal suggested by Pappano et al. (1999).

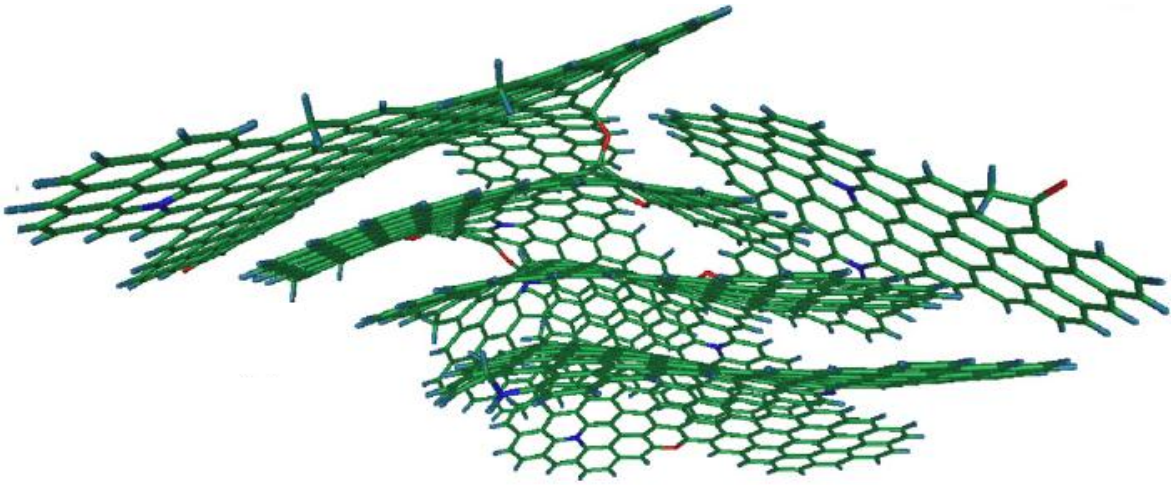

Fig. 1.2. An example micro-structure model for anthracite coal suggested by Pappano et al. (1999) and adopted and reprinted by Mathews and Chaffee (2012).

The porous structure of coal generally contains micropores and macropores (Flores, 2014). Micropores as part of the coal matrix have a radius less than 2nm (2×10^{-9}m) and make up approximately 70% of its total porosity. Macropores with a radius greater than 50nm (5×10^{-8}m) consist of a naturally occurring network of fractures called the cleat system. The transitional pores or mesopores with radius between 2 to 50nm do not generally appear in coal explaining why the coal. Therefore, due to the presence of

micropores and macropores, the coal is generally considered to be a dual porosity rock (Flores, 2014).

The gas transport in the coal seam usually includes the flow of gas through the naturally fractured porous network (cleats), diffusion into the organic coal matrix, and storage within the micropores in an adsorbed state. Nevertheless, there is a lack of understanding of what happens when the carbon dioxide is injected into a coal seam because the transport properties of the coal are highly related to the chemical and physical changes that occur during the adsorption and desorption processes.

The complex physical mechanisms and flows involved in the process of carbon sequestration in coal warrant more experimental investigation of this approach. Laboratory measurements are a cost effective way of investigating gas flow behavior and reactions in coals (Wold et al., 2008). Laboratory conditions are often well-controlled and readily-known and tend to provide a more complete data set. Therefore, laboratory experiments can play an important role in improving the understanding of permeability behaviour during gas sorption processes in coal. In addition, the experimental data are important for the development of numerical models, i.e. for validation of developed models (Pan and Connell, 2012).

The transport in the coal usually includes the flow of gas through the naturally fractured porous network (cleats), diffusion into the organic coal matrix. The storage includes the adsorption and desorption of gases on and from the coal matrix, as well as the stability of the adsorbed carbon dioxide on the coal.

Since, the transport properties of the coal are highly related to the chemical and physical changes that occur during the adsorption and desorption processes, there is a lack of understanding of what happens when the carbon dioxide is injected into a coal seam under in situ conditions. More importantly, there is a lack of understanding on the fate of adsorbed gas, i.e. extent of carbon dioxide release due to pressure depletion in the reservoir.

The prediction of the adsorption capacity and the long-term stability of the sequestered gas require knowledge of how the gas is held in place and what factors might induce its release (Ozdemir et al., 2003; White et al., 2005). Moreover, most of the laboratory investigations have mainly focused on gas sorption capacity measurements of coals, whereas the experimental investigation on the sorption kinetics of various gas species in coal has received very little attention.

1.2. Carbon sequestration in coal seam- field scale practice

In the last few decades, methane production from coalbeds (CBM) has led to extensive investigations into factors that affect adsorption capacity of coal to methane. The investigations were also focused on determination of the gas-in-place because of safety issues in coal mining (e.g. Levy et al., 1997; Bustin et al., 1998; Crosdale et al., 1998). However, studies of the capacity of coals to adsorb carbon dioxide under the in-seam conditions have been limited (White, et al., 2005).

In a study reported by Every and Dell'osso (1972), it was found that methane can be effectively removed from crushed coal by flowing a stream of carbon dioxide at ambient temperature through coal. Fulton et al. (1980) showed that a rapid loss of methane from coal occurred when carbon dioxide was injected during 90 days of testing. Subsequently, the concept of coal seam sequestration was first proposed in 1991 (Gunter et al., 1997).

Field experiences with carbon dioxide injection into deep coalbeds are however limited. The carbon sequestration in coal seams has been tested in a few projects in the USA, Canada, Poland, China and Japan, but is not yet commercially proven (Pan and Connell, 2012). The Allison unit in the San Juan basin is the first experimental carbon sequestration pilot, with about 366,000 metric tonnes of carbon dioxide injected over a 6-year period (Pan and Connell, 2012).

The Fenn and Big Valley carbon sequestration project has been performed in Alberta, Canada. After several carbon dioxide and nitrogen (N_2) injections and interval shut-in

sequences, it was concluded that carbon dioxide injectivity was greater than expected and it was attributed to weakening effect of carbon dioxide on coal (Gunter et al., 2005).

A carbon sequestration project has been carried out in a coal seam near the town of Yubari in northern Japan from 2004 to 2007 (Fujioka et al., 2010; Yamaguchi et al., 2005). The target coal seam was a 5-6m thick located at the depth of 900m. A variety of single well tests (micropilot tests) were conducted in the injection well, including initial water injection fall-off test and a series of carbon dioxide and nitrogen (N_2) injections. Low injectivity of carbon dioxide was observed as a result of reduction in coal permeability induced by swelling. The nitrogen (N_2) flooding test showed that the coal permeability did not return to the initial value after carbon dioxide and nitrogen (N_2) were repeatedly injected (Pan and Connell, 2012).

The RECOPOL carbon sequestration project has been performed in the upper Silesian coal basin in Poland (Pagnier et al., 2005; van Bergen et al., 2003). An existing coalbed methane well was used as production well with a new injection well drilled 150m away from it. The initial carbon dioxide injection was performed in 2004 in three seams of Carboniferous age in the depth interval between 900 and 1250m. The data showed that the permeability of the coal seams decreased with time as a result of swelling of the coal after contact with the carbon dioxide. Eventually, the coal was stimulated by fracking to increase the injectivity (Pan and Connell, 2012).

A carbon sequestration project has been also undertaken in Qinshui Basin China (Zhou et al., 2013; Wong et al., 2010). Before the carbon dioxide injection, the well was on methane production for 134 days. 192 metric tonnes of liquid carbon dioxide was injected into the coal seam through 13 injection cycles. The pressure build-up in the well was reported which was attributed to the permeability loss caused by carbon dioxide adsorption induced coal swelling (Pan and Connell, 2012).

Despite the mentioned field tests, very little information has been published and the outcomes of those field tests have largely remained inconclusive. Therefore, there is an

incomplete understanding of what happens when carbon dioxide is injected into a coal seam.

1.3. Potentials for carbon sequestration in coal in South Wales coalfield

There are two distinguished coalfields in Wales, the South Wales coalfield (from which the coal samples of this study have been taken) and the North Wales coalfield (Figure 1.3). The North Wales coalfield is a complex geological structure and therefore the coal mining in this area is not as extensive as that in South Wales (Jones et al., 2004). The South Wales coalfield, however, has been the subject of many geological studies over the years to the extent that it is probably the most studied area in the UK (Creedy, 1988). The main South Wales Coalfield comprises a sequence of over 2000m of Upper Carboniferous strata and is the second largest coalfield in Britain. The coal rank in the South Wales Coalfield varies across the basin, from high volatile bituminous coals in the south and east to anthracite coals in the north-western part of the coalfield (Bevins et al., 1996).

Coalbed methane has been exploited in the UK since the 1950s. In Lancashire, North Wales, South Wales and Scotland, coalbed methane produced via boreholes from virgin coal seams (VCBM), has been the subject of significant exploration effort. The project at Airth, north of Falkirk in Scotland is an example of production of gas and water from a single well. The total VCBM resource of these areas is thought to be about $2900x10^9m^3$ (Jones et al., 2004).

So far no project has been undertaken in the UK which includes injecting carbon dioxide into coal. A general assumption has been made that where coal seams are at depths below 1200m they are unlikely to be mined or gasified (Jones et al., 2004). There are vast areas of coal at depths below 1200m in the UK that are possibly too deep for mining and in situ coal gasification (Jones et al., 2004). Carbon sequestration projects that rely on injecting carbon dioxide into coal seams require significant coal seam permeability and this appears to be a major issue, especially for the UK coals (Jones et al., 2004). To date,

little work has been carried out in the UK on coal permeability, or to identify the obstacles to carbon sequestration in coal.

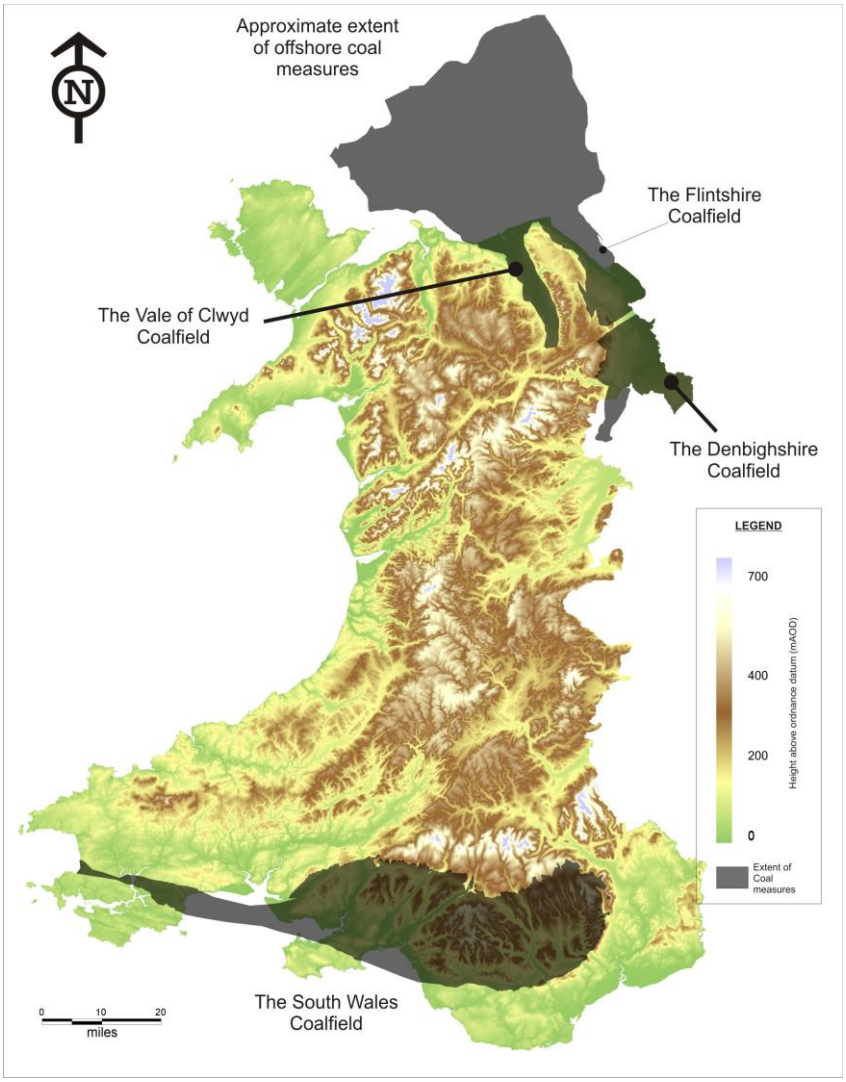

Fig. 1.3. The extent of the Welsh coalfields (Turner et al., 2008).

1.4. Objectives of the research

The aim of this study is to obtain a better understanding of the phenomena related to carbon sequestration process in coal through experimental investigation. An initial objective of this research was to design, construct and commission a laboratory facility capable of providing the required testing conditions such as the high gas pressure, high

stress conditions and controlled temperature, as well as being suitable for testing with gases such as Nitrogen (N_2), carbon dioxide (CO_2) and methane (CH_4).

The experimental program in this work aims to investigate the interactions between coal and various gas species and to provide further insight into the processes and mechanisms involved in coal-gas system.

In summary, the fundamental objectives of this study are as follows:

- To develop a laboratory facility for investigating the processes related to gas transport and reactions in coal at high pressure conditions.
- To investigate the adsorption/desorption behaviour of various gas species in coal for a broad range of gas pressures and under isothermal conditions.
- To study the kinetics of gas interaction with coal and the influential parameters/mechanisms on kinetics of gas sorption in coal.
- To assess the effect of effective stress and sorption-induced strain on coal permeability variations and gas flow behaviour.
- To evaluate and quantify the volumetric deformations of the coal due to interaction with reactive gases such as carbon dioxide, i.e. swelling/shrinkage.
- To obtain permeability and sorption properties of coal samples from South Wales coalfield.
- To obtain a better insight into the flow processes in coal and mechanisms involved in coal permeability evolution due to gas injection via theoretical modeling and numerical studies.

1.5. The scopes and limitations

The scope of the work undertaken in this thesis and in particular the limitations that are anticipated are listed below:

- The experimental works are conducted on dry samples only and the effect of water on the studied processes has not been considered.
- Gas pressures in the experimental works presented in this thesis are limited to 7MPa which was mainly due to the phase change of carbon dioxide at higher pressures, i.e. liquid phase/supercritical phase.
- The experiments are conducted under isothermal conditions, therefore the effect of temperature variation of the studied processes has not been considered.
- The adsorption/desorption measurements are conducted on powdered coal samples only. This was mainly due to the time constrains, i.e. by eliminating the lower process of gas diffusion process in coal.
- This research has considered the permeability and deformation of the intact coal under the isotopic stress conditions only, subsequently, the coal specimens are not subjected to triaxial stress conditions.

1.6. Thesis outline

This thesis is divided into nine consecutive chapters:

Chapter 1 presents an overview of the carbon sequestration in coal seams, the aim and objectives of this research and outline of the work.

Chapter 2 provides the technical review of the literature relevant to the aspects of this study. A brief review of the coal structure and its physical and chemical properties is provided in this chapter. The coal-gas interactions and effects of different parameters on gas adsorption/desorption in coal as well as coal permeability are reviewed. The experimental measurement methods are also described here. The literature review on experimental investigation of gas storage and displacement processes in coal is presented. The experimental apparatuses related to the gas-coal interaction studies are presented. Finally, a review on computational models relevant to coal-gas interactions is provided in this chapter.

Chapter 3 presents the details of the laboratory facility designed, constructed and commissioned as part of this study. The design considerations for the main analysing units, i.e. the manometric sorption apparatus and the triaxial core flooding system, are discussed. A number of example scenarios are analysed and the results are used as a guideline to select the measuring components such as the pressure transducers and flow meters. The specifications of the major components and the specific features of the constructed and commissioned experimental setup are also provided in this chapter.

Chapter 4 describes the material and methods used in the experimental investigations of this study. The preparation methods used to provide the coal samples for various tests are provided. The characterisation of the coal samples are also presented in this chapter. The methodologies adapted to investigate gas sorption behaviour in coal and gas flow and permeability measurements in coal are described in details. Lastly, the experimental procedure used for measurement of the volumetric deformation of the coal samples due to interactions with reactive gases and during gas injections into core samples is presented in this chapter.

Chapter 5 presents the experimental results of gas adsorption/desorption measurements on the coal samples using the manometric sorption apparatus. The excess and absolute adsorption isotherms of various gas species are measured under a broad range of gas equilibrium conditions. The effects of gas species on sorption behaviour in coal are assessed. In addition, the adsorption kinetics of various gas species in coal is investigated and a number of rate functions are examined to describe the kinetics behaviour of gases.

Chapter 6 presents the experimental results of the core flooding experiments using the high pressure triaxial system. The effects of variation in confining pressure and gas injection pressure on gas flow rates and coal permeability are investigated. Coal volumetric strains due to variations in effective stress and sorption-induced swelling/shrinkage are evaluated. The fate of adsorbed carbon dioxide in coal is investigated by performing sequential gas injections using various gas species.

Chapter 7 presents the experimental results of gas storage and displacement processes in coal. In these experiments, a methane saturated coal sample was subjected to nitrogen (N_2) and carbon dioxide (CO_2) injections. The results of gas breakthrough and displacement processes are presented. The effect of gas species and other factors in those processes are discussed in this chapter.

Chapter 8 presents the results of a series of theoretical modelling on coal permeability evolution due to gas injection. A theoretical approach and numerical model developed by Hosking (2014) is adopted which considers the effective physical and chemical mechanisms controlling the gas transport behaviour in coal. The application of the model to simulate the gas storage and displacement tests presented in chapter 7 is also presented in this chapter. The initial and boundary conditions are described as well as the material parameters used in the simulations. The simulated results are compared with the experimental data and material behaviour during the interactions with different gas species and displacement processes are discussed.

Chapter 9 presents the main conclusions drawn based on the findings of this research as well as suggestions for further research.

1.7. References

Adams, E.E. and Caldeira, K. 2009. Carbon Sequestration via Direct Injection into the Ocean. In: Steele, J.H. eds. *Encyclopedia of Ocean Sciences.* 2nd ed. Oxford: Academic Press, pp. 495-501.

Berlin, K., Sussman, R.M. and Hendricks, B. 2007. *Global warming and the future of coal, the path to carbon capture and storage.* Center for American Progress.

Bevins, R.E., White, S.C. and Robinson, D. 1996. The South Wales Coalfield: low grade metamorphism in a foreland basin setting? *Geology Magazine,* 133(6), pp. 739-749.

Bustin, R.M. and Clarkson, C.R. 1998. Geological controls on coalbed methane reservoir capacity and gas content. *International Journal of Coal Geology*, 38(66), pp. 3-26.

Creedy, D.P. 1988. Geological controls on the formation and distribution of gas in British Coal Measure strata. *International Journal of Coal Geology,* 10(1), pp. 1-31.

Crosdale, P.J., Beamish, B.B. and Valix, M. 1998. Coalbed methane sorption related to coal composition. *International Journal of Coal Geology*, 35(1-4), pp. 147-158.

Damen, K., Faaij, A.., Bergen, F.V., Gale, J. and Lysen, E. 2005. Identification of early opportunities for CO_2 sequestration-worldwide screening for CO_2-EOR and CO_2-ECBM projects. *Energy*, 30(10), pp. 1931-1952.

EIA, 2010. *Annual energy outlook 2010, with projections to 2035*. DOE/EIA-0383(2010), Washington: US Department of Energy.

Every, R.L. and Dell'osso, L. 1972. A new technique for the removal of methane from coal. *CIM Bulletin*, pp. 143-150.

Flores, R.M. 2014. *Coal and coalbed gas: fueling the future*. Waltham: Elsevier.

Fujioka, M., Yamaguchi, S. and Nako, M. 2010. CO_2-ECBM field tests in the Ishikari Coal Basin of Japan. *International Journal of Coal Geology*, 82(3-4), pp. 287-298.

Fulton, P.F., Parente, C.A., Rogers, B.A., Shah, N. and Reznik, A..A. 1980. A laboratory investigation of enhanced recovery of methane from coal beds by carbon dioxide injection. Paper SPE/DOE8930, In: *Proceeding of the First Annual SPE/DOE Symposium on Unconventional Gas Recovery*. Pittsburgh: pp. 65-72.

Gale, J. and Freund, P. 2001. Coal-bed methane enhancement with CO_2 sequestration worldwide potential. *Environmental Geosciences*, 8(3), pp. 210-217.

Gunter, W.D., Gentzis, T., Rottenfusser, B.A. and Richardson, R.J.H., 1997. Deep coalbed methane in Alberta, Canada: a fuel resource with the potential of zero greenhouse gas emissions. *Energy Conversion and Management*, 38(Supplement), pp. S217-S222.

Gunter, W.D., Mavor, M.J. and Robinson, J.R. 2005. CO_2 storage and enhanced methane production: Field testing at Fenn-Big Valley, Alberta, Canada, with application. In: Rubin, E.S., Keith, D.W., Gilboy, C.F., Wilson, M., Morris, T., Gale, J. and Thambimuthu, K. eds. *Proceedings of the 7th International Conference on Greenhouse Gas Control Technologies* 5- September 2004. Vancouver: Elsevier, pp. 413-421.

Hosking, L. 2014. *Reactive transport modelling of high pressure gas flow in coal*. PhD Thesis. Cardiff University.

Israelsson, P.H., Chow, A.C. and Adams, E.E. 2010. An updated assessment of the acute impacts of ocean carbon sequestration by direct injection. *International Journal of Greenhouse Gas Control*, 4(2), pp. 262-271.

Jones, J.M., Pourkashanian, M., Rena, C.D. and Williams, A. 1999. Modelling the relationship of coal structure to char porosity. *Fuel,* 78(4), pp. 1737-1744.

Jones, N.S., Holloway, S., Smith, N.J.P., Browne, M.A.E., Creedy, D.P., Garner, K. and Durucan, S. 2004. *UK coal resource for new exploitation technologies*. Keyworth, Nottingham: British Geological Survey.

Leach, A., Mason, C.F. and van't Veld, K. 2011. Co-optimization of enhanced oil recovery and carbon sequestration. *Resource and Energy Economics,* 33(4), pp. 893-912.

Levy, J.H., Day, S.J. and Killingley, J.S. 1997. Methane capacities of Bowen Basin coals related to coal properties. *Fuel*, 76(9), pp. 813-819.

Marzec, A. 1986. Macromolecular and molecular model of coal structure. *Fuel Processing Technology,* 14(1), pp. 39-46.

Mathews, J.P. and Chaffee, A. 2012. The molecular representations of coal - a review. *Fuel*, 96(1), pp. 1-14.

Ogawa, T., Nakanishi, S., Shidahara, T., Okumura, T. and Hayashi, E. 2011. Saline-aquifer CO_2 sequestration in Japan-methodology of storage capacity assessment. *International Journal of Greenhouse Gas Control*, 5(2), pp. 318-326.

Orr, F.M.Jr. 2009. Onshore geologic storage of CO_2. *Sience*, 325(5948), pp. 1656-1657.

Ozdemir, E., Morsi, B.I. and Schroeder, K. 2003. Importance of volume effects to adsorption isotherms of carbon dioxide on coals. *Langmuir*, 19(23), pp. 9764-9773.

Pagnier, H.J.M., Van Bergen, F., Kreft, E., Van Der Meer, L.G.H. and Simmelink, H.J. 2005. Field experiment of ECBM-CO_2 in the upper Silesian Basin of Poland (RECOPOL). In: *67th European Association of Geoscientists and Engineers Conference*. June 2005. Madrid: Society of Petroleom Engineers, pp. 3013-3015.

Pan, Z. and Connell, L.D. 2012. Modelling permeability for coal reservoirs: A review of analytical models and testing data. *International Journal of Coal Geology*, 92(1), pp. 1-44.

Pappano, P., Mathews, J.P. and Schobert, H.H. 1999. Structural determinations of Pennsylvania anthracites. *American Chemical Society's Division of Fuel Chemistry*, 44(1), pp. 567-70.

Reeves, S.R. and Schoeling, L. 2000. Geological sequestration of CO_2 in coalseams: Reservoir mechanisms field performance and econimics. *5th Internatioanl Conference on Greenhouse Gas Control Technologies*, Cairns, Australia.

Smith, D.H., Sams, W.N., Jikich, S. and Ertekin, T. 2002. Simulating carbon dioxide sequestration/ECBM production in coal seams: effects of permeability anisotropies and the diffusion-time constant. *In: SPE annual technical conference and exhibition*. Denver, pp. 156-163.

Speight, J.G. 2005. *Handbook of coal analysis.* Hoboken, New Jersey: John Wiley & Sons, Inc.

Thomas, L. 2002. *Coal geology*. Dargo Associates Ltd: Wiley Publishing.

Turner, M., Brabham, P., Griffiths, A., Williams, K. and Marsh, R. 2008. *Review of the offshore geology of Wales with relation to its potential for underground coal gasification. Report No. 3163.* Cardiff University Department of Engineering.

van Bergen, F., Pagnier, H.J.M., van der Meer, L.G.H., van den Belt, F.J.G., Winthaegen, P.L.A. and Westerhoff, R.S. 2003. Development of a field experiment of CO_2 storage in coal seams in the Upper Silesian Basin of Poland (Recopol). In: Gale, J. and Kaya, Y. eds. *Greenhouse Gas Control Technologies - 6th International Conference.* 2003. Oxford: Pergamon, pp. 569-574.

Vega, B. and Kovscek, A.R. 2010. *4- Carbon dioxide (CO_2) sequestration in oil and gas reservoirs and use for enhanced oil recovery (EOR)*. In: Maroto-Valer M. ed. *Woodhead Publishing Series in Energy*, Woodhead Publishing, pp. 104-126.

White, C.M., Smith, D.H., Jones, K.L., Goodman, A.L., Jikich, S.A., LaCount, R.B., DuBose, S.B., Ozdemir, E., Morsi, B.I. and Schroeder, K.T. 2005. Sequestration of carbon dioxide in coal with enhanced coalbed methane recovery- A review. *Energy and Fuel*, 19(3), p. 659-724.

White, C.M., Straeisar, B.R., Granite, E.J., Hoffman, J.S. and Pennline, H.W. 2003. Separation and capture of CO_2 from large stationary sources and sequestration in geological formations. *Journal of Air and Waste Management Association*, 53(6), pp. 645-715.

Wold, M.B., Connell, L.D. and Choi, S.K. 2008. The role of spatial variability in coal seam parameters on gas outburst behaviour during coal mining. *International Journal of Coal Geology*, 75(1), pp. 1-14.

Wong, S., Macdonald, D., Andrei, S., Gunter, W.D., Deng, X., Law, D., Ye, J., Feng, S., Fan, Z. and Ho, P. 2010. Conceptual economics of full scale enhanced coalbed methane production and CO_2 storage in anthracitic coals at South Qinshui basin, Shanxi, China. *International Journal of Coal Geology*, 82(3-4), pp. 280-286.

Zhang, D.F., Cui, Y.J., Liu, B., Li, S.G., Song, W.L. and Lin, W.G. 2011. Supercritical pure methane and CO_2 adsorption on various rank coals of China: experiments and modeling. *Energy and Fuel*, 25(1), pp. 1891-1899.

Zhou, F., Hou, W., Allinson, G., Wu, J., Wang, J. and Cinar, Y. 2013. A feasibility study of ECBM recovery and CO_2 storage for a producing CBM field in Southeast Qinshui Basin, China, *International Journal of Greenhouse Gas Control*, 19(1), pp. 26-40.

Yamaguchi, S., Ohga, K., Fujioka, M. and Muto, S. 2005. Prospect of CO_2 sequestration in the Ishikari Coal Field, Japan. In: Rubin, E.S., Keith, D.W., Gilboy, C.F., Wilson, M., Morris, T., Gale J. and Thambimuthu, K. eds. *Greenhouse Gas Control Technologies 7*, Oxford: Elsevier Science Ltd, pp. 423-430.

Yamazaki, T., Aso, K. and Chinju, J. 2006. Japanese potential of CO_2 sequestration in coal seams. *Applied Energy*, 83(9), pp. 911-920.

Yu, C., Ko, W., Chiao, C., Hwang, L. and Yang, M. 2013. Planning a pilot injection test for a 3000m deep saline aquifer in a preferred carbon sequestration site. *Energy Procedia*, 37(1), pp. 4960-4967.

Chapter 2

Literature Review

2.1. Introduction

In this chapter, a review of the recent developments and methodologies employed to investigate the interactions between coal and gases is presented. The aim of this chapter is to provide an overview of the aspects related to the processes involved in gas transport and interactions in coal. The experimental and theoretical studies related to carbon sequestration in coal have been also reviewed in this chapter.

A state-of-the-art review on apparatuses relevant to the experimental investigation of gas-coal interactions is presented in section 2.2. This includes a review of apparatuses related to gas adsorption/desorption isotherm measurements, apparatuses related to gas flow and permeability measurements (core flooding system) and apparatuses specifically developed for measurement of coal swelling/shrinkage due to interaction with gases.

In section 2.3, the experimental measurement methods frequently reported in the literature are reviewed. This includes various approaches for the measurements of gas adsorption/desorption isotherms, gas flow and permeability measurements in coal and swelling/shrinkage measurement during gas-coal interactions.

In Section 2.4, a detailed literature review on influential parameters in interactions between coal and various gas species is presented. Various parameters and their effects on gas sorption properties of coal are discussed. The experimental investigations relevant to the effective parameters on gas sorption in coal and their key findings are also reviewed in this section.

Section 2.5 presents a review on gas transport in coal. The macro-structure of coal and its fracture system are briefly reviewed. The key factors controlling the transport properties of coal and mechanisms involved in gas flow in coal are discussed. The effects of effective stresses and gas sorption on coal permeability are also discussed in this section.

Section 2.6 presents a review on the studies related to gas storage and recovery/displacement processes in coal, also known as enhanced coalbed methane

recovery (ECBM). This section specifically covers the experimental studies related to the processes involved in carbon sequestration in coal and methane recovery.

Section 2.7 presents a brief review on the computational modelling approaches related to the gas storage and replacement in coal with specific focus on carbon sequestration in coal.

In section 2.8, a summary and the concluding remarks of this chapter are presented.

2.2. A review on the experimental apparatuses

In this section, a state-of-the-art review on developed experimental apparatuses and facilities related to study of the interactions between coal and various gas species is presented. The main experimental measurements related to coal-gas interactions include: i) gas adsorption/desorption isotherm measurements, ii) gas flow and permeability measurements in coal samples under the confined conditions and iii) coal swelling/shrinkage measurements during coal-gas interactions.

2.2.1. Apparatuses related to gas sorption measurements

Based on the most common methods used for gas sorption measurements, i.e. volumetric/manometric and gravimetric methods, several apparatuses have been developed and used over the few years. The principal of each method and their detailed description will be provided later in this chapter, i.e. Section 2.3.1. Volumetric/manometric apparatuses have been commonly used for measurements of gas sorption properties of coal (e.g. van Hemert et al., 2009; Fitzgerald et al., 2005; Busch et al., 2003).

Figure 2.1 shows a schematic diagram of a manometric apparatus with two sets of reference cells and sample cells (Battistutta et al., 2010). This setup was employed to conduct sorption experiments of different gases on Selar Cornish coal from South Wales

coalfield. Busch et al. (2003) measured the adsorption/desorption isotherms for single and mixed gases using a manometric apparatus. van Hemert et al. (2009) adopted a manometric apparatus with an enlargeable reference cell to control the amount of the added and extracted gas.

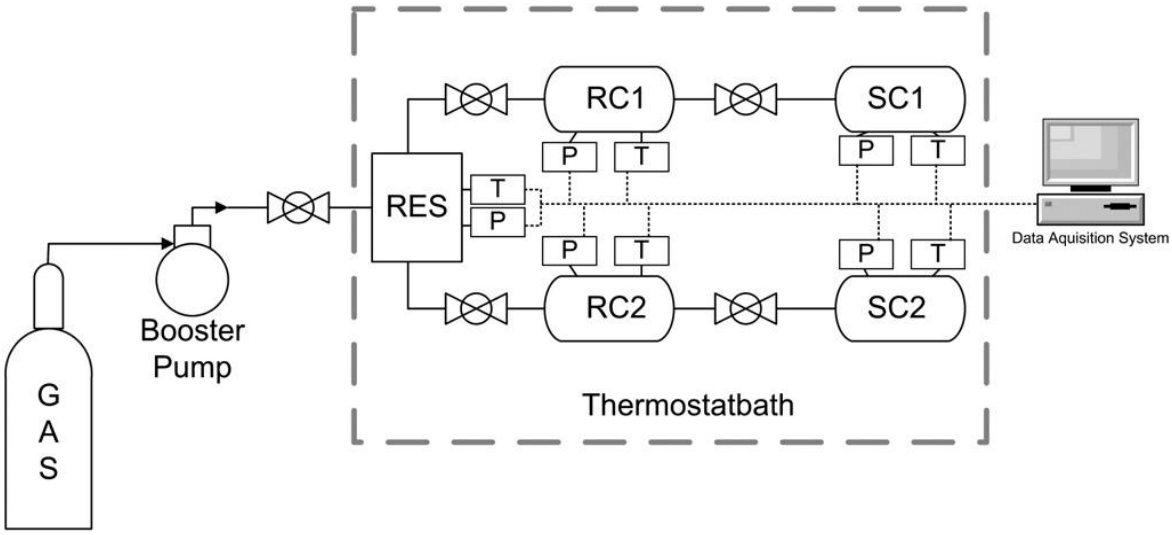

Fig. 2.1. Schematic diagram of a manometric apparatus with two sets of reference cells and sample cells (Battistutta et al., 2010); RES: reservoir, RC: reference cell, SC: sample cell, P: pressure transducer and T: thermocouple.

Figure 2.2 shows an schematic diagram of a volumetric apparatus that has been used to measure adsorption of CO_2, CH_2, N_2 and their mixture on wet coals (Fitzgerald et al., 2005; Mohammad et al., 2009; Sudibandriyo, 2004). As shown in Figure 2.2, a special pump (Ruska pump) has been used to provide constant gas pressure during gas sorption measurements. A volumetric setup comprising four pairs of reference and sample cells was used by Zhang et al. (2011).

Compared to the volumetric/manometric apparatuses, application of the gravimetric apparatus has been limited mostly due to relatively high cost associated with it. Figure 2.3 presents a schematic diagram of a gravimetric apparatus reported by Goodman et al. (2007). Day et al. (2008) conducted a series of excess sorption measurements on coal particles using a gravimetric system including a reference cell, a sample cell, a syringe pump and two electronic balances for each cell. Ottiger et al. (2008) and Fujii et al. (2009)

measured the adsorption of CO_2 and CH_4 on coal samples with a gravimetric setup equipped with a Rubotherm magnetic suspension balance.

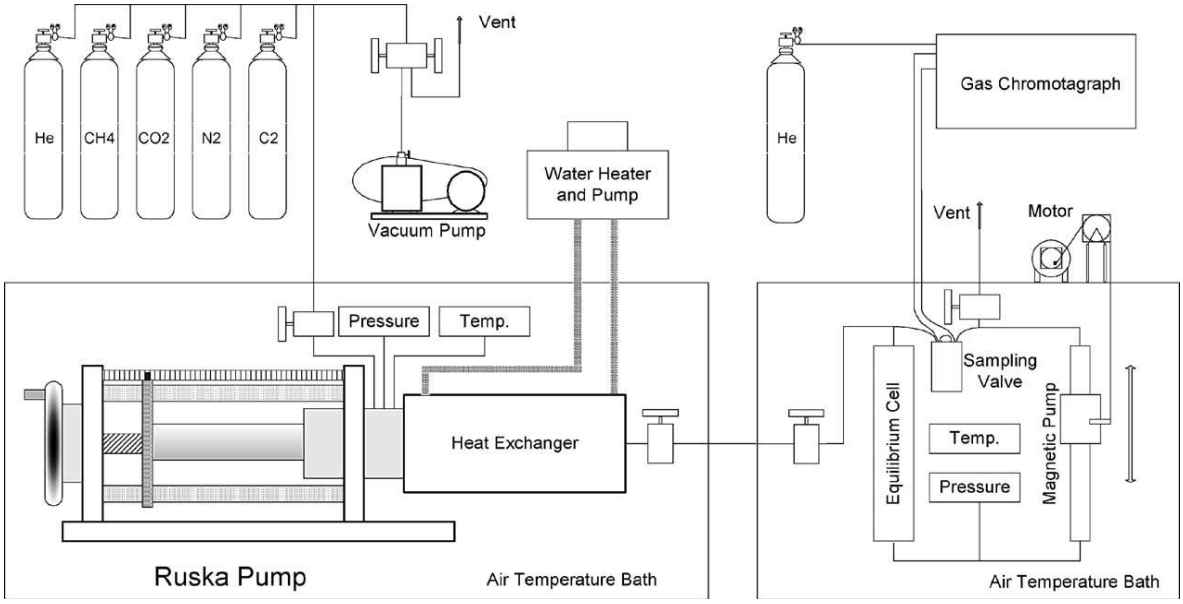

Fig. 2.2. Schematic diagram of a volumetric apparatus used by Fitzgerald et al. (2005).

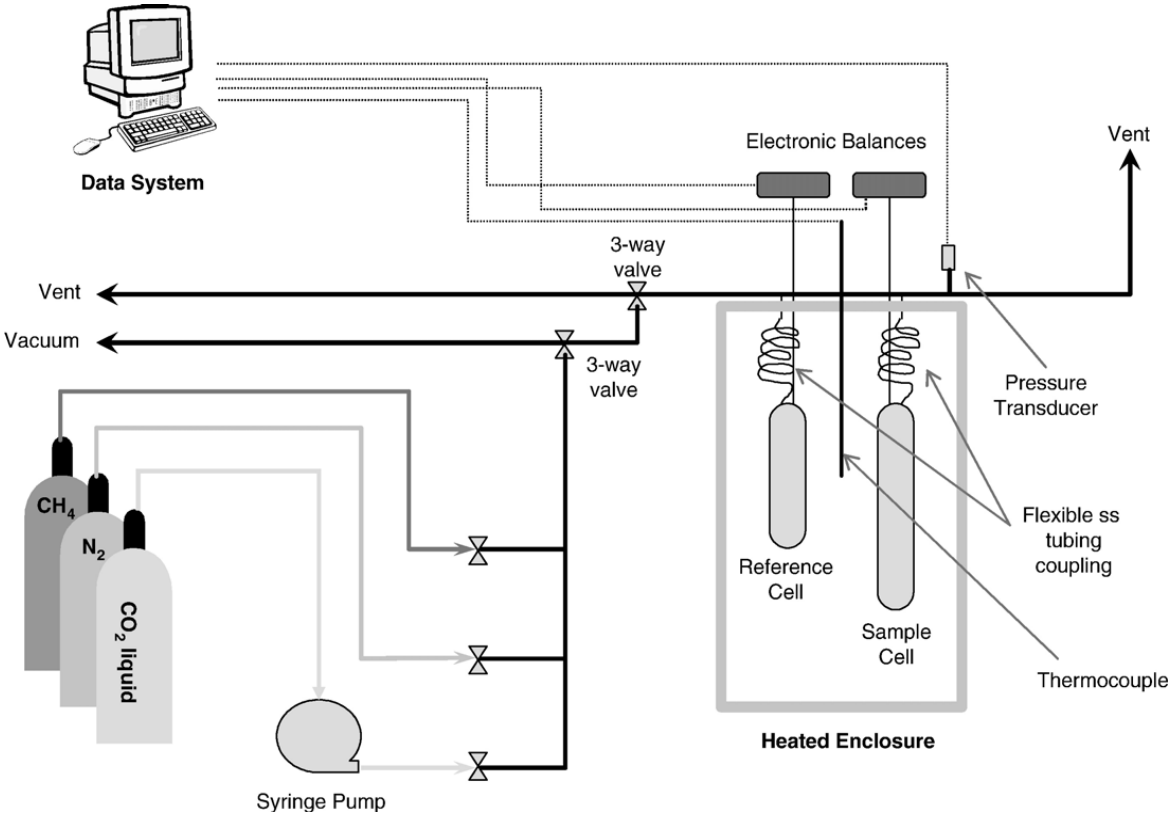

Fig. 2.3. A schematic diagram of a gravimetric apparatus reported by (Goodman et al., 2007) for measurement of CO_2-coal sorption isotherms.

2.2.2. Apparatuses related to gas flow and permeability measurements

Several experimental setups related to gas flow and permeability measurements have been constructed and used by other researchers in last few years. A TTSCP facility (True Triaxial Stress Coal Parameter) has been used by Massarotto et al. (2010) to measure the coal permeability to CO_2 using a quasi-steady flow method. Examples of the published works using this facility can be found in Massarotto et al. (2010), Wang et al. (2010), Wang et al. (2007) and Wang et al. (2011).

A high-pressure core flooding setup has been developed and used by Mazumder et al. (2006). This system comprises of a pressure cell for samples up to 500mm in length, an ISCO Syringe pump to control the gas flow, a micro gas chromatographer to analyse the composition of the produced gas. Examples of the published works using this apparatus can be found elsewhere e.g. Mazumder et al. (2006), Mazumder and Wolf (2008), van Hemert et al. (2012), Shi et al. (2008b).

Figure 2.4 presents the gas permeability measurement setup developed and used by Huy et al. (2010). The setup mainly consists of a Hassler core holder and two hydraulic pumps to provide the confining and axial stresses required. Three types of gas flow meter and flow controller with different capacities have been employed in this apparatus including a soap-film flow meter for measuring fracture aperture in coal. CO_2 gas has been used to measure the permeability of the coal samples under a range of effective stresses up to 6MPa (Huy et al., 2010).

Ranjith and Perera (2011) developed a high pressure triaxial apparatus to measure the mechanical properties and permeability of core samples at gas pressures up to 50MPa and confinement pressures up to 70MPa (Ranjith and Perera, 2011; Perera et al., 2011; Viete and Ranjith, 2006; Jasinge et l, 2011; Shukla et al., 2012, Vishal et al., 2013).

Harpalani and Mitra (2010) conducted gas permeability and sorption-induced strain measurements on coal samples using a triaxial system and a circumferential extensometer to monitor deformations of core.

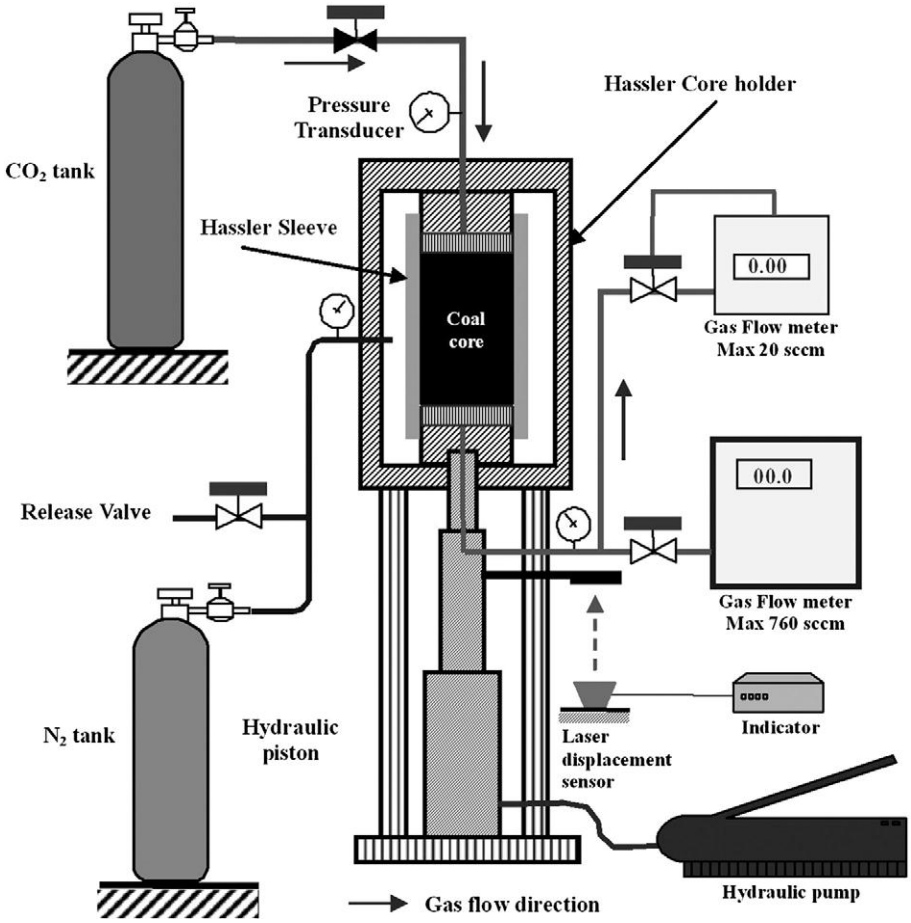

Fig. 2.4. Schematic diagram of the developed gas permeability measurement system at Kyushu University (Huy et al., 2010).

Chen et al. (2011) and Pan et al. (2010a) have used a triaxial multi-gas apparatus to measure gas adsorption, swelling and permeability for the core samples of coal utilising a transient method. Figure 2.5 shows a schematic diagram of the apparatus used by Chen et al. (2011).

A rock test rig especially designed for soft rocks was used by Kiyama et al. (2011) to investigate the coal swelling strain and permeability changes during CO_2 and N_2 injections under stress-constrained conditions. Four syringe pumps were employed to control the inlet/outlet fluids and piezoelectric transducers to measure the coal strain during gas injections. Similar setups with syringe pump utilisation have been developed and used by other researchers, e.g. Wang et al. (2013), Mazumder et al. (2006) and Lin (2010).

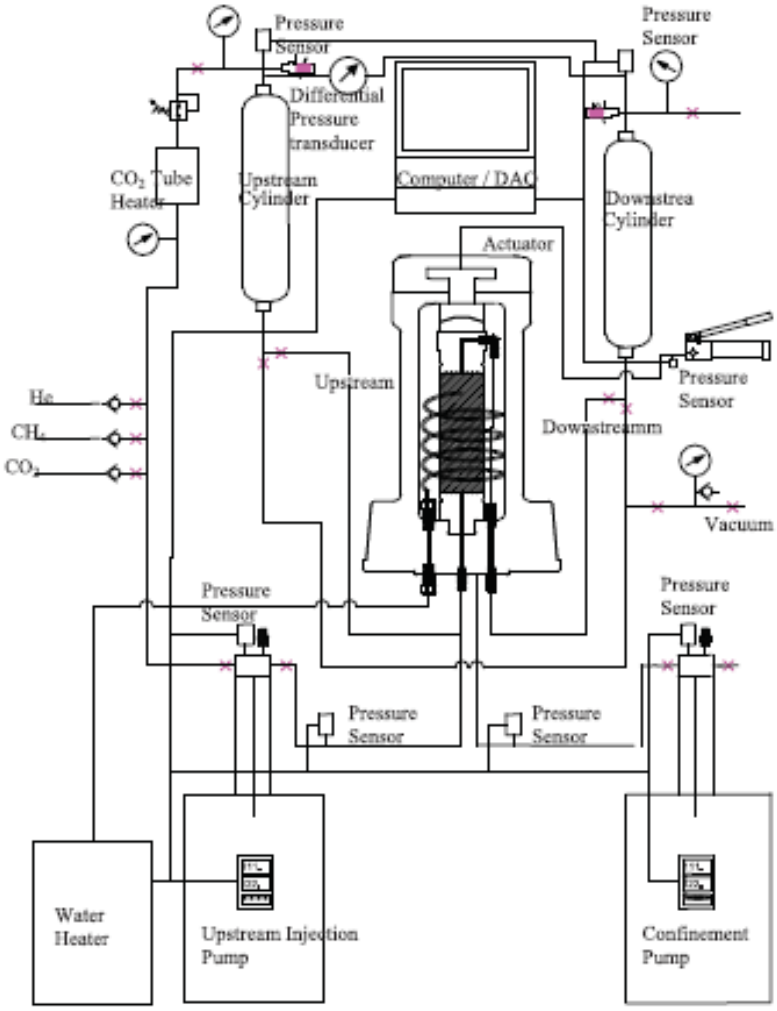

Fig. 2.5. A schematic diagram of a triaxial apparatus for gas flow and permeability measurement in coal based on transient method (Chen et al., 2011).

2.2.3. Apparatuses related to coal swelling/shrinkage measurements

Application of displacement transducers for measurement of swelling/shrinkage of coal samples due to interaction with gases is usually associated with the triaxial cells and core flooding system as mentioned in previous section. Nevertheless, the number of experimental apparatuses reported in the literature which have been specifically designed for the measurements of swelling/shrinkage or sorption-induced strain in coal during interaction with gases is very limited.

Duracan et al. (2009) developed an apparatus for measurement of sorption-induced strain on cubic coal blockes. As shown in Figure 2.6, the apparatus comprises a high

pressure cell with strain gauges directly glued on the surfaces of coal blocks (Duracan et al., 2009). Similar approch has been used by others. For instance, Harpalani and Mitra (2010) adopted three pressure cells and placed one core sample in each cell with three stain gauges attached to each sample. Majewska et al. (2010) performed coal swelling/shrinkage measurements on one block of coal sample and four strain gauges attached to its sides.

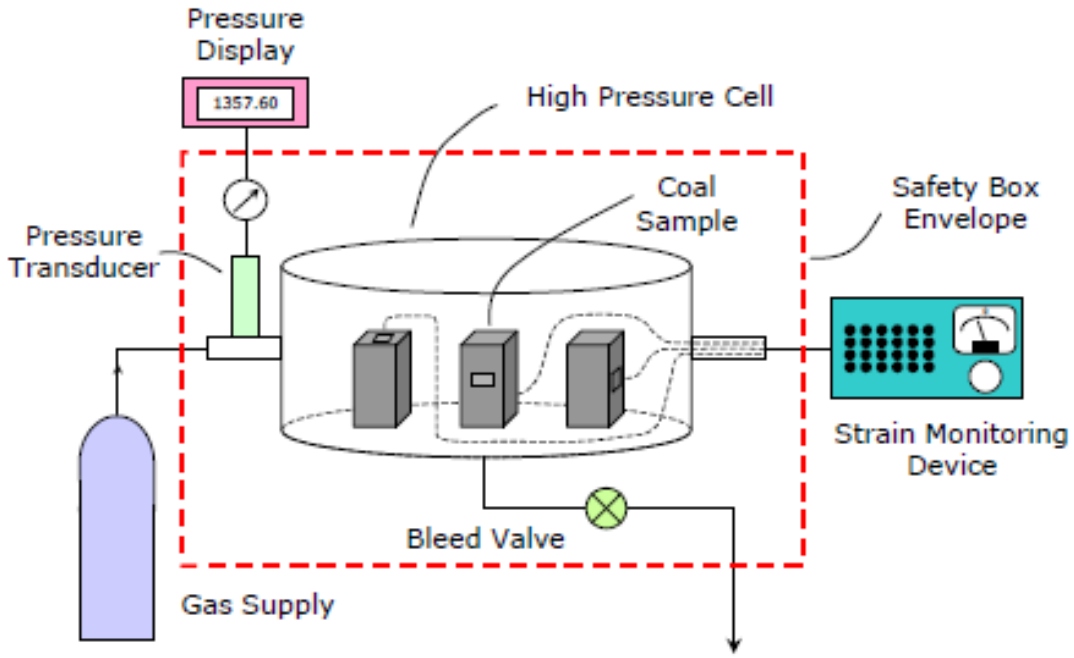

Fig. 2.6. The experimental set-up used for measurements of sorption-induced coal matrix deformation (from Durucan et al., 2009).

Another type of experimental apparatuses developed specifically for the measurement of sorption-induced strain in coal (swelling/shrinkage) is based on the optical method (He et al., 2010; van Bergen et al., 2009; Day et al., 2008; Robertson and Christiansen, 2007), an example of the optical apparatus used by Day et al. (2008) is presented in Figure 2.7. In this apparatus, the dimensional changes in blocks of coal within a pressure cell can be observed and recorded by means of digital cameras positioned above transparent windows of the cell.

From the review of the experimental apparatuses presented in this section, it can be perceived that there are a number of experimental apparatuses reported in the literature which have been developed specifically for a certain area of research, i.e. for gas adsorption/desorption measurements, gas flow and permeability measurements or swelling/shrinkage measurements. However, there is a lack of experimental apparatuses which are capable of producing a comprehensive set of data including all the areas mentioned above. In addition, the range of sample sizes used in these apparatuses is limited (mostly cylinder samples with diameters less than 0.05m).

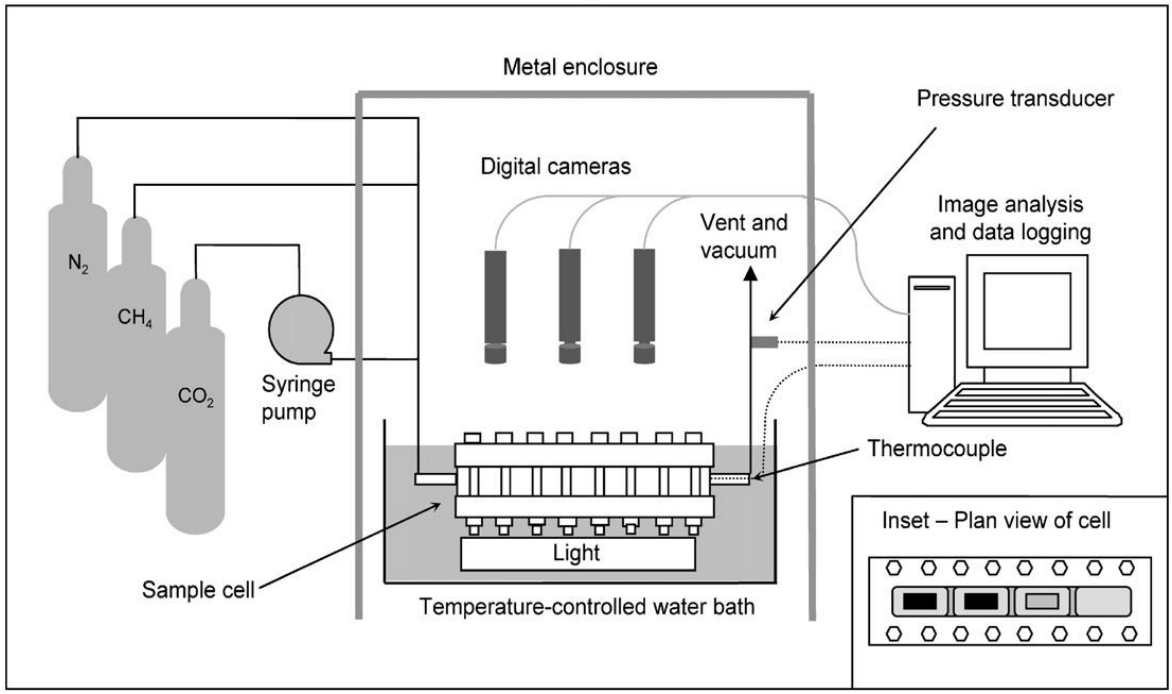

Fig. 2.7. Schematic diagram of the apparatus for measuring coal swelling based on optical method (From Day et al., 2008).

2.3. Experimental measurement methods

Gas transport and reactions in coal can involve different processes including i) gas adsorption/desorption, ii) gas flow in coal and iii) deformation effects and coal swelling/shrinkage. In this section, a detailed description of the most common methods that have been used to investigate the above processes is presented.

2.3.1. Gas adsorption/desorption measurement methods

Various experimental methods including gravimetric (Fujii et al., 2009; Day et al., 2008; Ottiger et al., 2008), volumetric (Fitzgerald et al., 2005), manometric (Siemons and Busch, 2007; van Hemert et al., 2009; Ozdemir, 2004), carrier gas and calorimetric techniques (Nelsen and Eggertsen, 1958), nuclear resonance (Sircar, 1999) and chromatographic analysis (Wakao et al., 1980) have been employed to obtain the adsorption/desorption isotherms of gases in coal. The accuracy of each method depends on the design of the measurement apparatus and the experimental conditions. Among the mentioned methods, the most frequently used methods for measuring adsorption/desorption isotherms are the volumetric (manometric) and gravimetric methods. Therefore, in this section these methods are briefly described and their advantages and disadvantages are discussed.

In the volumetric/manometric method, the adsorption isotherms are obtained by calculating the adsorbed amount of gas using the real gas behaviour and associated thermodynamic relationships. The manometric and volumetric methods are distinguished by the manner in which the gas is injected into the measurment cell. Systems which involve the measurement of a displaced volume at constant pressure “fixed-pressure” are true volumetric techniques and those which measure a pressure change for a constant volume “fixed-volume” are called manometric technique. Schematic diagrams of both methods are shown in Figure 2.8. These methods are well-known and established techniques and relatively inexpensive. However, reliable sorption measurement using these methods requires an accurate determination of the cell and void volumes. The amount of the adsorbed gas is calculated from the pressure measurements (manometric method) or pressure and volume measurements (volumetric method).

In both methods, the sample is placed in the sample cell and its volume is determined using helium pycnometry method. Helium pycnometry method will be described in detail in Chapter 4. In the volumetric method, the adsorption isotherm is determined by continuously decreasing the volume of the piston pump and thus increasing the gas pressure. In the manometric method (with fixed reference and void volumes), the

adsorption isotherm is determined by a stepwise increasing of the gas injection pressure in the reference cell. For the desorption measurements, the experimental procedures are similar to the adsorption measurements, except that it starts from the higher gas pressure and continues with stepwise gas pressure reduction.

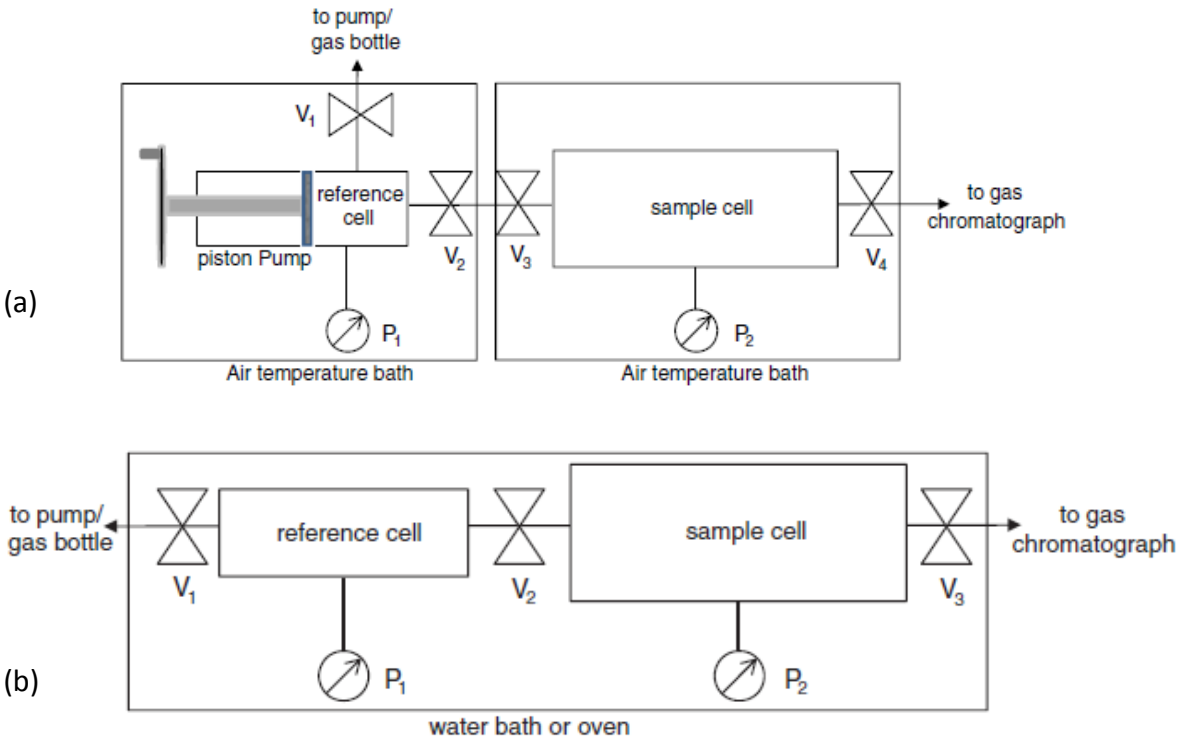

Fig. 2.8. Schematic diagrams of a) volumetric apparatus and b) manometric apparatus (from Busch and Gensterblum, 2011); V: valves and P: pressure gauges.

In the gravimetric method, the amount of the adsorbed gas is measured at constant pressure by means of an accurate balance, with the sample either suspended mechanically or by magnetic coupling across the wall of a high-pressure cell (Busch and Gensterblum, 2011). In this technique, a microbalance is used to measure the weight variations after accounting for the sample buoyancy. As shown in Figure 2.9, the system consists of an electromagnet linked to the balance and a permanent magnet at the top of the suspension system. More details related to the gravimetric method and calculation of the adsorption/desorption isotherms in this method have been provided by Ottiger et al. (2008), Day et al. (2008) and Fujii et al. (2009).

A comparison between the gravimetric method and volumetric/manometric method is provided in Table 2.1. Advantages and disadvantages of each method are summarised in this table.

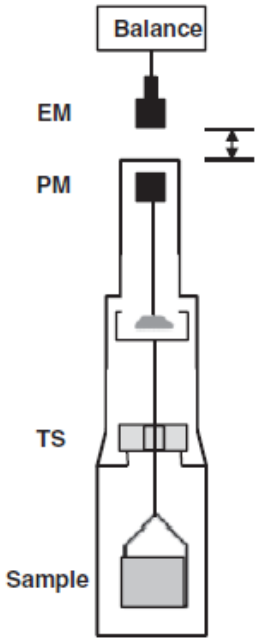

Fig. 2.9. Schematic diagram of a gravimetric apparatus; EM:electro magnet, PM: permanent magnet, TS: titanium sinker (from Busch and Gensterblum, 2011).

Table 2.1. A comparison between the gravimetric and volumetric/manometric methods.

Gravimetric method	**Volumetric / manometric method**
High precision and accuracy.	Well known and accepted technique.
Relatively fast due to direct measurement and less calibrations required.	Easy to develop for high-pressure measurements.
Sample preparation is easier.	Relatively inexpensive.
Most gravimetric devices are commercial and relatively expensive.	Larger errors due to the use of Equations of State (EoS).
The buoyancy error.	The hermetic seal can be challenging.
Nearby ground vibrations may cause inaccuracy of the measurements.	Not suitable for moist coal samples.

In addition to the volumetric and gravimetric methods mentioned above, alternative test methods to measure gas sorption on coal have been also reported in the literature. For

instance, a less conventional method for gas sorption measurement in coal has been reported by Hol et al. (2011). In this method, a cylindrical coal sample is jacketed in an annealed gold capsule and exposed to gas at constant pressure and temperature. Once the coal is saturated, the capsule is sealed. CO_2 is then allowed to be desorbed from the coal and flow into an inflatable aluminum-foil bag attached to the capsule. The volume of the bag and amount of CO_2 stored in the coal sample is then determined using the Archimedes method. Although, the capsule method used by Hol et al. (2011) can be time-consuming and expensive, the advantage of this method is that there is no need for Equation of State (EoS) to account for the gas compressibility.

2.3.2. Gas flow and permeability measurement methods

In order to investigate the flow processes in rock material, triaxial testing has been used more frequently especially for measurements at high pressure conditions. A primary advantage of the triaxial testing is the ability to simulate the in situ conditions (stress and pressure) at different depths (Ranjith and Perera, 2011; Harpalani and Mitra, 2010; Shen et al., 2011; Gillies et al., 1995). The confining pressure around the sample prevents the gas escape from preferential flow paths along the walls (Tarantino et al., 2009).

Various methods have been used by researchers to measure gas flow and permeability of rocks under the triaxial stress conditions. The most commonly used methods are i) the steady-state method, ii) unsteady-state method and iii) transient method.

The steady-state method is a routine permeability measurement method which is conducted on a core sample under confined conditions and by applying gas pressure to one end and measuring the flow rate and pressure differential under the steady-state conditions, as shown in Figure 2.10.a. One of the advantages of using the steady-state method is the possibility to perform several gas permeability measurements on the same sample and at different pore pressures (Carles et al., 2007). However measuring the steady-state permeability of tight rocks can be time consuming since reaching the equilibrium for the gas flow and pressure can be very slow (Shen et al., 2011; Carles et al.,

2007). Moreover some difficulties such as sample drying, condensation or leakage might occur in long duration steady-state experiments (Carles et al., 2007).

For the experiments based on the unsteady-state method, the outlet remains closed during the test. A gas pressure pulse is applied at the inlet and the decrease of the inlet pressure is analysed in order to obtain the permeability values. According to the Recommended Practices for Core Analysis (API RP, 1998), this method is particularly suitable for tight rocks with permeability less than 10μD ($1\times10^{-18}m^2$), due to the advantage of measuring the pressure instead of flow rate. The unsteady-state method is faster than steady-state method. However the absolute permeability is not given directly from the test and is calculated with Klinkenberg factors from existing correlations (Carles et al., 2007).

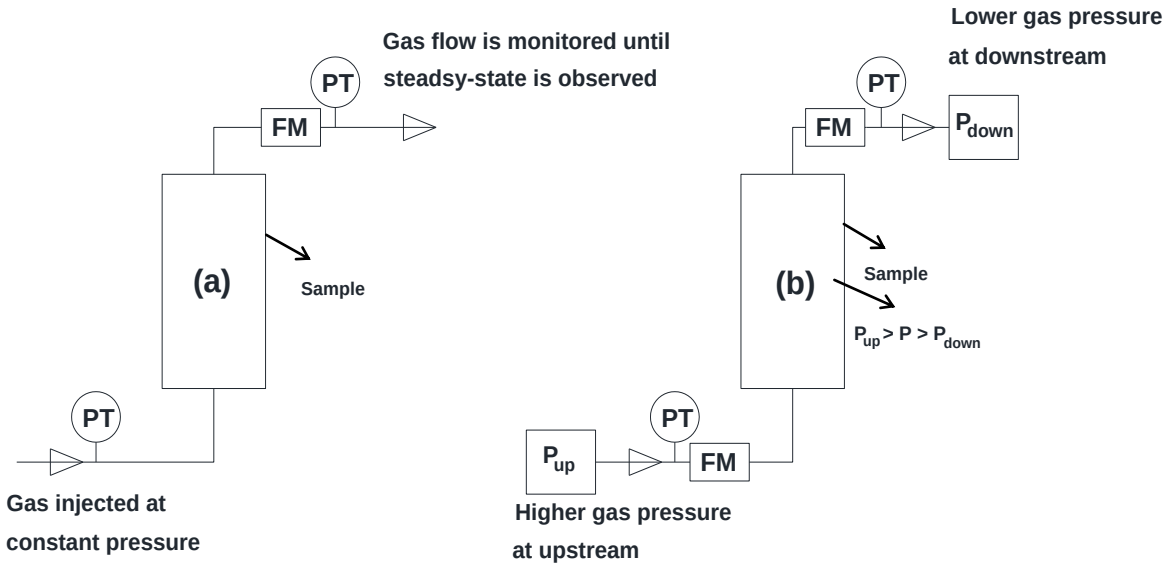

Fig. 2.10. Schematic diagram of gas flow and permeability measurements using a) steady-state method, b) transient method; PT and FM are pressure transducer and flow mete, respectively.

An alternative method of gas flow and permeability measurements in low permeability samples is the transient method (e.g. Chen et al., 2011; Brace et al., 1968; Hsieh et al., 1981). In this method, there are two gas cylinders at upstream and downstream of the sample. The upstream cylinder is charged to slightly higher than the sample pressure

while the downstream cylinder pressure is slightly lower than the sample pressure, as shown in Figure 2.10.b. Then gas is allowed to flow through the sample from the upstream cylinder to the downstream cylinder. Permeability is calculated from the pressure decay curve measured by a differential pressure transducer installed between the upstream and downstream cylinders.

The quasi-steady method has been also employed to measure gas permeability in which the mean gas flow rate is taken into account (Wang et al., 2010). Other less conventional methods for permeability measurement in rocks have been also reported in the literature, e.g. the Darcygas method for gas permeability measurement on crushed cores (Luffel, 1993), the Darcylog method for liquid permeability measurement on crushed cores (Egermann et al., 2005), Nuclear Magnetic Resonance or NMR (Kenyon, 1989; Timur, 1968), Image Analysis (Carles et al., 2007) and Mercury porosimetry curves (Swanson, 1981; Thomeer, 1983; Kamath, 1992). More details about these methods can be found in the mentioned works.

2.3.3. Swelling/shrinkage measurement methods

As stated previously, a limited number of studies have been reported in the literature which have conducted direct measurements of coal swelling/shrinkage due to gas adsorption or desorption. Direct swelling/shrinkage measurments are usually associated with application of stain gauges or displacement transducers attached to the surface of sample. In this approch cubic coal blocks are placed in a high pressure cell with strain gauges attached to each sides, as previously shown in Figure 2.6 (Duracan et al., 2009; Battistutta et al., 2010). Similar approche has been adopted by Majewska et al. (2010) with one block of coal and four strain gauges attached to its sides.

Another method for measurement of sorption-induced strain (swelling/shrinkage) is the optical method. In this method, the dimensional changes can be observed in blocks of coal placed within a pressure cell with glass windows, as previously shown in Figure 2.7. He et al. (2010), van Bergen et al. (2009), Day et al. (2008) and Robertson and

Christiansen (2007) have conducted coal swelling measurments on unconfined coal blockes using a pressure cell with transparent windows and digital cameras positioned above the windows.

The effect of different gases on coal swelling/shrinkage can be indirectly evaluated using excess adsorption/desorption isotherms (Kim et al., 2011; Ozdemir et al., 2004) In this method, the volumetric effects during adsorption/desortion isotherm measurements can be accounted for coal swelling (Siemons and Busch, 2007; Ozdemir et al., 2004).

The swelling/shrinkage measurement methods described above are usually conducted under the unconfined conditions and therefore the effect of confining pressure on gas transport properties of the sample and ite sorption-induced strain can not be considered. The effect of confining pressure on gas-coal interactions will be discussed in Section 2.4.6.

In order to account for the effect of confining pressure on coal swelling/shrinkage, triaixal cells and core flooding cells are frequently used (e.g. Lin, 2010; Li et al., 2013; De silva and Ranjith, 2012; Ranjith and Perera, 2011; Wang et al., 2010; Kiyama et al., 2011). In this method, axial and radial displacement transducers are attached to the core sample under the confined condition. Deformations of the sample due to variations in effective stress or swelling/shrinkage due to interaction with gases are recorded by displacement transducers.

In order to distinguish between the mechanical deformation of the sample due to changes in effective stresses from sorption-induced deformations, Harpalani and Mitra (2010) conducted a core flooding test with a non-adsorptiove gas, i.e. helium, under a range of effective stresses. The test was repeated for reactive gases such as CH_4 or CO_2 to estimate the sorption-induced deformations (swelling or shrinkage).

2.4. The interactions between coal and gases

The adsorption/desorption capacity of coal for various gas species and the stability of the adsorbed gases can be affected by a number of factors. These are related to coal

composition, gas properties and those affected by environmental conditions and variability. In this section, a number of important parameters/factors that can be influential in gas sorption in coals are briefly discussed and experimental studies relevant to each factor are reviewed.

2.4.1. Coal sorption capacity to gases

The adsorption/desorption capacity of coal for different gas species and stability of the adsorbed gases can be related to the coal composition, gas properties and environmental conditions such as temperature and water content (White et al., 2005). For instance, the sorption mechanism of carbon dioxide in coal is described to include both physical and chemical adsorption. The gas can be bound to the solid surface of coal by a direct chemical bond. In addition, adsorption of carbon dioxide on coal can occur mainly due to van der Waals and electrostatic forces between the coal surface and gas molecules (Wang et al., 2013). Carbon dioxide can be absorbed into the coal by penetrating into the elastic chains contained in coal and by filling of micropores smaller than its molecular size which can result in swelling of the coal matrix (Milewska-Duda et al., 2000).

Several experimental investigations have been reported on adsorption/desorption behaviour of different gases in coal, e.g. Busch et al. (2003), Ozdemir (2004), Fitzgerald et al. (2005), Siemons and Busch (2007), Gensterblum et al. (2010). The experimental studies on gas sorption kinetics in coal, however, have received very little attention in the literature.

The experimental investigation on powdered coal samples indicates that coal in general has higher adsorption tendency for CO_2 in comparison with CH_4 (e.g. Jessen et al., 2008; Pone et al., 2009; Sakurovs et al., 2010). In a few cases preferential adsorption of CH_4 over CO_2 in low rank coals has been reported (Busch et al., 2003). Due to the specific physical, chemical and electrical properties of different gas molecules and interactions of gases with functional groups on the coal surface, coal can present a selective sorption behaviour for CO_2 molecules over CH_4 molecules (Cui et al., 2004). Simulation studies at

molecular scale also confirm that CO_2 molecules can be more readily adsorbed to the coal in comparison with CH_4 molecules (Narkiewicz and Mathews, 2009). Linear molecules of CO_2 with smaller kinetic diameter can access to the pore spaces which are not accessible to the spherical methane molecules with larger kinetic diameter (Cui et al., 2004; Narkiewicz and Mathews, 2009). Additionally, the higher adsorption energies of the available smaller pores enhance the adsorption affinity of CO_2 molecules (Cui et al., 2004). In general, the amount of nitrogen (N_2) adsorbed on coal is reported as about half of CH_4 and CH_4 as about half of CO_2 (Levy et al., 1997).

2.4.2. Effects of the coal rank on sorption properties

The degree of alteration (or metamorphism) that occurs as a coal matures from peat to anthracite is referred to as the rank of the coal. Low-rank coals include lignite and sub-bituminous coals. These coals have a lower energy content because they have a low carbon content. They are lighter (earthier) and have higher moisture levels. As time, heat, and burial pressure all increase, the rank does as well. High-rank coals, including bituminous and anthracite coals, contain more carbon than lower-rank coals which results in a much higher energy content. They have a more vitreous appearance and lower moisture content than lower-rank coals (Thomas 2002). There are various classification systems for coal developed in different countries. A number of common classification systems are shown in Figure 2.11.

It has been reported that the gas adsorption/desorption capacity of coal varies significantly with coal rank. The adsorption capacities of CH_4 and CO_2 are dependent on the coal rank which is indicated by vitrinite reflectance coefficient ($R_{o\ max}$). The behaviour presents a U-shaped trend with coal rank (Zhang et al., 2011). This has been attributed to both morphological and surface chemistry properties of coal (Zhang et al., 2011). According to Gürdal et al. (2001), the micro-pore volume of coal decreases with an increase of vitrinite reflectance up to a value of approximately 1.1%. With further increase in vitrinite reflectance, the micro-pore volume increases again. This may explain

the relationship between the adsorption capacity and the coal rank. The micro-pore volume is related to the content of vitrinite (Zhang et al., 2011).

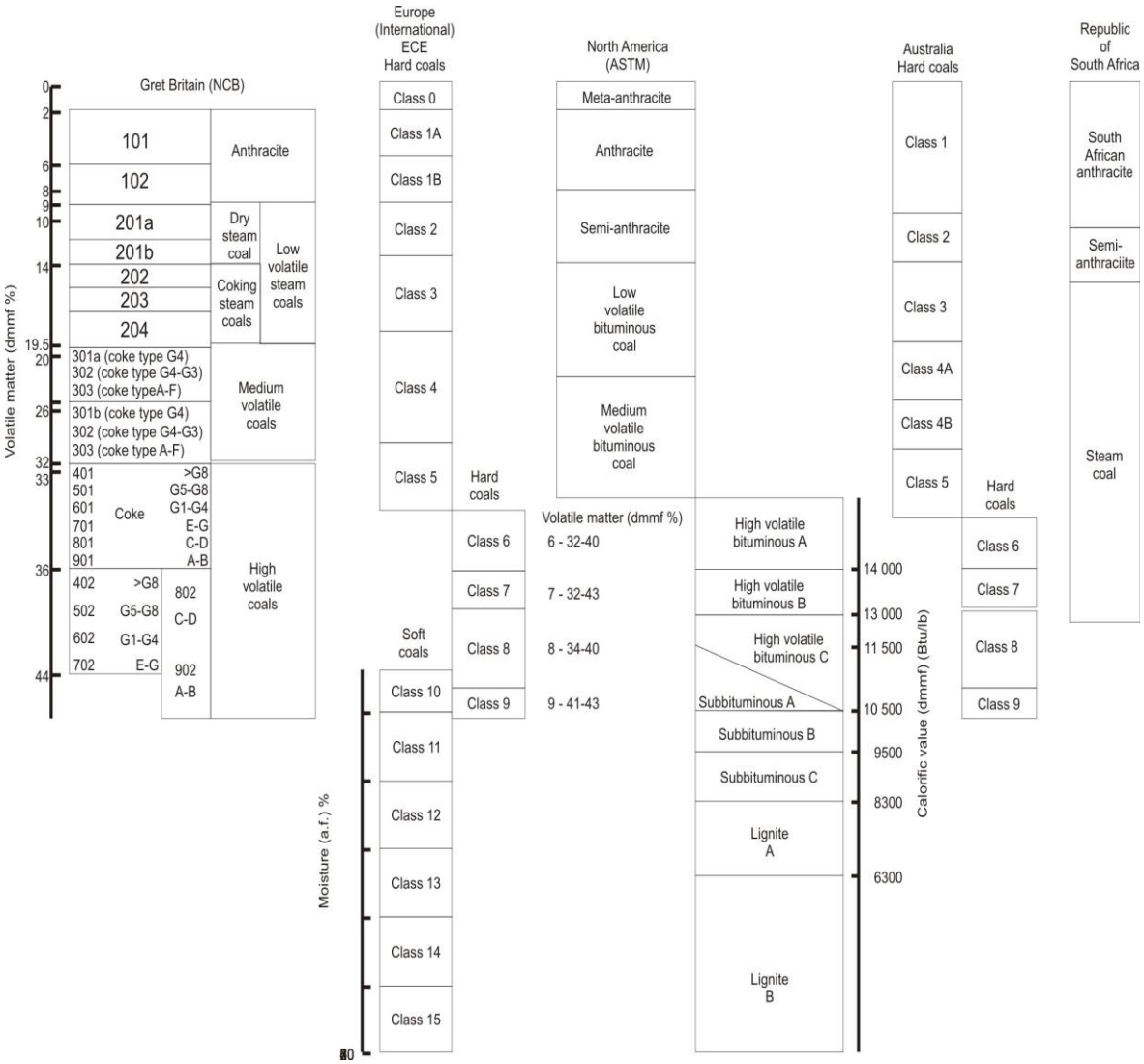

Fig. 2.11. Comparison of the different coal classification systems (adopted from Thomas, 2002).

In general, anthracite coals have higher adsorption capacity whilst the gas adsorption capability is reduced by the amount of volatile contents in bituminous coals (Kim, 1977). The experimental study of Laxminarayana and Crosdale (1999) on the adsorption of CH_4 on dry coals with different ranks from high volatile bituminous to anthracite, in Sydney Basin, Australia, indicated that the coal type, rank and mineral matter strongly influence the CH_4 sorption capacity of the coals.

2.4.3. Effects of the moisture content on sorption properties

Coal moisture content has been also found as an influential parameter on gas adsorption/desorption behaviour in coal. In general, adsorption capacity of coal decreases with increase in the water content (Day et al., 2008; Pan et al., 2010b). Day et al. (2008) stated that the adsorption capacity of coal for both CO_2 and CH_4 reduces up to a critical moisture level. Beyond the critical moisture level, the moisture content has no effect on the adsorption capacity. This is because water molecules only attach to the polar sites of the coal surface such as the hydroxyl groups and hydrophobic sites on coal surface remain available for adsorption of CO_2 or CH_4 (Day et al., 2008). In addition, in low rank coals, moisture has shown a greater effect on the sorption capacity than in high rank coals (Day et al., 2008). This can be because of the greater proportion of the polar sites in low rank coals (Day et al., 2008).

In general, the adsorption capacity of wet coal has been reported to be lower than those for dried coal (Ozdemir and Schreoder, 2009). Figure 2.12 presents a schematic diagram related to the effect of moisture content on sorption capacity of coal to methane as a function of temperature (Busch and Genstreblum, 2011).

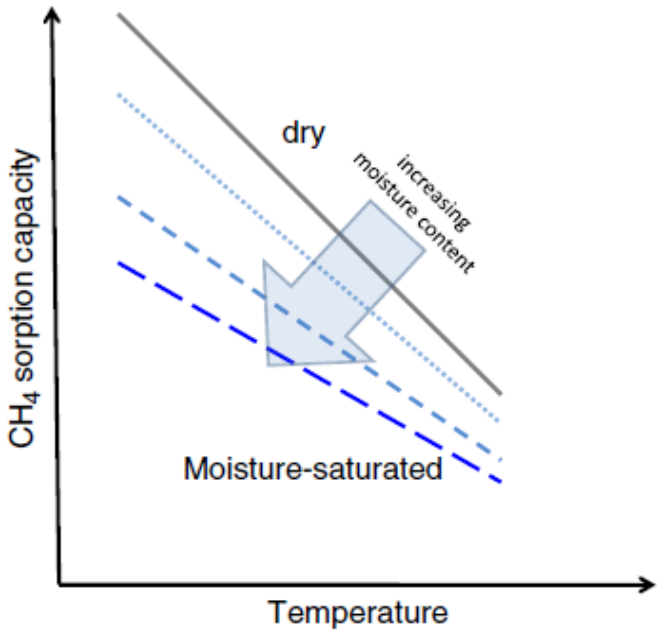

Fig. 2.12. Schematic diagram of the effect of moisture content on coal sorption capacity (Busch and Genstreblum, 2011)

The experimental results of Pan et al. (2010b) showed that moisture content has an additional impact on gas adsorption rate. The effect of moisture content on diffusion rate has been reported to be stronger for CH_4 than CO_2 (Pan et al., 2010b). It has been explained that water has different impacts on gas diffusion in pores with different sizes and the impact of moisture on CH_4 diffusion in micro-pores is stronger than CO_2, as it tends to dissolve into water more readily (Pan et al., 2010b).

Presence of water can affect the experimental results of gas sorption on coal (Busch and Genstreblum, 2011). Gas sorption capacities are typically reported on a dry-ash-free (daf) basis assuming no gas dissolution in water or sorption. Methane dissolution in water is negligible and therefore can be ignored (Busch and Genstreblum, 2011). For the case of CO_2 however, relevant amounts of gas dissolution in water have been reported depending on the sample moisture content (Busch et al., 2007).

2.4.4. Effects of temperature on sorption properties

Temperature is an influential factor in gas-coal interactions and needs to be monitored carefully during the experimental measurements. A small variation in gas temperature can result in a large error in the calculations and data interpretations. This is especially more significant at higher gas pressures. For instance, an error of 1K in the temperature measurement may result in a maximum error in calculated density of carbon dioxide at 10MPa gas pressure (Gensterblum et al., 2010).

Experimental studies related to the effect of temperature on gas sorption in coal indicate that the temperature variation may considerably decrease the adsorption capacity of gases in coals (e.g. Azmi et al., 2006; Ozdemir, 2004; Sakurovs et al., 2007). A significant decrease in the CH_4 adsorption in coal with increasing temperature was reported by Levy et al. (1997).

Laboratory studies of Schroeder et al. (2002) on CO_2 adsorption capacity of coals at different temperature ranges (20-50˚C) have shown a reduction in the adsorption capacity with increasing temperature especially at high gas pressures. Zhang et al. (2011)

attributed the reduction of adsorption capacities of coals at higher temperature to the greater energy required for replacement of the adsorbed molecules of methane at higher temperature.

Li et al. (2010) have shown that at gas pressures of more than 20MPa the temperature dependency of the CO_2 excess adsorption isotherms decreases to nearly zero and therefore the excess adsorption isotherms for different temperatures converge.

2.4.5. Effect of gas pressure on sorption properties

In general, the sorption capacity is assumed to increase with increase in gas pressure. Krooss et al. (2002) reported the experimental results of CH_4 and CO_2 adsorption isotherms on coal at pressures up to 20MPa. Their findings indicated that CH_4 adsorption behaviour follows a Langmuir-like trend and did not show any discrepancies at pressures up to 20MPa, whilst the excess and absolute adsorption isotherms of CO_2 showed an unusual decreasing pattern at higher pressures than at specific critical points. Similar observations have been reported by Li et al. (2010) and Weniger et al. (2010) on the adsorption behaviour of CO_2 and CH_4 at high pressures on different coals. They attributed the unusual shape of the high pressure adsorption isotherm of CO_2 to volume increase of adsorbed-phase at high pressures as well as swelling of the coal matrix.

Goodman et al. (2007) compared the results of CO_2 adsorption experiments conducted at different laboratories on the Argonne premium coal. They reported considerable discrepancy in the results of CO_2 adsorption isotherms at high pressures (Goodman, 2007). Higher uncertainties on the measurement of adsorption isotherms data at high pressures have also been reported by Sakurovs et al. (2010).

Bae et al. (2009) studied the pore accessibility of coal to CO_2 and CH_4 and concluded that at high pressures, beyond the critical gas pressure, the pores are essentially all accessible, indicating that adsorbing molecules can enter and leave the restricted pore spaces at a given temperature within practical time scales.

2.4.6. Effects of sample type and confining pressure on sorption properties

Although experiments using powdered coal samples provide a quick indication of the gas sorption capacity, underground storage takes place within compact coal seam blocks with complex porosity system including cleats, and therefore, it is necessary to account for in situ conditions specifically confining stress, for meaningful estimates. Pone et al. (2009) studied the sorption capacities of CO_2 and methane for a bituminous coal sample in a whole sample under confining stress and in powder form. The results of CH_4 and CO_2 sorption capacity measured on coal plug were then compared to powdered samples under unconfined conditions and showed a reduction in sorption capacity by up to 91% for CH_4 and up to 69% for CO_2 (Pone et al., 2009).

Such observations emphasise that it is necessary to use coal samples confined at representative in situ confining stress for reliable evaluation of the sorption capacities and sorption rates.

2.4.7. Effects of coal matrix swelling/shrinkage on sorption properties

Coals exhibit shrinkage/swelling behaviour during the interaction with gas species, therefore, the uptake or release of CO_2 and CH_4 is a combination of adsorption/desorption process and matrix swelling (Mazzotti et al., 2009). Day et al. (2008) studied the swelling behaviour of a powdered coal sample due to the adsorption of various gases up to 16MPa pressure and suggested that there is a direct relationship between the maximum swelling in coal versus the absolute percentage of adsorbed gas. The results indicate a high swelling percentage for CO_2 in comparison with other gases (i.e., 5 %). He et al. (2010) also reported the maximum swelling of 1.37% due to the CO_2 adsorption on two different coals at different gas pressures ranging from subcritical to supercritical. He et al. (2010) reported a reversible trend for gas sorption so that the swelling behaviour of coal sample during adsorption and desorption should follow a similar trend. It has been shown that volumetric strain due to the adsorption of CO_2 or methane follows a Langmuir-type model (Harpalani and Mitra, 2010; Mazzotti et al.,

2009). In order to extract the reliable data on the absolute adsorption capacity of CO_2 in coals, the isotherm results of the excess gas adsorbed in the coal has to be corrected with the matrix swelling (Mazzotti et al., 2009).

2.5. Gas transport in coal

Gas transport in coal is a multi-physical process dealing with sorption, diffusion and macroscopic flow, and plays an important role in achieving effective gas storage and displacement in target coal seams. In the case where CO_2 is injected into the coal seam, these processes become more complex due to interaction between CO_2 and CH_4 in terms of competitive adsorption and counter-diffusion (Wei et al., 2007a). This section aims to provide a review on gas transport properties of coal and related experimental studies.

2.5.1. Coal permeability to gases

Coal contains two kinds of cleats or fractures including face cleat and butt cleat which are nearly orthogonal to each other and perpendicular to the bedding surfaces (Flore, 2014), as shown in Figure 2.13. The face cleat is laterally extensive and continuous throughout the seam. The butt cleat is in most cases discontinuous, ending at an intersection with the face cleat generally at a right angle. Because of their continuity, face cleats usually control the flow of fluids in rock system. The diffusion of gas from the coal matrix to face cleats is generally controlled by butt cleats (Flore, 2014).

Generally, there are two types of gas flow in coals. First one is the laminar flow through the cleat system which is pressure-driven and can be described using Darcy's law. The second type of flow is diffusion in the coal matrix which is assumed to be concentration-driven and is usually modeled using Fick's law (Busch and Gensterblum, 2011).

The key parameter that controls the fluid flow in coal is the permeability of the coal. Coal permeability to gases is related to many factors, such as the cleat and fracture systems (Harpalani and Chen, 1997; Olson et al., 2009); porosity, gas pressure and mechanical

stresses (Somerton et al., 1975; Palmer and Mansoori, 1998; Sasaki et al., 2004), fracture orientation (Laubach et al., 1998) and effect of matrix swelling/shrinkage induced by gas sorption.

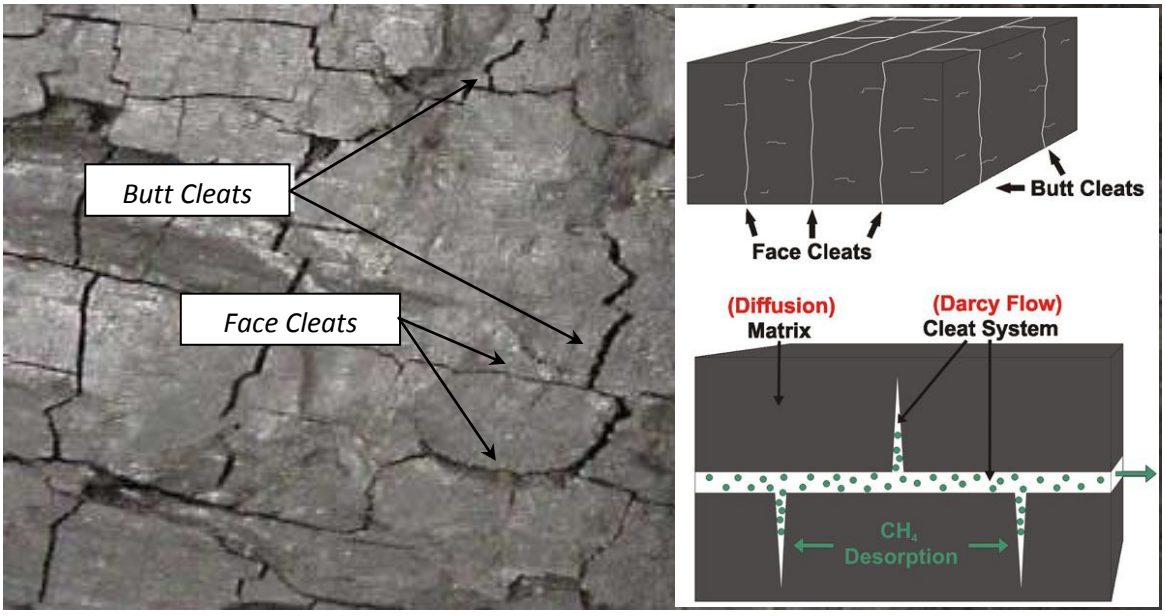

Fig. 2.13. Schematic diagram of cleats and fracture system in coal (adopted from ACRP Project, 2014 and KGS Energy Research Reports, 2006).

In general, the coal permeability decreases with increasing depth. A broad range of permeability values have been reported for coals. For instance, for the US coal seams, permeability of 5mD has been recorded at depths between 300-2500m depth (McKee et al., 1986). For the UK coals, however, permeability values reported in the literature are very limited. In general, the range of permeability values for the UK coals is reported to be low (Jones et al., 2004). Mazumder et al. (2006) have reported a permeability range of less than 0.1 to 3.5mD for the Selar Cornish semi-anthracite coal in South Wales. Durucan et al. (1995) reported 3mD coal permeability from Evergreen drilled well.

2.5.2. Effects of the effective stress on coal permeability

Coal permeability decreases with increase in the effective stress (Jasinge et al., 2011). An increase in effective stress causes pore space shrinkage, resulting in coal permeability

reduction for gas flow (Ranjith and Perera, 2011). The experimental results by Gawish and Al-Homadhi (2008) showed a decrease in the porosity and permeability with the increase in confining pressure. Jasinge et al. (2011) conducted a series of experimental tests and investigated the effects of effective stress on the permeability of coal.

A simplified relationship between the effective stress and permeability for coal has been presented by Sasaki et al. (2004):

$$\frac{k}{k_0} = exp(-\eta\sigma_{eff}) \tag{2-1}$$

where, k is the permeability of the coal (m^2), k_0 is the permeability of the coal at initial stress condition (m^2), σ_{eff} is the effective stress (MPa) and η is the stress attenuation coefficient (MPa^{-1}).

It should be mentioned that most of the experimental investigations related to the coal permeability variations with effective stress have been conducted under the non-zero strain conditions, i.e. the coal samples have been allowed to expand as a result of increase in gas pore pressure or decrease in effective stress. In in situ conditions, however, zero-strain conditions are expected (Harpalani and Mitra, 2010).

Harpalani and Mitra, (2010) conducted a series of experiments in which a core sample was injected by CO_2 under the uniaxial strain condition. The horizontal stress was adjusted to ensure zero strain, therefore no horizontal strain was allowed during CO_2 injection experiment. The horizontal stress was increased to achieve the desired zero horizontal strain condition expected under the in situ condition. However the excess stress required maintaining this condition was very large, resulting in sample failure. The results indicated that the excess stresses associated with injection of CO_2, i.e. as a result of CO_2 sorption-induced coal matrix swelling, are large. Therefore, the excess stresses generated might be sufficient to cause microfracturing and increased permeability and improved injectivity. Also, there might be a weakening effect resulting from repeated CO_2 injection, as has been found to be the case with thermal cycling of rocks (Harpalani and Mitra, 2010).

2.5.3. Effects of the gas adsorption/desorption on permeability

As stated previously, gas adsorption and desorption on coal matrix is an influential factor in coal permeability variations, i.e. by inducing swelling and shrinkage in coal matrix. Massarotto et al. (2007) observed permeability increases of between 100 to 1200% during CH_4 desorption, as compared to permeability decreases of 60 to 80% during CO_2 adsorption.

The coal matrix shrinkage from desorption of CH_4 can result in a permeability increase of an equal order of magnitude as the permeability loss from matrix swelling with CO_2 (Massarotto et al., 2010). According to Harpalani and Mitra (2010), CH_4 permeability reduction was approximately 25% of the original value, whereas the CO_2 permeability was found to be 40% less than the CH_4 permeability and 15% of the original value.

Coal exhibits shrinkage or swelling behaviour during the interaction with different gas species. Therefore, the uptake or release of CO_2 and CH_4 is a combination of adsorption or desorption processes as well as matrix swelling and shrinkage (Mazzotti et al., 2009). The amount of swelling depends on a variety of parameters, including the structure and properties of coal, gas composition, confining stress, pore pressure, temperature, fracture geometry and moisture content (Wang et al., 2013). In the microscopic level, the extension of the carbon-carbon bond (C-C) during the adsorption process is the dominant responsible mechanism for the swelling of coal matrix (Wang et al., 2010). The swelling of the coal matrix induced by CO_2 adsorption has been also attributed to the viscoelastic relaxation of strained, glassy/rubbery and highly cross-linked macromolecular structure of coal (Karacan, 2003; Larsen, 1988, 1995, 2004; Mazumder et al., 2006).

In general, there is a relationship between the coal swelling and amount of CO_2 adsorbed by the coal. At low pressures (below a few atmospheres), swelling is low and generally unaffected by the amount of gas adsorbed. However, at elevated pressures, swelling increases nearly linearly with the amount of CO_2 adsorbed (van Bergen et al., 2009). At pressures higher than 8MPa, the gas adsorption continues to increase but the coal matrix

volume remains constant, i.e. no coal matrix swelling occurs (Kelemen et al., 2006; Harpalani and Mitra, 2010; Gensterblum et al., 2010).

He et al. (2010) reported a maximum swelling of 1.37% due to the CO_2 adsorption on two different coals at different gas pressures ranging from subcritical to supercritical. Day et al. (2008) measured CO_2 and CH_4 induced swelling in three Australian coals at temperatures up to 55°C and gas pressures up to 15MPa. The results showed a maximum volumetric swelling of 1.7% - 1.9%, whereas, methane-induced coal swelling was found to be half of the CO_2 induced-swelling. Jasinge et al. (2011) observed a maximum volumetric swelling of 1.3% when a CO_2 pressure of 0.15MPa was applied on a low rank coal (with carbon content of 65.8%). They have also reported volumetric swellings of 0.60% and 0.36% for samples with a carbon content of 78.3% and 83.8%, respectively.

Harpalani and Mitra (2010) carried out a test to investigate the deformations of the coal sample caused by variations in effective stresses as well as deformations induced by gas sorption. The coal samples were first subjected to helium (He) injections. Since helium is a non-adsorptive gas, the volumetric strain measured during helium injections was purely related to the mechanical compression of the coal. The coal samples were then subjected to CO_2 and CH_4 injections and the effects of gas sorption induced deformations were evaluated (Harpalani and Mitra, 2010).

It has been shown that the volumetric strain of coal due to CO_2 or CH_4 adsorption follows a Langmuir-type model (Harpalani and Mitra, 2010; Mazzotti et al., 2009). In order to extract reliable data on the absolute adsorption capacity of CO_2 in coals, the isotherm results of the excess gas adsorbed in coal has been suggested to be corrected for the matrix swelling using a Langmuir-type model (Mazzotti et al., 2009).

2.6. Gas storage and displacement in coal

The majority of the experimental studies on gas storage and recovery in coal reported in the literature have been mostly focused on the aspect of enhanced coal bed methane

recovery or ECBM (e.g. van Hemert et al., 2012; Wang et al., 2010; Mazumder and Wolf, 2008). In this study, however, the focus has been mainly on the gas storage and displacement processes in coal and the methane recovery from coal has been considered as a by-product.

The experimental procedure for studying the gas storage and displacement/recovery processes in coal is relatively similar to the gas flow and permeability measurement method described in Section 2.3.2 (the steady-state method). The only difference is that for the case of gas storage and displacement experiment (ECBM), the coal sample is first saturated with CH_4 and then CO_2 or N_2 or a mixture of both gases is injected into the sample. The composition of the outflow gas is then monitored to evaluate the breakthrough time of the injected gas, displacement of gases and the rate of gas storage or recovery.

van Hemert et al. (2012) conducted a series of gas storage and recovery experiments (ECBM) on Nottinghamshire coal sample by injecting N_2, CO_2 and mixtures of N_2 and CO_2 at 8MPa gas pore pressure and under confining pressure of 12MPa and temperature of 318K. A summary of the experimental results reported by van Hemert et al. (2012) including the amount of N_2 or CO_2 injected and CH_4 production for each gas species is presented in Table 2.2.

Wang et al. (2010) carried out a series of gas storage and displacement experiments on high volatile bituminous coal samples from Bowen coal basin, Australia. The results of CO_2 storage and CH_4 recovery reported by Wang et al. (2010) are presented in Figure 2.14. Under a steady condition, the amount of the adsorbed CO_2 was reported to be two orders of magnitude higher as compared with the desorbed CH_4 from coal (Wang et al., 2010).

Connell et al. (2011) performed a gas displacement experiment with N_2 on a coal sample from Bowen basin, Australia at two gas injection pressures, i.e. 2MPa and 10MPa. The core samples were initially saturated with methane. Prior to the core flooding tests, a series of coal characterisation tests was performed on the core sample including the adsorption isotherms, swelling with gas adsorption, geomechanical properties and cleat

compressibility. This information was used in the history matching of the core floods to reduce the amount of unknown parameters (Connell et al., 2011).

Table 2.2. The results of N_2 and CO_2 storage and CH_4 recovery experiments conducted by van Hemert et al. (2012).

Injection gas	Initial CH_4 content (mol)	Produced CH_4 (mol)
N_2	0.793	0.70
N_2	-	0.67
N_2/CO_2	0.799	0.79
N_2/CO_2	0.806	0.76
N_2/CO_2	0.848	0.76
N_2/CO_2	0.897	0.80
CO_2	0.875	0.81
CO_2	1.055	0.98
N_2	1.316	0.81

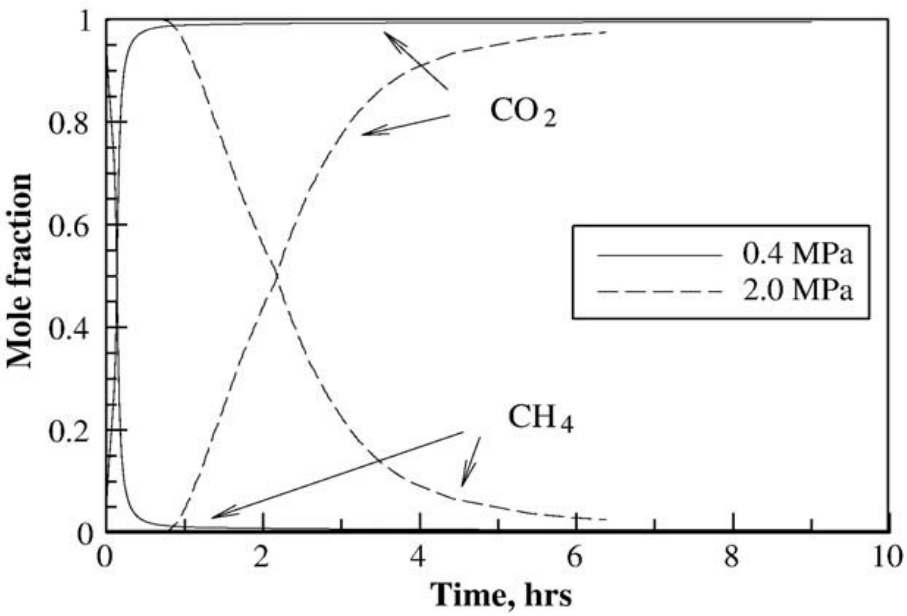

Fig. 2.14. Experimental results of gas storage and recovery test performed by Wang et al. (2010).

Mazumder and Wolf (2008) conducted a series of core flooding experiments on dry and wet coal samples from the Beringen coal mines in Belgium, the Silezia coalfield in Poland

and the Tupton coalfields in UK. The effect of moisture was evident from the low sweep efficiency (Mazumder and Wolf, 2008).

Jessen et al. (2008) used ground coal with a mean size of the coal particles of 0.25mm from a coalbed in the Powder River Basin, Wyoming. The coal particles were formed into a coalpack by pressing the ground coal into cylindrical shapes. CH_4, CO_2 and N_2 sorption isotherms, as well as porosity and permeability measurements were conducted before gas storage and displacement experiments. A series of gas storage and displacement experiments were conducted using N_2 or CO_2 to displace CH_4. In these experiments, the cleat structure was not preserved. Thus, such data were of limited value to characterise permeability behaviour and flow properties of the natural coal.

Yu et al. (2008) performed gas storage and displacement experiments on coal samples originated from the Jincheng and Luan mines, Qinshui basin, North China. First sample was saturated with CH_4. CO_2 injection at 4.5MPa was then carried out. Compared with the CH_4, the CO_2 fraction in outflow gas was reported to be very small and the initial CH_4 displacement with CO_2 was not associated with CO_2 release. With increase of replaced-CH_4 volume, the discharge capacity of CO_2 increased slowly. With CO_2 breakthrough, the fraction of CO_2 was reported to be increased slowly during CH_4 displacement.

Tsotsis et al. (2004) performed gas storage and displacement experiments to study the mechanisms involved in CO_2 sequestration for a highly volatile bituminous coal from Jamestown coal seam in Illinios. After degassing the coal sample using vacuum, the core was saturated with CH_4. Then, the CO_2 sequestration experiment was performed. As the CO_2 was injected into the core, the outflow rate was measured and its composition was continuously analysed. The result of this work can be found in Tsotsis et al. (2004).

From the review presented above, it can be observed that the emphasis in majority of the published works has been on the efficiency of the process in terms of CO_2 storage or methane recovery, whereas the gas displacement process and its effect on permeability evolution of the coal have received very little attention.

In addition, the number of experimental studies on gas storage and displacement in coal reported in the literature are still limited. Therefore, currently there is a lack of experimental data with high level of accuracy and resolution which can be used as validation exercises for the improvement and development of the numerical models.

2.7. Theoretical aspects and computational modelling studies

The common conceptual model applied to coal is the dual porosity model in which storage of gas is mostly considered in the coal matrix whilst Darcy's law is applied in its fracture system (Gan et al., 1972; Mazumder and Wolf, 2008; Shi and Durucan, 2005; Pan and Connel, 2012). The coal consists of a non-uniform porosity system including a dispersed fracture/cleat network and blocks of rock matrix. The transport process in cleat is mainly advection whilst diffusion is the dominant transport process in the matrix (Shi and Durucan, 2005). The three mechanisms identified for gas diffusion in coals are the molecular diffusion, the Knudsen diffusion and the surface diffusion (Shi and Durucan, 2005; Wei et al., 2007b). The diffusion mechanism in meso-pores and micro-pores (<2nm) are suggested to be similar to Knudson and surface diffusion respectively, whilst diffusion in the macropores is similar to the molecular diffusion process (Wei et al., 2007b). Figure 2.15 illustrates the concept of the dual porosity system in coal and the flow regimes.

During gas injection into the coal, the physical and chemical interactions between the gas and coal can change the stress conditions and subsequent deformation in coal can affect the transport and reaction processes via changes in the porosity and permeability. The major physical and chemical mechanisms responsible for this behaviour are reported as follows (Somerton et al., 1975; Reucroft and Patel, 1986):

i) Fracture width in coal or fracture porosity and permeability which can be influenced by changes in effective stress.

ii) Mechanical compression and expansion of the matrix blocks.

iii) Gas sorption-induced strain in the coal matrix.

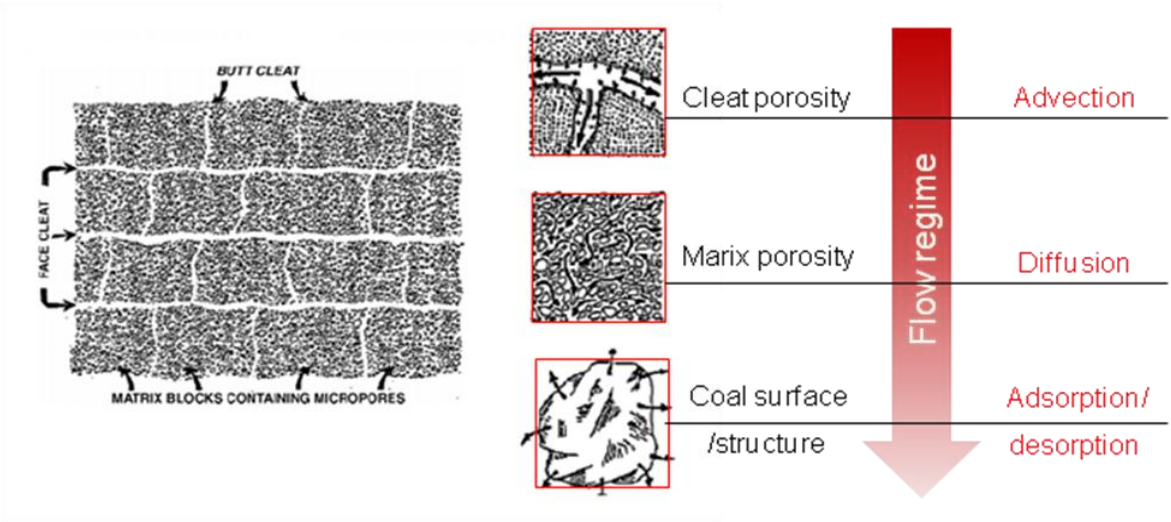

Figure 2.15. The dual porosity system and different flow regimes in coal (modified after Shi and Durucan, 2005).

A number of analytical models reported in the literature have considered the deformation of the coal by relating the physical and chemical mechanisms mentioned above with the porosity and permeability evolutions in coal (e.g. Palmer and Mansoori, 1998; Shi and Durucan, 2004; Cui and Bustin, 2005). A review of the deformation models can also be found in Palmer (2009) and Pan and Connell (2012). The majority of the deformation models have developed based on the field-scale conditions, i.e. with the assumption of uniaxial strain, which limits their application for the laboratory-scale conditions with hydrostatic confinement. More details related to modeling of coal permeability evolutions due to interaction with gases will be provided in Chapter 8.

As stated previously, the gas adsorption on coal is usually described by a Langmuir-type isotherm, indicating that the adsorption is dominated by micropore-filling process (Mazzotti et al., 2009) In many approaches adopted for the simulations of gas storage and displacement processes, Langmuir equation has been used as a simple method and has shown a good correlation with the experimental data (Busch and Gensterblum, 2011). Ozdemir et al., (2003) provided a review on methods for modeling the adsorption and desorption isotherms on coal. Various modeling approaches for adsorption/desorption isotherms have been also discussed by Fitzgerald et al. (2005) and Sakurovs et al. (2007).

Zou-Tang et al. (2009) presented a coupled flow and deformation numerical simulation for CO_2 sequestration with enhanced methane recovery in coal (CO_2-ECBM). The flow of gas (or supercritical fluid) was considered as purely advective reactive flow coupled with a non-linear elastic deformation. The hydraulic conductivity was linked to the effective stress using an exponential relationship. In addition, a Langmuir-style isotherm model has been incorporated in the flow equation (Zuo-tang et al., 2009).

Wu et al. (2010) presented a coupled flow and deformation model assuming the coal system as an elastic and dual-porosity medium. The flow of gas in matrix and fracture was assumed to be purely advective and with first order sink/source between matrix and fracture. The hydraulic conductivity in matrix and fracture was linked to the elastic strain-stress model which incorporates the effects of gas pressure variation in matrix and fracture as well as the sorption-induced swelling in the system (Wu et al., 2010).

Recently, more attempts have been made to advance the modelling processes in CBM/ECBM to quantify the complex coal-gas interactions. Shi and Durucan (2003) presented a model for competitive displacement of adsorbed CH_4 by CO_2 injection using a bi-disperse pore-diffusion model that accounts for both macro- and micro pore diffusion in the coal matrix. In this model, for each gas component in the cleats, macro/micropores, mass conservation law is applied along with binary gas mixture equilibrium isotherm equations. The flow regime in the cleat was considered purely as advection flow whilst an advective-diffusive flow was assumed in the macropore. An extended Langmuir equation for adsorption isotherm of multiple gases was incorporated in the formulation. The model was applied to analyse the performance of a laboratory core flooding experiment.

Zhu et al. (2007) provided a coupled gas flow and deformation model. In their approach, a linear elastic medium was assumed. However the coupling between the matrix shrinkage/swelling due to the chemical interactions was provided through a gas pressure dependant permeability coefficient. In this modelling approach the system was considered as dry system and the flow of water or liquid was not studied (Zhu et al., 2007).

Wei et al. (2007a, 2010) developed a numerical model in order to simulate the displacement of gases during gas injection into coal. A triple porosity gas reactive transport model was developed using mass conservation in micro-fracture, meso/macro porosity and micro porosity in the matrix. The dominant flow mechanism in the micro-fracture was assumed to be advection whilst the process of diffusion was considered in the case of the flow in meso/macro porosity (bulk diffusion and micro porosity). The adsorption induced swelling effects were considered using a stress dependant permeability and porosity in which the net stress is related to the variation in the chemical/gas concentrations. The model has been tested against a CO_2 displacement laboratory investigation in the University of Queensland, Australia (Wei et al., 2010; Wei et al., 2007a).

Jessen et al. (2008) presented a numerical simulation of a laboratory scale in which an injection test of CO_2 in coal has been reported. The model was based on the single phase advective flow of gas formulation in which the extended Langmuir adsorption isothermal for multi-gases is incorporated as the adsorption/desorption term. The model was validated against the experimental results of gas displacement of pure carbon dioxide (CO_2), nitrogen (N_2) and various mixtures in Powder River Basin coal samples (Jessen et al., 2008).

Shi et al. (2008a) also developed a numerical model describing a two-phase (i.e. gas and water) advective flow in the cleat. The extended Langmuir equation for multiple-gas systems was used in order to calculate the equilibrium adsorbed gas amount in the matrix which depends on the gas pressure in the cleat. The model was used for simulation of competitive displacement of CH_4 by injection of supercritical CO_2 based on laboratory scale simulation on a large diameter dry coal (Shi et al., 2008a).

A computational modelling work based on a numerical model of coupled thermal, hydraulic, chemical and mechanical behaviour of geomaterials (COMPASS, i.e. the **Co**de for **M**odelling **Pa**rtially **S**aturated **S**oils) has been developed by Thomas and co-workers at the Geoenvironmental Research Centre, Cardiff University (e.g. Thomas and He, 1998; Seetharam, 2003; Vardon, 2009; Sedighi; 2011; Masum, 2012). The model is based on a

mechanistic approach in which physical, chemical and mechanical processes are included in an additive manner with inter-related couplings being accommodated in the governing equations of the model. The main features of ground behaviour included in COMPASS are: i) the heat transfer via the mechanisms of conduction, convection and latent heat of vaporisation, ii) moisture transfer which includes water and vapour flow due to various driving potentials, iii) transfer of gas phase or air, iv) transport of multicomponent chemicals present in the liquid and gas phases, v) geochemical reactions including heterogeneous and homogenous reactions between/in solid, liquid and gas phases and vi) deformation behaviour which is based on stress-strain equilibrium, considering appropriate constitutive relationships describing the behaviour of soil or rock. The model has been extensively applied to study the coupled behaviour of unsaturated soils, in particular, the behaviour of highly compacted swelling clays in relation to geological disposal of high level radioactive waste (e.g. Thomas et al., 2003; Thomas and Sedighi, 2012).

Hosking (2014) further developed an existing coupled Thermal-Hydroulic-Chemical/gas-Mechanical formulation in COMPASS to include the processes of reactive gas flow in coal relevant to the application of carbon sequestration in coal and methane recovery. In the present study, the model developed by Hosking (2014) has been used for further assessment and insight into mechanisms involved in the processes of gas transport and reactions in coal. More details related to the theoretical formulation are provided in Chapter 8 and Appendix A of this thesis or can be found in Hosking (2014). The results of the numerical simulations are presented in Chapter 8.

2.8. Conclusions

A summary of the state-of-the-art apparatuses related to the experimental investigations of carbon sequestration in coal has been provided in this chapter. The experimental measurement methods for gas adsorption/desorption isotherms and gas transport in coal have been reviewed. The key factors and influential parameters on coal interactions with gases, gas transport in coal and gas storage and displacement processes in coal were

reviewed in details. Finally, studies on computational modelling relevant to carbon sequestration in coal were briefly reviewed.

The review on the experimental apparatuses showed that despite increasing number of developed experimental apparatuses in recent years, there is still lack of experimental apparatuses which are capable of producing a comprehensive set of data related to various aspects of coal-gas interactions, i.e. measurement of i) gas sorption properties of coals, ii) gas flow and permeability in coal and iii) swelling/shrinkage of coal matrix induced by gas adsorption/desorption.

From the literature review conducted in this study, it can be concluded that in the past, most of the experimental works related to gas adsorption/desorption in coals have reported the sorption capacities of coal to different gases at equilibrium conditions, whereas, the kinetics of the adsorption/desorption processes has received very little attention.

Although in recent years the number of experimental works conducted on gas flow and permeability measurements in coal has increased, there are some areas of research that have not been investigated experimentally. For instance, the fate of adsorbed CO_2 in coal and the swelling behaviour of coal due to desorption of CO_2 during gas flooding experiments are yet to be understood. Similarly, the experimental data related to gas storage and displacement processes in coal is very limited, especially on the aspects of coal permeability evolution due to interaction with gases. Production of such data is very important for better understanding and obtaining new insights into the mentioned processes as well as providing validation exercises for the development of numerical models.

Finally, the review of the literature related to reactive gas transport in coal suggests that little information exist bout coal from South Wales coalfield. Accordingly, further laboratory investigations including coal characterisation, gas adsorption/desorption isotherm measurements, core flooding experiments and gas flow and permeability measurements are of importance. More specifically, none of the experimental data

mentioned above is available for the coal from 6t-seam of South Wales coalfield from which the coal samples of this study have been provided.

2.9. References

ACRP Project, 2014. *Permeability: degree of fracturing. ACRP Project- C14015.* [Online]. Available at: http://eis.uow.edu.au/outburst/html/Factors/fracturing.html [Accessed: 1 April 2014].

API RP, 1998. *Recommended practices for core analysis*. *Recommended Practice 40*. American Petroleum Institute.

Azmi, A.S., Yusup, S. and Muhamad, S. 2006. The influence of temperature on adsorption capacity of Malaysian coal. *Chemical Engineering and Processing,* 45(5), pp. 392-396.

Bae, J.-S., Bhatia, S.K., Rudolph, V. and Massarotto, P. 2009. Pore accessibility of methane and carbon dioxide in coals. *Energy and Fuels*, 23(6), pp. 3319-3327.

Battistutta, E., van Hemert, P., Lutynski, M., Bruining, H. and Wolf, K.H. 2010. Swelling and sorption experiments on methane, nitrogen and carbon dioxide on dry Selar Cornish coal. *International Journal of Coal Geology,* 84(1), pp. 39-48.

Brace, W.F., Walsh, J.B. and Frangos, W.T. 1968. Permeability of granite under high pressure. *Journal of Geophysical Research*, 73(6), pp. 2225-2236.

Busch, A. and Gensterblum, Y. 2011. CBM and CO_2-ECBM related sorption processes in coal: A review. *International Journal of Coal Geology*, 87(2), pp. 49-71.

Busch, A., Gensterblum, Y. and Krooss B.M. 2003. Methane and CO_2 sorption and desorption measurements on dry Argonne premium coals: pure components and mixtures. *International Journal of Coal Geology*, 55(2-4), pp. 205-224.

Busch, A., Gensterblum, Y. and Krooss, B.M. 2007. High-pressure sorption of nitrogen, carbon dioxide, and their mixtures on argonne premium coals. *Energy and Fuels*, 21(3), pp.1640-1645.

Carles, P., Egermann, P., Lenormand, R. and Lombard, J. 2007. Low permeability measurements using steady-state and transient methods. *The International Symposium of the Society of Core Analysts,* Calgary, Canada. 10-14 September 2007.

Chen, Z., Pan, Z.J., Liu, J.S., Connell, L.D. and Elsworth, D. 2011. Effect of the effective stress coefficient and sorption-induced strain on the evolution of coal permeability: Experimental observations. *International Journal of Greenhouse Gas Control,* 5(5), pp. 1284-1293.

Connell, L.D., Sander, R., Pan, Z., Camilleri, M. and Heryanto, D. 2011. History matching of enhanced coal bed methane laboratory core flood tests. *International Journal of Coal Geology*, 87(2), 128-138.

Cui, X., Bustin, R.M. and Dipple, G. 2004. Selective transport of CO_2, CH_4 and N_2 in coals: insights from modeling of experimental gas adsorption data. *Fuel*, 83(3), pp. 293-303.

Cui, X. and Bustin, R.M. 2005. Volumetric strain associated with methane desorption and its impact on coalbed gas production from deep coal seams. *AAPG Bulletin*, 89(9), pp. 1181-1202.

De Silva, P.N.K. and Ranjith, P.G. 2012. Advanced core flooding apparatus to estimate permeability and storage dynamics of CO_2 in large coal specimens. *Fuel*, 104, pp. 417-425.

Day, S., Fry, R. and Sakurovs, R. 2008. Swelling of Australian coals in supercritical CO_2. *International Journal of Coal Geology*, 74(1), pp. 41-52.

Durucan, S., Ahsan, M. and Shi, J-Q. 2009. Matrix shrinkage and swelling characteristics of European coals. *Proceedings of the 9th International Conference on Greenhouse Gas Control Technologies (GHGT-9),* 16-20 November, 2008. Washington DC: Elsevier Science, pp. 3055-3062.

Durucan, S., Daltaban, T.S., Shi, J.Q. and Sinka, I.C. 1995. Coalbed methane well stimulation: the effect of structural and geotechnical parameters on connectivity in coal seams. *In: Planning for Profit Coalbed Methane in the UK and Europe Conference,*30-31 March, 1995.London, pp. 30-31.

Egermann, P., Lenormand, R., Longeron, D. and Zarcone, C. 2005. A fast and direct method of permeability measurements on drill cuttings. *SPE Reservoir Evaluation & Engineering*, 8(4), pp. 269-275.

Fitzgerald, J.E., Pan, Z., Sudibandriyo, M., Robinson, J.R.L., Gasem, K.A.M. and Reeves, S. 2005. Adsorption of methane, nitrogen, carbon dioxide and their mixtures on wet Tiffany coal. *Fuel*, 84(18), pp. 2351-2363.

Flores, R.M. 2014. *Coal and coalbed gas: fueling the future*. Waltham: Elsevier.

Fujii, T., Sato, Y., Lin, H., Inomata, H. and Hashida, T. 2009. Evaluation of CO_2 sorption capacity of rocks using a gravimetric method for CO_2 geological sequestration. *Energy Procedia*, 1(1), pp. 3723-3730.

Gan, H., Nandi, S.P. and Walker, Jr.P.L. 1972. Nature of the porosity in American coals. *Fuel,* 51(4), pp. 272-277.

Gawish, A. and Al-Homadhi, E. 2008. Relative permeability curves for high pressure. High Temperature Reservoir Conditions. *Oil and Gas Business* [Online]. Available at: http://www.ogbus.ru/eng/authors/Gawish/Gawish_1.pdf.

Gensterblum, Y., van Hemert, P., Billemont, P., Battistutta, E., Busch, A., Krooss, B.M., De Weireld, G. and Wolf, K.H.A.A. 2010. European inter-laboratory comparison of high pressure CO_2 sorption isotherms II: Natural coals. *International Journal of Coal Geology,* 84(2), pp. 115-124.

Gillies, A.D.S., Gray, I. and Ham, Y. 1995. Measurement of coal permeability using large samples. *Proceedings of International Symposium on Management and Control of High Gas Emissions and Outbursts in Underground Coal Mines*. Wollongong: March, 1995. Australia: Coal Assosation, pp. 317-321.

Goodman, A.L., Busch, A., Bustin, R.M., Chikatamarla, L., Day, S., Duffy, G.J., Fitzgerald, J.E., Gasem, K.A.M., Gensterblum, Y., Hartman, C., Jing, C., Krooss, B.M., Mohammed, S., Pratt, T., Robinson, Jr.R.L., Romanov, V., Sakurovs, R., Schroeder, K. and White, C.M. 2007. Inter-laboratory comparison II: CO_2 isotherms measured on moisture-equilibrated Argonne premium coals at 55°C and up to 15MPa. International Journal of Coal Geology, 72(3-4), pp. 153-164.

Gürdal, G. and Yalçın, M.N. 2001. Pore volumes and surface area of the Carboniferous coals from the Zonguldak basin (NW Turkey) and their variations with rank and maceral composition. *International Journal of Coal Geology,* 48(1), pp. 133-144.

Harpalani, S. and Chen, G. 1997. Influence of gas production induced volumetric strain on permeability of coal. *Geotechnical and Geological Engineering*, 15(4), pp. 303-25.

Harpalani, S. and Mitra, A. 2010. Impact of CO_2 injection on flow behavior of coalbed methane reservoirs. *Transport in Porous Media,* 82(1), pp.141-156.

He, J., Shi, Y., Ahn, S., Kang, J.W. and Lee, C. 2010. Adsorption and desorption of CO_2 on Korean coal under subcritical to supercritical conditions. *The Journal of Physical Chemistry*, 114(14), pp. 4854-4861.

Hol, S., Peach, C.J., Spiers, C.J., 2011. A new experimental method to determine the CO_2 sorption capacity of coal. *Energy Procedia*, 4(1), pp. 3125-3130.

Hosking, L. 2014. *Reactive transport modelling of high pressure gas flow in coal*. PhD Thesis. Cardiff University.

Hsieh, P.A., Tracy, J.V., Neuzil, C.E., Bredehoeft, J.D. and Silliman, S.E. 1981. A transient laboratory method for determining the hydraulic properties of 'tight' rocks - I. Theory. *International Journal of Rock Mechanics and Mining Sciences and Geomechanics Abstracts*, 18(3), pp. 245-252.

Huy, P.Q., Sasaki, K., Sugai, Y. and Ichikawa, S. 2010. Carbon dioxide gas permeability of coal core samples and estimation of fracture aperture width. *International Journal of Coal Geology,* 83(1), pp. 1-10.

Jasinge, D., Ranjith, P.G. and Choi, S.K. 2011. Effects of effective stress changes on permeability of latrobe valley brown coal. *Fuel* 90(3), pp. 1292-1300.

Jessen, K., Tang, G.Q. and Kovscek, A. 2008. Laboratory and simulation investigation of enhanced coalbed methane recovery by gas injection. *Transport in Porous Media,* 73(2), pp. 141-159.

Jones, N.S., Holloway, S., Smith, N.J.P., Browne, M.A.E., Creedy, D.P., Garner, K. and Duracan S. 2004. *UK coal resource for new exploitation technologies.* Department of Trade and Industry. Report No. Coal R271 DTI/Pub URN 04/1879.

Kamath, J., Boyer, R.E. and Nakagawa, F.M. 1992. Characterisation of core-scale heterogeneities using laboratory pressure transients, *SPE Formation Evaluation*, 7(3), pp. 219-227.

Karacan, C.O. 2003. Heterogeneous sorption and swelling in a confined and stressed coal during CO_2 injection. *Energy and Fuels*, 17(6), pp. 1595-1608.

Kelemen, S.R., Kwiatek, L.M. and Lee, A.G.K. 2006. Swelling and sorption response of selected Argonne premium bituminous coals to CO_2, CH_4, and N_2. *In Proceedings of International CBM Symposium*. Tuscaloosa, Alabama.

Kenyon, W.E. 1989. A three-part study of NMR longitudinal relaxation properties of water saturated sandstones. *SPE Formation Evaluation*, 3(3), pp. 622-636.

KGS Energy Research Reports, 2006. *Integrated subsurface carbon sequestration and enhanced coalbed natural gas recovery using cement kiln emissions, Wilson County, Kansas.* [Online]. Available at: http://www.kgs.ku.edu/PRS/publication/2006/2006-13/p2-03.html [Accessed: 15 May 2014].

Kim, A.G. 1977. *Estimating methane content of bituminous coalbeds from adsorption data*. *Report No. RI 8245*. Washangton: U.S. Department of Interior, Bureau of Mines.

Kim, H.J., Shi, Y., He, J., Lee, H.H. and Lee, C.H. 2011. Adsorption characteristics of CO_2 and CH_4 on dry and wet coal from subcritical to supercritical conditions. *Chemical Engineering Journal*, 171(1), pp. 45-53.

Kiyama, T., Nishimoto, S., Fujioka, M., Xue, Z., Ishijima, Y., Pan, Z. and Connell, L.D. 2011. Coal swelling strain and permeability change with injecting liquid/supercritical CO_2 and N_2 at stress-constrained conditions. *International Journal of Coal Geology*, 85(1), pp. 56-64.

Krooss, B.M., van Bergen, F., Gensterblum, Y., Siemons, N., Pagnier, H.J.M. and David, P. 2002. High-pressure methane and carbon dioxide adsorption on dry and moisture equilibrated Pennsylvanian coals. *International Journal of Coal Geology*, 51(2), pp. 69-92.

Larsen, J.W. 2004. The effects of dissolved CO_2 on coal structure and properties. *International Journal of Coal Geology*, 57(1), pp. 63-70.

Larsen, J.W., Hall, P. and Wernett, P.C. 1995. Pore structure of Argonne Premium coals. *Energy and Fuel*, 9(2), pp. 324-330.

Larsen, J.W. and Wernett, P. 1988. Pore structure of Illinois No. 6 coal. *Energy and Fuel*, 2(5), pp. 719-720.

Laubach, S.E., Marrett, R.A., Olson, J.E. and Scott, A.R. 1998. Characteristics and origins of coal cleat: A review. *International Journal of Coal Geology*, 35, pp. 175-207.

Laxminarayana, C. and Crosdale, P.J. 1999. Role of coal type and rank on methane sorption characteristics of Bowen Basin, Australia coals. *International Journal of Coal Geology*, 40(4), pp. 309-325.

Levy, J.H., Day, S.J. and Killingley, J.S. 1997. Methane capacities of Bowen Basin coals related to coal properties. *Fuel*, 76(9), pp. 813-819.

Li, D., Liu, Q., Weniger, P., Gensterblum, Y., Busch, A. and Krooss, B.M. 2010. High-pressure sorption isotherms and sorption kinetics of CH_4 and CO_2 on coals. *Fuel*, 89(3), pp. 569-580.

Li, J., Liu, D., Yao, Y., Cai, Y. and Chen, Y. 2013. Evaluation and modeling of gas permeability changes in anthracite coals. *Fuel*, 111(1), pp. 606-612.

Lin, W. 2010. *Gas sorption and the consequent volumetric and and permeability change coal*. PhD Thesis, Stanford University.

Luffel, D.L., Hopkins, C.W. and Shettler, P.D. 1993. Matrix permeability measurements of gas productive shales. *SPE 26633, In Proceedings of the 68th Annual Technical Conference and Exhibition of the SPE,* Houston.

Majewska, Z., Majewski, S. and Ziętek, J. 2010. Swelling of coal induced by cyclic sorption/desorption of gas: experimental observations indicating changes in coal structure due to sorption of CO_2 and CH_4. *International Journal of Coal Geology*, 83(4), pp. 475-483.

Massarotto, P., Golding, S.D., Bae, J.S., Iyer, R. and Rudolph, V. 2010. Changes in reservoir properties from injection of supercritical CO_2 into coal seams- A laboratory study. *International Journal of Coal Geology*, 82(3-4), pp. 269-279.

Massarotto, P., Golding, S.D., Iyer, R., Bae, J.S. and Rudolph, V. 2007. Adsorption, porosity and permeability effects of CO_2 geosequestration in Permian coals. *In: International Coalbed Methane Symposium. Alabama, USA*. CD ROM Paper 0727.

Masum, S. 2012. Modelling of reactive gas transport in unsaturated soil – a coupled thermo-hydro-chemical-mechanical approach. PhD Thesis, Cardiff University.

Mazumder, S., Karnik, A. and Wolf, K.H. 2006. Swelling of coal in response to CO_2 sequestration for ECBM and its effect on fracture permeability. *SPE Journal*, 11(3), pp. 390-398.

Mazumder, S. and Wolf, K. 2008. Differential swelling and permability change of coal in response to CO_2 injection for ECBM. *International Journal of Coal Geology*, 74(2), pp. 123-138.

Mazzotti, M., Pini R., and Storti G., 2009. Enhanced coalbed methane recovery. *The Journal of Supercritical Fluids*, 47(3), pp. 619-627.

McKee, C.R., Bumb, A.C., Way, S.C., Koenig, R.A., Reverand, J.M. and Brandenburg, C.F. 1986. Using permeability vs depth correlations to assess the potential for producing gas from coal seams. *Methane from Coal Seams Technology*, 9(7), pp. 415-426.

Milewska-Duda, J., Duda, J., Nodzenski, A. and Lakatos, J. 2000. Absorption and adsorption of methane and carbon dioxide in hard coal and active carbon. *Langmuir*, 16(12), pp. 5458-5466.

Mohammad, S., Fitzgerald, J.E., Robinson, J.R.L. and Gasem, K.A.M. 2009. Experimental uncertainties in volumetric methods for measuring equilibrium adsorption. *Energy and Fuel,* 23(1), pp. 2810-2820.

Narkiewicz, M.R. and Mathews, J.P. 2009. Visual representation of carbon dioxide adsorption in a low-volatile bituminous coal molecular model. *Energy and Fuels*, 23(1), pp. 5236-5246.

Nelsen, F.M. and Eggertsen, F.T. 1958. *Improvements in or relating to method and apparatus for the estimation of surface areas of solids*. British Patent 831639,30.4.

Olson, J.E., Laubach, S.E. and Lander, R.H. 2009. Natural fracture characterization in tight gas sandstones: integrating mechanics and diagenesis. *AAPG Bulletin*, 93 (11), pp. 1535-1549.

Ottiger, S., Pini, R., Storti, G. and Mazzotti, M. 2008. Competitive adsorption equilibria of CO_2 and CH_4 on a dry coal. *Adsorption*, 14(4-5), pp. 539-556.

Ozdemir, E. 2004. *Chemistry of the adsorption of carbondioxide by Argonne Premium coals and a model to simulate CO_2 sequestration in coal seams*. PhD Thesis. University of Pittsburgh.

Ozdemir, E. and Schroeder, K. 2009. Effect of moisture on adsorption isotherms and adsorption capacities of CO_2 on coals. *Energy and Fuels*, 23(1), pp. 2821-2831.

Ozdemir, E., Morsi, B.I. and Schroeder, K. 2003. Importance of volume effects to adsorption isotherms of carbon dioxide on coals. *Langmuir*, 19(23), pp. 9764-9773.

Ozdemir, E. Morsi, B.I. and Schroeder, K. 2004. CO_2 adsorption capacity of argonne premium coals. *Fuel,* 83(7-8), pp. 1085-1094.

Palmer, I. 2009. Permeability changes in coal: Analytical modeling. *International Journal of Coal Geology*, 77(1-2), pp. 119-126.

Palmer, I. and Mansoori, J. 1998. How permeability depends on stress and pore pressure in coal beds- a new model. *SPE Reservoir Evaluation and Engineering*, 1 (6), pp.539-544.

Pan, Z. and Connell, L.D. 2012. Modelling permeability for coal reservoirs: A review of analytical models and testing data. *International Journal of Coal Geology*, 92(1), pp. 1-44.

Pan, Z., Connell, L.D. and Camilleri, M. 2010a. Laboratory characterisation of coal reservoir permeability for primary and enhanced coalbed methane recovery. *International Journal of Coal Geology,* 82(3-4), pp. 252-261.

Pan, Z., Connell, L.D., Camilleri, M. and Connelly, L. 2010b. Effects of matrix moisture on gas diffusion and flow in coal. *Fuel*, 89(11), pp. 3207-3217.

Perera, M.S.A, Ranjith, P.G, Choi, S.K. and Airey, D. 2011. The effects of sub-critical and super-critical carbon dioxide adsorption-induced coal matrix swelling on the permeability of naturally fractured black coal. *Energy*, 36(11), pp.6442-6450.

Pone, J.D.N., Halleck, P.M. and Mathews, J.P. 2009. Sorption capacity and sorption kinetic measurements of CO_2 and CH_4 in confined and unconfined bituminous coal. *Energy and Fuels*, 23(9), pp. 4688-4695.

Ranjith, P.G. and Perera, M.S.A. 2011. A new triaxial apparatus to study the mechanical and fluid flow aspects of carbon dioxide sequestration in geological formations. *Fuel*, 90(8), pp. 2751-2759.

Reucroft, P.J. and Patel, H. 1986. Gas-induced swelling in coal. *Fuel*, 65(6), pp. 816-820.

Robertson, E.P. and Christiansen, R.L. 2007. Modeling laboratory permeability in coal using sorption-induced-strain data. *SPE Reservoir Evaluation and Engineering*, 6(3), pp. 260-269.

Sakurovs, R., Day, S. and Weir, S. 2010. Relationships between the critical properties of gases and their high pressure sorption behavior on coals. *Energy and Fuels*, 24(1), pp. 1781-1787.

Sakurovs, R., Day, S., Weir, S. and Duffy, G. 2007. Application of a modified Dubinin-Radushkevich equation to adsorption of gases by coals under supercritical conditions. *Energy and Fuels*, 21(2), pp. 992-997.

Sasaki, K., Fujii, K., Yamaguchi, S., Ohga, K., Hattori, K. and Kishi, Y. 2004. CO_2 gas permeability and adsorption of coal samples in consideration of CO_2 sequestration into coal seams. *Journal of the Mining and Materials Processing Institute of Japan*, 120 (8), pp. 461-468.

Schroeder, K., Ozdemir, E. and Morsi, B.I. 2002. Sequestration of carbon dioxide in coal seams. *Journal of Energy and Environmental Research,* 2(1), pp. 54-63.

Sedighi, M. 2011. *An investigation of hydro-geochemical processes in coupled thermal, hydraulic, chemical and mechanical behaviour of unsaturated soils*. PhD Thesis, Cardiff University.

Seetharam, S.C. 2003. An investigation of the thermro/hydro/chemical/mechanical behaviour of unsaturated soils. PhD Thesis, Cardiff University.

Shen, J., Qin Y., Wang G.X., Fu X., Wei C. and Lei B. 2011. Relative permeabilities of gas and water for different rank coals. *International Journal of Coal Geology*, 86(2-3), pp. 266-275.

Shi, J.Q. and Durucan, S. 2003. A bidisperse pore diffusion model for methane displacement desorption in coal by CO_2 injection. *Fuel,* 82(10), pp. 1219-1229.

Shi, J-Q. and Durucan, S. 2004. Drawdown induced changes in permeability of coalbeds: A new interpretation of the reservoir response to primary recovery. *Transport in Porous Media*, 56(1), pp. 1-16.

Shi, J.Q. and Durucan, S. 2005. CO_2 storage in deep unminable coal seams. *Oil & Gas Science and Technology-Rev.IFP,* 60(3), pp. 547-558.

Shi, J.Q., Durucan, S. and Fujioka, M. 2008a. A reservoir simulation study of CO_2 injection and N_2 flooding at the Ishikari coalfield CO_2 storage pilot project, Japan. *International Journal of Greenhouse Gas Control,* 2(1), pp. 47-57.

Shi, J., Mazumder, S., Wolf, K. and Durucan, S. 2008b. Competitive methane desorption by supercritical CO_2 injection in coal. *Transport in Porous Media*, 75(1), pp. 35-54.

Shukla, R., Ranjith, P., Choi, S. and Haque, A. 2012. A novel testing apparatus for hydromechanical investigation of rocks: Geo-sequestration of carbon dioxide. *Rock Mechanics and Rock Engineering*, 45(6), pp. 1-13.

Siemons, N. and Busch, A. 2007. Measurement and interpretation of supercritical CO_2 sorption on various coals. *International Journal of Coal Geology*, 69(4), pp. 229-242.

Sircar, S. 1999. Gibbsian surface excess for gas adsorptions revisited. *Industrial and Engineering Chemistry Research*, 38(10), pp. 3670-3682.

Somerton, W.H., Soylemezoglu, I.M. and Dudley, R.C. 1975. Effect of stress on permeability of coal. *International Journal of Rock Mechanics and Mining Science and Geomechanics Abstracts,* 12(1), pp. 129-145.

Sudibandriyo, M. 2004. Measurement of methane, nitrogen and carbon dioxide adsorption on wet selected coals. *Proceedings of Seminar Nasional Teknologi Proses Kimia VI.* Jakarta, March 31, 2004, pp. 1-9.

Swanson, B.F. 1981. A simple correlation between permeability and mercury capillary pressures. *Journal of Petroleum Technology*, 33(12), pp. 2498-2504.

Tarantino, A., Romero, E. and Cui, Y.J. eds. 2009. *Laboratory and field testing of unsaturated soils.* Reprinted from Geotechnical and Geological Engineering, Springer.

Thomas, H.R. and He, Y. 1998. Modelling the behaviour of unsaturated soil using an elasto-plastic constitutive relationship. *Géotechnique,* 48(5), pp. 589-603.

Thomas, H.R., Cleall, P.J., Chandler, N., Dixon, D. and Mitchell, H.P. 2003. Water infiltration into a large-scale in-situ experiment in an underground research laboratory. *Géotechnique*, 53(2), pp. 207-224.

Thomas, H.R. and Sedighi, M. 2012. *Modelling the engineering behaviour of highly swelling clays.* Keynote Paper in Proceeding of the 4th International Conference on Problematic Soils. pp. 21-33.

Thomas, L. 2002. *Coal geology*. Dargo Associates Ltd: Wiley Publishing.

Thomeer, J.H.M. 1983. Air permeability as a function of three pore network parameters. *Journal of Petroleum Technology*, 35(4), pp. 809-814.

Timur, A. 1968. An investigation of permeability, porosity and residual water saturation relationships. *The Log Analyst*, 9(4), pp. 8-17.

Tsotsis, T.T., Patel, H., Najafi, B.F., Racherla, D., Knackstedt, M.A. and Sahimi, M. 2004. Overview of laboratory and modelling studies of carbon dioxide sequestration in coalbeds. *Industrial and Engineering Chemistry Research*, 43(12), pp. 2887-2901.

van Bergen, F., Spiers, C., Floor, G. and Bots, P. 2009. Strain development in unconfined coals exposed to CO_2, CH_4 and Ar: Effect of moisture. *International Journal of Coal Geology,* 77(1-2), pp. 43-53.

van Hemert, P., Bruining, H., Rudolph, E.S.J, Wlof, K.A.A. and Mass, J.G. 2009. Improved manometric setup for the accurate determination of supercritical carbon dioxide sorption. *Reviw of Scientific Instrumments*, 80(3), 035103.

van Hemert, P., Wolf, K.A.A. and Rudolph, E.S.J. 2012. Output gas stream composition from methane saturated coal during injection of nitrogen, carbon dioxide, a nitrogen-carbon dioxide mixture and a hydrogen-carbon dioxide mixture. *International Journal of Coal Geology,* 89, pp. 108-113.

Vardon, P.J. 2009. A three-dimensional numerical investigation of the thermo-hydromechanical behaviour of a large-scale prototype repository. PhD Thesis, Cardiff University.

Viete, D.R. and Ranjith, P.G. 2006. The effect of CO_2 on the geomechanical and permeability behaviour of brown coal: implications for coal seam CO_2 sequestration. *International Journal of Coal Geology*, 66(3), pp. 204-216.

Vishal, V., Ranjith, P.G. and Singh, T.N. 2013. CO_2 permeability of Indian bituminous coals: Implications for carbon sequestration. *International Journal of Coal Geology,* 105, pp. 36-47.

Wakao, N., Kaguei, S. and Smith, J.M. 1980. Adsorption chromatography measurements. Parameter Determination. *Industrial and Engineering Chemistry Fundamentals Journal,* 19(4), pp. 363-367.

Wang, F., Zhu, Z., Massarotto, P. and Rudolph, V. 2007. Mass transfer in coal seams for CO_2 sequestration. *AIChE Journal*, 53(4), pp. 1028-1049.

Wang, G.X., Wei, X.R., Wang, K., Massarotto, P. and Rudolph, V. 2010. Sorption-induced swelling/shrinkage and permeability of coal under stressed adsorption/desorption conditions. *International Journal of Coal Geology*, 83(1), pp. 46-54.

Wang, G.G.X., Zhang, X., Wei, X., Fu, X., Jiang, B. and Qin, Y. 2011. A review on transport of coal seam gas and its impact on coalbed methane recovery. *Frontiers of Chemical Science and Engineering,* 5(2), pp. 139-161.

Wang, S., Elsworth, D. and Liu, J. 2013. Permeability evolution during progressive deformation of intact coal and implications for instability in underground coal seams. *International Journal of Rock Mechanics and Mining Sciences,* 58(1), pp. 34-45.

Wei, X., Massarotto, P., Wang, G., Rudolph, V. and Golding, S.D. 2010. CO_2 sequestration in coals and enhanced coalbed methane recovery: New numerical approach. *Fuel*, 89(5), pp. 1110-1118.

Wei, X.R., Wang, G.X., Massarotto, P., Golding, S.D. and Rudolph, V. 2007a. Numerical simulation of multicomponent gas diffusion and flow in coals for CO_2 enhanced coalbed methane recovery. *Chemical Engineering Science*, 62(16), pp. 4193-4203.

Wei, X.R., Wang, G.X., Massarotto, P., Golding, S.D. and Rudolph, V. 2007b. A review on recent advances in the numerical simulation for coalbed-methane-recovery process. *SPE Reservoir Evaluation & Engineering,* 10(6), pp. 657-666.

Weniger, P., Kalkreuth, W., Busch, A., Krooss, B.M. 2010. High-pressure methane and carbon dioxide sorption on coal and shale samples from the Paraná Basin, Brazil. International Journal of Coal Geology, 84(3-4), pp. 190-205.

White, C.M., Smith, D.H., Jones, K.L., Goodman, A.L., Jikich, S.A., LaCount, R.B., DuBose, S.B., Ozdemir, E., Morsi, B.I. and Schroeder, K.T. 2005. Sequestration of carbon dioxide in coal with enhanced coalbed methane recovery- A review. *Energy and Fuel*, 19(3), p. 659-724.

Wu, Y., Liu, J., Elsworth, D., Chen, Z., Connell, L. and Pan, Z. 2010. Dual poroelastic response of a coal seam to CO2 injection. *International Journal of Greenhouse Gas Control*, 4(4), pp. 668-678.

Yu, H., Zhou, L., Guo, W., Cheng, J. and Hu, Q. 2008. Predictions of the adsorption equilibrium of methane/carbon dioxide binary gas on coals using Langmuir and ideal adsorbed solution theory under feed gas conditions. *International Journal of Coal Geology*, 73(2), pp. 115-129.

Zhang, D.F., Cui, Y.J., Liu, B., Li, S.G., Song, W.L. and Lin, W.G. 2011. Supercritical pure methane and CO_2 adsorption on various rank coals of China: experiments and modeling. *Energy and Fuel*, 25(1), pp. 1891-1899.

Zhu, W.C., Liu, J., Sheng, J.C. and Elsworth, D. 2007. Analysis of coupled gas flow and deformation process with desorption and Klinkenberg effects in coal seams. *International Journal of Rock Mechanics and Mining Sciences,* 44(7), pp. 971-980.

Zuo-tang, W., Guo-xiong, W., Rudolph, V., Diniz da Costa, J.C., Pei-ming, H. and Lin, X. 2009. Simulation of CO_2-geosequestration enhanced coal bed methane recovery with a deformation-flow coupled model. *Procedia Earth and Planetary Science*, 1(1), pp. 81-89.

Chapter 3

Apparatus Design, Construction and Commissioning

3.1. Introduction

This chapter describes the design considerations related to the experimental facility which has been constructed and commissioned as part of this study. As stated in Chapter 1, the experimental set up has been primarily designed to study the coal-gas interactions and flow behaviour of gases in coal. The laboratory facility developed includes three main analysing units: i) a manometric sorption apparatus, ii) a triaxial core flooding system and iii) ancillary system such as the gas supply unit and the gas analysing unit.

The principal objective of this chapter is to present the detailed design considerations that have been incorporated to evaluate the specification required for selecting the essential measuring instruments such as the pressure transducers and flow meters.

In Section 3.2, the design considerations for the manometric sorption apparatus are discussed. The design specifications related to 1) appropriate pressure transducers capable of reading gas pressure variations during the experiments with reasonable accuracy, 2) a manometric apparatus capable of providing high equilibrium pressures are discussed. A number of scenarios have been defined to evaluate the mentioned considerations. For each scenario, the range of gas pressure variations during the gas adsorption process has been predicted using back-calculation analysis. The excess and absolute adsorption isotherms are also predicted for the conditions given in each scenario. The outcome is then considered as a guideline to finalise the specifications of the manometric sorption apparatus.

Section 3.3 presents the design considerations for the triaxial core flooding system. For this system, the focus was to adopt an appropriate gas flow meter capable of reading the lowest and the highest gas flow rates that may occur during the core flooding experiments. A number of example scenarios have been defined with regards to a range of sample sizes, sample permeabilities and gas injection pressures. The gas flow rates are estimated for each scenario. The results have been used to specify the range of flow meters required for the system.

The detailed specifications of the apparatuses constructed and commissioned for the main analysing units and ancillary system are provided in Section 3.4.

Finally, an overview of the developed experimental facilities and the specific features are provided as conclusions in Section 3.5.

3.2. The manometric sorption apparatus

3.2.1. Design considerations

The principle of manometric measurement technique has been described in Chapter 2. In a manometric adsorption/desorption test, the gas pressure and temperature are key variables that are measured. The gas volume is then calculated knowing the gas pressure and temperature in accordance with ideal gas low (Condon, 2006). A water bath or oven is commonly used to control the temperature of the entire system in a manometric apparatus. Therefore, the temperature of the system can be easily measured and controlled during the test. The measurement of gas pressure, however, is more complicated. Various types of pressure transducers are commercially available depending on the application case. Therefore, the first consideration here was to select an appropriate pressure transducer.

With regards to the application of the manometric apparatus, several factors have been considered in the selection of a suitable pressure transducer, including:

- The range of gas pressures within the system, i.e. the lowest and highest pressure readings.

- The pressure resolution which can be defined as the ability of the transducer to record the smallest pressure variations in the system.

The maximum gas pressure of 20MPa was found to be sufficiently high with respect to the application considered for this study, i.e. gas transport and reactions in deep geological formations (coal seams) with the depths up to 2000m. Therefore, the range of

gas pressure to be provided in the adsorption cell was defined to be between 1 and 20MPa.

The pressure resolution is a key factor for accurate recording the smallest pressure variations within the system as a result of gas sorption on sample. This can be calculated based on the ratio of the smallest pressure variation to the pressure range. The pressure range is the pressure values over which a transducer is intended to measure, specified by their upper and lower limits. The pressure transducers with higher resolution can minimise the measurement errors and enhance the overall accuracy of the measured adsorption/desorption isotherms. The resolution of the pressure transducer is highly influenced by its pressure range. In general, the pressure transducers with broader pressure range have lower pressure resolution. This, in turn, can increase the level of the uncertainties and errors that may arise during the measurements. On the other hand, high-resolution transducers can be relatively expensive and may impose unnecessary cost. Therefore, the major concern here was to adopt a cost effective pressure transducer with an optimum pressure resolution and capable of recording a broad range of gas pressures.

Another consideration was to design a manometric apparatus which is capable of producing accurate and reliable experimental data for a broad range of gas pressures. Since, the adsorption/desorption isotherms are usually presented based on a range of gas equilibrium pressures, it was important to design a manometric apparatus which is capable of providing high pressure equilibrium conditions. The parameters that directly control the range of equilibrium pressure in a manometric apparatus were identified as (Gensterblum et al., 2010; Mohammad et al., 2009):

- The ratio of the sample cell to the reference cell (V_{SC}/V_{RC}).
- The void volume in the sample cell (V_v), i.e. the volume of the sample cell unoccupied by the solid particles of the sample.

In general, a smaller ratio of the sample cell to the reference cell and smaller void volume in the sample cell can lead to higher equilibrium pressure (Gensterblum et al., 2010).

However, the manometric measurement of sorption isotherms at high pressures can impose some uncertainties regarding the amount of the adsorbed or desorbed gas (Gensterblum et al., 2010; Mohammad et al., 2009). In addition, a large V_{SC}/V_{RC} (between 1 and 10) may result in lower errors (Gensterblum et al., 2010). However, the latter may also lead to a much lower pressure equilibrium which is not favored. Therefore, one of the critical factors in minimising the uncertainties mentioned above is to optimise the ratio of the sample cell to the reference cell and to minimise the void volume in the sample cell.

Once the design considerations were identified, the influential parameters such as the ratio of the sample cell to the reference cell, and size of the void volume in the sample cell were evaluated via a number of example scenarios. Details of the example scenarios and the defined conditions for each scenario are presented in the following section.

3.2.2. Scenarios and analysis conditions

A number of scenarios were developed to evaluate the design considerations discussed above. The influential parameters mentioned in previous section were used to define the conditions of the scenarios, as follows:

1) The scenarios were categorised based on the ratio of the sample cell to the reference cell, i.e. V_{SC}/V_{RC} was assumed to be 0.5, 1.0 and 2.0.
2) Each scenario was then divided into two subdivisions. For subdivision (a), the sample cell was assumed to be packed with a powder sample resulting in a very small void volume left, i.e. $V_v/V_{SC}<0.1$. In the case of subdivision (b), the sample cell was partially filled with the sample resulting in a large void volume remained in the cell, i.e. $V_v/V_{SC}>0.5$.

Figure 3.1 shows a schematic diagram of the example scenarios defined for evaluating the design considerations. In order to estimate the gas pressure variations during gas adsorption process and to predict the results of gas adsorption isotherms, a series of

back-calculation analyses were carried out. In order to consider the effect of temperature on gas pressure variations, the analysis of each scenario was repeated for a range of temperature, i.e. 313K and 328K. The methodology used in the analysis of the example scenarios is described in the following section.

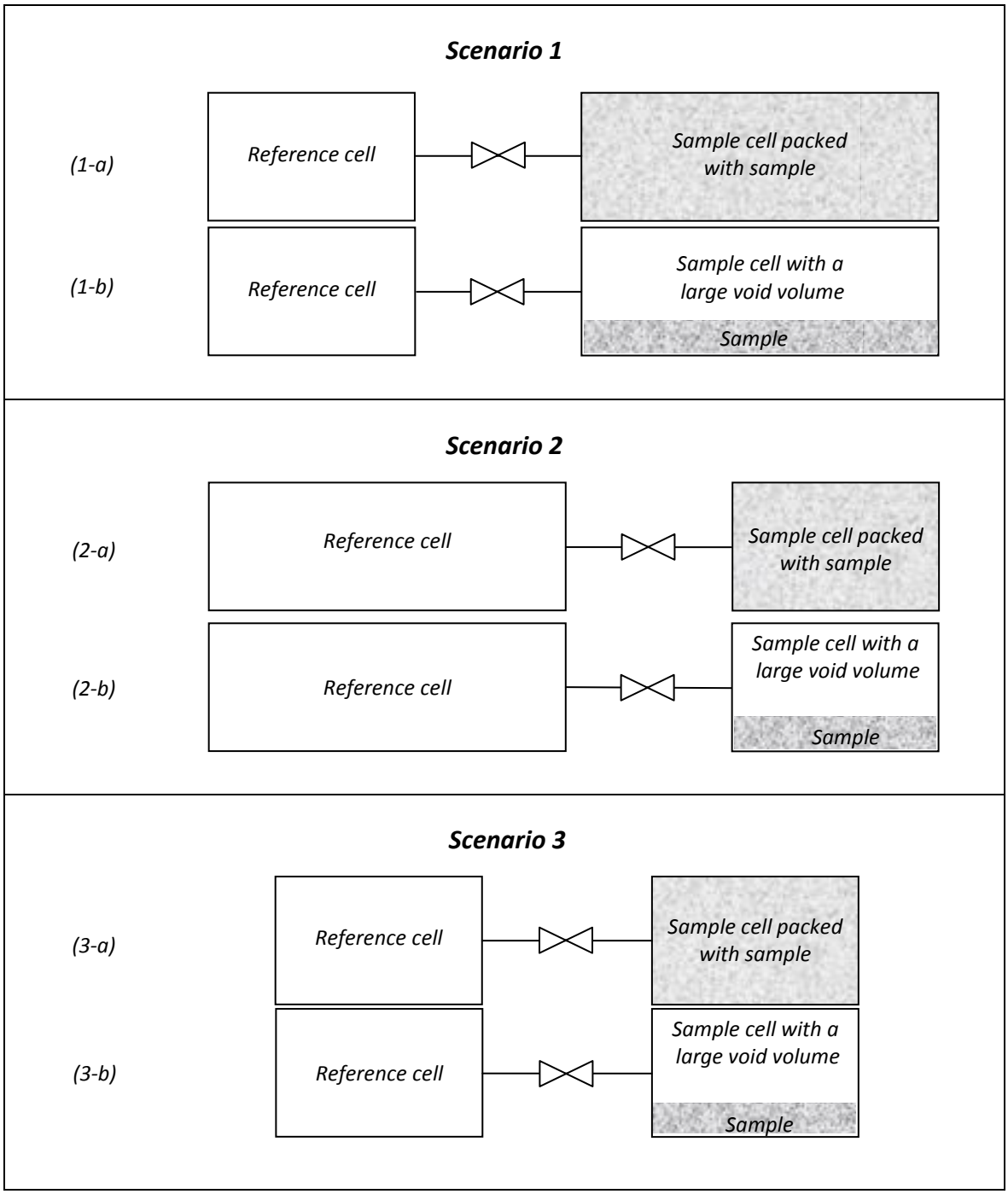

Fig. 3.1. Schematic diagram of the defined conditions for scenarios 1, 2 and 3.

3.2.3. Estimations of the gas pressure variations

As stated in Chapter 2, the calculation of the amount of gas adsorbed/desorbed in the manometric system is calculated based on the variations of gas pressure at constant temperature measured in the reference cell and sample cell. The mass conservation law dictates that the amount of the gas (moles) in the system remains constant (Condon, 2006):

$$n_1 = n_2 \tag{3-1-a}$$

$$n_2 = n_3 + n_{ads}^{ex} \tag{3-1-b}$$

where, n_1 is the initial amount of free gas (mol) in the reference cell, n_2 is the amount of free gas in both reference cell and sample cell immediately after connecting the cells, n_3 is the amount of free gas (mol) at equilibrium state. n_{ads}^{ex} is the excess amount of adsorbed gas (mol).

Based on the ideal gas law, equations (3-1-a) and (3-1-b) can be expanded as (Condon, 2006):

$$\frac{P_1V_1}{Z_1RT} = \frac{P_2V_2}{Z_2RT} \tag{3-2-a}$$

$$\frac{P_2V_2}{Z_2RT} = \frac{P_3V_3}{Z_3RT} + n_{ads}^{ex} \tag{3-2-b}$$

where, P_1, P_2 and P_3 are the gas pressures (Pa) in the reference cell initially, after connecting the cells and at equilibrium state, respectively. Z_1, Z_2 and Z_3 are the corresponding gas compressibility factors to P_1, P_2 and P_3, respectively. R is the universal gas constant (J/mol.K) and T is gas temperature (K). V_1, V_2 and V_3 are the free gas volumes at each stage that can be defined as:

$$V_1 = V_{RC} \tag{3-3}$$

$$V_2 = V_3 = (V_{Rc} + V_{sc}) - V_s \tag{3-4}$$

where, V_{RC} is the volume of the reference cell (m^3), V_{SC} is the volume of the sample cell (m^3) and V_s is the volume of the solid particles of the sample (m^3).

In a real experiment, the parameters P_1, P_2 and P_3 are the known values, i.e. are obtained from direct measurements. Therefore, Z_1 to Z_3 can be estimated using relevant equation of state. The amount of gas excess adsorption/desorption is then calculated based on the estimated values. At the stage of the design, however, the experimental parameters (gas pressure variations) are not available. Therefore, a back-calculation analysis was carried out to predict the gas pressure variations during gas adsorption process as well as assessing the excess and absolute gas adsorption isotherms.

Equation (3-2) cannot be solved with an analytical method due to the number of unknowns. Therefore, a numerical method, i.e. Secant method (Süli and Mayers, 2003) was used to solve the equation and estimate the variables for a range of gas injection pressures. It should be mentioned that in these analyses, the material properties associated with CO_2 and powdered coal have been used due to their relevance to the application of this study. The required input parameters for equation (3-2) are defined, as follows:

- **Gas injection pressure (P_1):** As stated previously, the range of gas pressure for the laboratory facilities designed and constructed as part of present study has been considered to be between 1 and 20MPa.

- **Temperature (T):** the components of the manometric apparatus such as the pressure transducers were selected to work under a range of temperature values while their level of accuracy should remain consistent. In order to consider a range of temperature on pressure variations, average geothermal gradient at the depth of 1000-1500m were estimated as 313K-328K (40°C-55°C) based on the relationships between the geothermal gradient and depth (Han et al., 2010). More details related to the estimation of the geothermal gradients will be provided in Chapter 4.

- **Gas compressibility factor (Z):** The Peng-Robinson Equation of State (PR-EoS) has been used to estimate the gas compressibility factors (Z) for a range of gas pressures (P_g) up to 20MPa (Peng and Robinson, 1976):

$$P_g = \frac{RT}{V_m - b} - \frac{a\alpha}{V_m^2 + 2bV_m - b^2} \quad (3\text{-}5)$$

where, V_m is the molar volume (m^3/mol). Parameters *a*, *b* and α are the coefficients related to the non-ideality of gases and are expressed based on the critical properties of gases and acentric factor. Further details can be found in (Peng and Robinson, 1976).

- **Volume of the cells (V_{RC} and V_{SC}):** In this calculations, two sizes of cell volumes were considered for the reference cell and sample cell to be $1\times10^{-4}m^3$ or $5\times10^{-5}m^3$. The range of sample sizes was found to be sufficiently large for accommodating both powdered samples and small intact rocks.

- **The volume of the sample (V_s):** Volume of the sample was estimated based on the defined sample mass (m_s) for each scenario, knowing the density of the solid and by using the mass-volume relationship (Murthy, 2003), given as:

$$V_s = \frac{m_s}{\rho_s} \quad (3\text{-}6)$$

where, m_s is the mass weight of the solid material (kg) and ρ_s is the density of the solid which can be estimated as (Murthy, 2003):

$$G_s = \frac{\rho_s}{\rho_w} \quad (3\text{-}7)$$

where, G_s is the specific gravity and ρ_w is the density of the water (kg/m^3), i.e. 1000kg/m^3. The specific gravity (G_s) for a fine powdered coal, for instance, has been given as 1.5 (Tateishi, 1980). Therefore, the density was calculated to be 1500kg/m^3.

- **The void volume of the sample cell (V_v):** The void volume of the sample cell (V_v) is calculated as:

$$V_v = V_{sc} - V_s \quad (3\text{-}8)$$

Table 3.1 summarises the values related to the volumes of the reference cell, the sample cell and the amounts of the sample considered for analysis of the scenarios.

Table 3.1. The values of the sample volume and void volume considered in the development of scenarios.

Scenario		V_{SC}/V_{RC} (-)	V_{RC} (m^3)	V_{SC} (m^3)	m_s (kg)	V_s (m^3)	V_v (V_{SC}-V_s) (m^3)	V_v/V_s (-)
1	a	2	5.0×10^{-5}	1.0×10^{-4}	0.140	9.3×10^{-5}	6.7×10^{-6}	0.1
	b	2	5.0×10^{-5}	1.0×10^{-4}	0.050	3.3×10^{-5}	6.7×10^{-5}	2.0
2	a	0.5	1.0×10^{-4}	5.0×10^{-5}	0.065	4.3×10^{-5}	6.7×10^{-6}	0.2
	b	0.5	1.0×10^{-4}	5.0×10^{-5}	0.020	1.3×10^{-5}	3.7×10^{-5}	2.8
3	a	1	5.0×10^{-5}	5.0×10^{-5}	0.060	4.0×10^{-5}	1.0×10^{-5}	0.3
	b	1	5.0×10^{-5}	5.0×10^{-5}	0.010	6.7×10^{-6}	4.3×10^{-5}	6.5

- **Adsorption parameters (n_{ads}^{ex})**: The excess adsorption (n_{ads}^{ex}) can be expressed in terms of the absolute adsorption (Gensterblum et al., 2010):

$$n_{ads}^{ex} = n_{ads}^{abs}\left(1-\frac{\rho_{gas}}{\rho_{ads}}\right) \tag{3-9}$$

where, ρ_{gas} and ρ_{ads} are the density of the free gas (kg/m^3) at equilibrium condition and the density of the adsorbed-phase (kg/m^3), respectively. The absolute adsorption (n_{ads}^{abs}) can be calculated using Langmuir equation (Langmuir, 1918), given as:

$$n_{ads}^{abs} = \frac{n_L.P_3}{P_L + P_3} \tag{3-10}$$

where, n_L and P_L are the Langmuir parameters for adsorption capacity (mol/kg) and pressure (MPa), respectively.

The adsorption parameters such as the Langmuir coefficients and adsorbed-phase density are obtained from the literature, i.e. for the Selar Cornish coal from South Wales coalfield (Gensterblum et al., 2010). The Selar Cornish coal was preferred as it was found to be in proximity of the 6ft coal seam from which the coal samples of present study have been collected. The average Langmuir parameters (n_L and P_L) for the Selar Cornish coal at 318K have been reported to be 1.92mol/kg and 1.35MPa, respectively. The average adsorbed-phase density of CO_2 on a similar coal has been reported as 1174kg/m^3 (Gensterblum et al., 2010).

3.2.4. Results of analysis

Figures 3.2 and 3.3 show the pressure reduction due to the gas adsorption for scenarios (1-a) and (1-b), respectively. As shown in these Figures, the pressure reduction in scenario (1-a) is larger than that observed from scenario (1-b). This can be attributed to the larger amount of adsorbent (coal sample) in scenario (1-a). The results of gas pressure variations related to the lower temperature range (313K) show a slight decrease at higher pressure conditions which might be related to variations in compressibility of gas at higher pressures.

The smallest pressure reductions during the adsorption process for scenarios (1-a) and (1-b) were estimated to be 0.67MPa and 0.02MPa, respectively. The pressure resolutions were then calculated by dividing above values by overall pressure range, i.e. 20MPa. As a result, the minimum pressure resolutions required under scenarios (1-a) and (1-b) are estimated to be 0.033MPa and 0.001MPa, respectively.

Figures 3.4 and 3.5 present the range of pressure variations due to gas adsorption on coal for scenarios (2-a) and (2-b), respectively. The results show that the range of pressure decrease due to gas adsorption on coal is very small, especially in scenario (2-b). This can be related to the larger volume of the reference cell and therefore larger amount of injected gas and the small amount of adsorbent in the sample cell.

The minimum pressure variation for scenarios (2-a) and (2-b) were estimated to be 0.13MPa and 0.05MPa, respectively and therefore, the minimum pressure resolutions required for those scenarios are 0.007MPa and 0.003MPa, respectively.

Figures 3.6 and 3.7 show the results of pressure decrease in the adsorption cell as a result of gas adsorption on coal for scenarios (3-a) and (3-b), respectively. From the results, the amount of pressure decrease in scenario (3-a) is much larger than those for scenario (3-b) which is related to the large amount of adsorbent in the sample cell.

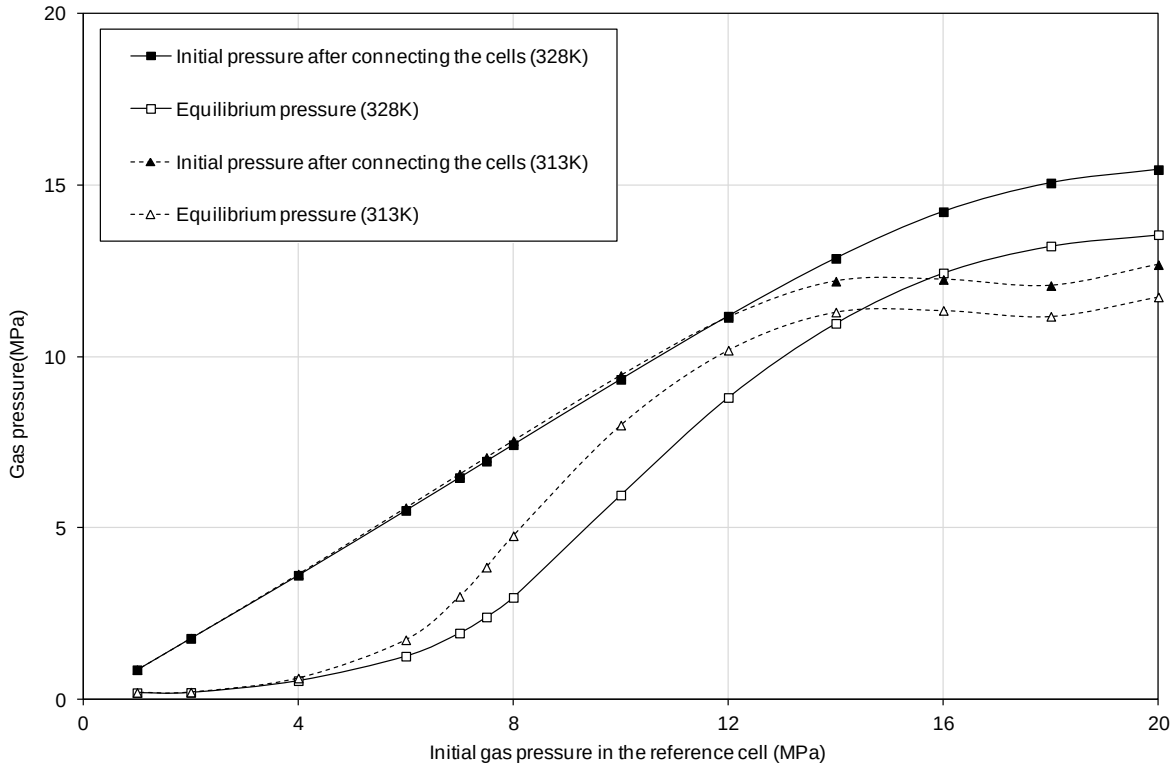

Fig. 3.2. Scenarios 1-a: Gas pressure variations in the adsorption cell as a result of CO_2 adsorption on coal at 328K and 313K.

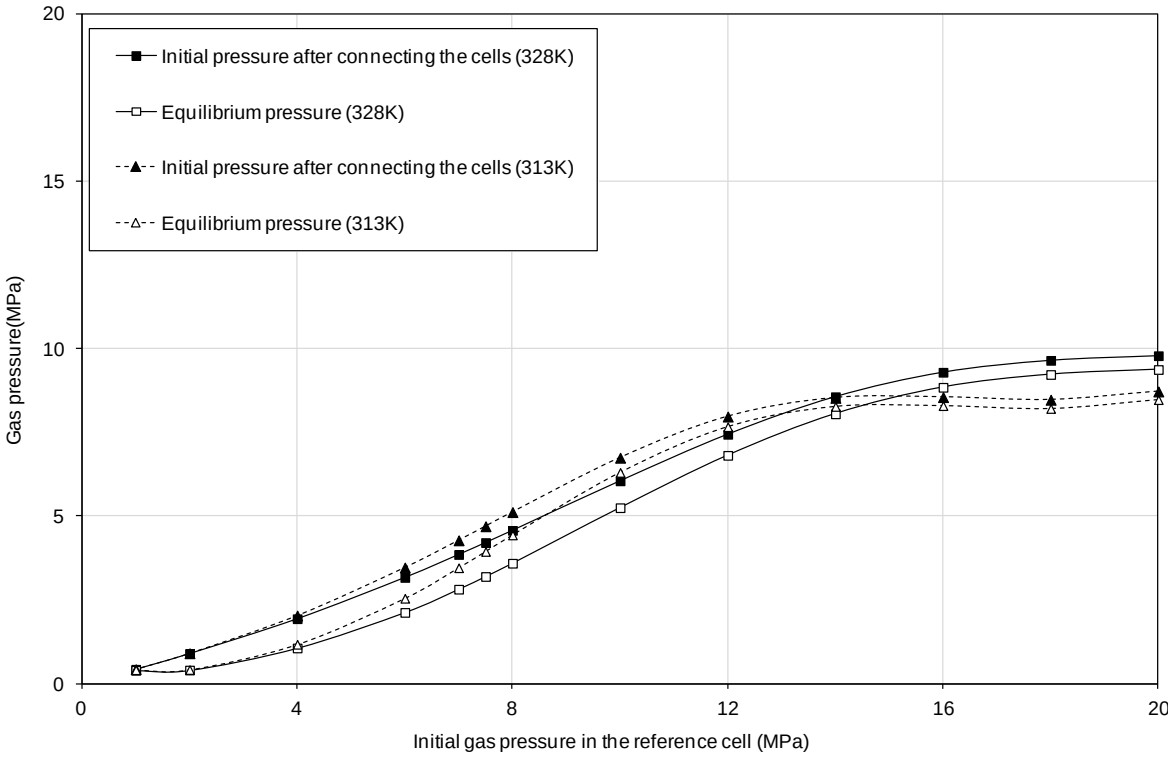

Fig. 3.3. Scenarios 1-b: Gas pressure variations in the adsorption cell as a result of CO_2 adsorption on coal at 328 and 313K.

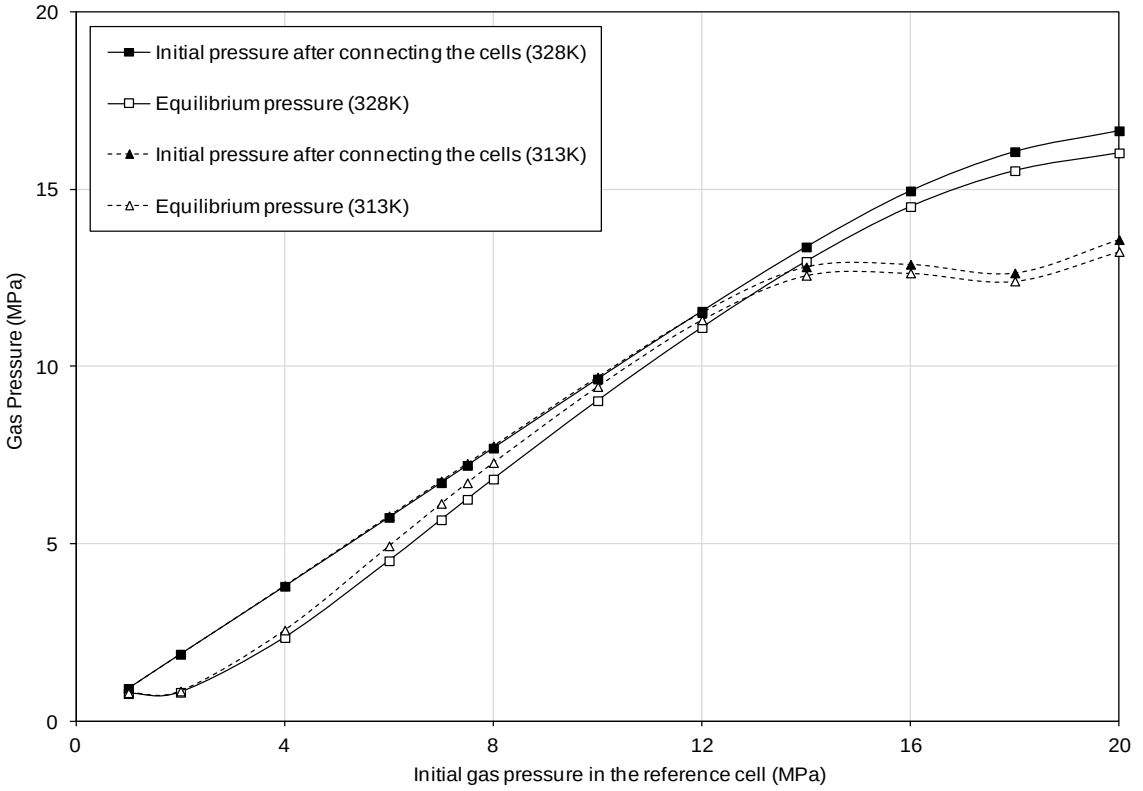

Fig. 3.4. Scenarios 2-a: Gas pressure variations in the adsorption cell as a result of CO_2 adsorption on coal at 328 and 313K.

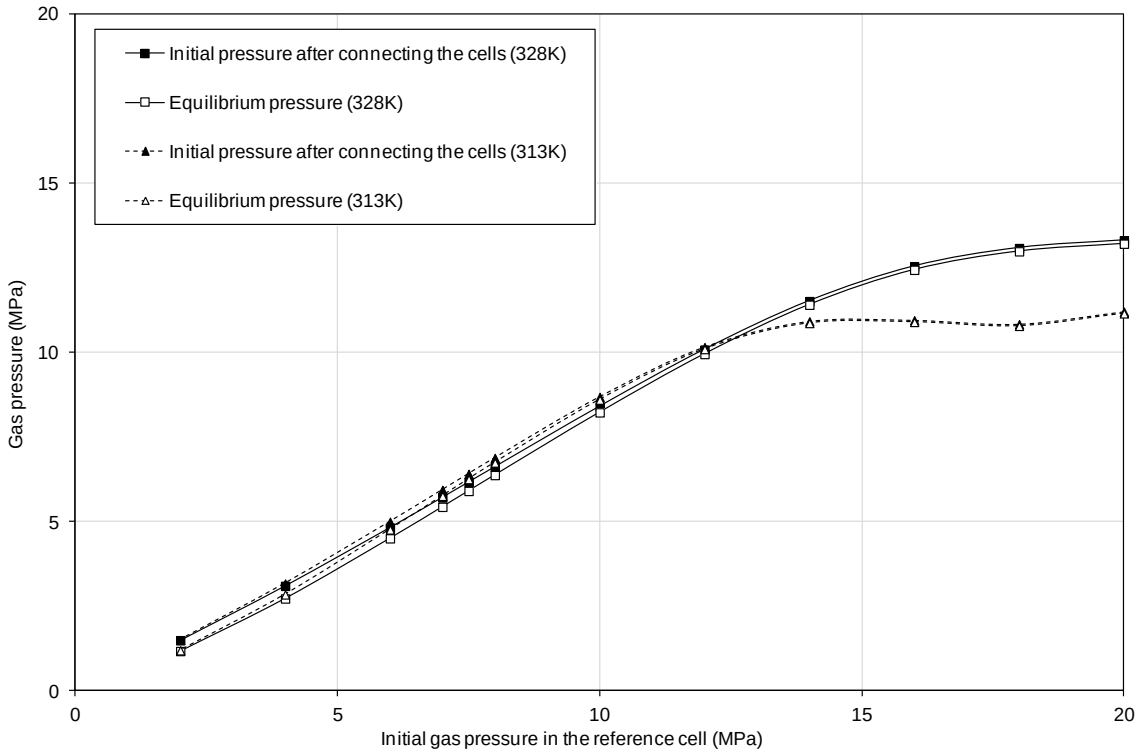

Fig. 3.5. Scenarios 2-b: Gas pressure variations in the adsorption cell as a result of CO_2 adsorption on coal at 328 and 313K.

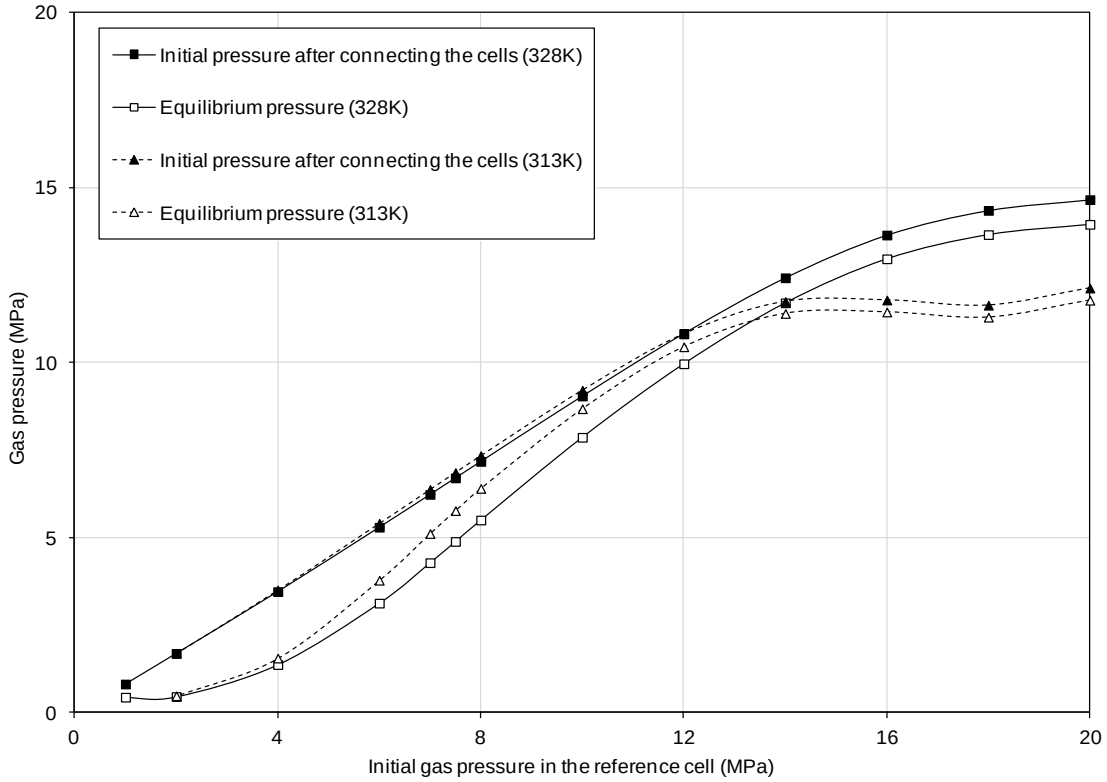

Fig. 3.6. Scenarios 3-a: Gas pressure variations in the adsorption cell as a result of CO_2 adsorption on coal at 328 and 313K.

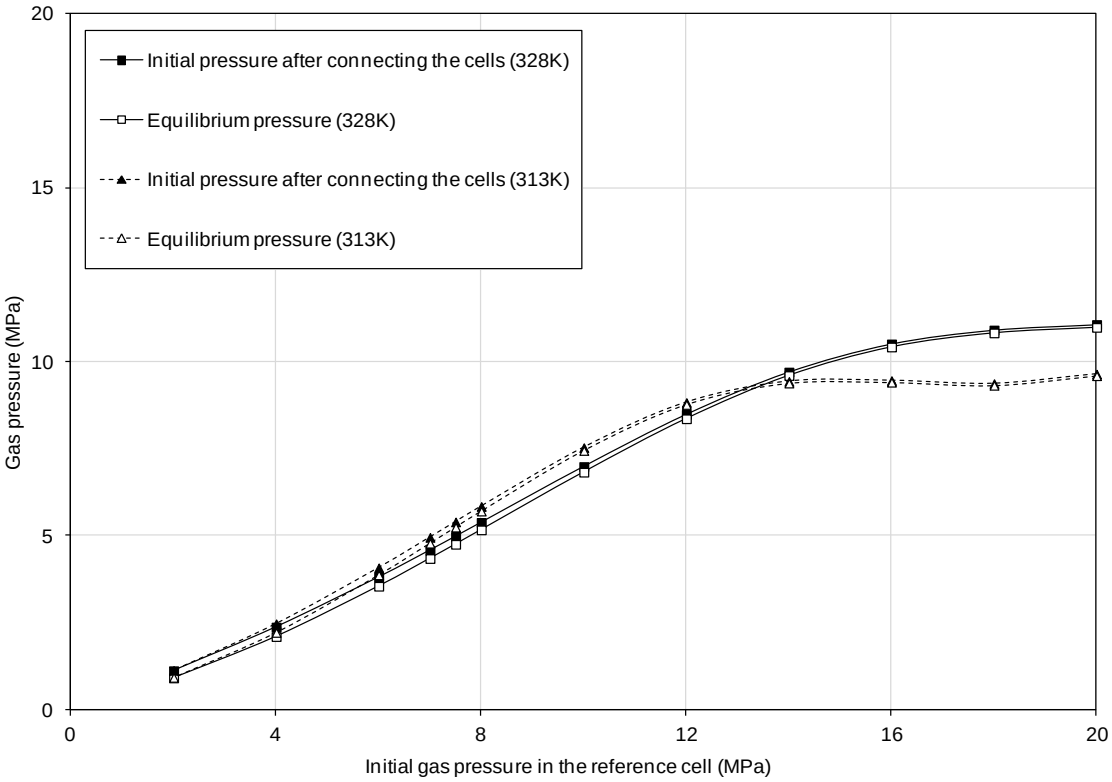

Fig. 3.7. Scenarios 3-b: Gas pressure variations in the adsorption cell as a result of CO_2 adsorption on coal at 328 and 313K.

The minimum pressure variation for scenarios (3-a) and (3-b) were estimated to be 0.38MPa and 0.05MPa, respectively. The minimum pressure resolution required for scenarios (3-a) and (3-b) are 0.017MPa and 0.002kPa, respectively.

Figures 3.8 and 3.9 compare the excess and absolute adsorption isotherms of the scenarios (1-a) and (1-b), respectively. The results of both scenarios show similar trends for the amount of absolute gas adsorption on coal. However, the amount of excess adsorption in the scenario (1-b) changed considerably compared with the scenario (1-a). This can be attributed to the amount of coal in the sample cell and therefore higher rate of coal swelling due to the effect of CO_2 on coal (Mazzotti et al., 2009). The coal matrix swelling induced by the adsorbed CO_2 and its effect on excess adsorption will be discussed in detail in Chapter 5. The results of the analysis for scenario (1-a) show a higher final equilibrium pressure. In addition, the effect of temperature on the amount of excess adsorption was found to be considerable especially at higher pressures.

Figures 3.10 and 3.11, provide a comparison between the excess and absolute adsorption isotherms related to the scenarios (2-a) and (2-b), respectively. The amounts of the absolute CO_2 adsorption for both scenarios were found to be similar. The amounts of the excess adsorption, however, were found to be different which can be related to the differences in the amount of adsorbent (coal sample) in the sample cell. The results also show that in the scenario (2-a), the final equilibrium pressure is higher than that for the scenario (2-b).

Figures 3.12 and 3.13 present the results of the excess and absolute adsorption isotherms for the scenarios (3-a) and (3-b), respectively. Similar to the other scenarios, the results of absolute gas adsorption show similar trends. However, the amount of excess adsorption slightly change in the scenario (3-b) compared to the scenario (3-a) due to the differences in the amount of coal sample. For both scenarios, the effect of temperature on the amounts of excess adsorption was found to be considerable, especially at higher equilibrium pressures. Moreover, the scenario (3-a) provided higher final equilibrium pressure compared to those for the scenario (3-b).

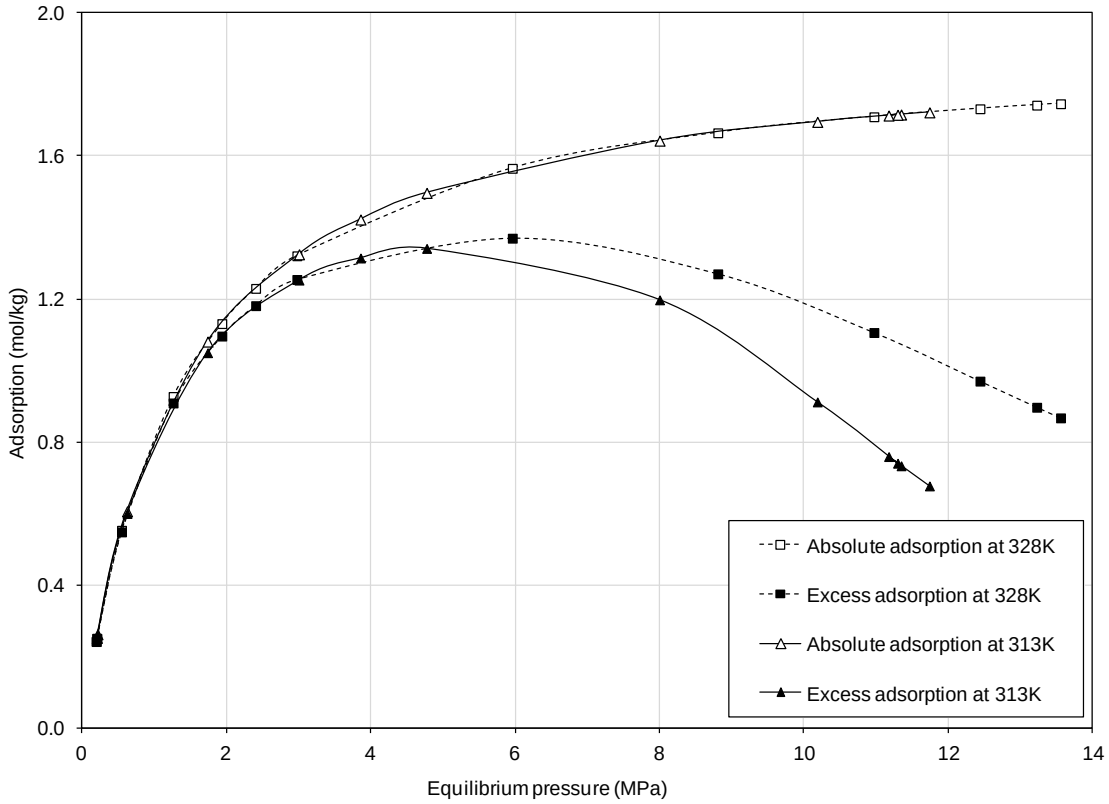

Fig. 3.8. Scenario 1-a: CO_2 excess and absolute adsorption isotherms at 328K and 313 K.

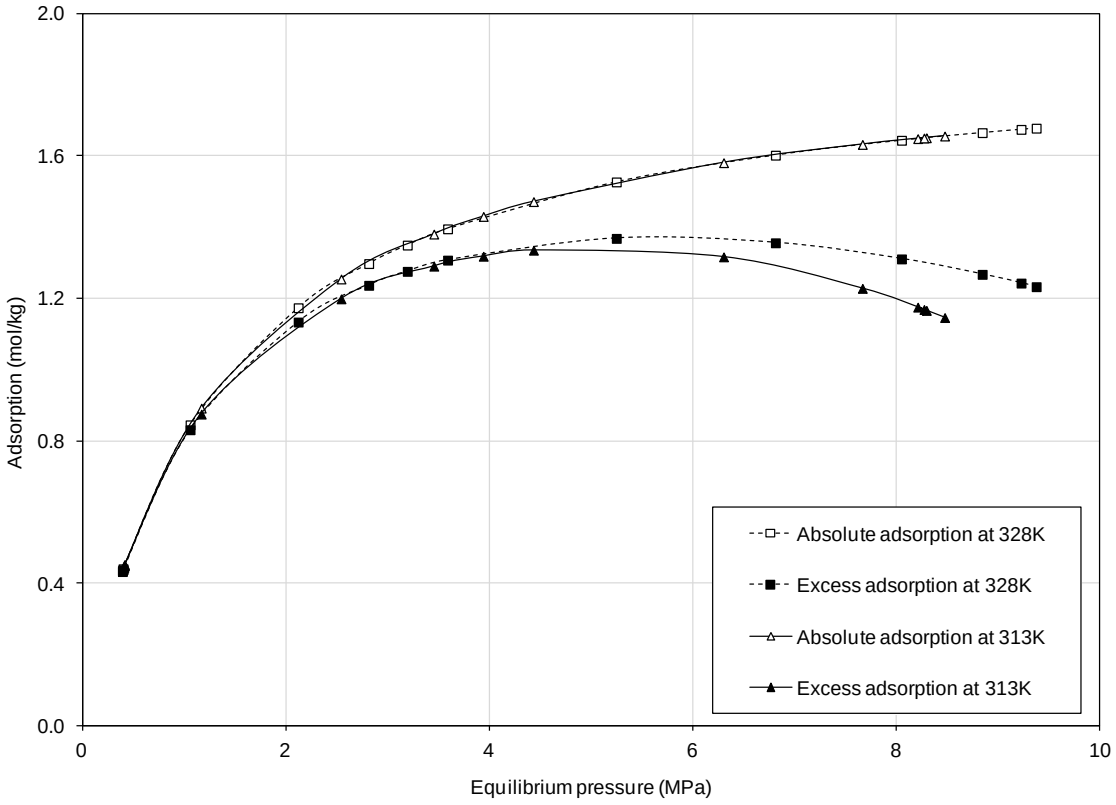

Fig. 3.9. Scenario 1-b: CO_2 excess and absolute adsorption isotherms at 328K and 313 K.

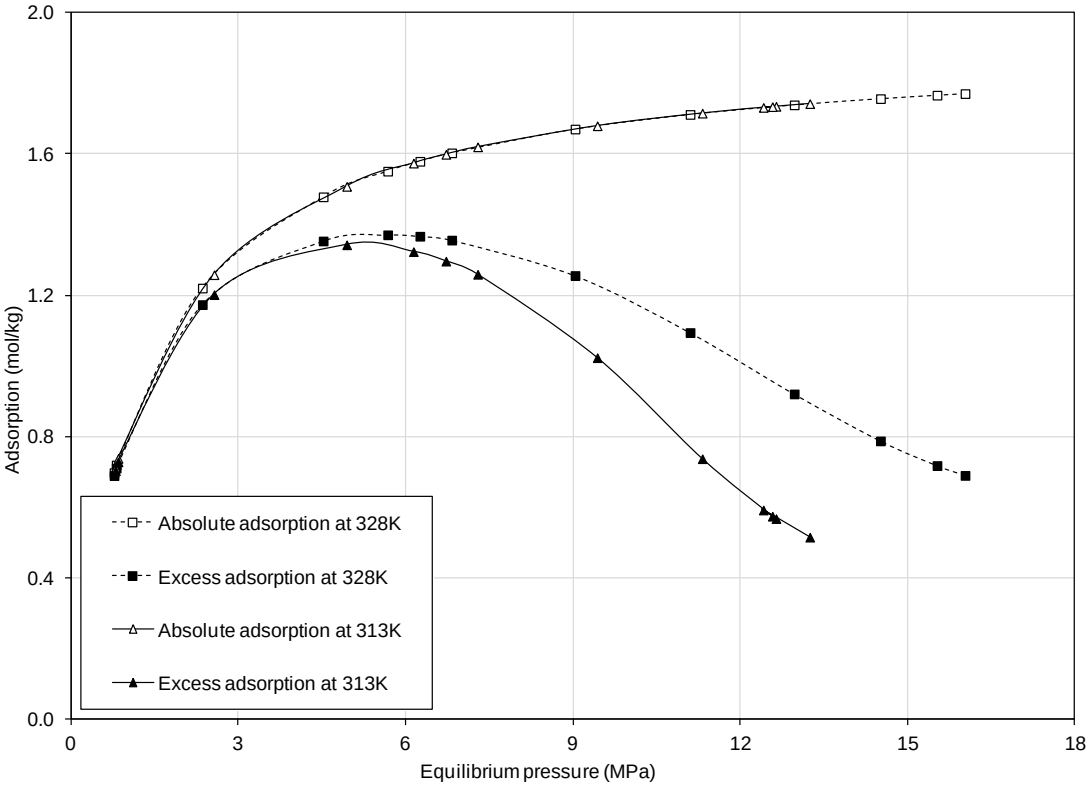

Fig. 3.10. Scenario 2-a: CO_2 excess and absolute adsorption isotherms at 328K and 313 K.

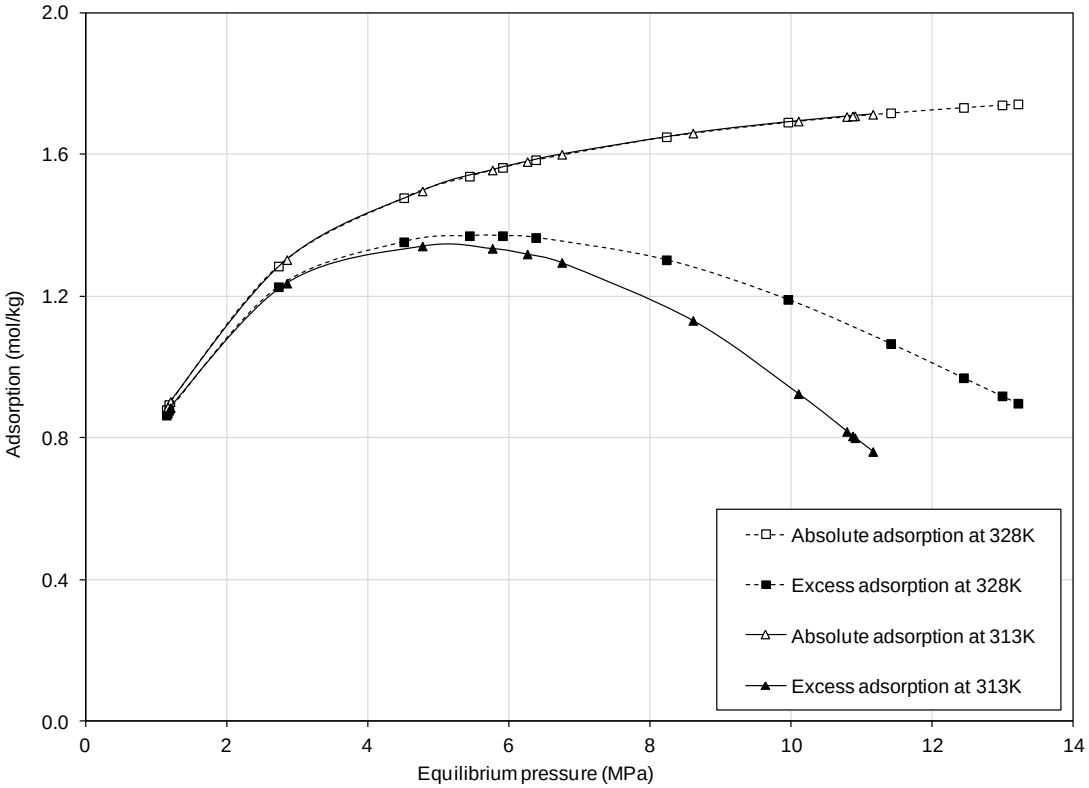

Fig. 3.11. Scenario 2-b: CO_2 excess and absolute adsorption isotherms at 328K and 313 K.

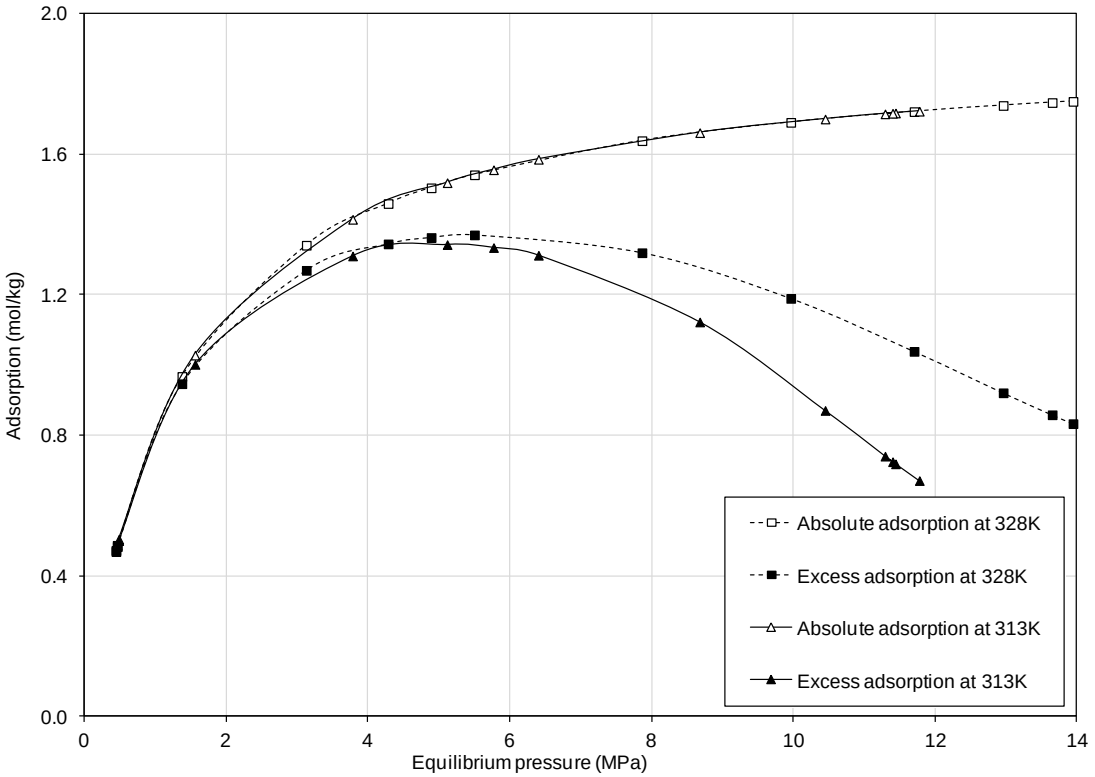

Fig. 3.12. Scenario 3-a: CO_2 excess and absolute adsorption isotherms at 328K and 313K.

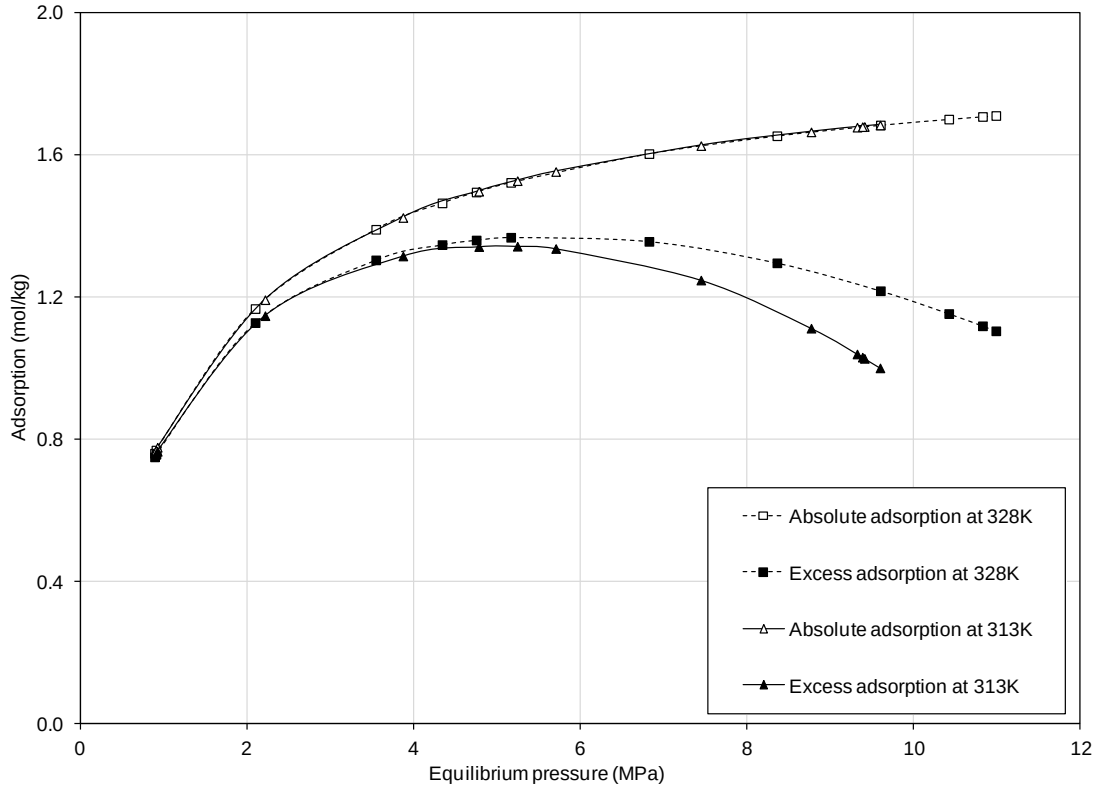

Fig. 3.13. Scenario 3-b: CO_2 excess and absolute adsorption isotherms at 328K and 313K.

3.2.5. Concluding remarks on the design considerations

In order to select the optimised scenario with regards to the design considerations, the results presented in previous section are compared in Table 3.2.

Table 3.2. Comparison of the results of different scenarios after accounting for the design considerations.

Scenarios		Design considerations			
		***Minimum required* pressure resolution (MPa)**		**Maximum equilibrium pressure (MPa)**	
1	a	0.033	(√)	13.5	(√)
	b	0.001	(×)	9.5	(×)
2	a	0.006	(×)	16	(√)
	b	0.002	(×)	13	(√)
3	a	0.017	(√)	14	(√)
	b	0.002	(×)	11	(×)

(√): The results of analyses for the defined scenario are in agreement with the design considerations; (×): The results do not fulfill the design considerations.

From the information in Table 3.2, scenarios (1-a) and (3-a) are found to be in agreement with both design considerations. However, the scenario (1-a) provides slightly lower equilibrium pressures and due to its larger sample volume more pressure steps are required to achieve the final equilibrium pressure. The scenario (3-a), however, requires less pressure steps to reach to the final equilibrium pressure (due to its smaller sample cell) and therefore, the equilibrium state can be achieved faster.

The results of the minimum pressure resolution required for each scenario show that most of the scenarios except scenarios (1-a) and (3-a) require pressure transducers with very high pressure resolutions, e.g. resolutions higher than 0.002MPa. Such transducers are difficult to obtain and expensive options. The scenarios (1-a) and (3-a), however, require a reasonable pressure resolution with respect to the commercially available pressure transducers. Further details regarding the resolution of the adopted pressure transducers are provided in Section 3.4.2.

In conclusion, the scenario (3-a) has been found as the appropriate and optimised scenario with regards to the design considerations of this study. Therefore, it was decided to construct the adsorption cell unit based on the scenario (3-a). Details of the constructed and commissioned manometric sorption apparatus is provided in Section 3.4.

3.3. The triaxial core flooding system

3.3.1. Design considerations

The principal of the core flooding technique has been described in Chapter 2. In this section, the design considerations of the triaxial core flooding system developed for the purpose of this study are discussed and the methodology employed to evaluate the design considerations is described.

One of the important parameters to be accurately measured in permeability measurement experiments is the flow rate. For that, an appropriate flow meter is required to be incorporated into the flow measurement system. The flow meters should be capable of accurately measuring the lowest and highest possible flow rates that may occur during the experiments. Similar to the manometric sorption apparatus, real experimental data were not available at this stage. Therefore, a number of scenarios have been defined which are based on a range of influential parameters on gas flow rates. The gas flow rates are then estimated and the results are considered as a guideline to define the specifications of the flow meters with an appropriate range to be incorporated into the system.

3.3.2. Scenarios and analysis conditions

As stated previously, several factors were considered for defining the example scenarios for the evaluation of the range of gas flow rates, expected during the core flooding experiments. Figure 3.14 shows a schematic diagram of the scenarios which have been defined based on a range of sample sizes and permeabilities.

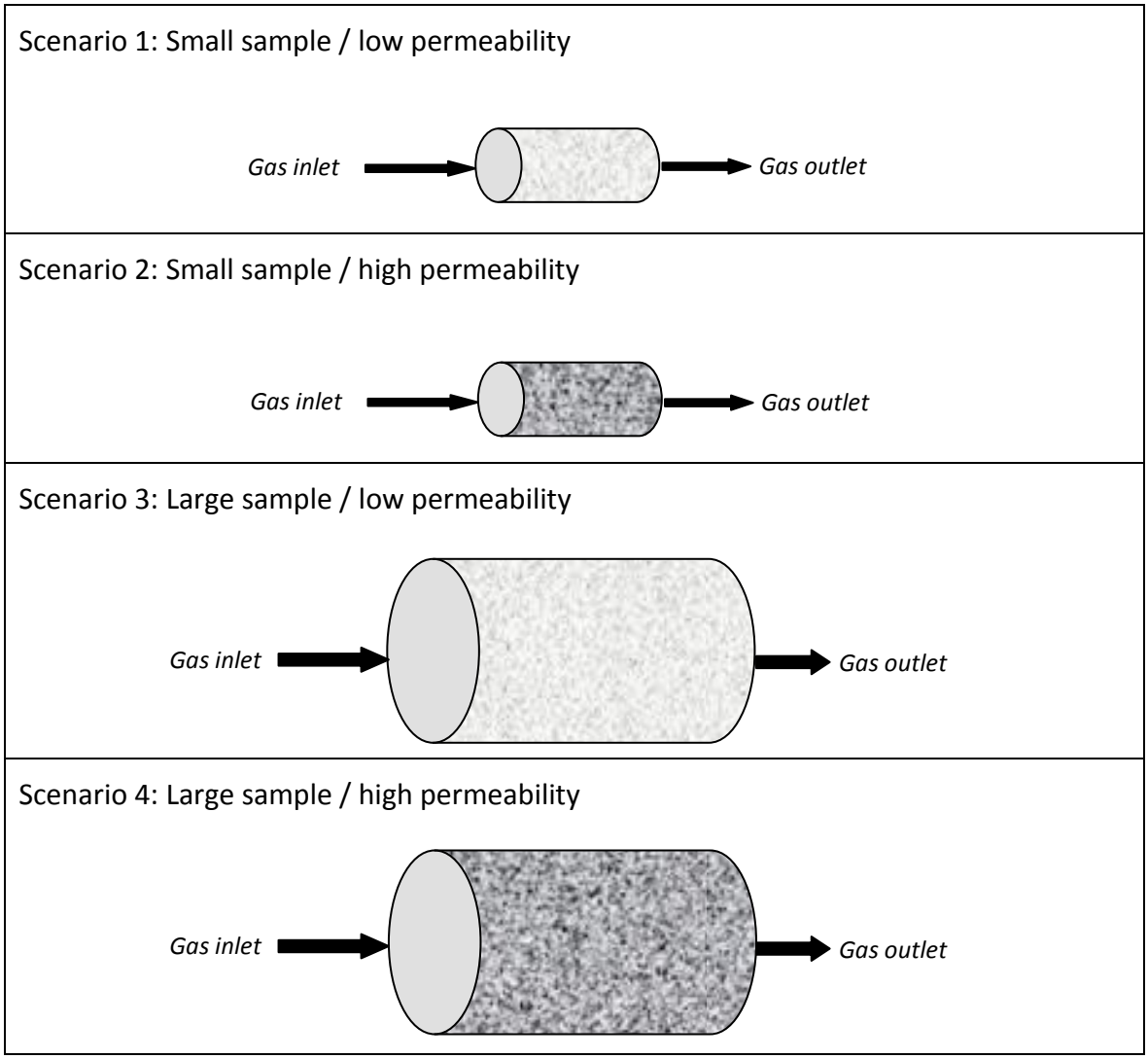

Fig. 3.14. Initial conditions defined in scenarios 1 to 4 in order to evaluate the range of gas flow rates anticipated during the core flooding experiments.

As shown in Figure 3.14, in the scenario 1, the smallest sample size and the lowest permeability range have been considered. The values for the sample sizes and permeabilities will be provided in the following section. For the scenario 2, the sample size is similar to those for the scenario 1. The permeability of the sample, however, was considered to be within the high range in scenario 2. In the scenario 3, the largest sample size was considered with lower permeability range. Similar to the scenario 3, the largest sample size was considered in the scenario 4 with the permeability value within the higher range.

3.3.3. Estimation of the range of gas flow rates

The range of gas flow rates were calculated based on Darcy's equation for gases (Carman, 1956):

$$Q_0 = \frac{k_g A(P_{up}^2 - P_{down}^2)}{2\mu_g L P_0} \quad (3\text{-}11)$$

where, Q_0 is the volumetric rate of flow at reference pressure (m^3/s), k_g is the gas permeability coefficient (m^2), μ_g is the gas viscosity (Pa.s), L is the sample length (m), P_0 is the reference pressure (Pa), A is the cross-sectional area of the sample (m^2), P_{up} is the upstream gas pressure (Pa), and P_{down} is the downstream gas pressure (Pa).

In order to estimate the range of possible gas flow rates in the system, a range of values were considered for the parameters mentioned in equation (3.11), as follows:

- **The range of gas pressure:** As stated in Section 3.2, the experimental apparatus of this study has been designed to tolerate gas pressures up to 20MPa. This would allow replicating the ground conditions in terms of pore pressure and confining pressure for the depths up to 2000m. Therefore, the experimental gases can be injected at upstream of the sample at pressures up to 20MPa. The gas pressure in downstream of the sample is considered at atmospheric pressure (0.1MPa). Therefore, the range of gas pressures to be applied in the calculations is between 0.1MPa and 20MPa. Similar to previous sections, the material properties associated with CO_2 and coal have been used due to their relevance with the application of this study.

- **Permeability of the sample to gases:** There are limited published coal permeability measurements for the UK coals (DECC, 2010; Jones, 2004). Based on the literature review conducted in Chapter 2, the gas permeability of targeted coal seams in the South Wales is expected to be low, i.e. less than $3\times10^{-15}m^2$ (3mD). However, this value might vary depending on the depth and gas injection pressure. Therefore, due to limited information about permeability of the South Wales coals and

uncertainties about the depth of which samples will be provided, calculations in this section were carried out based on a permeability range of $1\times10^{-17}m^2$ to $3\times10^{-15}m^2$ (0.01 to 3mD).

- **Sample size:** As stated in Chapter 1, one of the objectives for the design of the triaxial flooding system is to develop a triaxial facility which is capable of accommodating various sample sizes. The influential factors in defining the range of sample sizes to be used in the triaxial cell are the limitations related to the sample coring as well as the cost. Providing a small diameter core sample (<20mm) from a highly fractured coal without damaging its structure can be very difficult. On the other hand constructing a triaxial cell for samples with a very large diameter (>100mm) can be expensive. Therefore, it was decided to define a reasonable range of sample diameters to be accommodated in the triaxial cell. The range of core samples was defined to be between 0.025m and 0.01m with their lengths of up to twice their diameter.

- **Gas viscosity:** The viscosity of gases (μ_g) has been calculated based on the Sutherland formula as function of temperature (Smits and Dussauge, 2006):

$$\mu_g = \mu_{g0}\frac{T_0 + C}{T + C}\left(\frac{T}{T_0}\right)^{3/2} \tag{3-12}$$

where, μ_{g0} is the reference viscosity (Pa·s) at reference temperature T_0 (K), and C is the Sutherland's constant depending on gas species. It should be mentioned that the range of gas temperatures considered in these analyses is 313 and 328K, based on the discussion provided in Section 3.2.3.

The results of the gas flow rates for the example scenarios based on the range of gas injection pressures and sample sizes described above are presented in the following section.

3.3.4. Results of analysis

The results of estimated gas flow rates for scenarios 1 to 4 are presented in Figures 3.15 to 3.18, respectively. From Figure 3.15, the range of gas flow in the scenario 1 was found to be very low which is related to the low permeability of the sample. According to the results, gas flow rate is expected to increase with the increase in gas pressure and reaches to a maximum value of approximately $12.5\times10^{-6}m^3/s$.

Figure 3.16 shows the results of gas flow rates estimated for the scenario 2. From the results, it can be observed that the gas flow rates are considerably high due to high permeability value considered in this scenario, i.e. $1\times10^{-15}m^2$. The maximum gas flow rate at 20MPa gas injection pressure is approximately $3.7\times10^{-3}m^3/s$.

Figure 3.17 presents the results of gas flow rates based on the initial conditions defined for the scenario 3. The highest flow rate of $200\times10^{-6}m^3/s$ is expected in this scenario.

From Figure 3.18, the results of gas flow rates for the scenario 4 provided the highest range of gas flow rates compared to other scenarios. The results show that the gas flow rate in this scenario can be as high as $60\times10^{-3}m^3/s$.

3.3.5. Concluding remarks on the design considerations

A summary of the input data and the final results of the scenarios 1 to 4 are presented in Table 3.3. According to the results, a broad range of gas flow rates from 13×10^{-6} to $60\times10^{-3}m^3/s$ can be expected during the experimental measurements.

It should be mentioned that the results presented in Figures 3.15 to 3.18 are based on Darcy's law and related to the gas phase only. The permeability changes due to the variations in effective stress, swelling/shrinkage of sample and interactions of sample with various gas species have not been included in these analyses. The results from these analyses are only considered as a guideline to specify an appropriate flow meter capable of reading the gas flow rates under a broad range of gas pressures.

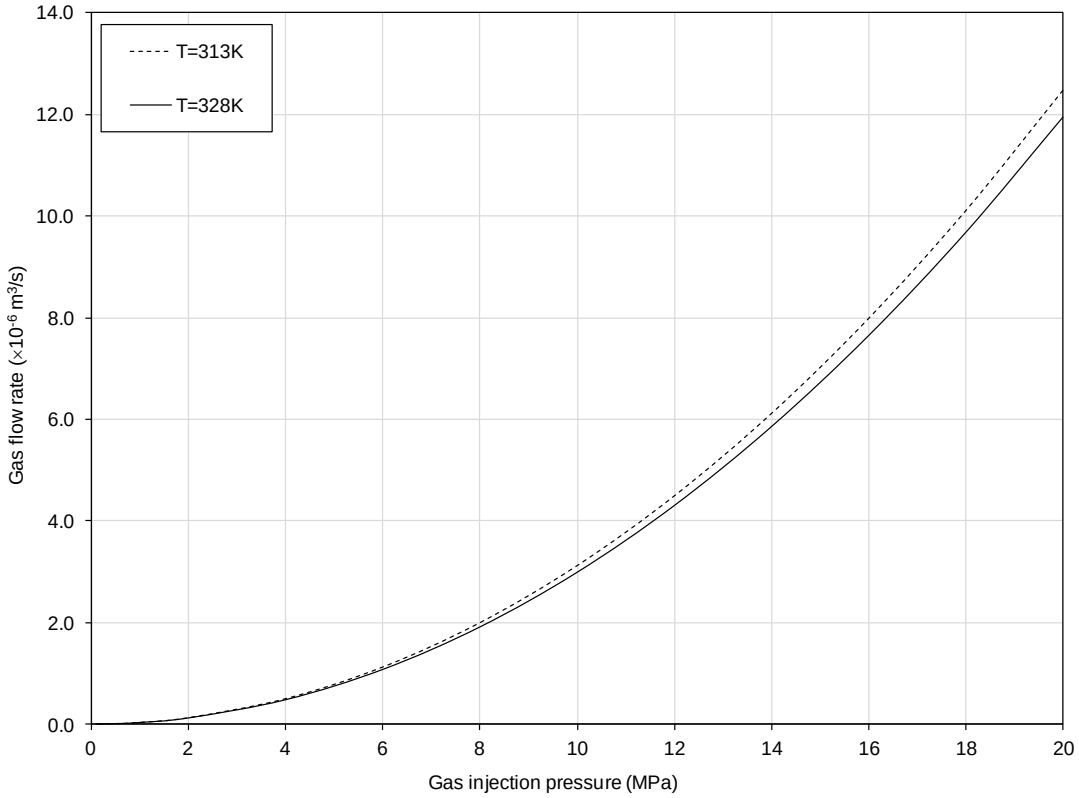

Fig. 3.15. Estimated gas flow rates based on scenario 1.

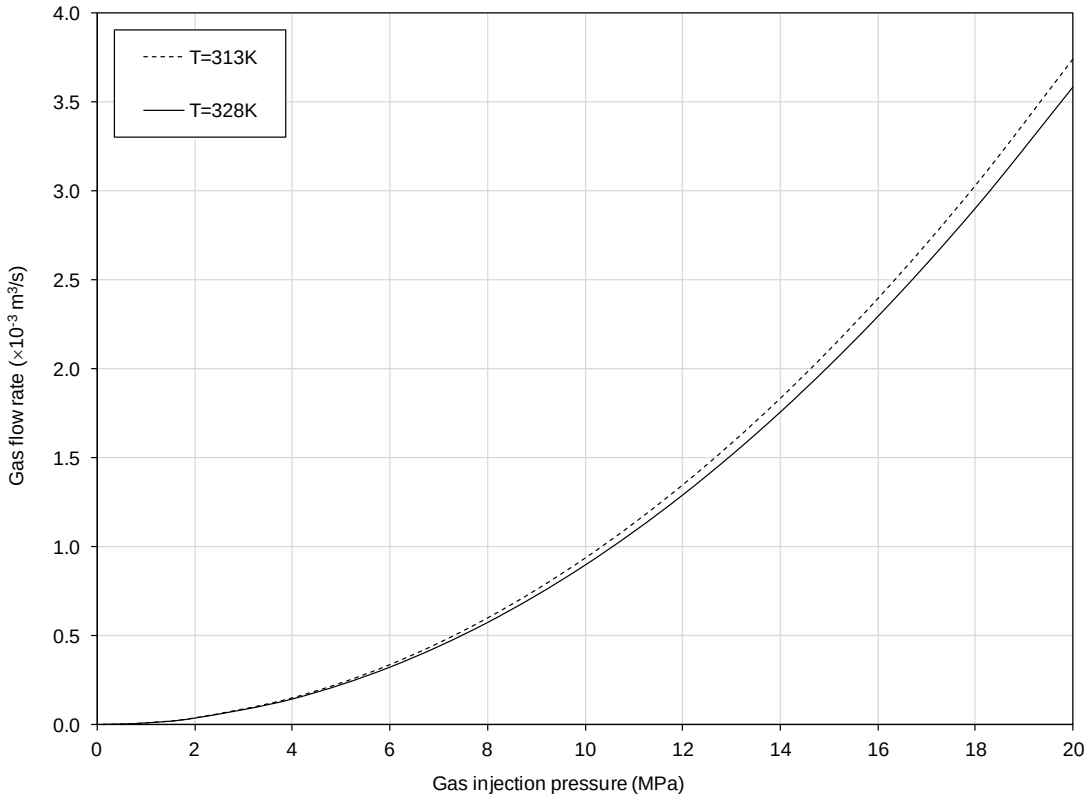

Fig. 3.16. Estimated gas flow rates based on scenario 2.

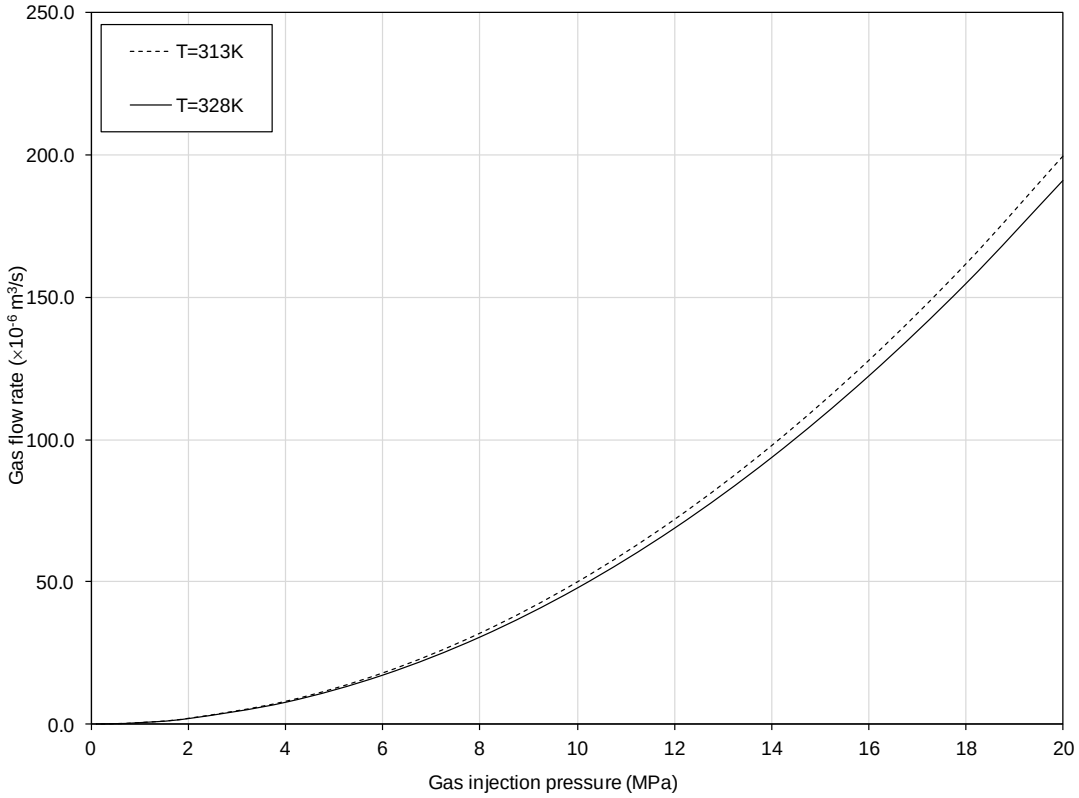

Fig. 3.17. Estimated gas flow rates based on scenario 3.

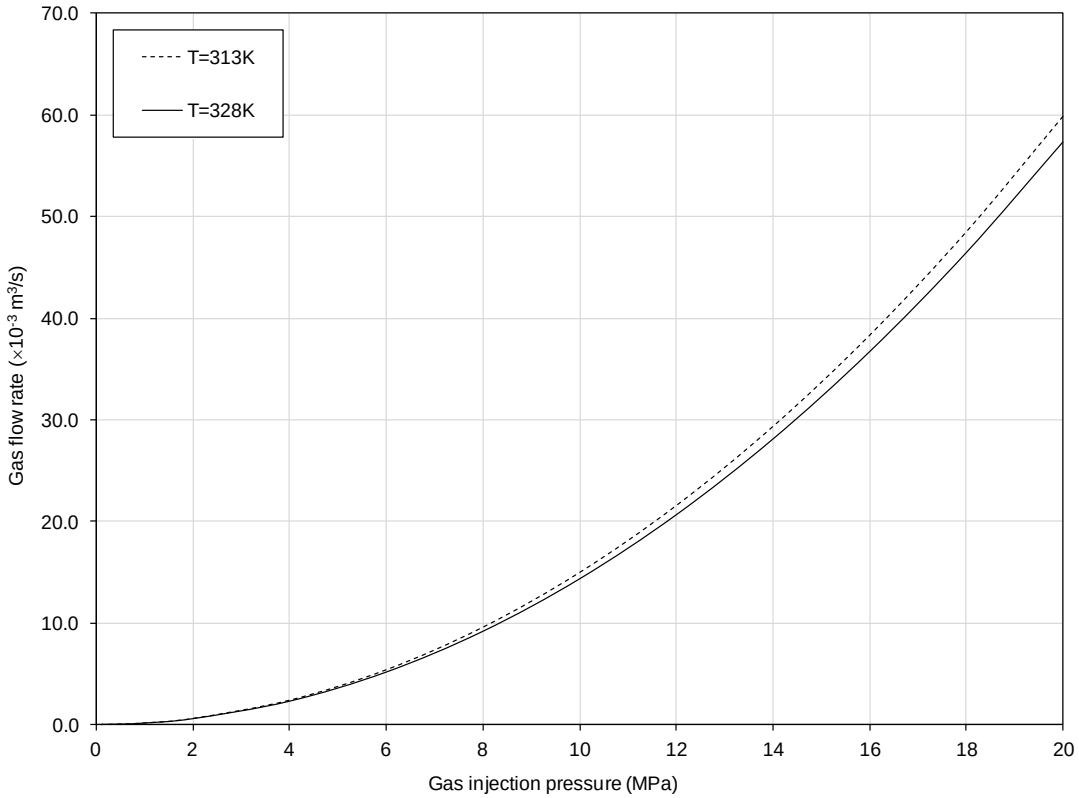

Fig. 3.18. Estimated gas flow rates based on scenario 4.

Most of commercially available flow meters are limited to a certain range of gas flow rates. For instance, some flow meters are designed for low flow rates up to $1.7\times10^{-6}m^3/s$ (100mL/min) and some are designed to measure high flow rates up to $17\times10^{-6}m^3/s$ (1L/min). Alternative broader-range flow meters such as the Coriolis Mass Flow Meters are expensive and their cost exceeds the resources of the equipment design in this study.

Table 3.3. Summary of the input data and final results for scenarios 1 to 4.

Parameter	Scenario			
	1	2	3	4
Sample diameter and length (m)	D:0.025,L:0.05	D:0.025,L:0.05	D:0.01,L:0.02	D:0.01,L:0.02
Permeability (m^2)	1×10^{-17}	3×10^{-15}	1×10^{-17}	3×10^{-15}
Maximum upstream pressure (MPa)	20	20	20	20
Downstream pressure (MPa)	0.1	0.1	0.1	0.1
Viscosity of CO_2 at 313K (Pa.s)	1.57×10^{-5}	1.57×10^{-5}	1.57×10^{-5}	1.57×10^{-5}
Viscosity of CO_2 at 328K (Pa.s)	1.64×10^{-5}	1.64×10^{-5}	1.64×10^{-5}	1.64×10^{-5}
Maximum gas flow rate (m^3/s)	13×10^{-6}	4×10^{-3}	199×10^{-6}	60×10^{-3}

In conclusion, it was decided to adopt a relatively cost-effective Mass Flow Meter capable of measuring high flow rates up to $17\times10^{-6}m^3/s$ (1L/min). Instead, for the experiments with high permeable samples, higher injection pressures can be avoided so that the gas flow rate would not exceed the upper limit of the flow meters.

3.4. Construction and commissioning

The high pressure experimental facilities have been constructed and commissioned as part of this study based on the design considerations discussed in the previous sections. The system is capable of working under high pressure conditions up to 20MPa and temperatures up to 338K (65°C). A schematic diagram of the developed laboratory facility is presented in Figure 3.19. This facility consists of three main sections, including:

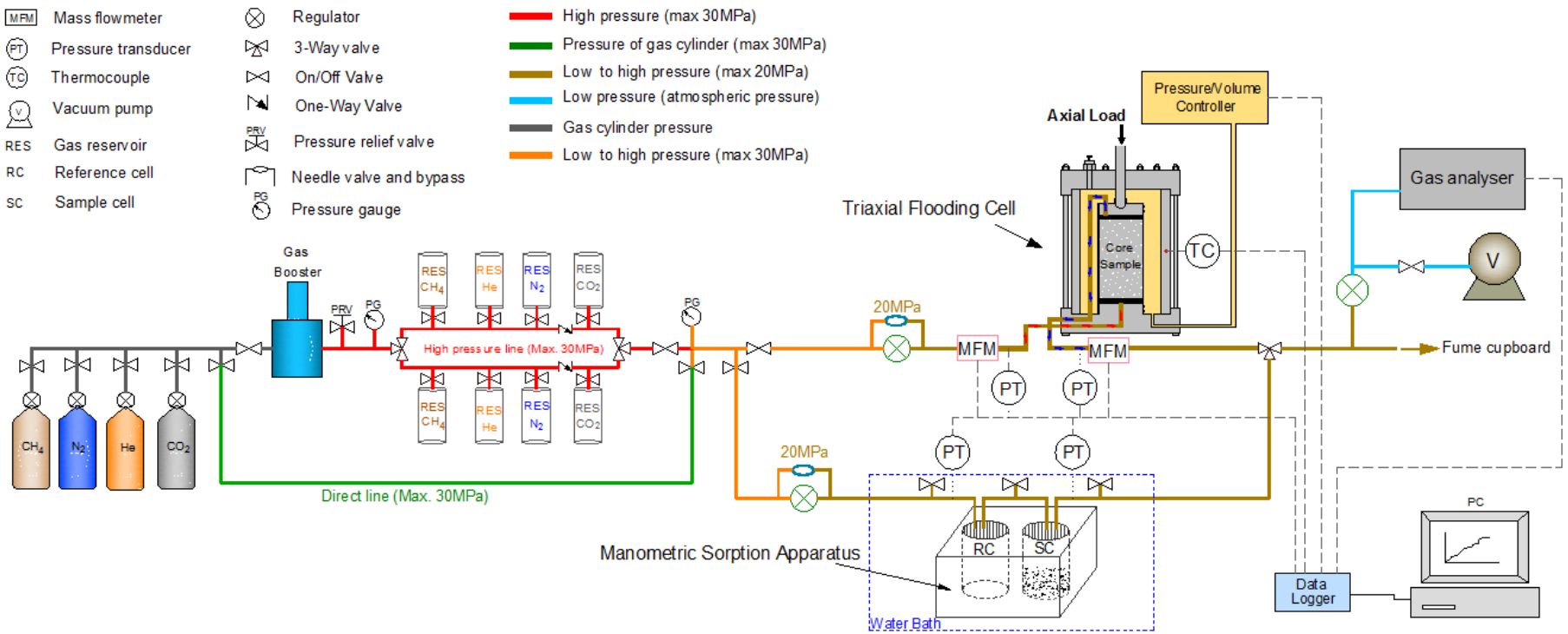

Fig. 3.19. A schematic diagram of the developed laboratory facility.

- A manometric sorption apparatus.
- A triaxial core flooding system.
- The ancillary system including the gas supply unit and the gas analysing unit.

Detail specifications of the constructed and commissioned facility are provided in the following sections.

3.4.1. The adsorption/desorption cell

The apparatus has been designed for high pressure gases such as supercritical CO_2 which is known to be highly corrosive. Therefore, it was decided to use stainless steel 316 (SS-316) which is known to be corrosion resistant, in the cells body and the connecting tubes. The adsorption cell comprises a double-ended twin cavity block of SS-316 with caps (Figure 3.20) constructed by GDS Instruments for the purposes of this study. The cavity on the left-hand side is considered as the reference cell and the cavity on the right-hand side is considered as the sample cell. The cells have a volume of approximately 150cm^3 each excluding the dead volume of the tubes and the valves. The entire system has been designed to tolerate high pressures up to 20MPa and high temperatures up to 338K (65°C). Nitrile and Viton o-rings have been used as seal between the cell body and the cap.

3.4.2. Pressure transducers

Two in-line pressure transducers were employed for the adsorption cell, one for the reference cell and one for the sample cell (Figure 3.21). According to the results of analysis presented in previous sections, the pressure transducers were purchased based on the minimum pressure resolution required, i.e. 0.017MPa (17kPa). The transducers were purchased from GDS Instruments, with 0.002MPa (2kPa) resolution and 0.15% accuracy.

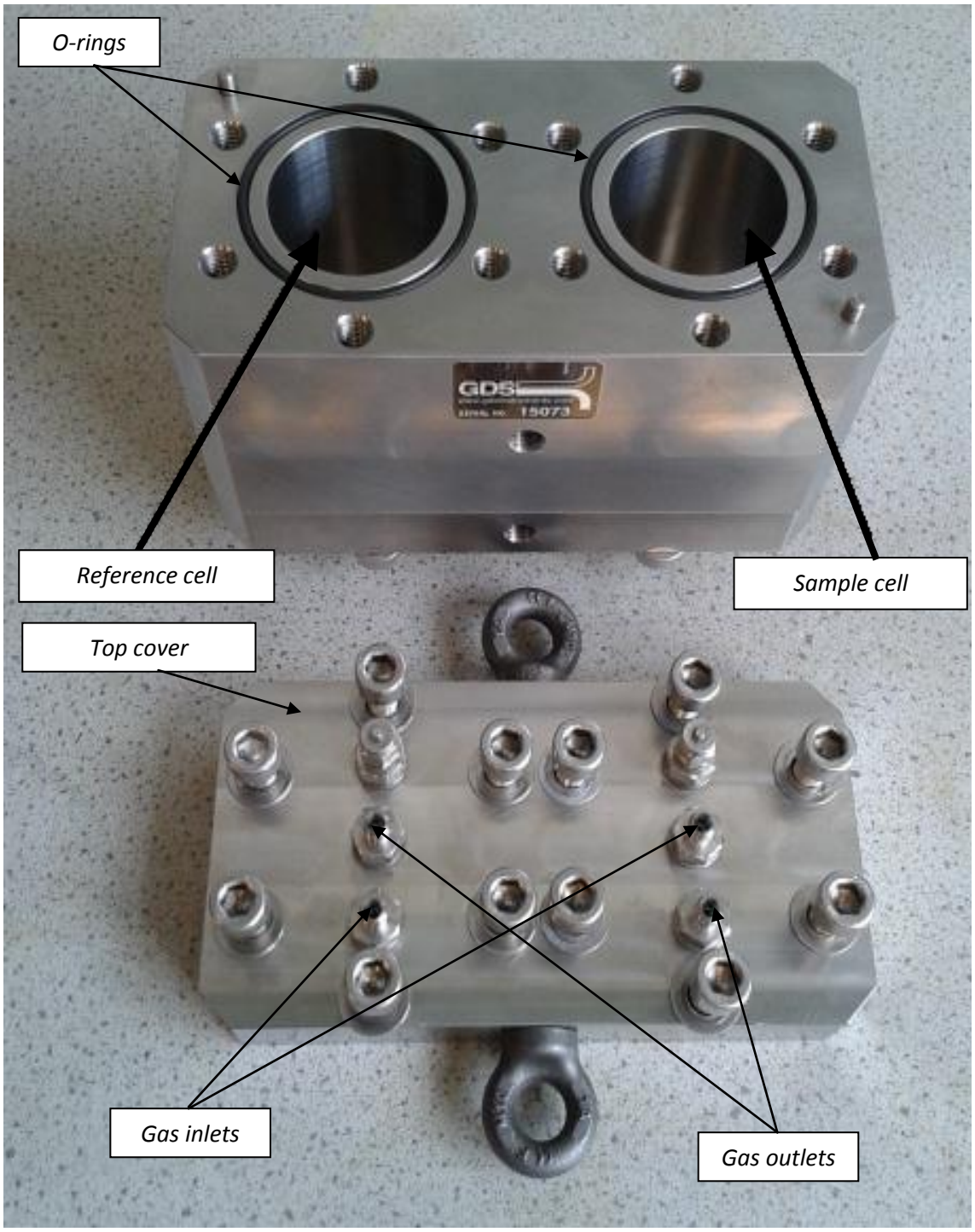

Fig. 3.20. Adsorption cell including a reference cell and a sample cell.

3.4.3. Needle valves and tubes

For the experimental conditions of this study, needle valves were found to be the most suitable type of valve as it allows a precise regulation of gas flow through the system.

Since the orifice is small and the force advantage of the fine-threaded stem is high, needle valves are usually easy to shut off completely with a finger tight pressure. Three stainless steel needle valves have been employed for the adsorption cell, as shown in Figure 3.21. Flexible tubes (SS-316 with O/D of 1/8˝) connect the valves and the transducers to the cells.

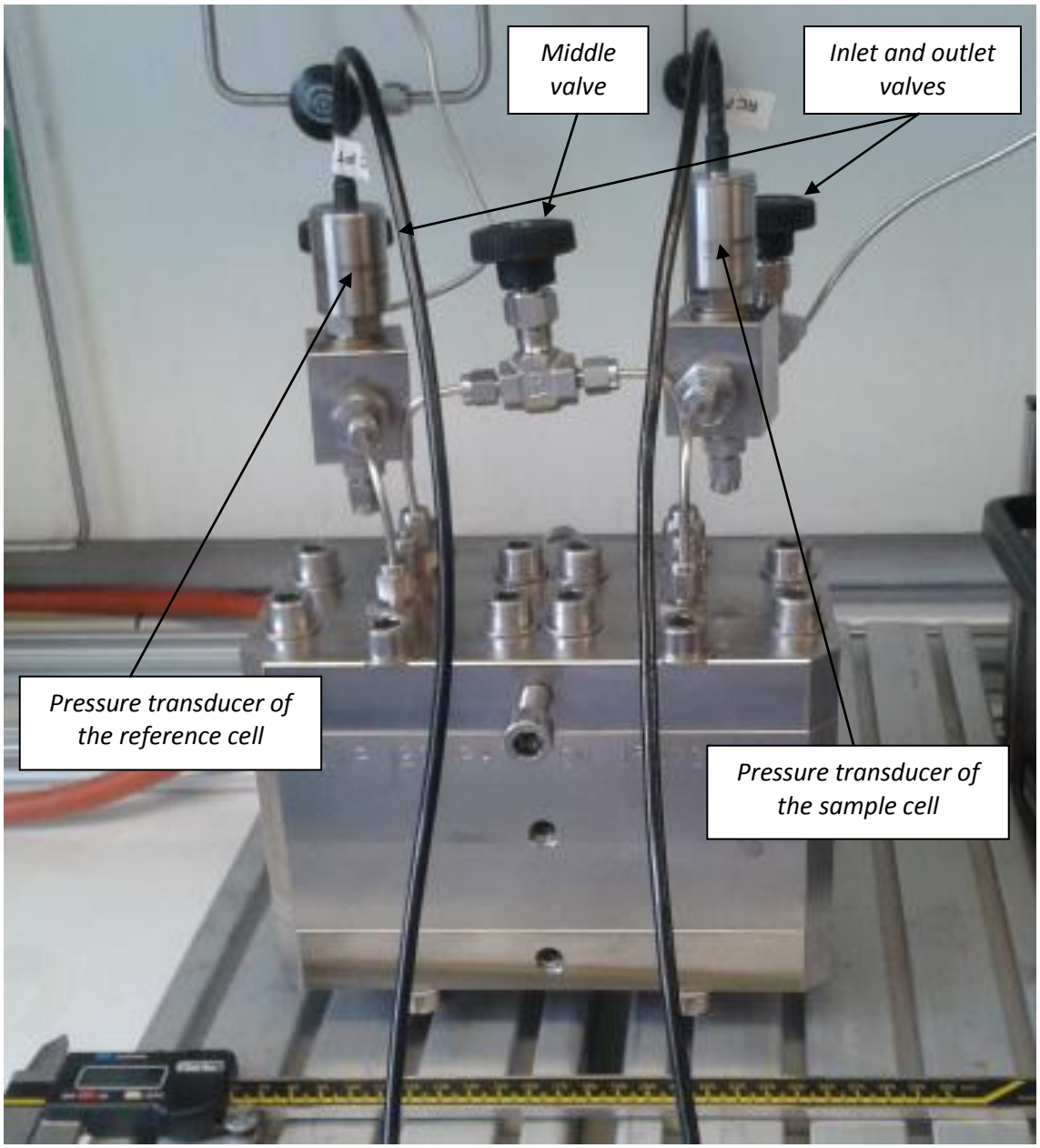

Fig. 3.21. Arrangement of the pressure transducers and three needle valves.

3.4.4. Water bath and temperature controller

A bespoke stainless steel water tank was designed in this study to be able to accommodate the temperature controller as well as the adsorption cell, the pressure transducers, the needle valves and the connecting tubes, as shown in Figure 3.22. The stainless steel water tank with the dimensions of 0.3×0.3×0.3m was constructed by the Engineering Workshop of the Cardiff University.

Deionised water was used as heat transfer liquid and a Thermo Haake temperature controller has been employed to provide a constant temperature inside the water bath with accuracy of ±0.01K (Figure 3.22). In order to minimise the heat loss, the water tank was covered with isolating material and strong cling film was used to cover the tank during long-term experiments to minimise the water evaporation and the heat loss. Excess water evaporation may lead to the exposure of the adsorption cell to the atmospheric temperature and therefore resulting in non-isothermal conditions during the test. The temperature controller may also be damaged if the water level falls below a certain value.

3.4.5. Volume calibration cylinder

The helium pycnometry method was used in this study for void volume measurements in the adsorption cell. A stainless steel double-ended cylinder was purchased from Swagelok as a calibration cylinder including a valve and a rupture disc (Figure 3.23.1). The cylinder is pressure rated to 12.4MPa (1800psig) with calibrated internal volume of 489.18cm^3±0.35%. A heater mat with a thermocouple and two isolating pieces have been used to provide an isothermal condition around the calibration cylinder. More details related to the volume calibration cylinder and helium pycnometery method will be provided in Chapter 4.

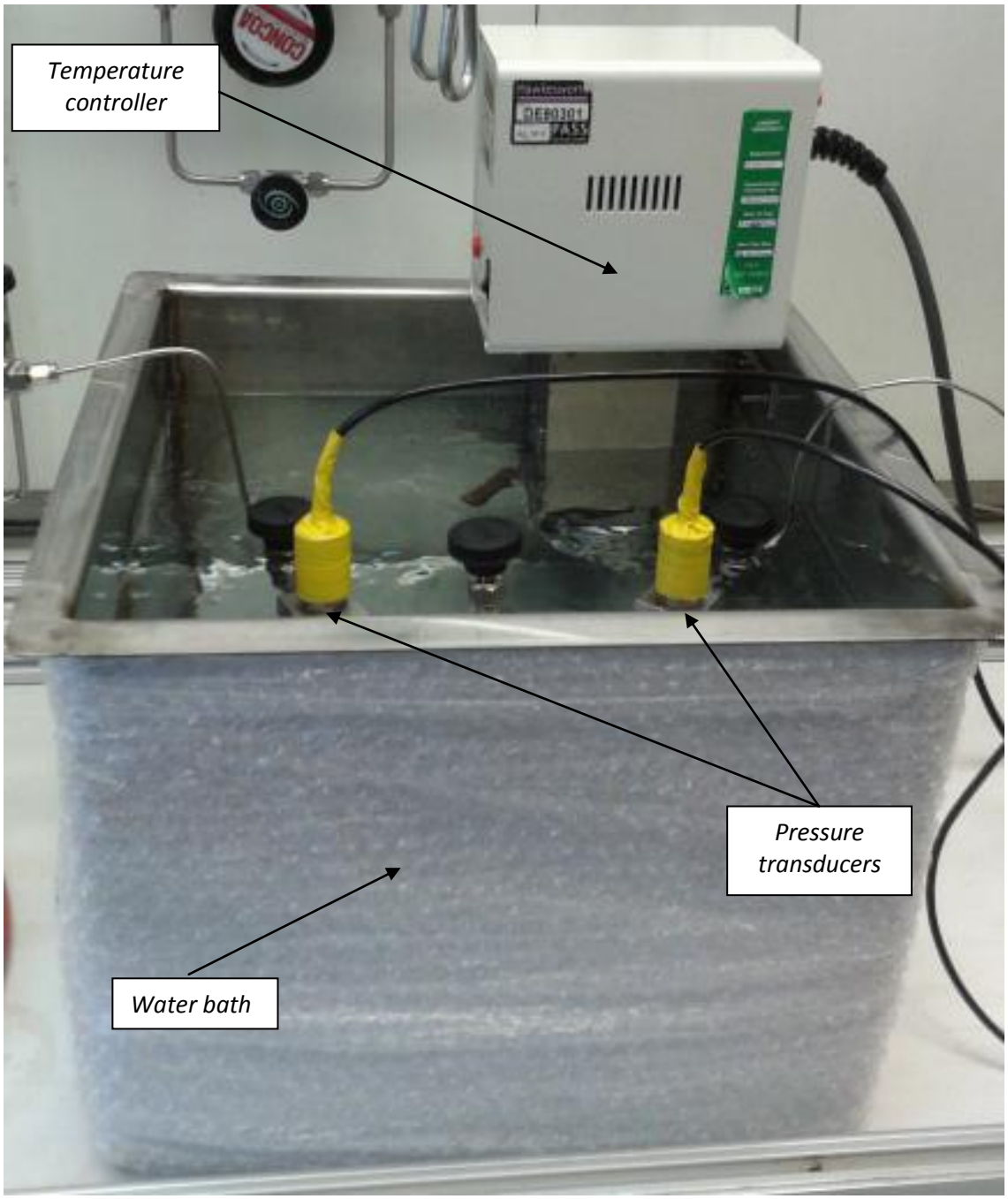

Fig. 3.22. Adsorption cell is placed inside the water bath with a temperature controller. Pressure transducers are covered with waterproof tape to protect from water.

3.4.6. Vacuum pump

A vacuum pump has been employed to evacuate the entire system including the dead volumes inside the pipes and the valves to avoid any contamination of injecting gases with the residual gases from previous tests. The ATEX certified vacuum pump was

purchased from Buchi with final vacuum of approximately -0.09MPa (Figure 3.23.2). The ATEX certification was necessary since the flammable gases such as methane are to be used in the system.

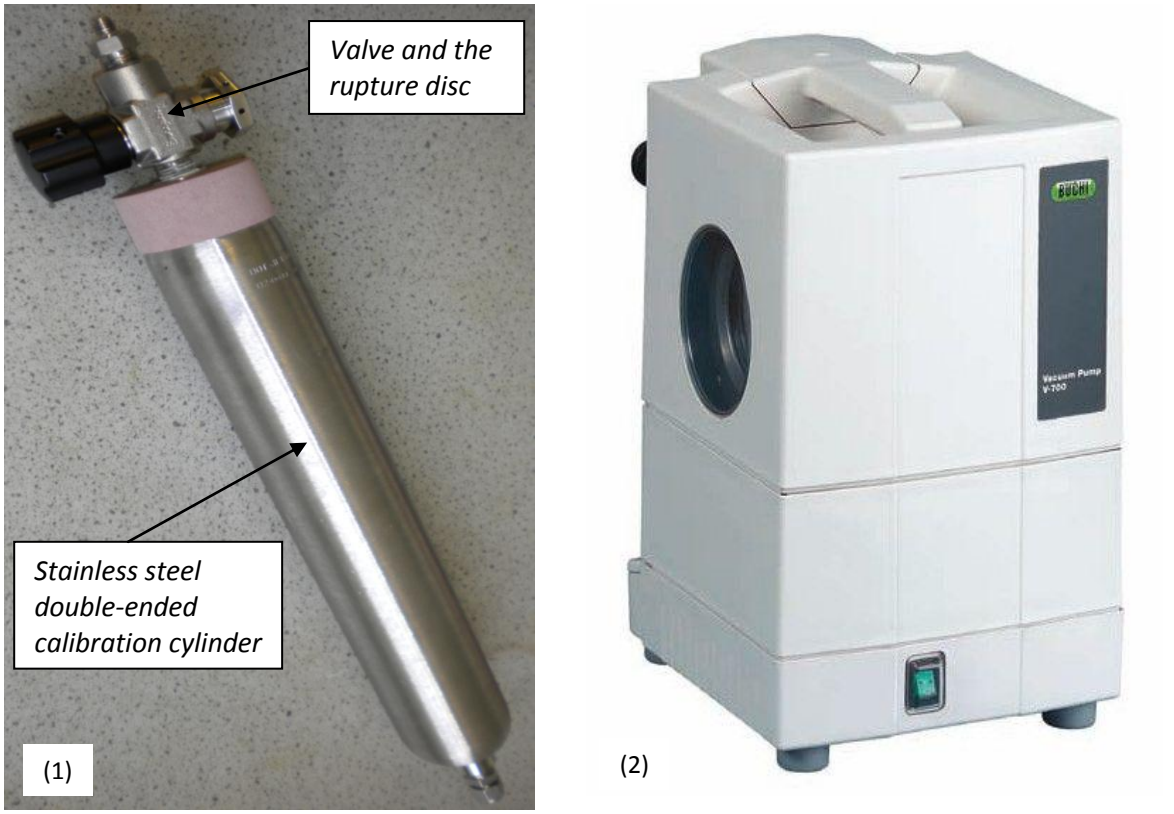

Fig. 3.23. 1) Calibration cylinder, 2) Vacuum pump.

3.4.7. The triaxial cell

Based on the design considerations for the triaxial core flooding system, presented in Section 3.3, the essential parameters such as the ranges of gas pressures, sample size, gas flow rate, material type (SS-316) and the requirements for temperature control system were provided for the manufacturer, GDS Instruments, for construction of the triaxial cell and its related components (Figure 3.24).

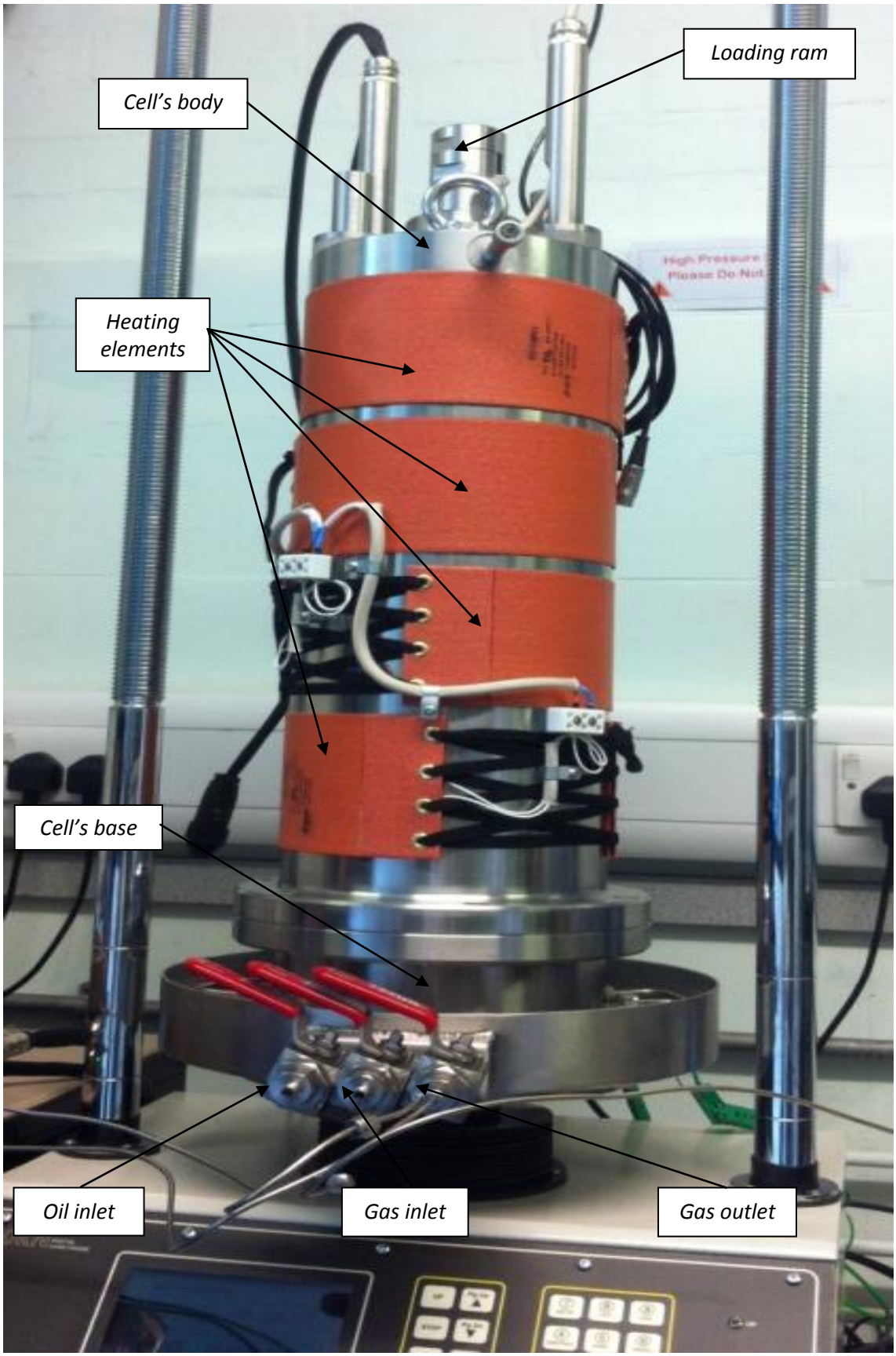

Fig. 3.24. The high pressure triaxial cell and its components, mounted on the load frame.

The triaxial cell accommodates an internal submersible load cell and the local strain transducers for samples with diameters up to 0.07m (two axial and one radial displacement transducers). The cell also includes:

- One base pedestal and one top-cap.
- Two cell pressure connections.
- Three pore/back pressure connections.

The core sample sits within a rubber sleeve and a hydraulic load is applied to the outside of the sleeve in order to apply confining pressures on the core, simulating the overburden pressure. The test gas enters the high pressure cell and passes through a porous plate at the bottom of the sample. Then, it leaves the cell through a similar arrangement at the top after having passed through the test core.

3.4.8. The loading system

An electro-mechanical digital loading frame (Figure 3.25) has been employed to generate axial loads up to 50,000kg.m/s^2 (50kN), applied through a loading ram. The loading system consists of a loading frame and a load cell. The cell base rests on the circular bottom plate and load is applied via movement of the circular plate upward. The loading rate and direction can be controlled using the control box, which has been attached to the loading frame with rates of strain from 1.67×10^{-10} to 1.67×10^{-4}m/s. A high pressure (64MPa) internal submersible load cell is placed between the loading shaft and the top of the loading frame including load ram, load button and electrical connection for data interface with accuracy of 0.1% of Full Range Output (FRO).

3.4.9. The confining system

The confining system is used to provide the pressure required for the testing rock sample by pressurising the hydraulic oil in the confinement cell. The confining system consists of a 32MPa pressure/volume controller with a 2×10^{-4}m^3 oil reservoir (Figure 3.26) with a

volume accuracy of 0.1%. Volume changes can be measured and displayed to $1\times10^{-9}m^3$ (0.001cc). The pressure accuracy is 0.1% of Full Range and pressure can be regulated and displayed to 0.008MPa.

In order to provide the hydraulic forces around the sample (confining pressure), silicone oil 350 Polydimethylsiloxane has been used. Silicone oil has been recommended by ASTM STP-977 (1988) as the most suitable hydraulic liquid to be used in the triaxial cells. Compared to other cell liquids such as de-aired water, glycerin, castor oil and liquid paraffin, silicone oil 350Cs does not pass through the rubber membrane during high pressure tests. It has also shown minimum effect of the rubber membrane (ASTM STP 977, 1988). A liquid suction pump is used to transfer silicone oil from the oil tank to the triaxial cell and vice versa.

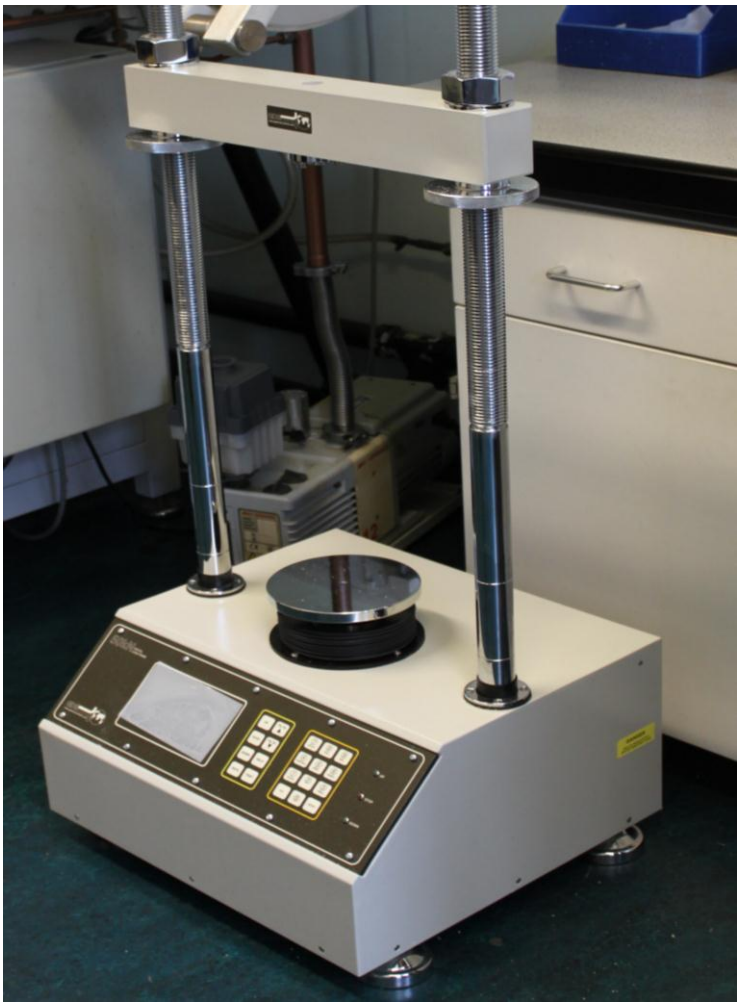

Fig. 3.25. The 50kN load frame.

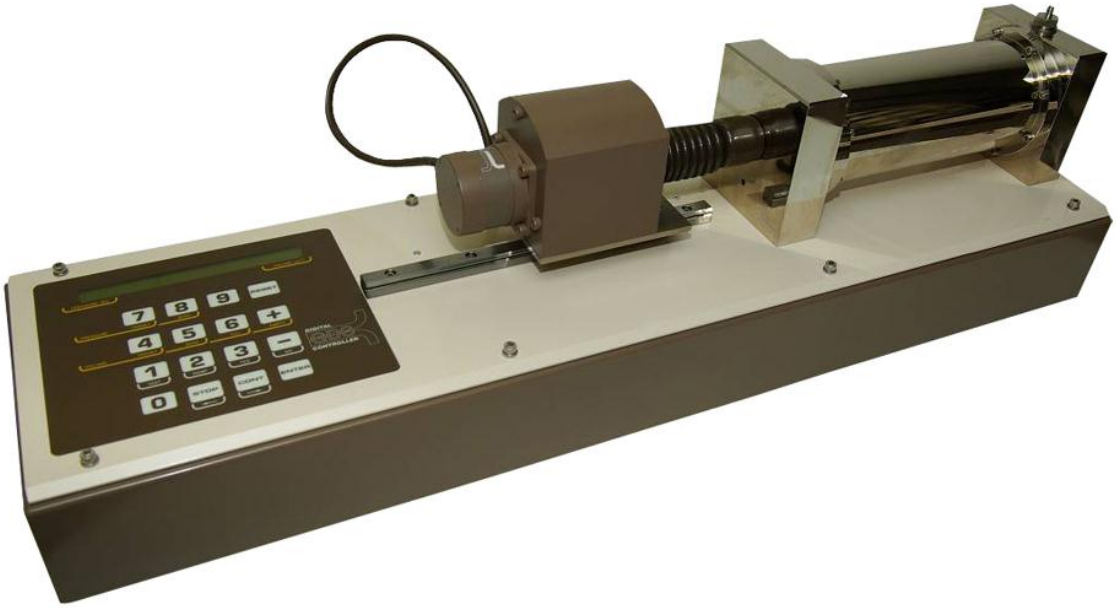

Fig. 3.26. Advanced pressure/volume controller (ADVDPC).

3.4.10. Temperature control system

Since, the experimental set up has been designed to simulate the ground conditions, it is important that the sample inside the high pressure triaxial cell is kept at a constant temperature corresponding to the ground temperature. In order to control the temperature of the testing sample and providing isothermal conditions, a climate control system has been installed on the high pressure cell. The system comprises four heating elements, as shown in Figure 3.24 and a programmable controller. Heating elements provide constant temperature around the sample from ambient temperature to up to 338K (65°C). An aluminum cover with environmental insulation is designated to buffer the cell from changes in atmospheric temperature.

Temperature control for other components such as the pipeline, the valves and the pressure transducers consists of two glass-fibre heating tapes. Each heater tape is 2m long and flexible enough to bend around the pipelines and the connections.

A digital three-zone temperature controller has been incorporated with the heater tapes to control the temperature and to provide an isothermal condition for the pipeline. The

thermal gradient within the sample is measured using three thermocouples attached to the top, middle and bottom of the sample.

3.4.11. Measurement system

The measurement system for the triaxial core flooding apparatus consists of two flow meters, two pressure transducers, three thermocouples and four displacement transducers. All these components are linked to a data logger and their specifications are as follows:

- **Flow meters:** Digital mass flow meters have been designated to measure the inlet and outlet gas flow, at upstream and downstream of the sample, respectively. The flow meters are specified with flow rates of 3×10^{-7} to $23\times10^{-7}m^3/s$ (20-1000 mLn/min). The flow meters are capable of working under both subcritical and supercritical conditions with pressures up to 20MPa and accuracy of 0.5%.

- **Pressure transducers:** The pressure range in the triaxial core flooding system is expected to be from atmospheric pressure (0.1MPa) to a maximum pressure of 20MPa. The pressure control system includes a pressure/volume controller to control the confining pressure and a high pressure regulator with a needle valve to control the pressure of inlet gas. Two 32MPa in-line pore pressure transducers measure the inlet and the outlet gas pressures with accuracy of 0.15%.

- **Displacement transducers:** Two axial and one radial high pressure Linear Variable Differential Transformer (LVDT) local strain transducers manufactured by GDS Instruments have been employed to measure the volumetric deformation of the sample with accuracy better than 0.1% of Full Range Output. The LVDT transducers have a maximum operating pressure of 200MPa in non-conductive oil only. The transducers are for the core samples with diameters of 0.07m only (70mm ±5mm) and capable of working at temperatures up to 333K (60°C).

In addition, a ±0.025m displacement transducer with an accuracy of 0.25% has been used to measure the axial displacement of the sample due to increase or decrease in axial loads applied by the load frame.

3.4.12. Gas supplying unit

The gas supplying system was designed to deliver different gases with controlled pressure and temperatures to both the manometric sorption apparatus and the triaxial core flooding system. The Pressure range supplied by this system covers subcritical and supercritical conditions up to a maximum pressure of 30MPa. The gas temperature can also be adjusted to up to 338K (65°C).

The range of gas flow rates discussed in Section 3.3 was a key factor in specifying the requirements of the gas supplying unit. Therefore, for a low pressure low flow experiment, the experimental gas is to be supplied directly from the gas cylinder. For a high pressure high flow experiment, however, ancillary equipments such as a gas booster and gas reservoirs are incorporated into this unit to ensure that the gas supply remains steady throughout the experiment.

The unit mainly consists of:

- Four gas cylinders including CO_2, N_2, CH_4 and He.
- An air driven gas booster.
- Four pairs of high pressure gas reservoirs.
- Regulators, valves, stainless steel pipelines and high pressure flexible hoses.

The gas supply system accommodates up to four different pure or mixed gas cylinders. It also includes two sets of pipelines, direct and indirect. The direct line connects the gas cylinders to the analysing units directly if the gas pressure of the cylinder is sufficiently high for the specific experiment. The maximum pressure in this line depends on maximum pressure of the gas cylinder. The gas pressure can be regulated using high

pressure regulators on each cylinder. The indirect line is used if the gas pressure inside the cylinder is lower than the experimental pressure. The indirect line comprises a gas booster to pressurise the gas and a set of gas reservoirs to store the pressurised gases to be used for high gas demand experiments, i.e. high pressure/high flow rate. Details of the components are provided in the following sections.

3.4.12.1. Gas cylinders

The gas cylinders are mainly supplied by British gas supplier BOC in standard full-size cylinders. Table 3.4 presents the specifications of the cylinders for the main gases to be used in the experimental work of present study. Each cylinder is equipped with a regulator. An electric CO_2 vaporiser is used for the CO_2 cylinder as the CO_2 cylinders are normally provided in liquid form.

Table 3.4. Specifications of gas cylinders used in this study.

Gas	Cylinder size	Gross weight (kg)	Max. Pressure at 15°C (MPa)	Purity (%)
Helium (He)	L (0.16×0.23m)	87	23	99.99
Carbon dioxide (CO_2)	LK (0.15×0.23m)	99	5	99.99
Nitrogen (N_2)	W(0.15×0.23m)	85	23	99.99
Methane (CH_4)	L (0.16×0.28m)	87	23	99.95

3.4.12.2. Gas booster

An air driven gas booster (model AG-62-50341) manufactured by Haskel International is employed to pressurise gases to the required experimental pressures (Figure 3.27). Syringe pumps are commonly used for pressurising the experimental gases (Hol et al., 2011; Ozdemir and Schroeder, 2009; Mazumder et al., 2006). In this study, however, adopting a gas booster was preferred due to the cost compared to the syringe pump. One limitation of the gas booster is that it has a limited capacity and providing the required volumes of pressurised gas might be time consuming, especially for the experiments with high gas demand. In order to overcome this problem, high pressure vessels are provided as gas reservoirs which are described in the next section.

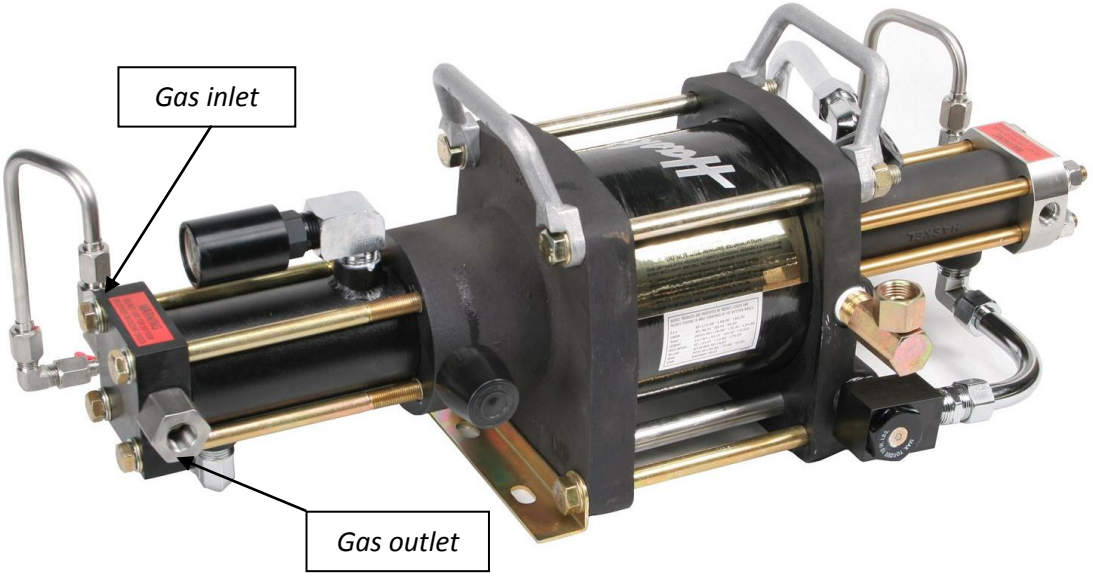

Fig. 3.27. Air-driven Haskel booster.

3.4.12.3. Gas reservoirs

For each gas type, two diving cylinders, one in duty and one on standby, are designated as illustrated in Figure 3.28. The diving cylinders are rated to a maximum pressure of 30MPa with internal volume of 0.012m^3(12L). A regulator adjusts the gas pressure to the desired experimental pressure and conducts the gas from the reservoirs to the experimental units. A pressure relief valve (PRV) is also incorporated into the pipeline with maximum set pressure of 31MPa.

3.4.13. Gas analysing unit

In order to investigate the interaction between the sample and various gas species, the composition of outflow gases is determined using an X-Stream general purpose gas analyser manufactured by Emerson. The X-STREAM gas analyser is a standard 19"/3HU version (Figure 3.29). It comprises two gas channels, one for CO_2 and one for CH_4. Both channels have a defined range of 0 to 100%. Gas analyser can be controlled via a web browser interface. The advantage of this analyser is that it is relatively fast and it is capable of analysing the gas samples simultaneously and continuously over a long period of time. Calibration procedure is also relatively easy.

Fig. 3.28. Gas reservoirs including four pairs of diving cylinders (one standby and one in duty), secured inside a metal rack.

Prior to each test, the gas analyser is calibrated using N_2 as zeroing gas and CO_2 and CH_4 as span gases (experimental gases). According to the manufacturer, the optimum gas flow for this gas analyser is $1.7\times1^{-5}m^3/s$ (1L/min). Therefore, in order to adjust the gas flow, outflow gas is passed through a low flow rotameter mounted on the wall and equipped with a needle valve to adjust the gas flow. The excess gas is then passed through a one-way valve and eventually is vented to the atmosphere via a fume cupboard.

Fig. 3.29. X-STREAM Enhanced XEGP - General purpose gas analyser.

3.5. Conclusions

Based on the objectives of this study, a high pressure laboratory facility has been designed, constructed and commissioned as part of this study to investigate the adsorption/desorption capacity of coal to different gases as well as the reactive gas transport processes in coal.

In conclusion, the specific features of the designed laboratory facility are summerised, as follows:

- Depending on the type of the experiment, a broad range of sample sizes from powdered samples to small intact rocks can be used in the manometric sorption apparatus.

- Due to the relatively small size of the sample cell in the manometric sorption apparatus, it is expected that reaching to the equilibrium state is fast and therefore less time consuming.

- For the triaxial core flooding system, a broad range of stress conditions up to 20MPa can be provided which replicate the ground conditions up to 2000m depths.

- Mechanical expansion/compression of the sample due to variations in effective stress condition, i.e. variations in gas pore pressure or confining pressure, as well as the swelling/shrinkage of the sample due to gas adsorption or desorption can be investigated using the triaxial system and displacement transducers.

- Processes of CO_2 sequestration in coal and enhanced methane recovery (ECBM) using CO_2 and N_2 can be replicated for a broad range of ground conditions, using the triaxial core flooding system.

- The composition of the outflow gases can be analysed simultaneously using the X-STREAM gas analyser for the core flooding experiments. The gas analyser is also capable of working continuously in long-term experiments.

- All components used in the developed facility are compatible with both subcritical and supercritical gas conditions as well as flammable gases such as CH_4.

3.6. References

ASTM Standards, 1988. *ASTM STP-977, 1988*. Advanced triaxial testing of soil and rock. In: *Donaghe R.T., Chaney R.C and Silver M.L. eds.* West Conshohocken, PA: ASTM International.

Carman, P.C. 1956. *Flow of gases through porous media*. London: Butterworths.

Condon, J.B. 2006. *Surface area and porosity determinations by physisorption, measurements and theory*. Amsterdam, Elsevier.

DECC, 2010. *The unconventional hydrocarbon resources of Britain's onshore basins - Coalbed Methane (CBM)*. Depaertment of Energy and Climate Change.

Gensterblum, Y., van Hemert, P., Billemont, P., Battistutta, E., Busch, A., Krooss, B.M., De Weireld, G. and Wolf, K.H.A.A. 2010. European inter-laboratory comparison of high pressure CO_2 sorption isotherms II: Natural coals. *International Journal of Coal Geology,* 84(2), pp. 115-124.

Han, W.S., Stillman, G.A., Lu, M., Lu, C., McPherson, B.J. and Park, E. 2010. Evaluation of potential nonisothermal processes and heat transport during CO_2 sequestration. *Journal of Geophysical Research: Solid Earth,* 115(B7), pp. 1978-2012.

Hol, S., Peach, C.J. and Spiers, C.J. 2011. Applied stress reduces the CO_2sorption capacity of coal. *International Journal of Coal Geology*, 85(1), pp. 142-128.

Jones, N.S., Holloway, S., Smith, N.J.P., Browne, M.A.E., Creedy, D.P., Garner, K. and Duracan S. 2004. *UK coal resource for new exploitation technologies.* Department of Trade and Industry. Report No. Coal R271 DTI/Pub URN 04/1879.

Langmuir, I. 1918. The Adsorption of Gases on Plane Surfaces of Glass, Mica and Platinum. *Journal of American Chemical Society*, 40(9), pp. 1361-1403.

Mazumder, S., Karnik, A. and Wolf, K.H. 2006. Swelling of coal in response to CO_2 sequestration for ECBM and its effect on fracture permeability. *SPE Journal*, 11(3), pp. 390-398.

Mazzotti, M., Pini R., and Storti G., 2009. Enhanced coalbed methane recovery. *The Journal of Supercritical Fluids*, 47(3), 619-627.

Mohammad, S., Fitzgerald, J.E., Robinson, J.R.L. and Gasem, K.A.M. 2009. Experimental uncertainties in volumetric methods for measuring equilibrium adsorption. *Energy and Fuel,* 23(1), pp. 2810-2820.

Murthy, V.N.S. 2003. *Geotechnical Engineering: Principles and practices of soil mechanics and foundation engineering*. New York: Marcel Dekker.

Ozdemir, E. and Schroeder, K. 2009. Effect of moisture on adsorption isotherms and adsorption capacities of CO_2 on coals. *Energy and Fuels*, 23(1), pp. 2821-2831.

Peng, D-Y. and Robinson, D.B. 1976. A new two-constant equation of state. *Industrial and Engineering Chemistry Fundamentals*, 15(1), pp. 59-64.

Smits, A.J. and Dussauge, J.P. 2006. *Turbulent Shear Layers in Supersonic Flow.* 2nd ed. New York: American Institute of Physics.

Süli, E. and Mayers D.F. 2003. *An introduction to numerical analysis*. Cambridge: The University Press.

Tateishi, T. 1980. *Method for preventing sedimentation of finely powdered coal in colloidal fuel*. US-Patent 4202670.

Chapter 4

Material and Methods

4.1. Introduction

This chapter presents the material properties and methods which were employed to conduct the experimental studies of this research. The main objective of this chapter is to provide the details of the experimental procedures and measurement methods that have been utalised to investigate the flow and interactions of high pressure gases with coal using the developed laboratory facilities described in Chapter 3.

In section 4.2, a brief description about the coal samples used in this study is presented. The sampling procedure and details of preparation of powdered coal samples for adsorption/desorption measurements and intact samples for core flooding tests are included in this section.

Section 4.3 describes the coal characterisation tests carried out on coal samples in this study. This section explains the standard methods that have been followed during the coal characterisation. The results of the Proximate and Ultimate analyses of coal samples are presented. The physical characteristics such as density and porosity of the coal samples are also provided in this section.

The methodology used to define the temperature during gas adsorption/desorption measurements and core flooding experiments is described in Section 4.4.

In Sections 4.5, the manometric method adopted for measuring the gas excess adsorption/desorption isotherms in coal is provided in detail. In addition, the helium pycnometry method that has been adopted for calibration of the void volumes (internal volumes) of the reference cell and the sample cell is described in this section.

Section 4.6 presents the experimental procedure related to the gas flow and permeability measurements using the triaxial core flooding system. Step by step assembling procedure used for the triaxial cell and preparations required for the measuring instruments such as the displacement transducers are provided here. The steady-state gas permeability measurement method employed for the permeability measurements in this study is described in this section.

The methodology adopted for the estimation of the volumetric deformations of the coal samples during core flooding experiments has been provided in Section 4.7. This includes the measurement methods of sorption-induced swelling/shrinkage in coal as well as the volumetric strain of the coal sample as a result of variations in effective stress conditions, i.e. mechanical deformations.

The concluding remarks about material properties and the experimental methods are summarised in Section 4.8.

4.2. Coal samples and sample preparation methodology

Coal samples for this study were obtained from the Unity Mine in South Wales, UK with coordinations of 285592E, 202432N. Blocks of coal with dimensions approximately between 0.5m and 1m were collected from 6-ft seam located at 550m depth. Figure 4.1 shows the location of the Unity Mine and other active mines in the area.

Since coal rapidly and irreversibly adsorbs atmospheric oxygen, efforts were made to maintain the samples isolated from the atmospheric environment immediately after collection from the site. The coal samples were sealed using cling film. The sealed samples were then labeled and transferred to the laboratory. The coal samples were removed from the seal whenever required to be placed in the sample cell for testing or to be prepared for coring.

4.2.1. Preparation of the powdered coal samples

In order to conduct adsorption or desorption experiments, the coal samples were ground down to a certain size range to achieve equilibrium over a practical period of time, as recommended by Massarotto et al. (2010).

The procedure used for preparation of powdered sample was based on ASTM D-2013 including drying, crushing, dividing, and mixing the sample. Following ASTM D-2013 and in

order to minimize any moisture contamination, air-drying of samples were undertaken. The air-drying stage is important as the presence of excess moisture within the coal sample can influence the coal properties such as sorption capacity, surface area, pore size, density, and porosity (Speight, 2005; Ozdemir, 2004).

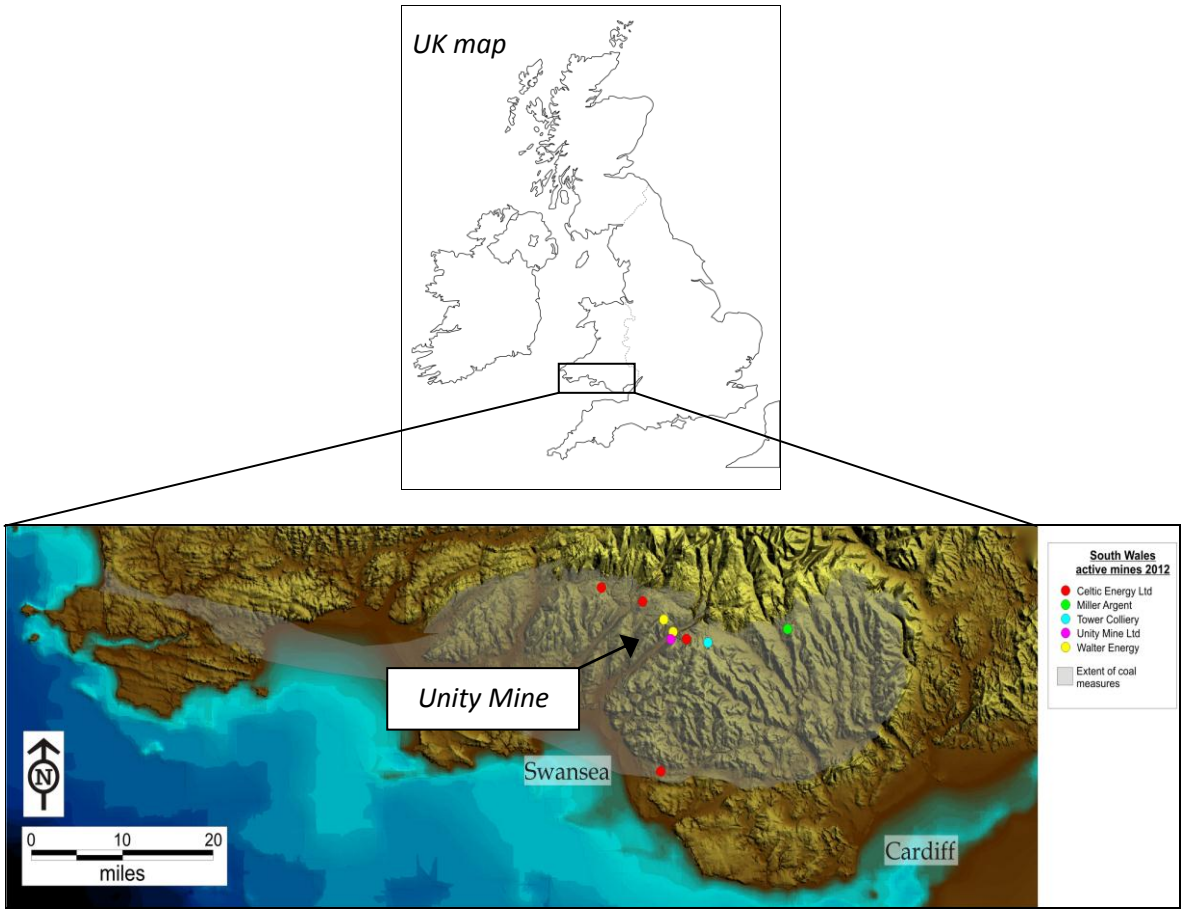

Fig. 4.1. South Wales Coalfield and the locations of the Unity mine and other active mines in the region.

Crushed and ground samples for coal characterisation testing were passed through a 212µm sieve (ASTM D-5142; ASTM D-5373). For the adsorption and desorption measurements, the crushed samples were size distributed using a series of sieves ranging from 0.5mm to 2mm (Figure 4.2). Size-distributed samples were sealed and labeled separately in air-tight containers, and then were stored in a refrigerator to be used in the experiments.

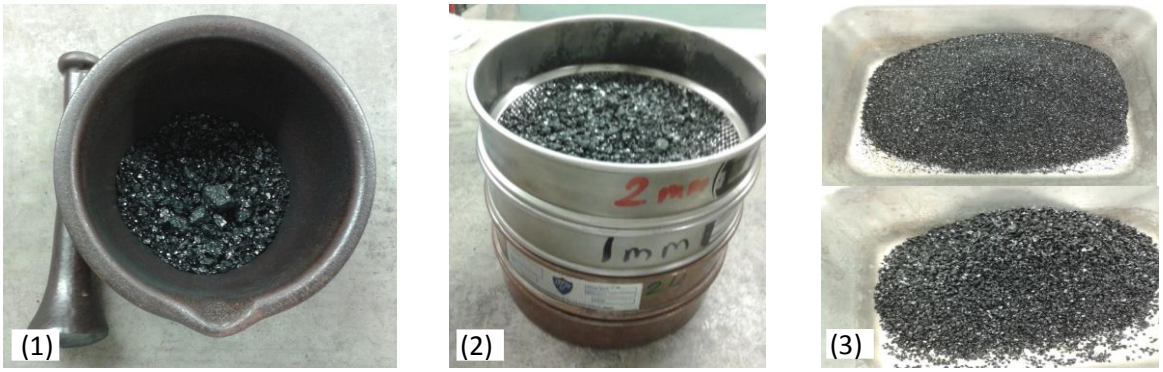

Fig. 4.2. Sample preparation for adsorption/desorption tests; 1) Crushing/grounding, 2) Sieving, 3) Size-distributed and air-dried samples.

4.2.2. Preparation of the core samples

The core samples were drilled out of large blocks of coal using a coring machine, as shown in Figure 4.3. A diamond core drill bit with 0.07m internal diameter was used to drill the core samples. The core samples were then cut into the required lengths using a diamond saw. Special care was taken during the coring and cutting processes to minimise breakage or damage to the coal structure. Any small breakage especially around the edges could potentially damage or puncture the rubber membrane of the sample during triaxial core flooding tests and under the high confining pressures and therefore had to be removed. Among many cut samples the most suitable samples with minimum damage on their structure and minimum broken edges were selected to be used in the triaxial cell.

In order to prevent breakage of the coal samples under high stress conditions, the ends of the specimens were ground and made parallel to each other using a fine sand paper. This would allow a uniform distribution of the axial stresses to both ends of the sample. The core samples were then air-dried for 24hr and wrapped carefully in a cling film. The samples were stored in a refrigerator to be used for the tests. Table 4.1 summarises the initial properties of the core samples used for gas flow and permeability measurements (Sample A) and N_2-ECBM and CO_2-ECBM experiments (Sample B). Although both samples have been drilled from a single block of coal, the slight differences in bulk density values

may be related to the heterogeneity nature of the coals, e.g. ash content, the thickness and number of micro and macro-scale interlayers in coal (ASTM-STP 661, 1978).

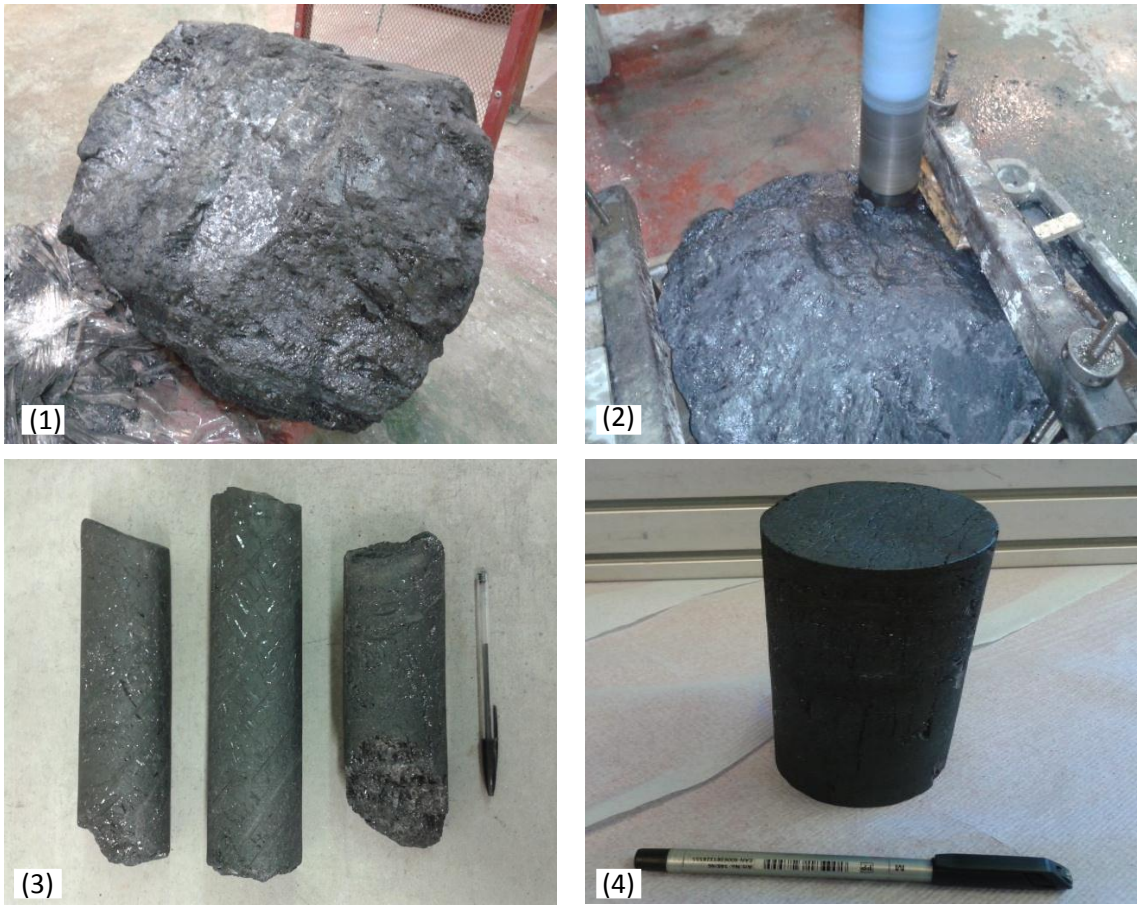

Fig. 4.3. Sample preparation for the triaxial cell; 1) A large block of coal from the coal mine, 2) A coring machine with a 70mm diamond core drill bit, 3) The coal samples after the coring, 4) The coal sample after cutting the ends and polishing.

Table 4.1. The properties and initial conditions of the core samples used in this study.

Properties	**Sample A**	**Sample B**
Moisture condition	Air-dried	Air-dried
Sample diameter, *m*	0.07	0.07
Sample length, *m*	0.12	0.12
Air-dried weight, *kg*	0.61	0.63
Bulk density, kg/m^3	1337	1398

4.3. Coal characterisation tests

A series of coal characterisation analyses have been conducted to determine parameters such as moisture content, ash content, and volatile matter as well as elemental compositions including sulphur content and carbon content. Table 4.2 presents the list of coal characterisation tests that have been carried out including the standard methods adopted for each test. The experimental procedure and the results are presented in the following sections.

Table 4.2. Summary of the coal characterisation tests conducted in this study.

Experiment	Parameter	Method
Proximate analysis	Moisture content, *%*	BS 1016-104.1
	Ash content, *%*	BS 1016-104.3
	Volatile Matter, *%*	BS 1016-104.4
	Fixed Carbon content, *%*	-
Ultimate Analysis	Carbon content, *%*	BS 1016-106.4.2: 1996 BS 1016-106.1.1
	Sulphur content, *%*	BS 1016-106.4.2: 1996 BS 1016-106.1.1
Bulk Density	Bulk Density, kg/m^3	-
Porosity	Porosity, *%*	Rodrigues and Lemos de Sousa (2002)

4.3.1. The Proximate analysis

Proximate analysis has been developed as a simple means of determining the distribution of products obtained when the coal sample is heated under specified conditions (BS 1016-104). The Proximate analysis carried out included:

- Moisture content.
- Volatile matter, consisting of gases and vapours.
- Fixed carbon content, i.e. the non-volatile fraction of coal.

- Ash content, i.e. the inorganic residue remaining after combustion.

The moisture content, the volatile matter and the ash content were all determined by subjecting the coal to prescribed temperature for a certain time intervals, suggested by BS 1016-104. The residue remaining after combustion at the final temperature is called ash. The fixed carbon was defined as the difference of these three values summed and subtracted from 100 (BS 1016-104).

The results of the Proximate analysis are presented in Figure 4.4. The moisture content was estimated to be 1.2%. The amount of the volatile matter was calculated to be 9.6%. The amount of ash content and fixed carbon of the coal samples were estimated to be 4.9% and 84.4%, respectively.

4.3.2. The Ultimate analysis

The standard method for the Ultimate analysis of coal and coke (BS 1016-106) includes the determination of elemental carbon, hydrogen, sulphur, and nitrogen, together with the ash in the material as a whole. Oxygen is usually calculated by difference. In this study, based on availability of the method, only sulphur and carbon contents were measured, and their total difference from 100 was reported as combination of the other elements.

The results of the Ultimate analysis for coal sample of this study are also presented in Figure 4.4. As the Figure shows, the weight percentage of elemental carbon and sulphur were estimated to be 86.4% and 0.8%, respectively, with 12.8% as the difference for other elements.

4.3.3. The density and porosity of coal

In order to estimate the bulk density of the coal, the cylindrical samples (core samples) were air-dried for 24hr at room temperature. Samples volume and mass were then

measured carefully. Using the mass-volume relationship (equation 3-6), the average buck density for the coal samples was found to be approximately 1495kg/m^3.

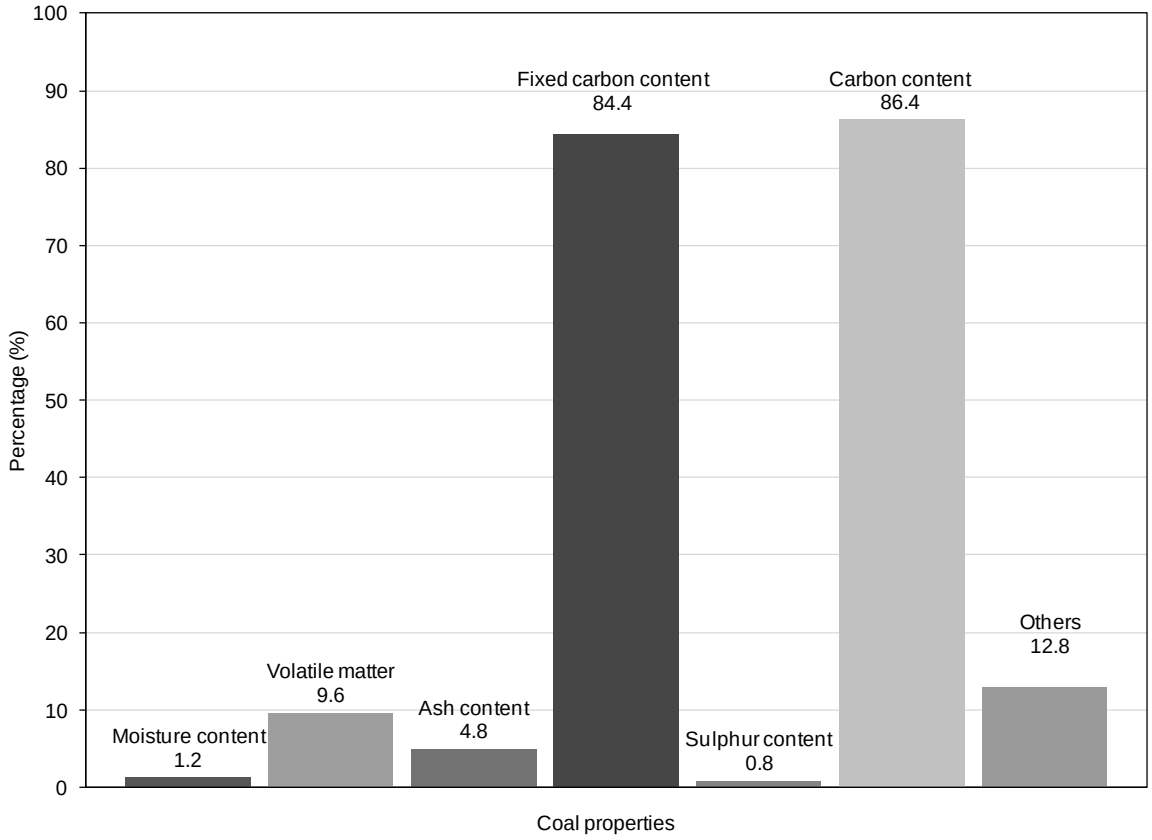

Fig. 4.4. Results of the Proximate and Ultimate analyses on coal sample of this study.

The porosity of the coal sample was estimated using the approximation between coal rank and porosity proposed by Rodrigues and Lemos de Sousa (2002). The carbon content of the coal sample from the Proximate analysis was used to estimate the average coal porosity in accordance with approach proposed by Rodrigues and Lemos de Sousa (2002). As shown in Figure 4.5, the range of coal porosity based on the carbon content measured, i.e. 84%, was estimated to be approximately 2.5 to 6%.

A comparison between the results of the coal characterisations for coal sample of this study and those for various ranks of coal reported by Speight (2005) is provided in Table 4.3. From this comparison it can be confirmed that the coal sample of this study can be classified as an anthracite coal.

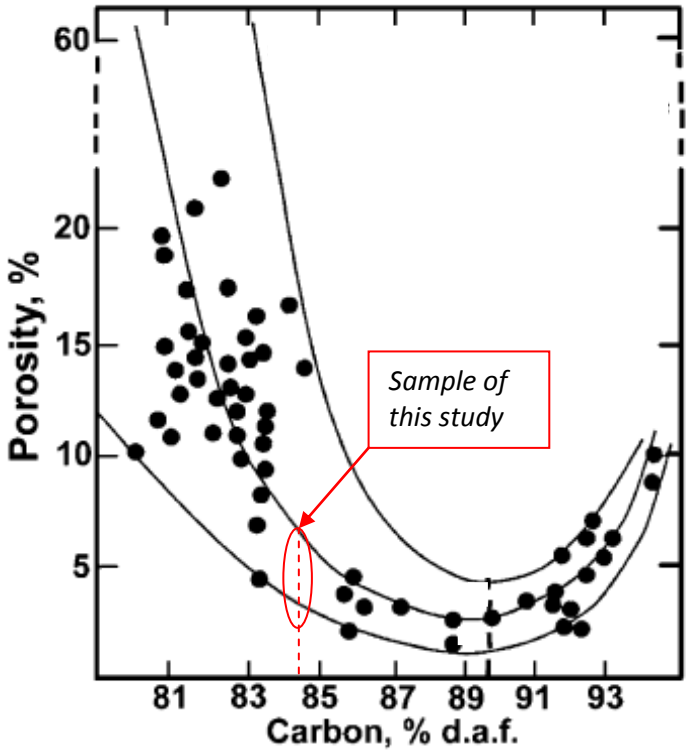

Fig. 4.5. Relationship between porosity and coal rank as reported by Rodrigues and Lemos de Sousa (2002).

Table 4.3. Comparison between coal characterisation results for coal sample in this study and those for various ranks of coals reported by Speight (2005).

Coal properties	Coal sample of this study	Anthracite	Bituminous	Sub-bituminous	Lignite
Moisture (%)	1.19	3–6	2–15	10–25	25–45
Volatile matter (%)	9.56	2–12	15–45	28–45	24–32
Fixed carbon (%)	84.39	75–85	50–70	30–57	25–30
Ash (%)	4.85	4–15	4–15	3–10	3–15
Sulfur (%)	0.79	0.5–2.5	0.5–6	0.3–1.5	0.3–2.5
Hydrogen (%)	-	1.5–3.5	4.5–6	5.5–6.5	6–7.5
Carbon (%)	86.42	75–85	65–80	55–70	35–45
Nitrogen (%)	-	0.5–1	0.5–2.5	0.8–1.5	0.6–1.0
Oxygen (%)	-	5.5–9	4.5–10	15–30	38–48
Btu/lb	-	12000–13500	12000–14500	7500–10000	6000–7500
Density (kg/m^3)	1495.85	1350–1700	1280–1350	1350–1400	1400–1450

4.4. The experimental temperature

The temperature set for the experimental tests was selected based on the in-situ conditions of the coal seam. As such data was not available for the coal samples collected from the Unity mine, the experimental temperature was estimated based on the relationships between the geothermal gradient and depth (Han et al., 2010). The ranges of temperature profile at depths up to 1000m are given as (Han et al., 2010):

$$T_g = T_{ave} + 0.025h, \text{ and} \tag{4-1}$$

$$T_g = T_{ave} + 0.035h \tag{4-2}$$

where, T_g is the ground temperature (°C) at depth h (m) and T_{ave} is the average surface temperature (°C). The diagram shown in Figure 4.6 presents two temperature profiles resulting from equations (4-1) and (4-2).

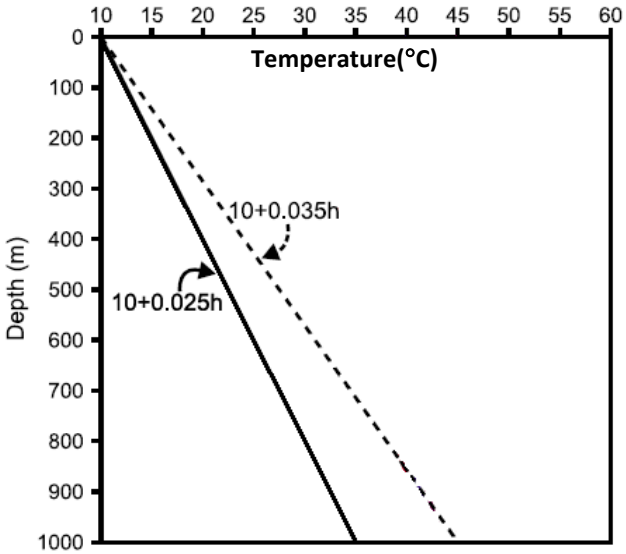

Fig. 4.6. The variation of temperature with depth suggested by Han et al. (2010).

Based on the information provided by Met Office, the average surface temperature of approximately 283K (10°C) has been reported in Wales (Met Office, Wales 1971-2000 averages). Considering the depth at which the coal samples of this study have been collected, i.e. approximately 550m, and by substituting the above values into equations (4-1) and (4-2), the average ground temperature representing the 550m depth is 298K (25°C).

4.5. Adsorption/desorption measurements method

In Chapter 2, various experimental methods related to measurements of gas adsorption/desorption isotherms in coals were discussed. As presented in Chapter 3, the manometric method has been adopted in this study for measuring the excess adsorption/desorption isotherms of different gas species. The manometric apparatus has also been described in Chapter 3. The procedure adopted for these measurements is as follows.

First, the powdered coal sample was carefully weighed to the nearest mg and placed inside the sample cell. Changeable 2 μm filter papers were used to prevent coal particles entering the valves and pipes during the experiment. The loaded cell was then placed inside the water bath and temperature was set to 298K. The measurements were carried out after a few hours to provide thermal equilibration within the system. The pressure transducers were then calibrated at atmospheric pressure.

Figure 4.7 shows a schematic flow diagram of the step by step experimental procedure adopted for manometric measurements. Prior to each test, a vacuum pump was used to evacuate the entire system including the pipes, valves and cells to avoid potential contaminations of injecting gas with the remaining gases from previous tests.

The volumes of the reference cell and the sample cell were measured before and after placing the sample in the sample cell using helium pycnometry method. The details of the helium pycnometry method will be described in section 4.5.1.

In order to determine the gas adsorption isotherm, the gas was admitted to the reference cell at desired pressure. The number of moles of the gas (n_{inj}) in the reference cell was calculated based on the pressure, temperature and volume of the reference cell, based on the ideal gas law, given as (Condon, 2006):

$$n_{inj} = \frac{P_{ref} V_{ref}}{Z_{ref} RT} \tag{4-3}$$

where, P_{ref} is the gas pressure in the reference cell (Pa), V_{ref} is the volume of the reference cell (m^3), Z_{ref} is the compressibility factor, R is the universal gas constant (J/mol.K), and T is the temperature (K). The compressibility factors for CO_2, CH_4 and N_2 gases, as described in Chapter 3, have been calculated based on PR-EOS proposed by Peng and Robinson (1976), i.e. equation (3-5).

The reference cell was then connected to the sample cell. At this stage, gas pressure decreases depending on the void volume (V_v). Immediately after admitting the gas to the sample cell, a sudden fluctuation in gas pressure and temperature may be observed which decays gradually after a short time. This is attributed to the adiabatic (Joules-Thomson) cooling of injected gas (Han et al., 2011; Gruszkiewicz et al., 2009). Pressure decrease continues until the system reaches to the equilibrium condition. The above steps were repeated until the final pressure level was achieved.

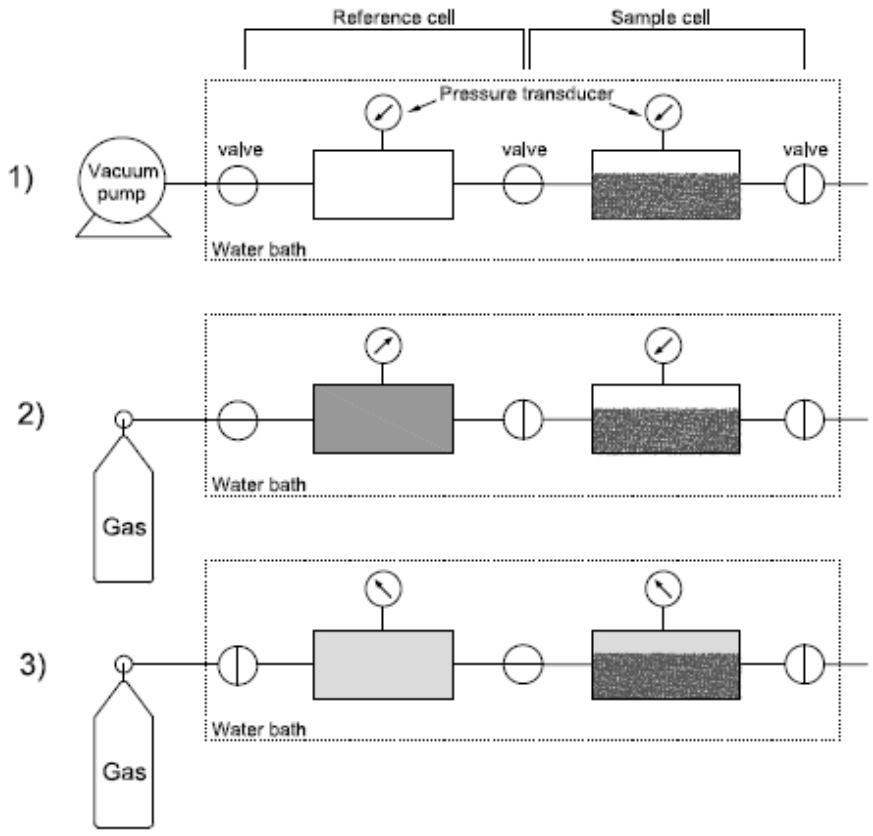

Fig. 4.7. Schematic diagram of the manometric method, 1) prior to each test, the system is evacuated by a vacuum pump, 2) gas is injected into the reference cell with required pressure, and 3) the cells are connected by opening the middle valve. Steps 2 and 3 are repeated until the final pressure level was achieved.

The amount of the unadsorbed gas (n^{ex}_{unads}) was calculated from the conditions of free gas at equilibrium, using (Condon, 2006):

$$n^{ex}_{unads} = \frac{P_{eq}\left(V_{ref} + V_v\right)}{Z_{eq}RT} \tag{4-4}$$

where, P_{eq} is the pressure of free gas at equilibrium (Pa), Z_{eq} is the compressibility factor of the free gas.

The excess adsorption (n^{ex}_{ads}) was then calculated directly from the experimental measurements using the mass balance between the reference cell and the sample cell at each step of gas injection (Condon, 2006):

$$n^{ex}_{ads} = n_{inj} - n^{ex}_{unads} \tag{4-5}$$

By substituting equations (4-3) and (4-4) into equation (4-5), the excess adsorption can be calculated as (Condon, 2006):

$$n^{ex}_{ads} = \frac{1}{RT}\left[\frac{P_{ref}V_{ref}}{Z_{ref}} - \frac{P_{eq}\left(V_{ref} + V_v\right)}{Z_{eq}}\right] \tag{4-6}$$

The cumulative quantity of gas introduced through the reference cell into the sample cell was evaluated by summing up the quantities introduced in each pressure step. Gensterblum et al. (2010) recommended maximum of 20 pressure steps in the manometric method due to the errors for each pressure step that may have an incremental effect on error development in the final step.

The estimate of the total amount of excess adsorbed gas ($n^{ex}_{ads(total)}$) at the end of the j_{th} step was determined from:

$$n^{ex}_{ads(total)} = \sum_{i=1}^{j} n^{ex}_{i} \tag{4-7}$$

The excess adsorption isotherms are typically plotted as the total excess amount of gas adsorbed versus gas equilibrium pressure.

The assumption of a zero-volume adsorbed phase in equation (4-6) can affect the accuracy of the absolute amount adsorbed. At low pressures, the gas phase has lower specific density than the adsorbed phase and the volume of the adsorbed phase is negligible (Gensterblum et al., 2010). As pressure increases, the adsorbed-phase volume (V_{ads}) increases, and the size of the void volume decreases. Therefore, at higher pressures, the excess adsorption underpredicts the absolute amount adsorbed into the coal. The absolute adsorption isotherms can then be approximated by the following function (Gensterblum et al., 2010):

$$n_{ads}^{ex} = n_{ads}^{abs}\left(1 - \frac{\rho_{free}}{\rho_{ads}}\right) \tag{4-8}$$

where, n_{ads}^{abs} is the absolute adsorption (mol/kg), ρ_{free} is the density of free gas at equilibrium (kg/m^3), and ρ_{ads} is the density of adsorbed-phase (kg/m^3).

The density of the free gas was calculated from direct measurements and using relevant equation of state, i.e. PR-EOS. However, determination of the density of adsorbed-phase required certain assumptions. More discussion on methods for estimation of adsorbed-phase density are provided in Chapter 5 where the results of adsorption/desorption isotherms are discussed.

4.5.1. The helium pycnometry

As stated previously, the helium expansion or helium pycnometry method has been adopted to determine the void volumes of the reference cell and the sample cell before and after the sample was placed in the sample cell. The advantage of using helium is that the helium gas has the smallest molecule size and penetrates the small pores easier. In addition, helium is a non-reactive gas and therefore, it does not react with the coal inside

the sample cell. The void volume in this method can be determined from the measured values of the temperature, pressure and volume of the injected gas.

The unknown volume of the cell including the dead volumes of the valves and the pipes were determined by injecting a known quantity of helium from a calibration cylinder (pycnometer) into the cell. The pycnometer is a vessel or a container with a precisely known volume. As described in Chapter 3, in this study a Swagelok stainless steel cylinder has been adopted as calibration cylinder or pycnometer (Figure 4.8). The cylinder is a double-ended sample cylinder, pressure rated to 12.4MPa (1800psig). It includes a high pressure needle valve and a rupture disc. A heater mat and a thermocouple with a temperature controller were used to provide the isothermal condition during the measurements.

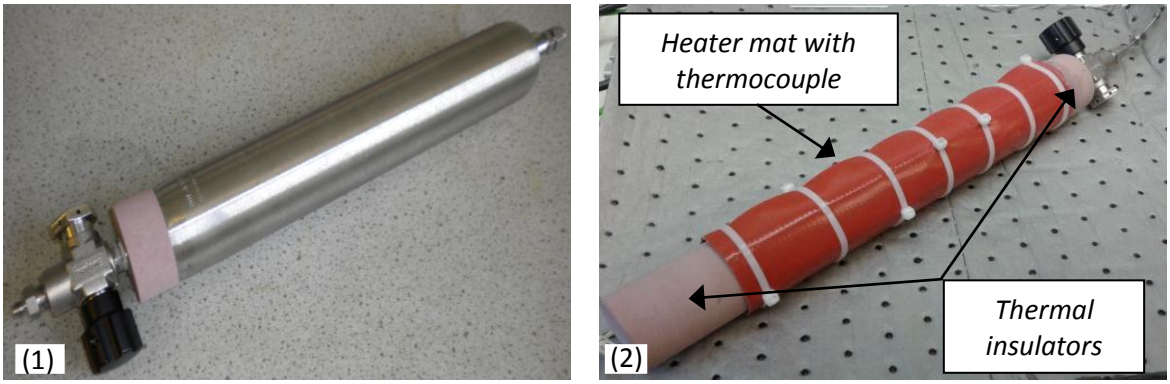

Fig. 4.8. 1) Volume calibration cylinder, 2) Calibration cylinder after attaching the heater mat, thermocouple and thermal insulators.

In order to calibrate the internal volume of the calibration cylinder, a procedure used for volume measurement of the manual glassware i.e. water pycnometry was adopted which was as following:

1. First, the empty calibration cylinder was weighed.
2. It was then filled with deionised and de-aired water and reweighed.
3. Water temperature was recorded during the measurements.
4. The density of water was calculated according to its temperature.

5. The weight difference was then calculated as the weight of the water
6. The volume of the calibration cylinder was calculated by dividing the water mass to the density of water calculated.

The above procedure was repeated several times and the average value for the volume of the calibration cylinder was found to be 489.2cm^3.

Figure 4.9 shows an example of a helium pycnometry test performed which comprised three consecutive pressure steps (A, B and C) to determine the void volume of the loaded sample cell. Circled numbers on the graph indicates the gas pressure in 1) calibration cylinder, 2) in calibration cylinder connected to the reference cell, and 3) in calibration cylinder connected to the reference cell and the sample cell.

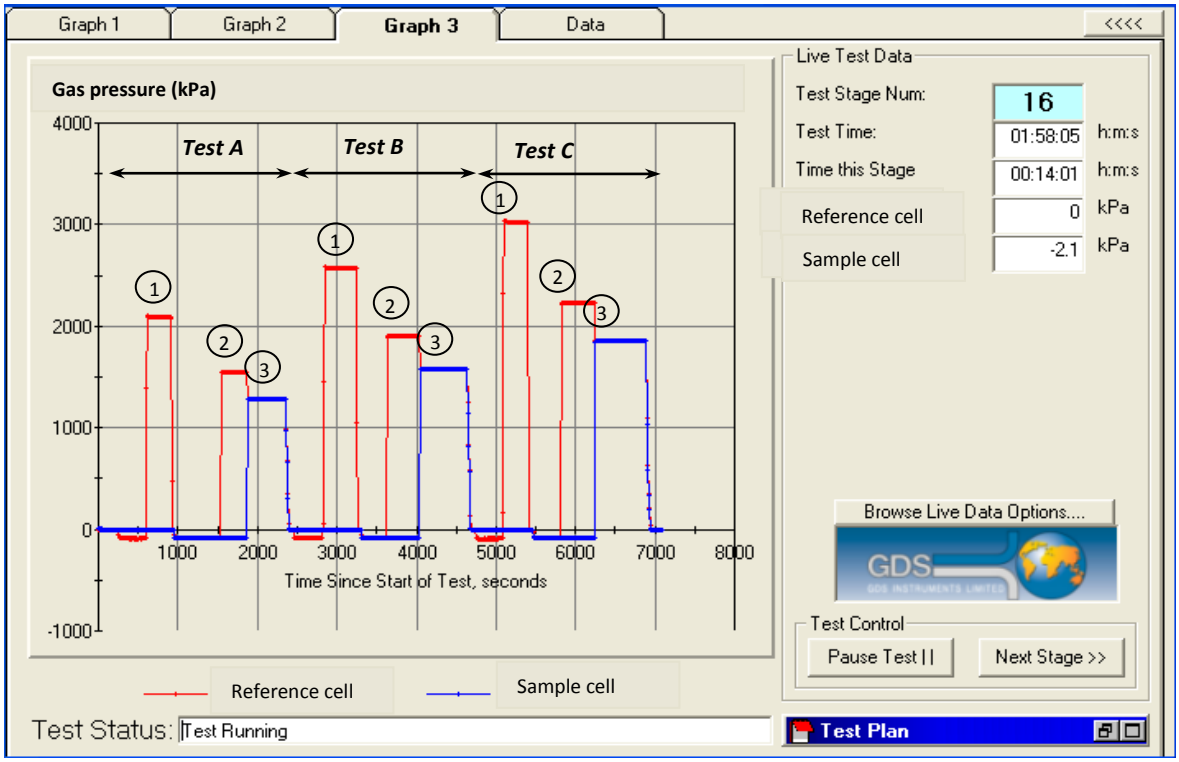

Fig. 4.9. An example of the results of void volume measurements using helium pycnometry method with 3 sequential gas injection pressures.

The void volume (V_{void}) of each cell was calculated using (Pan et al., 2010):

$$V_{void} = \frac{\left(\frac{PV}{Z_{He}T}\right)_{cylinder}}{\left(\frac{P_2}{Z_{He2}T} - \frac{P_1}{Z_{He1}T}\right)_{cell}} \quad (4\text{-}9)$$

where, V is the volume of gas injected from calibration cylinder (m^3), Z_{He} is the compressibility factor of helium. Subscripts "cell" and "cylinder" refer to the conditions in the cell and cylinder, respectively, and subscripts "*1*" and "*2*" refer to the conditions in the cell before and after injection of gas from the cylinder, respectively.

The compressibility factor of helium (Z_{He}) is given as (Sudibandriyo, 2004):

$$Z_{He} = 1 + \frac{(1.47\times10^{-3} - 4.78\times10^{-6}T + 4.92\times10^{-9}T^2)}{P} \quad (4\text{-}10)$$

where, T is the temperature (K) and P is the pressure (atm).

Determining the void volume was carried out carefully as small errors may have a large impact on the mass balance calculation (Gensterblum et al., 2010). In this study in order to minimise the errors, all void volume measurements were performed in multiple series of helium pycnometeries at several gas injection pressures.

In order to investigate the effect of the initial gas injection pressure on the accuracy of the measured void volume, a number of helium pycnometeries were also performed at several initial injection pressures. The results of the volumes estimated for both the reference cell and the sample cell are presented in Figure 4.10. At low pressures, the margin of the errors was much larger. As the initial pressure was increased the estimated values for both reference cell and sample cell showed more convergence. In other words, improved accuracy has been achieved with increasing the initial injection pressures. In addition, the pressure transducers used have a broad range of pressure (20MPa), and their accuracy improves at higher pressures. Therefore, it was concluded that in order to improve the accuracy of the void volume measurements, all measurements should be performed at initial gas injection pressures higher than 1MPa.

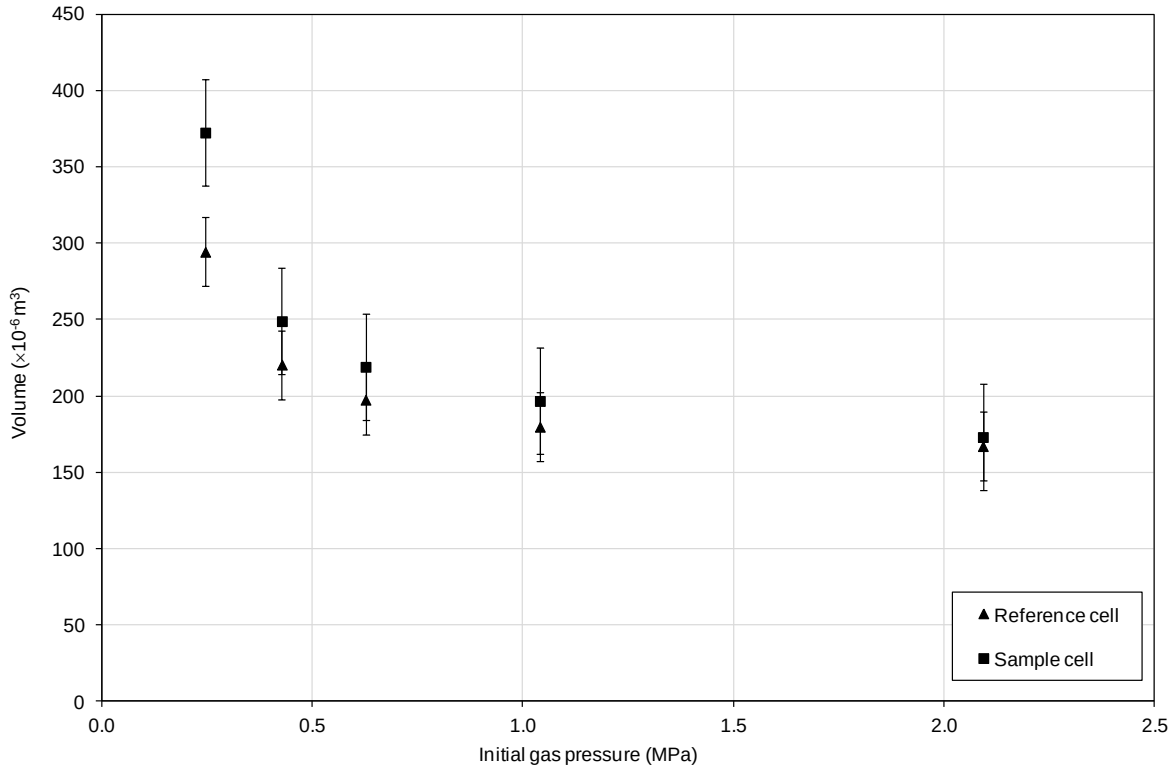

Fig. 4.10. The results of the helium pycnometry performed at several initial gas pressures.

In order to evaluate the precision of the volume measurements with the calibration cylinder, data from several volume measurements for an empty reference cell were analysed. The initial gas pressures in these measurements were ranging between 2 and 4.5MPa. After analysing the results an error margin of ±0.79% was found which is within the acceptable range. Similar analysis was also performed for the empty and loaded sample cell. Similar to the reference cell, the error margin for the empty sample cell was very small. However, for the loaded sample cell the margin of error was slightly larger. This can be attributed to mechanical compression or expansion of the sample during gas injection/extraction process (Mohammad et al., 2009). Another possibility is to lose a small fraction of fine sample particles during gas extraction and vacuum processes. The latest issue however was minimised by using proper filter papers inside the sample cell.

4.6. Core flooding tests

In this section, the experimental procedure used for gas transport studies including assembling the core sample in the triaxial cell and preparing the triaxial cell and related components is described step by step. In addition, the methodology that has been employed to measure the gas flow and permeability of the coal samples to different gases are described in detail.

The processes of sampling, coring and cutting the coal samples were described in Section 4.2. After initial measurements (dimensions and weight), the core sample was wrapped with a thick PTFE tape before placing in a silicon rubber sleeve, as shown in Figure 4.11. The PTFE was used as a non-reactive material which prevents gas diffusion through the rubber membrane into the silicone oil as well as protecting the membrane from any sharp edges that may have remained on the coal surface.

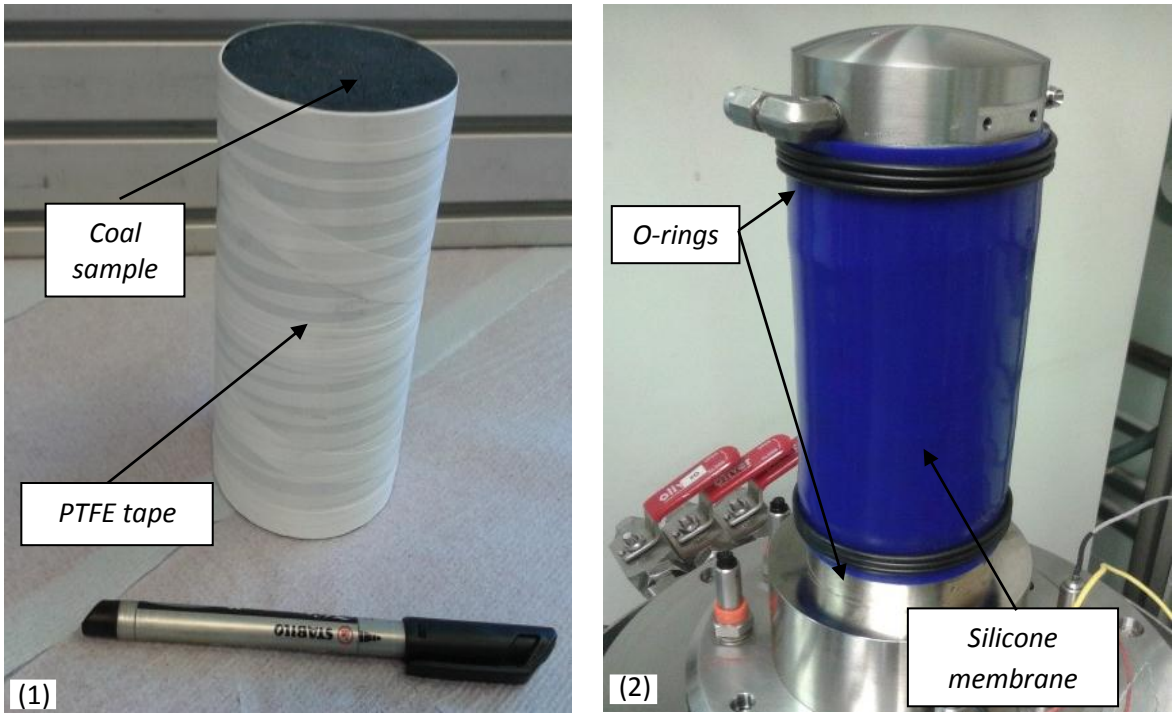

Fig. 4.11. Preparation of the core samples for the triaxial cell, 1) Sample is wrapped with the PTFE tape, 2) Sample is placed in a silicone rubber membrane and secured to the top and the bottom of the cell using the O-rings.

In this study, a 1.5mm thick blue silicone rubber has been used as membrane. In comparison with other materials such as Latex and Nitrile, silicone rubber proved to be stronger material against puncturing and less reactive with chemicals especially with CO_2 gas. O-rings were used to secure both ends of the membrane to the base and top of the cell and to prevent gas leakage into the silicone oil or vice versa.

The displacement transducers, two axials and one radial were attached afterwards to the sample, as shown in Figure 4.12. Three thermocouples were also attached to the top, middle and bottom of the sample to record the temperature variations across the sample during the test.

The top cap was then placed and cell was filled with the silicone oil using a manual oil pump. At this stage, the air bobbles trapped inside the cell or inside the silicone oil were removed. Air bobbles are highly compressible compared to the silicone oil which can affect the performance of the pressure controller.

The inlet and outlet pipes were connected as well as the pressure transducers and the mass flow meters. Both pressure transducers and flow meters have been regularly calibrated throughout the test to achieve the accuracy required. The temperature of the system was set to 298K and kept constant throughout the test. At this point the cell was ready to apply the confining pressure.

A certain amount of confining pressure i.e. 1MPa was applied to avoid oil leakage into the sample during the vacuum process. A vacuum of approximately -0.03MPa to -0.05MPa was applied at downstream of the sample while upstream valve was closed. Depending on the sample conditions, the vacuum process can take few hours to more than a day. After vacuuming the sample, downstream valve was closed and experimental gas was injected at upstream. The applied gas pressure at this stage was very low i.e. 0.2MPa and was increased slowly. It is important that in such experiment, sudden increases of gas pressure or confining pressures should be avoided as it might result in gas or oil leakage as well as failure of the membrane or sample. The upstream pressure was increased step by step to the desired level. Gas injection at fixed pressure was continued to saturate the

sample with gas. Depending on the test conditions and gas type, saturation of the sample can be achieved within few hours or few days. In present study, in most cases saturation has been achieved within 3 to 6 days. The condition for achieving the saturation state was based on pressure decrease less than 0.05MPa over 24hr as suggested by van Hemert et al. (2012).

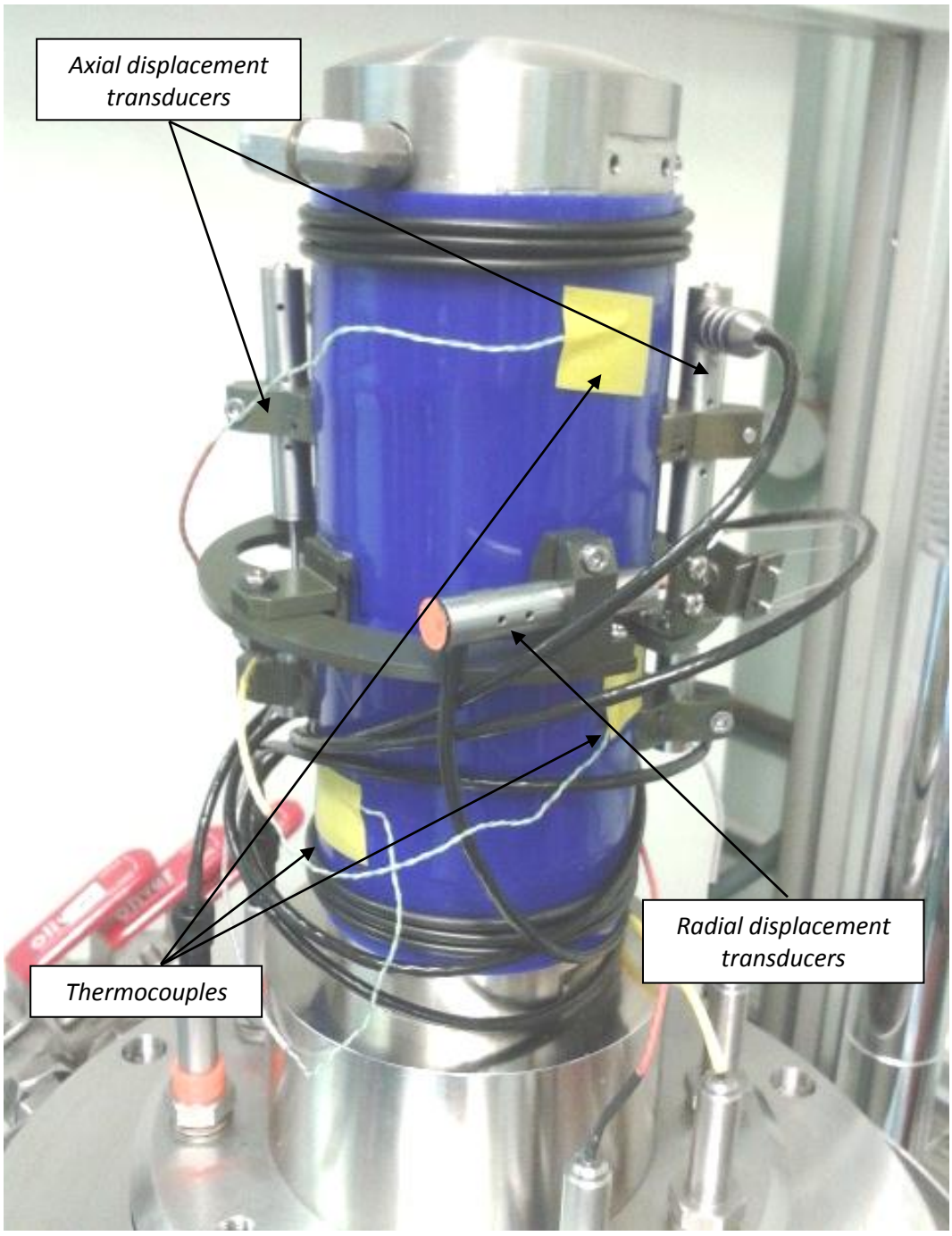

Fig. 4.12. Displacement transducers and thermocouples attached to the sample in the triaxial cell.

4.6.1. Gas flow measurements

Steady-state method has been used to estimate the permeability of the coal samples to various gases. Table 4.4 presents an example of the steps taken to increase the confining pressure and gas pressure during flow rate measurements. The confining pressure was maintained at desired pressure and increased step by step. The gas pressure at upstream was fixed at pressures defined in Table 4.4. The downstream pressure was kept at atmospheric pressure (0.1MPa) at all time. Once the steady-state flow rate was achieved, gas pressure at upstream was increased to the next level. Figures 4.13 to 4.18 present examples of the experimental measurements during the first series of gas flow rate measurements using helium on coal sample A. The effective stresses were calculated as the difference of the confining pressure and the mean pore gas pressure. The mean pore gas pressures were estimated as the average gas pressures at upstream and downstream of the sample.

Table 4.4. Experimental steps of the gas injection pressure and confining pressure during gas flow rate measurements on coal sample A.

Confining pressure (MPa)	Gas injection pressure (MPa)
1	0.2
	0.4
	0.6
2	0.6
	1
	1.5
3	1.5
	2
	2.5
4	2.5
	3
	3.5
5	3.5
	4
	4.5
6	4.5
	5
	5.5

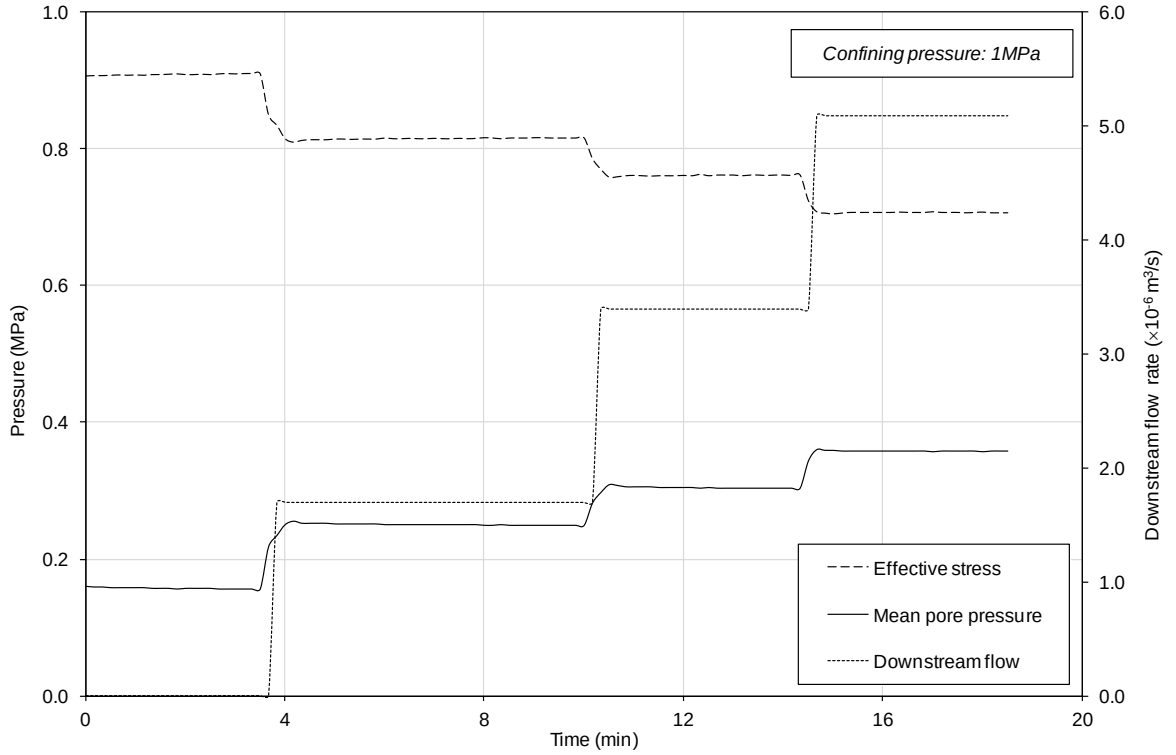

Fig. 4.13. Experimental results of He flow rate measurements at 1MPa confining pressure (temperature 298K).

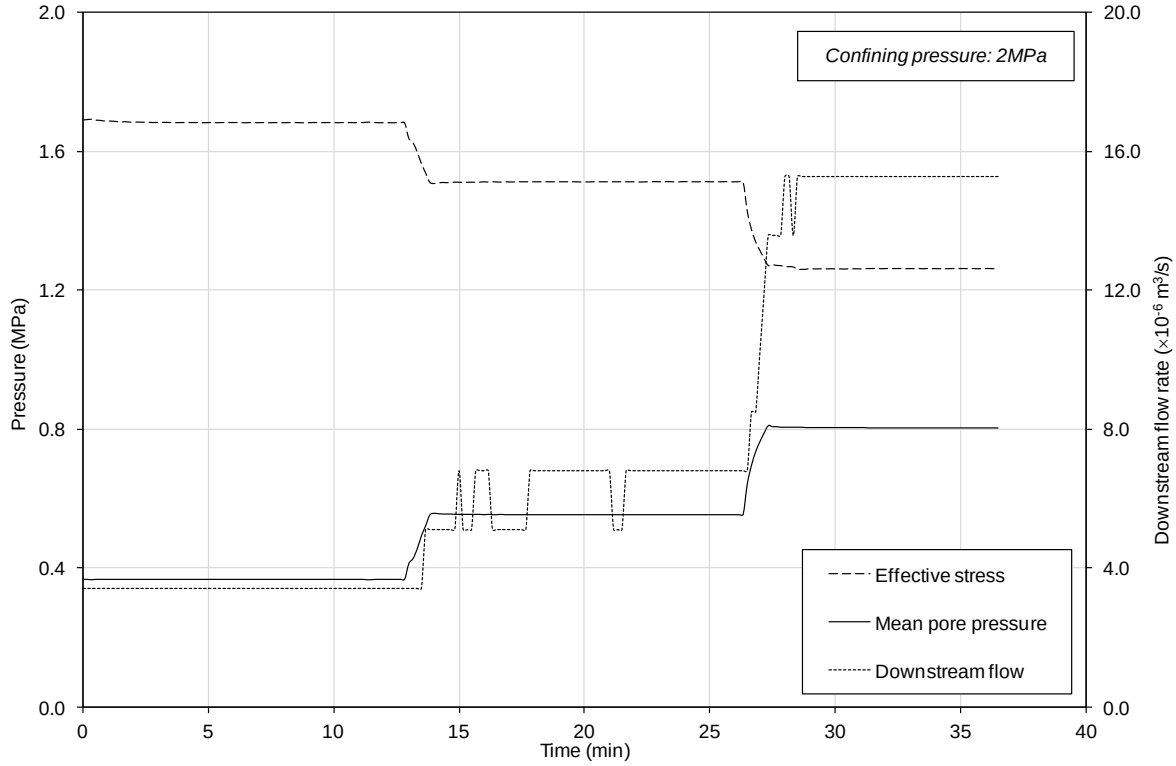

Fig. 4.14. Experimental results of He flow rate measurements at 2MPa confining pressure (temperature 298K).

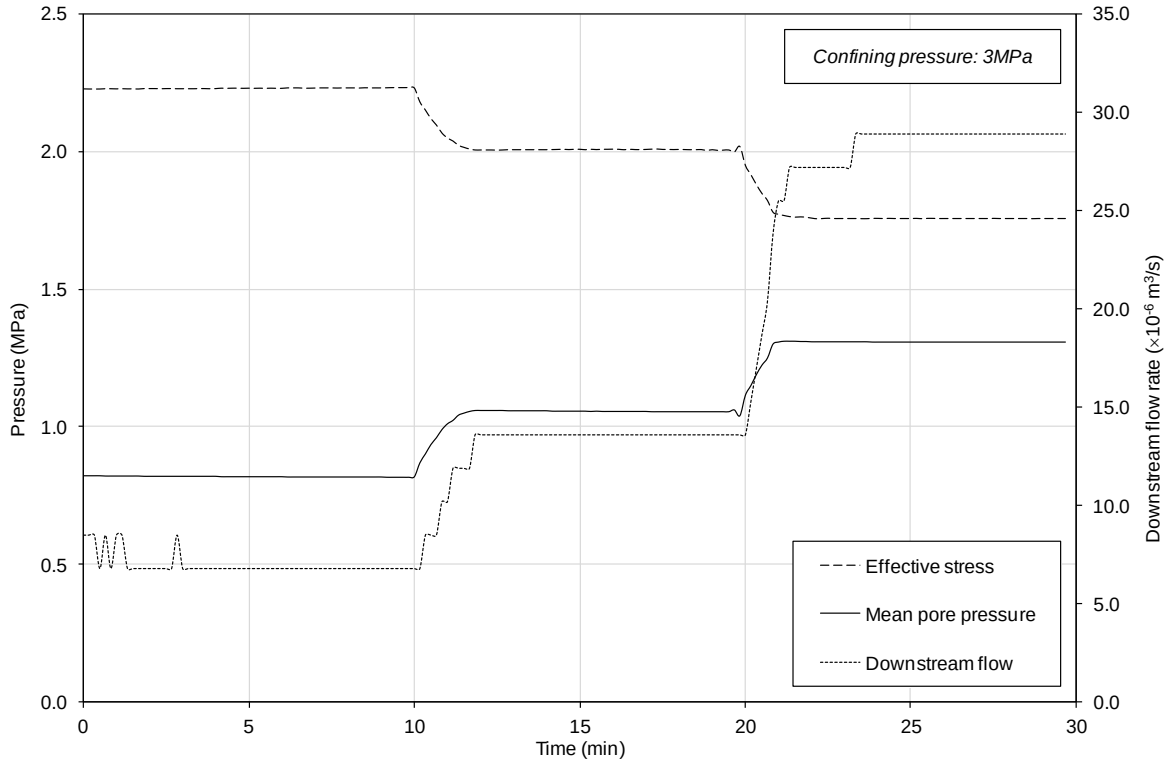

Fig. 4.15. Experimental results of He flow rate measurements at 3MPa confining pressure (temperature 298K).

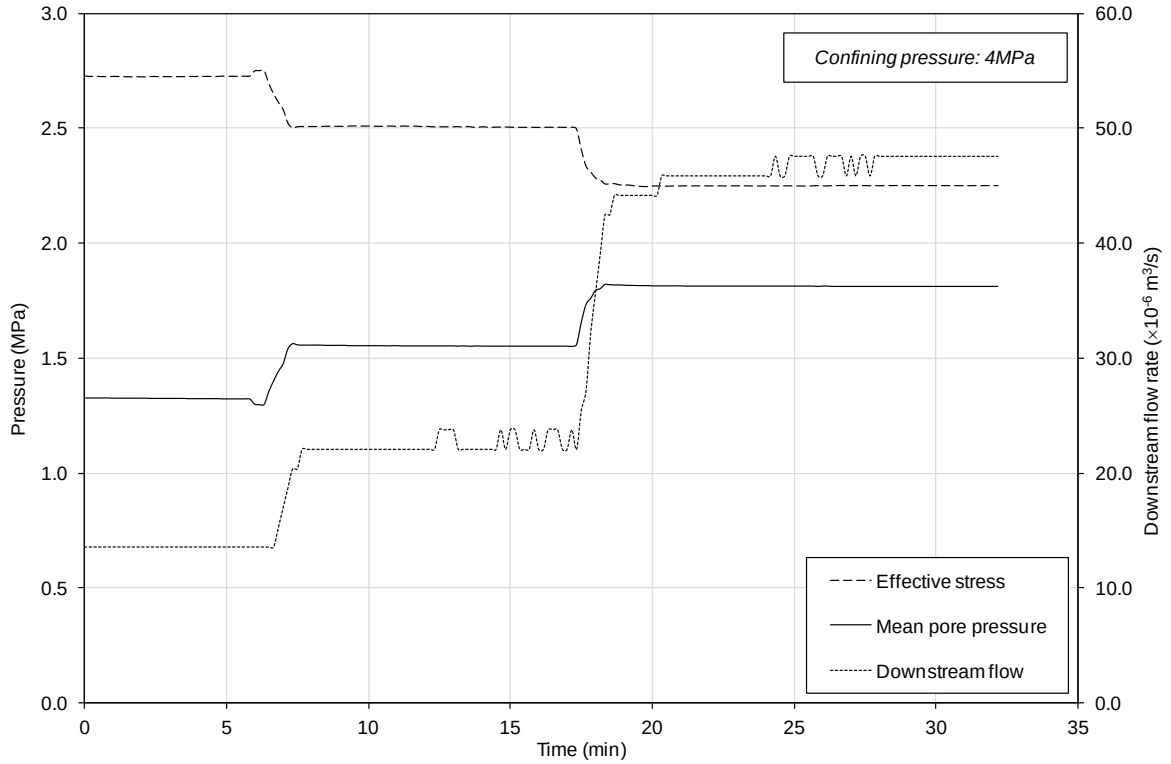

Fig. 4.16. Experimental results of He flow rate measurements at 4MPa confining pressure (temperature 298K).

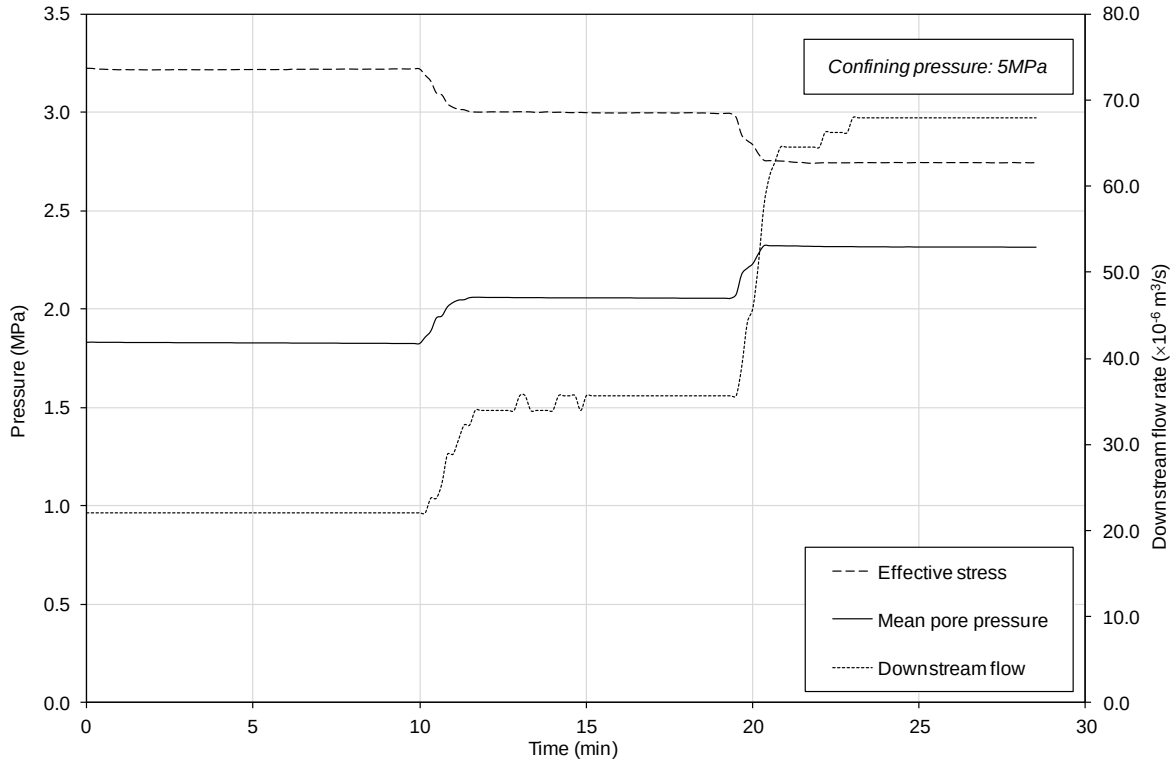

Fig. 4.17. Experimental results of He flow rate measurements at 5MPa confining pressure (temperature 298K).

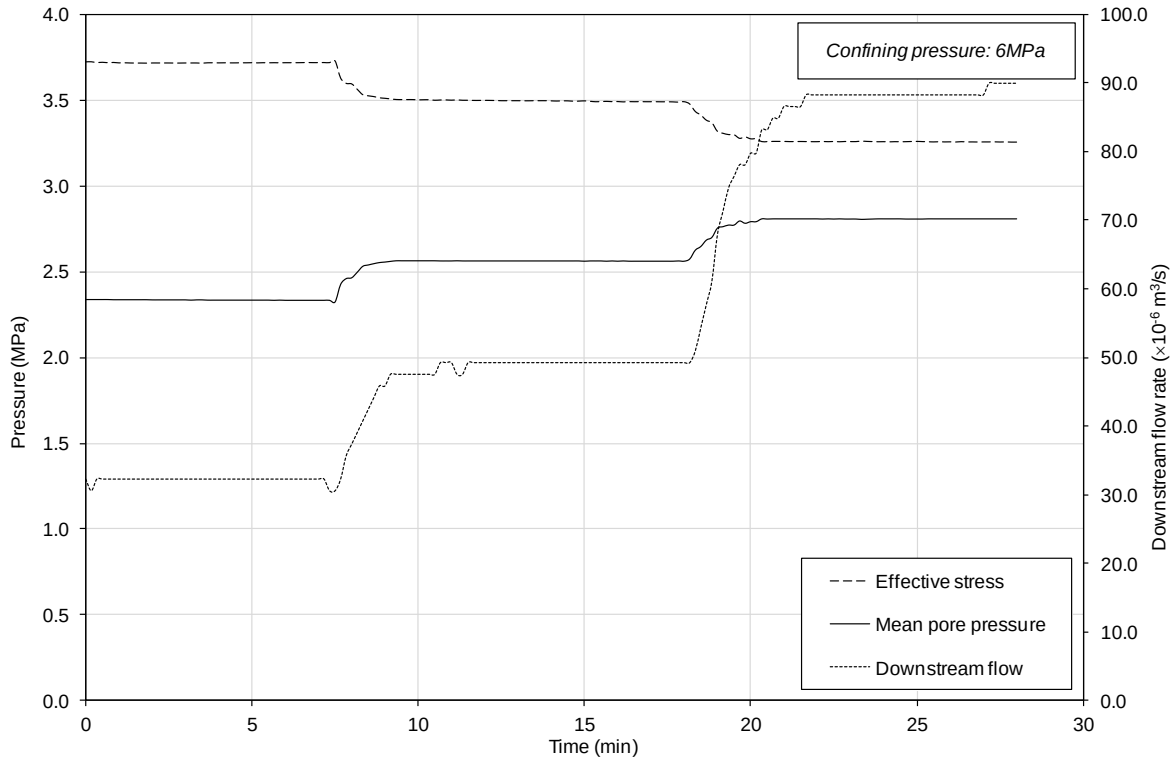

Fig. 4.18. Experimental results of He flow rate measurements at 6MPa confining pressure (temperature 298K).

4.6.2. Calculation of coal permeability to gases

At each steady-state condition the permeability of the coal sample to experimental gases was calculated using Darcy's law. In the case of gases, the rate of flow changes from point to point as the pressure decreases, but the mass rate of flow must remain constant (Carman, 1956). Using the Darcy's law, permeability of the samples to gases can be calculated as (Carman, 1956):

$$k_g = \frac{2Q_0\mu_g LP_0}{A(P_{up}^2 - P_{down}^2)} \tag{4-11}$$

where, k_g is the gas permeability coefficient (m^2), Q_0 is the volumetric rate of flow at reference pressure (m^3/s), μ_g is the gas viscosity (Pa.s), L is the sample length (m), P_0 is the reference pressure (Pa), A is the cross-sectional area of the sample (m^2), P_{up} is the upstream gas pressure (Pa), and P_{down} is the downstream gas pressure (Pa).

The viscosity of gases (μ_g) has been calculated based on the Sutherland formula as function of temperature (Smits and Dussauge, 2006):

$$\mu_g = \mu_{g0}\frac{T_0 + C}{T + C}\left(\frac{T}{T_0}\right)^{3/2} \tag{4-12}$$

where, μ_{g0} is the reference viscosity (Pa·s) at reference temperature T_0 (K), and C is the Sutherland's constant depending on gas species.

The methodology described in this section has been used to analyse the experimental results of this study which will be presented in Chapters 6 and 7.

4.7. Coal swelling and shrinkage measurement

The experimental methods for measurements of swelling/shrinkages in coal as a result of interaction with reactive gases were reviewed in Chapter 2. In the triaxial system of this study, the volumetric strain of the core sample can be estimated in two ways:

- To use the local displacement transducers to measure the axial, radial, and volumetric strain of the core sample.

- To use volume of the displaced silicone oil in the oil pump (pressure controller) to estimate the total volumetric strain of the core sample.

The first method is beneficial when axial pressure is applied to the sample and anisotropic deformation is expected. The volumetric strain of the sample can also be estimated in this method by using two axial and one radial displacement transducers. The major disadvantage of this method is that the local displacement transducers are extremely sensitive to vibrations and if they are not properly attached to the membrane, it is likely that they may fail before or during the measurements e.g. due to adhesive failure when in contact with silicone oil. Displacement of the transducers may also occur when the triaxial cell is filling up with the silicone oil.

In the second method, the volumetric strain of the sample can be estimated using the displaced oil volume inside of the oil pump. In this method, directional or anisotropic deformations cannot be measured. However, this method was found to be more reliable compared to the first method for the experiment in which only volumetric strain of the sample is measured and no axial pressure is applied. The only restrain here is that the silicone oil is to some extent a compressible fluid and its compressibility should be taken into account when volumetric strain of the sample is calculated.

Since the experimental investigations of this study have been conducted under the isotropic confining pressures, the second method has been employed to assess the volumetric deformations of the coal samples. The results of volumetric deformations of the sample during flooding experiments using various gas species will be presented in Chapter 6.

The details of the methodology used in this study to estimate the compression rate of the silicone oil and to calculate the volumetric deformations of the coal sample are provided in the following section.

4.7.1. Compressibility of the silicone oil

In order to estimate the compression rate of the silicone oil, a laboratory experiment was conducted at isothermal condition of 298K. First, the volume of the oil pump was set to zero. Then, the silicone oil inside the pump was pressurised. The oil pressure was increased gradually to a maximum value of 6MPa while volume changes of the pump were recorded. Figure 4.19 shows the results of the volumetric compression of the silicone oil in response to pressure increases up to 6MPa. The results showed that at low pressures (less than 0.5MPa) the silicone oil is highly compressible. As the pressure increases, the compression rate was found to remain almost constant. As shown in Figure 4.19, the average compression rate of the silicone oil at 298K has been estimated to be $1.06\times10^{-7}m^3$/MPa.

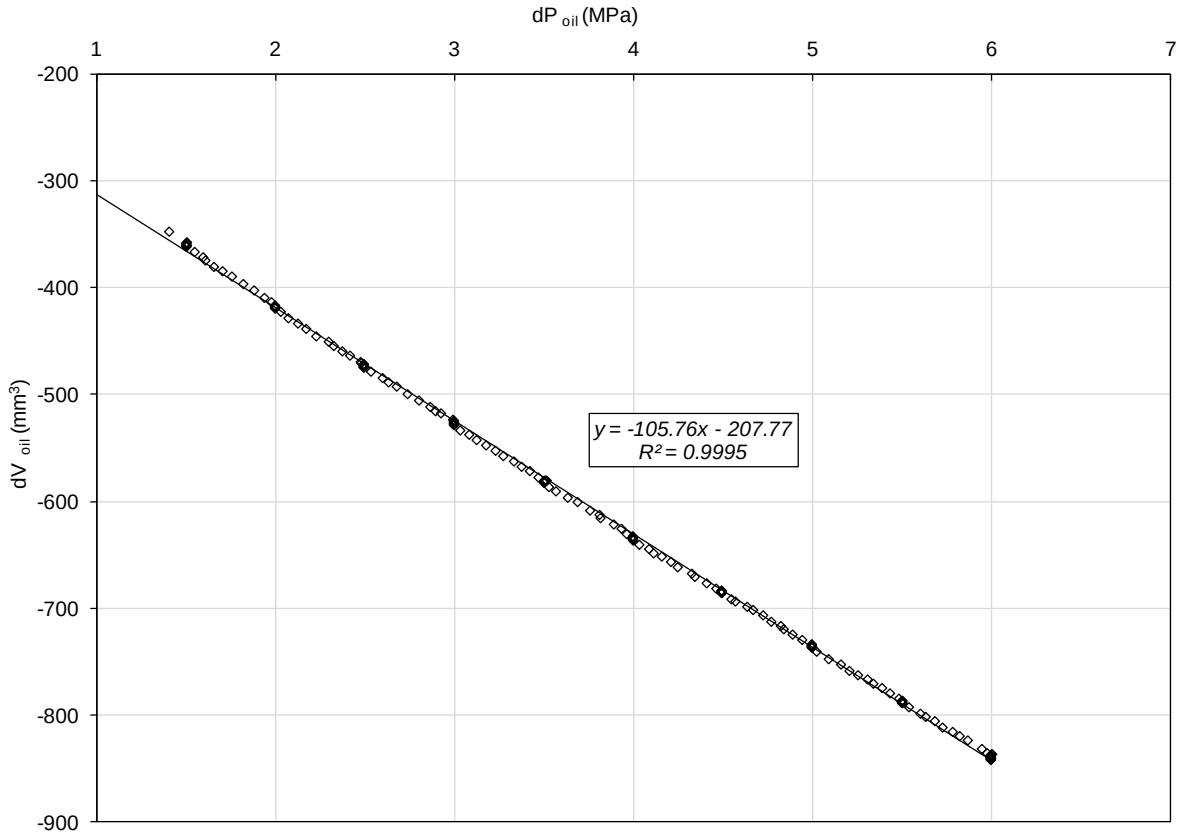

Fig. 4.19. Variation of the volume of silicone oil due to pressure increases up to 6MPa at 298K.

The total volumetric strain of the coal sample (ε_v) associated with 1MPa pressure increase was then calculated as:

$$\varepsilon_v = \frac{dV_{oil} - 1.06 \times 10^{-7}}{V_{s0}} \times 100 \tag{4-13}$$

where, ΔV_{oil} is the displaced volume of the silicone oil inside the pump (m^3), and V_{s0} is the initial volume of the coal sample (m^3).

As stated previously, the experimental results of volumetric strain measurements on coal sample A of this study will be presented in Chapter 6.

4.8. Conclusions

Details of the sampling procedure and preparation methods for both powdered coal samples and core samples are presented in this chapter. Powdered coal samples were used in coal characterisation tests and adsorption/desorption measurements, using the manometric sorption apparatus. The core samples were used for gas flow and permeability measurements in coal using the triaxial core flooding system.

The physical and chemical properties of the coal samples were investigated. The results of Proximate and Ultimate analyses showed that the coal samples of this study were high rank coals with 86% carbon content. The average bulk density and porosity of the coal samples were estimated to be 1496kg/m^3 and 6%, respectively.

The experimental temperature for this study was estimated to be 298K based on the average geothermal gradient of the region (South Wales) at the depth of which the coal samples have been obtained.

The manometric method adopted for adsorption and desorption measurements on coal was described in detail including the procedure for experimental measurements as well as the calculation methods. In addition, the levels of accuracy and precision for the

helium pycnometry method adopted for the void volume measurements were examined and found to be within the acceptable ranges.

The step by step preparation of the triaxial system for core flooding experiments and gas flow measurements under confined conditions have been presented. The Steady-state method that was used for the gas flow and permeability measurements is described and some examples of experimental results from the first helium flow measurements are presented.

The methodology used to measure the volumetric strain of the coal sample during the core flooding experiments is described. The volume of the displaced silicone oil inside the oil pump was used to evaluate the volumetric strain of the core sample. The compression rate of the silicone oil at the corresponding experimental temperature was measured and accounted in the calculations of volumetric deformations.

4.9. References

ASTM Standards, 2012. *ASTM D-2013. Standard practice of preparing coal samples for analysis. vol. 05.06.* West Conshohocken, PA: ASTM International.

ASTM Standards, 2009. *ASTM D-5142. Standard test methods for Proximate analysis of the analysis sample of coal and coke by instrumental procedures. vol. 05.06.* West Conshohocken, PA: ASTM International.

ASTM Standards, 2013. *ASTM D-5373. Standard test methods for instrumental determination of carbon, hydrogen, and nitrogen in laboratory samples of coal. vol. 05.06.* West Conshohocken, PA: ASTM International.

ASTM Standards, 1978. *ASTM STP-661, 1978*. Field description of coal. In: *Dutcher, R.R. eds.* West Conshohocken, PA: ASTM International.

British Standards Institution, 1999. *BS 1016-104.1:1999*. *Methods for analysis and testing of coal and coke. Proximate analysis, determination of moisture content of the general analysis test sample.* Milton Keynes: BSI.

British Standards Institution, 1998. *BS 1016-104.3:1998. Methods for analysis and testing of coal and coke.* Milton Keynes: BSI.

British Standards Institution, 1998. *BS 1016-104.4:1998. Methods for analysis and testing of coal and coke.* Milton Keynes: BSI.

British Standards Institution, 1996. *BS 1016-106.1.1: 1996. Methods for analysis and testing of coal and coke. Ultimate analysis of coal and coke. Determination of carbon and hydrogen content, high temperature combustion method.* Milton Keynes: BSI.

British Standards Institution, 1996. *BS 1016-106.4.2:1996, Methods for analysis and testing of coal and coke. Ultimate analysis of coal and coke. Determination of total sulfur content, high temperature combustion method.* Milton Keynes: BSI.

Carman, P.C. 1956. *Flow of gases through porous media*. London: Butterworths.

Condon, J.B. 2006. *Surface area and porosity determinations by physisorption, measurements and theory*. Amsterdam, Elsevier.

Gensterblum, Y., van Hemert, P., Billemont, P., Battistutta, E., Busch, A., Krooss, B.M., De Weireld, G., and Wolf, K.H.A.A. 2010. European inter-laboratory comparison of high pressure CO_2 sorption isotherms II: Natural coals. *International Journal of Coal Geology*, 84(2), pp. 115-124.

Gruszkiewicz, M.S., Naney, M.T., Blencoe, J.G., Cole, D.R., Pashin, J.C. and Carroll R.E. 2009. Adsorption kinetics of CO_2, CH_4 and their equimolar mixture on coal from the Black Warrior Basin, West-Central Alabama. *International Journal of Coal Geology,* 77(1-2), pp. 23-33.

Han, W.S., Kim, K-Y., Lu, M., McPherson, B.J., Lu C. and Lee, S-Y. 2011. Injectivity changes and associated temperature disequilibrium: numerical study. *Energy Procedia,* 4, pp. 4552-4558.

Han, W.S., Stillman, G.A., Lu, M., Lu, C., McPherson, B.J. and Park, E. 2010. Evaluation of potential nonisothermal processes and heat transport during CO_2 sequestration. *Journal of Geophysical Research: Solid Earth,* 115(B7), pp. 1978-2012.

Met Office, *Wales 1971-2000 ave*rages [Online]. Available at: http://www.metoffice.gov.uk/ climate/uk/averages/ 19712000 /areal/wales.html [Accessed: May 2011].

Massarotto, P., Golding, S.D., Bae, J.S., Iyer, R. and Rudolph, V. 2010. Changes in reservoir properties from injection of supercritical CO_2 into coal seams- A laboratory study. *International Journal of Coal Geology*, 82(3-4), pp. 269-279.

Mohammad, S., Fitzgerald, J.E., Robinson, J.R.L. and Gasem, K.A.M. 2009. Experimental uncertainties in volumetric methods for measuring equilibrium adsorption. *Energy and Fuel,* 23, pp. 2810-2820.

Ozdemir, E. 2004. *Chemistry of the adsorption of carbondioxide by Argonne Premium coals and a model to simulate CO_2 sequestration in coal seams.* PhD Thesis. University of Pittsburgh.

Pan, Z., Connell, L.D. and Camilleri, M. 2010. Laboratory characterisation of coal reservoir permeability for primary and enhanced coalbed methane recovery. *International Journal of Coal Geology,* 82(3-4), pp. 252-261.

Peng, D.Y. and Robinson, D.B. 1976. A new two-constant equation of state. *Industrial and Engineering Chemistry Fundamentals*, 15(1), pp. 59-64.

Rodrigues, C.F. and Lemos de Sousa, M.J. 2002. The measurement of coal porosity with different gases. *International Journal of Coal Geology*, 48(3-4), pp. 245-251.

Smits, A.J. and Dussauge, J.P. 2006. *Turbulent Shear Layers in Supersonic Flow.* 2nd ed. New York: American Institute of Physics.

Speight, J.G. 2005. *Handbook of coal analysis.* Hoboken, New Jersey: John Wiley & Sons, Inc.

Sudibandriyo, M. 2004. Measurement of methane, nitrogen and carbon dioxide adsorption on wet selected coals. *Proceedings of Seminar Nasional Teknologi Proses Kimia VI.* Jakarta, March 31, 2004, pp. 1-9.

van Hemert, P., Wolf, K.A.A. and Rudolph, E.S.J. 2012. Output gas stream composition from methane saturated coal during injection of nitrogen, carbon dioxide, a nitrogen-carbon dioxide mixture and a hydrogen-carbon dioxide mixture. *International Journal of Coal Geology,* 89, pp. 108-113.

Chapter 5

Gas Adsorption/Desorption Behaviour in Coal

5.1. Introduction

This chapter presents the results of the gas adsorption/desorption measurements on the coal samples based on the methodology described in Chapter 4. The main objectives of the study presented in this chapter are: i) to better understand and quantify the adsorption/desorption behaviour of different gas species in coal under equilibrium conditions, ii) to explore the kinetics of the adsorption behaviour of various gases in coal. In addition, this chapter provides a number of the material parameters that are required for the numerical modelling presented in Chapter 8.

Section 5.2 presents the results of the excess adsorption measurements of N_2, CH_4 and CO_2 in powdered coal for up to 6MPa gas pressure.

In Section 5.3, the amount of the absolute adsorption calculated for each measurement is provided. The volumetric effects of the reactive gases e.g. swelling/shrinkage of coal due to interaction with gases are included and discussed. The Langmuir equation has been employed to present the amounts of the absolute adsorptions of each gas.

The desorption behaviour of the gases studied from the coal samples under isothermal conditions are presented and discussed in Section 5.4.

In Section 5.5, the results of the adsorption kinetics of the gas species in coal are presented. The kinetic aspects of different gases during adsorption are investigated using the first-order and second-order rate functions.

Finally, concluding remarks of the experimental results related to this chapter are provided in Section 5.6.

5.2. The excess adsorption isotherms

The manometric sorption apparatus described in Chapter 3 was used to conduct the experimental measurements of the gas adsorption/desorption isotherms on the coal

sample from the Unity mine located in South Wales. The powdered coal samples (0.05kg) with particle size distribution ranging between 0.5 and 1mm were used in this study. Experimental temperature was set to 298K in all experiments and kept constant throughout the tests. The helium pycnometry test was also performed to measure the void volumes of the reference cell and sample cell.

Prior to each test, the coal sample was subjected to vacuum of approximately -100kPa for a period of 24hrs to remove the residual gases from the system. First, N_2 adsorption measurement was performed at ascending injection pressure steps up to 7MPa, followed by the desorption measurement at descending pressure steps. A similar procedure was then repeated by changing the experimental gas to CH_4 and CO_2, respectively.

The excess adsorption isotherms were determined for N_2, CH_4 and CO_2 gases based on equations (4-4) to (4-7). Figure 5.1 to 5.3 show the results of the excess adsorption isotherms for N_2, CH_4 and CO_2, respectively.

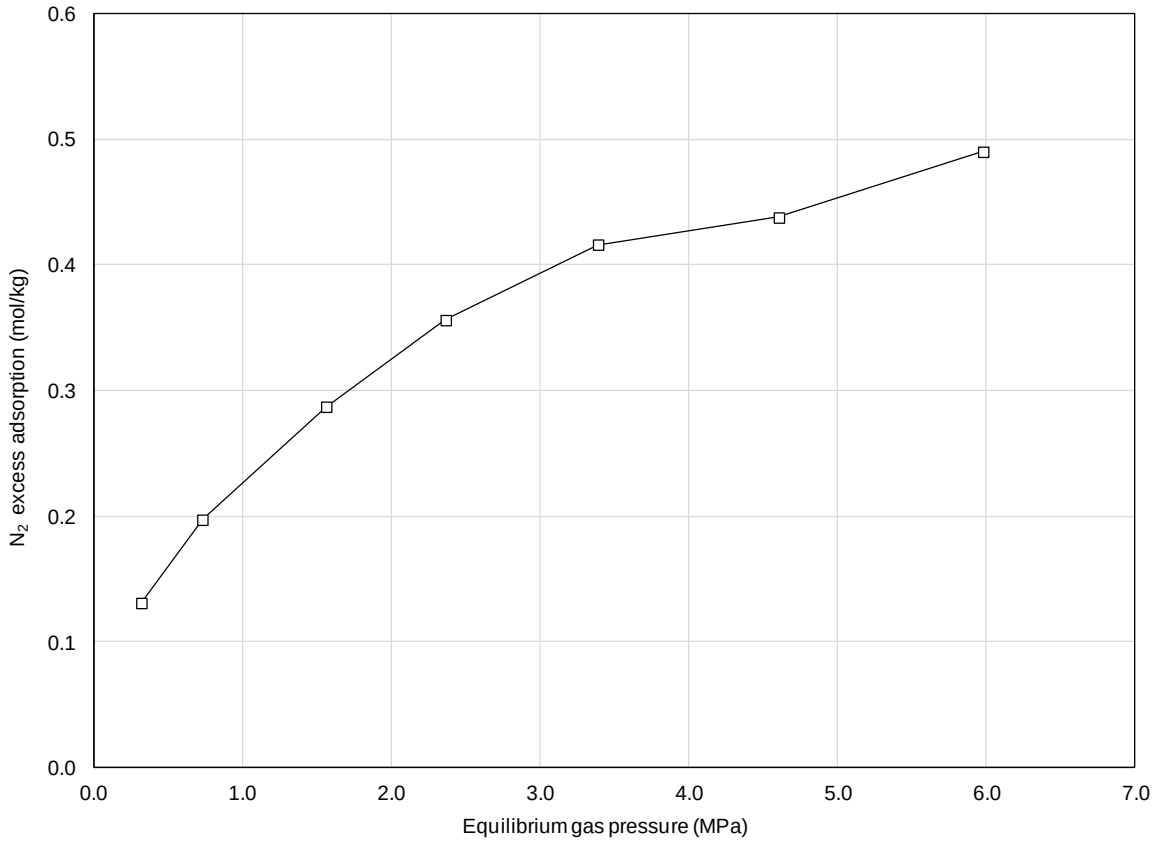

Fig. 5.1. Excess adsorption of N_2 gas on the coal sample at 298K.

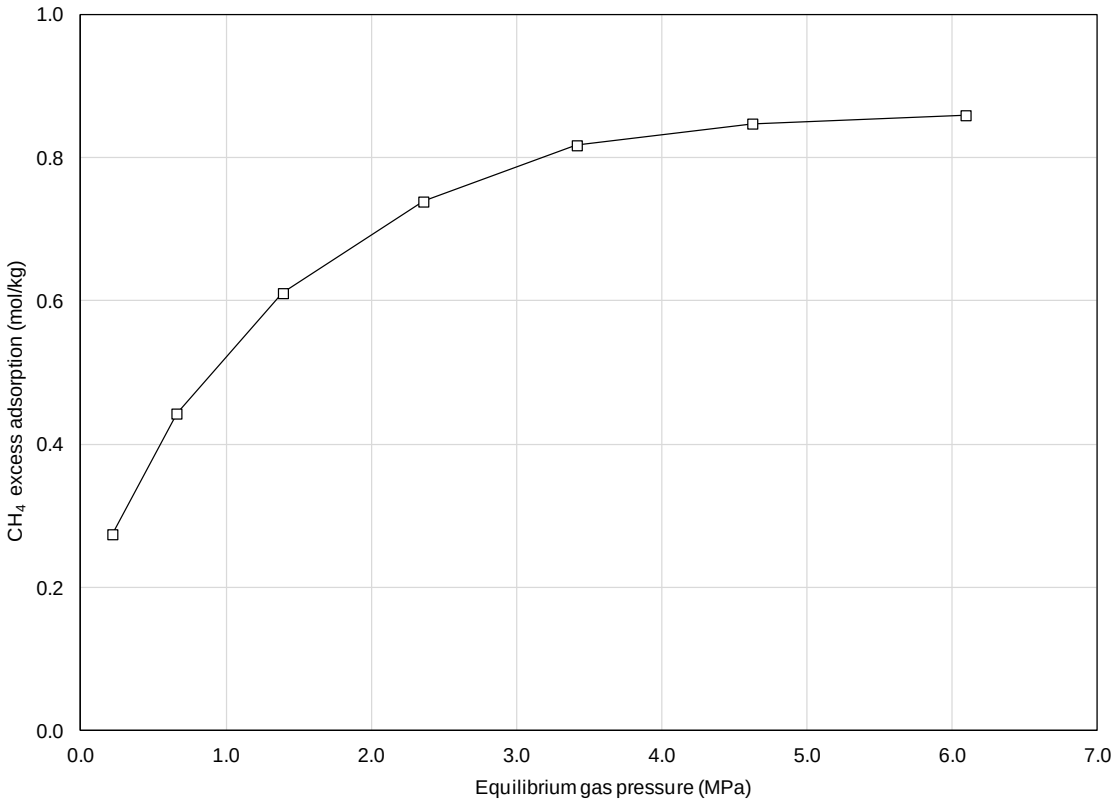

Fig. 5.2. Excess adsorption of CH_4 gas on the coal sample at 298K.

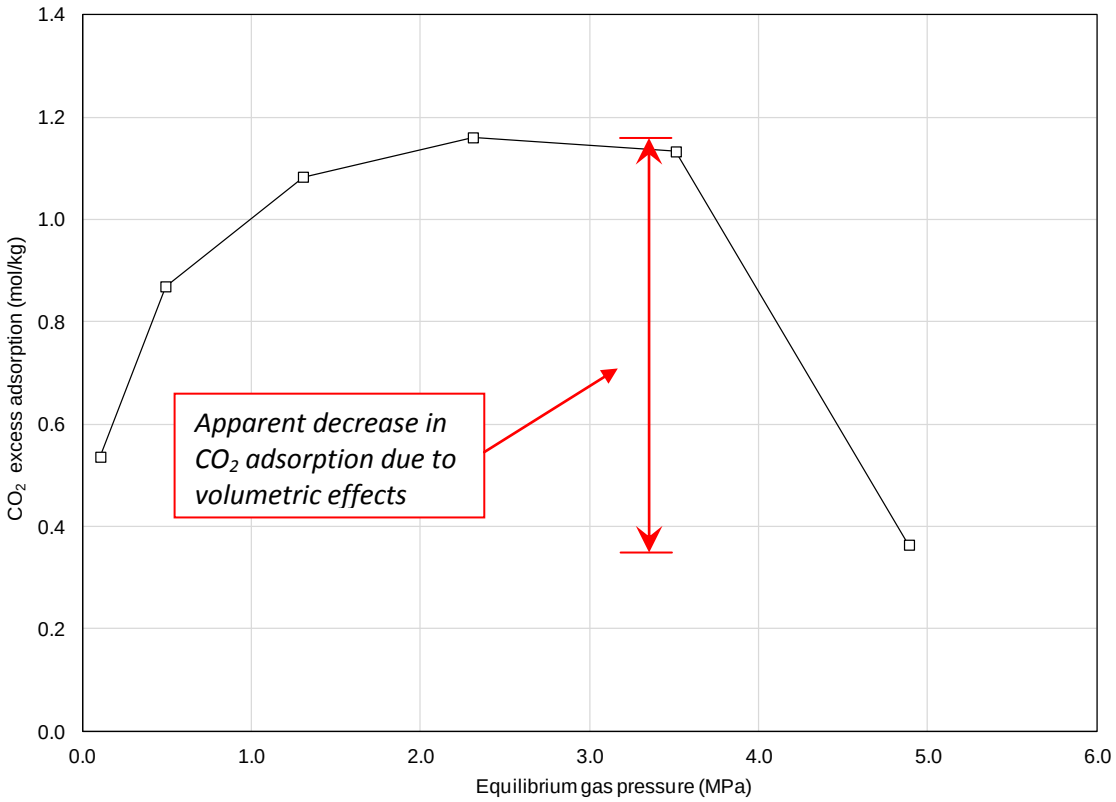

Fig. 5.3. Excess adsorption of CO_2 gas on the coal sample at 298K.

As shown in Figure 5.1, the amount of N_2 excess adsorption has increased gradually with the increase in gas pressure and reached to a maximum value of 0.49mol/kg at equilibrium pressure of 6MPa. In the case of CH_4, the excess adsorption has increased with the increase in gas pressure and has reached to a maximum value of 0.86mol/kg at equilibrium pressure of approximately 6MPa (Figure 5.2). For the case of CO_2, however, a different adsorption behavior was observed, as shown in Figure 5.3. The excess adsorption has gradually increased and reached to a maximum value of 1.2mol/kg at approximately 3MPa, followed by a sharp decrease.

The decrease in the excess adsorption of CO_2 is related to the volumetric effects that can occur during the CO_2 adsorption/desorption processes (Siemons and Busch, 2007). The volumetric effects have collectively increased the sample volume and reduced the void volume of the cell during the experiment. This effect becomes more visible when the volume increase can no longer be compensated by the gas uptake in the coal porous structure. This led to an apparent decrease in the adsorption behaviour, as shown in Figure 5.3. The volumetric effects on the adsorption behaviour observed and the correction method for obtaining the absolute amounts are discussed in the following section.

5.3. The absolute adsorption isotherms

As stated in Chapter 4, the excess adsorption/desorption isotherms are obtained directly from the experimental measurements of parameters such as gas pressure, volume and temperature. Therefore, the effect of adsorbed-phase volume and the volumetric effects of gases on coal are not included in the calculation of excess amounts.

For calculating the amounts of the absolute adsorption, however, those effects need to be taken into account, especially for CO_2 which can impose higher volumetric effects on coal due to higher swelling/shrinkage effects as observed in Figure 5.3. The steps followed to calculate the absolute adsorption isotherms include:

1. Applying appropriate values for the adsorbed-phase densities of different gas species (using equation 4-8).
2. Accounting for the volumetric effects of gas species on coal related to swelling/shrinkage of coal.

The first step was to apply the adsorbed-phase densities. Different approaches have been suggested to estimate the density of the adsorbed-phase gases. Approaches based on the extrapolations of the experimental results have been suggested, e.g. Humayun and Tomasko (2000); Gensterblum et al. (2010). Theoretical approaches have also been used, e.g. Ozdemir (2004), Sudibandriyo et al. (2003). The values of the adsorbed-phase densities given in the literature have been reviewed in Chapter 2. In this study and in order to maintain the consistency of the reported values for all the three gases (N_2, CH_4 and CO_2), the values of the adsorbed-phase densities reported by Fitzgerald et al. (2005) have been used. The adsorbed-phase densities for N_2, CH_4 and CO_2 were considered to be 808, 421 and 1180kg/m^3, respectively (Fitzgerald et al., 2005). Equation (4-8) was then used to estimate the absolute adsorption amounts for different gases by applying relevant adsorbed-phase densities mentioned above.

The second step was to account for the volumetric effects of the adsorptive gases on coal. In general, the volumetric effects can be categorized as:

1. Coal swelling/shrinkage due to gas adsorption/desorption (Ozdemir et al., 2004).
2. Dissolution or absorption of gas into coal (Siemons and Busch, 2007; Milewska-Duda et al., 2000).
3. Volumetric changes of coal samples at higher pressures due to compression or shrinkage (Ozdemir et al., 2003).
4. The uncertainties associated with the helium pycnometry measurements (Malbrunot et al., 1997).

The mentioned factors can impose a level of uncertainty in determination and calculation of the absolute adsorption/desorption isotherms. An approach to include these effects is

to assume a parameter for volumetric correction and apply that to the excess adsorption/desorption measurements. The correction parameter accounts for combined volumetric effects associated with gas interaction with coal especially for CO_2 gas (Siemons and Busch, 2007).

In this approach, the value for the volumetric correction is applied over the entire pressure range and the absolute amount of the adsorbed CO_2 is expressed by an appropriate adsorption function such as the Langmuir function (Langmuir, 1918):

$$n_L^{abs} = \frac{n_L P_{eq}}{P_L + P_{eq}} \tag{5-1}$$

where, n_L^{abs} is the Langmuir absolute adsorption (mol/kg), P_{eq} is the equilibrium pressure (Pa), n_L and P_L are the Langmuir parameters for adsorption capacity (mol/kg) and pressure (Pa), respectively.

The Langmuir parameters control the curve fit in the low pressure region where the volume of the adsorbed-phase is negligible, while the adsorbed-phase density is important in the high pressure region.

The procedure adopted for the inclusion of the volumetric effects, considered into the Langmuir parameters (n_L and P_L) is as following:

1. The amount of the absolute adsorption was determined using both equation (4-8) and the results of the excess adsorption measurements (open squares in Figures 5.4 to 5.6).
2. Initial values were considered for the Langmuir parameters and the Langmuir absolute adsorption was determined using equation (5-1).
3. The sum of the squared differences between steps 1 and 2 with a target function (f_T) was calculated. The target function was minimised with respect to the Langmuir parameters:

$$f_T = (n_{ads}^{abs} - n_L^{abs})^2 \tag{5-2}$$

4. The void volume was modified to find an optimal value of the target function.
5. The Langmuir parameters were then modified to find an optimal value of f_T.
6. Steps 4 and 5 were repeated until no further minimisation for f_T could be obtained. For the implementation of this optimisation procedure, the Excel solver function was utilised.

Figures 5.4 to 5.6 present the results of the excess and absolute adsorption isotherms (dashed and solid curves) of N_2, CH_4 and CO_2, respectively. As stated earlier, the volumetric effects of N_2 and CH_4 gases were small and therefore their Langmuir isotherms showed a good agreement with the experimental results (Figures 5.4 and 5.5). For CO_2, however, the volumetric effects were significant as the deviation between the Langmuir model and experimental results shows an increase with the increase in gas pressure which has reached a maximum deviation of 66% at 4.9MPa equilibrium gas pressure (Figure 5.6).

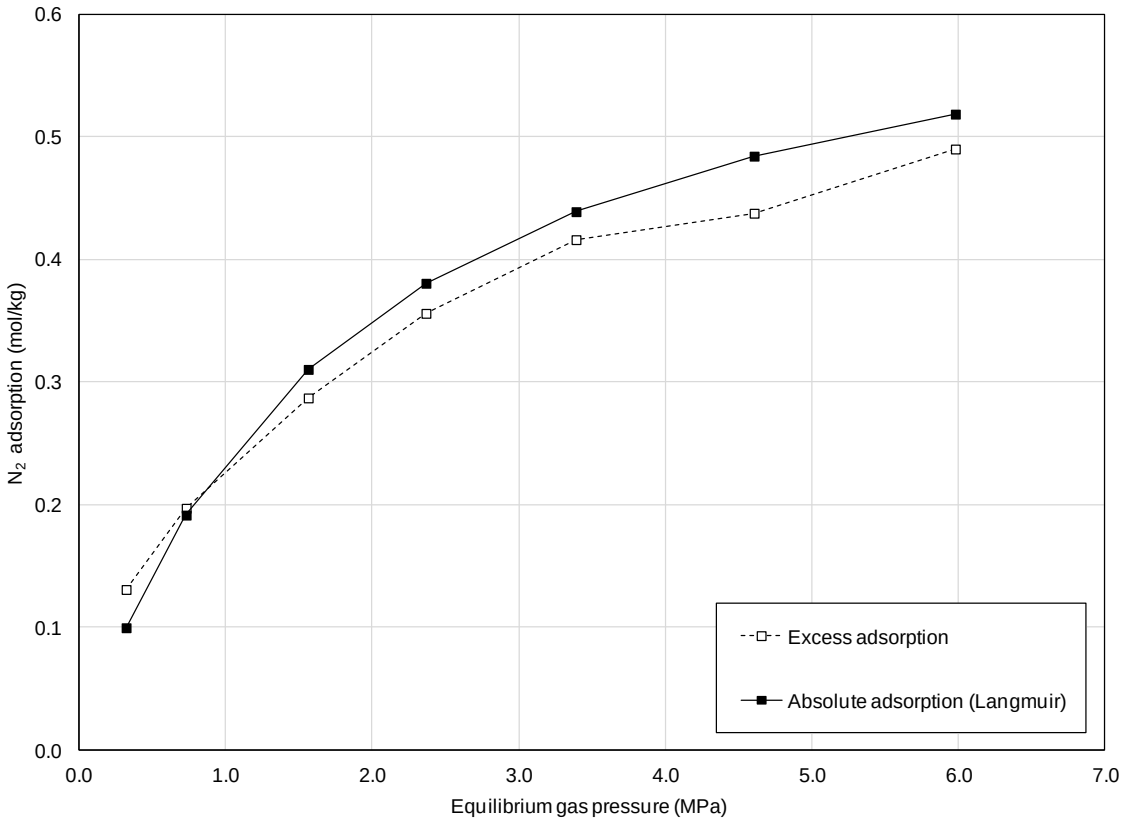

Fig. 5.4. The N_2 excess and absolute adsorption isotherms at 298K.

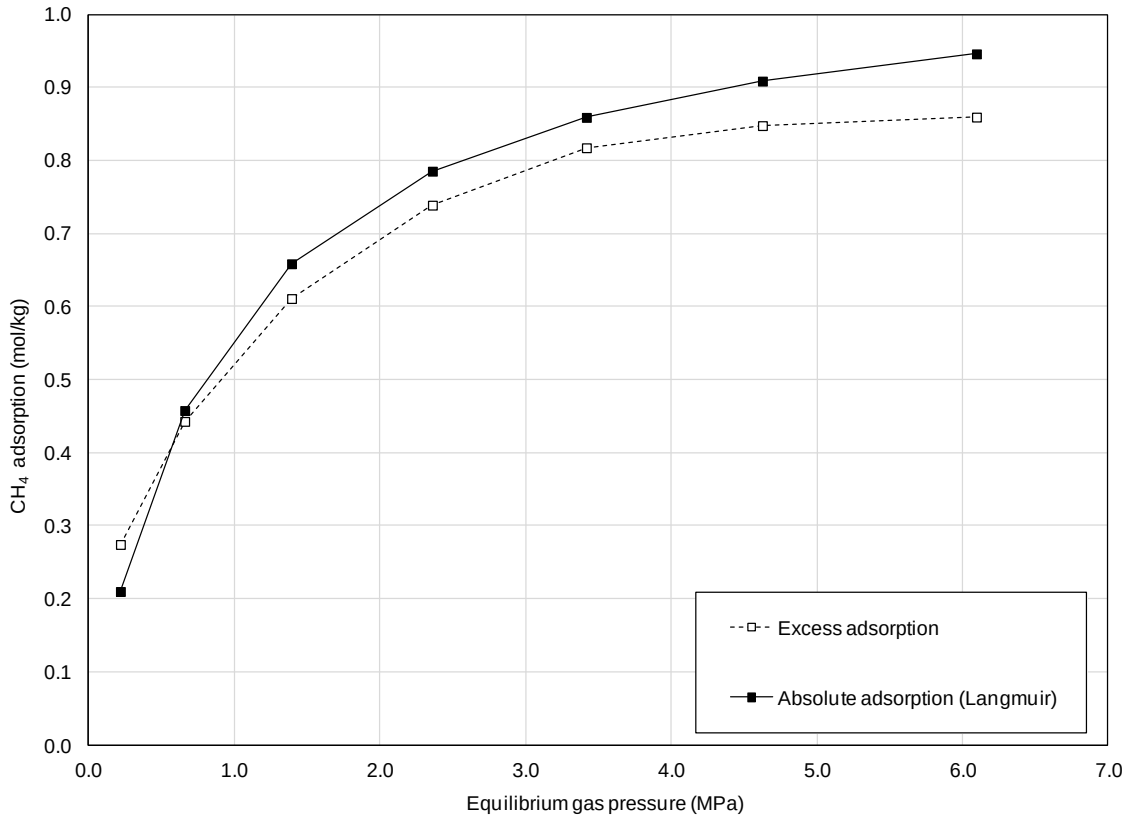

Fig. 5.5. The CH_4 excess and absolute adsorption isotherms at 298K.

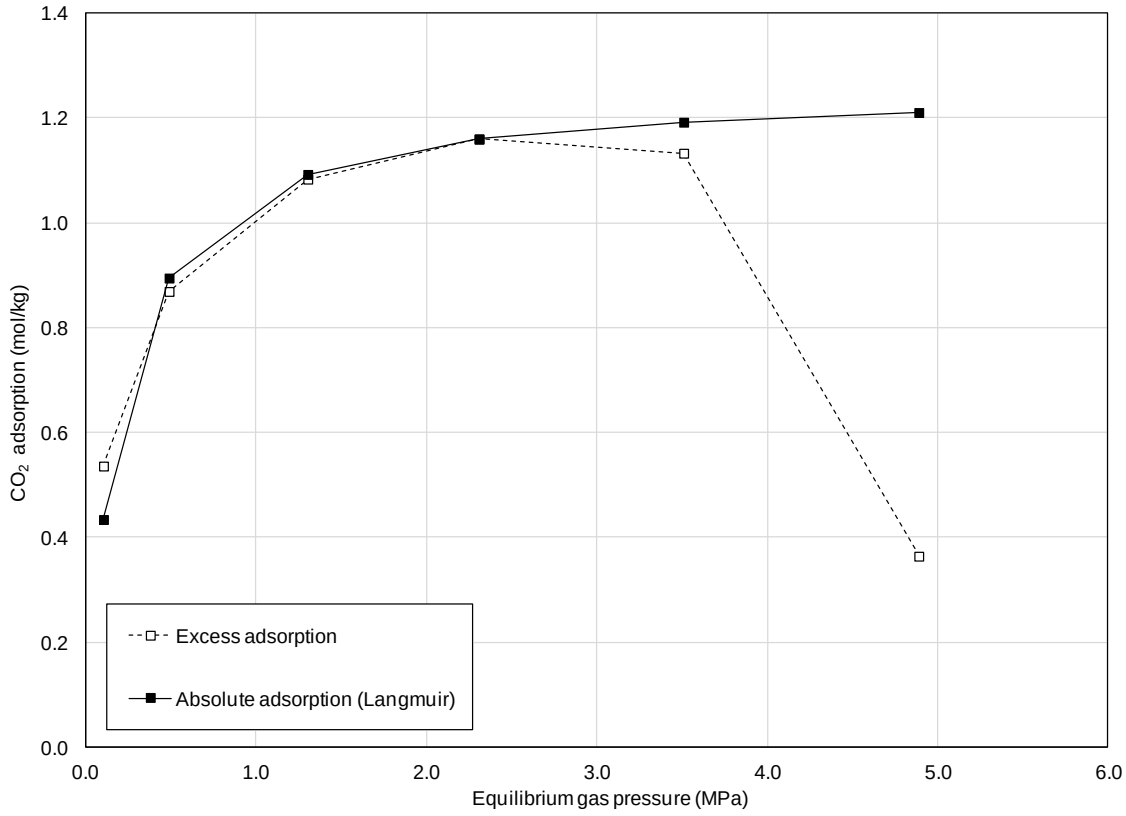

Fig. 5.6. The CO_2 excess and absolute adsorption isotherms at 298K.

According to the results, the total N_2 absolute adsorption was found to be 0.52mol/kg, whereas the total amount of CH_4 absolute adsorption was obtained to be approximately twice the N_2 adsorption capacity, i.e. maximum of 0.95mol/kg at equilibrium pressures of 6MPa. In the case of CO_2, the absolute adsorption increased with the increase in gas pressure to a maximum value of 1.21mol/kg at final equilibrium pressure of approximately 4.9MPa.

As stated in previous chapters, there is limited information about the adsorption or desorption isotherms of coals in South Wales. Semi-anthracite Selar Cornish coal is the only coal from the South Wales coalfield that has been the subject of testing for the gas adsorption/desorption capacity (Battistutta et al., 2010; Gensterblum et al., 2010; Siemons and Busch, 2007). For the Selar Cornish coal, Gensterblum et al. (2010) reported a maximum CO_2 excess adsorption of 1.37mol/kg at corresponding pressure of approximately 5.9MPa. Battistutta et al. (2010) estimated the amount of CO_2 absolute adsorption capacity of Selar Cornish coal to be 1.4mol/kg at 4.1MPa and 318K.

He et al. (2010) estimated the maximum CO_2 excess adsorption of 1.4mol/kg for an anthracite coal from Korea (Kyungdong coal) at 3MPa pressure and 298K. For a dry South Korean anthracite coal at 318K, Kim et al. (2011) reported the CO_2 excess adsorption to be 1.47mol/kg at 7.5MPa and the CH_4 excess adsorptions to be 0.46mol/kg at 5MPa.

The values of the adsorption capacity of the coal sample studied here are in general in the range of the values reported for anthracite and semi-anthracite coals. However, the value for CO_2 adsorption amount on coal sample of this study was found to be slightly lower than those reported for the Selar Cornish coal. Table 5.1 presents a summary of the results of gas adsorption isotherm measurements conducted in this study.

As given in Table 5.1, the absolute adsorption of CO_2 was 2.3 and 1.3 times higher than those obtained for N_2 and CH_4, respectively. As stated in Chapter 2, the higher capacity of coal to adsorb CO_2 is attributed to its higher affinity (adsorption energy) to coal compared to other gases under the same isothermal conditions (Wu et al., 2011; Dutta et al., 2011; Cui et al., 2004). In addition, CO_2 can be absorbed into the coal structure to a great extent

(Milewska-Duda et al., 2000; Busch and Gensterblum, 2011). The molecular sieving effect of coal has also been reported for the selective uptaking of gases such as CO_2 where the pore sizes are sufficiently small and are in the range of the kinetic diameters of CO_2 (Larsen et al., 1995; Larsen and Wernett, 1988).

The higher capacity of coal to adsorb CH_4 compared to N_2 can be explained by higher affinity of CH_4 (Cui et al., 2004). The absorption effect in this case is negligible as the amount of CH_4 absorbed into coal is much lower than in the case of CO_2 (Milewska-Duda et al., 2000).

Table 5.1. Summary of the results of gas adsorption isotherm measurements conducted on coal sample of this study.

Gas type	Excess adsorption *(mol/kg)*	Absolute adsorption *(mol/kg)*	Adsorbed-phase density *(kg/m^3)*	Langmuir parameters for adsorption isotherms	
				P_L (MPa)	*n_L (mol/kg)*
N_2	0.49	0.52	808	1.86	0.68
CH_4	0.86	0.95	421	0.90	1.09
CO_2	0.36	1.21	1180	0.20	1.26

5.4. Gas desorption behaviour

A similar procedure mentioned in previous sections for gas adsorption isotherms was repeated to estimate the gas desorption isotherms. Similar values of the adsorbed-phase densities and Langmuir were used to produce desorption isotherm trends. Figures 5.7 to 5.9 show the adsorption and desorption isotherms of N_2, CH_4 and CO_2, respectively. The results of adsorption have been presented to provide a comparison between the adsorption and desorption behaviour and hysteresis.

Table 5.2 presents the values obtained for the Langmuir parameters for gas desorption isotherms.

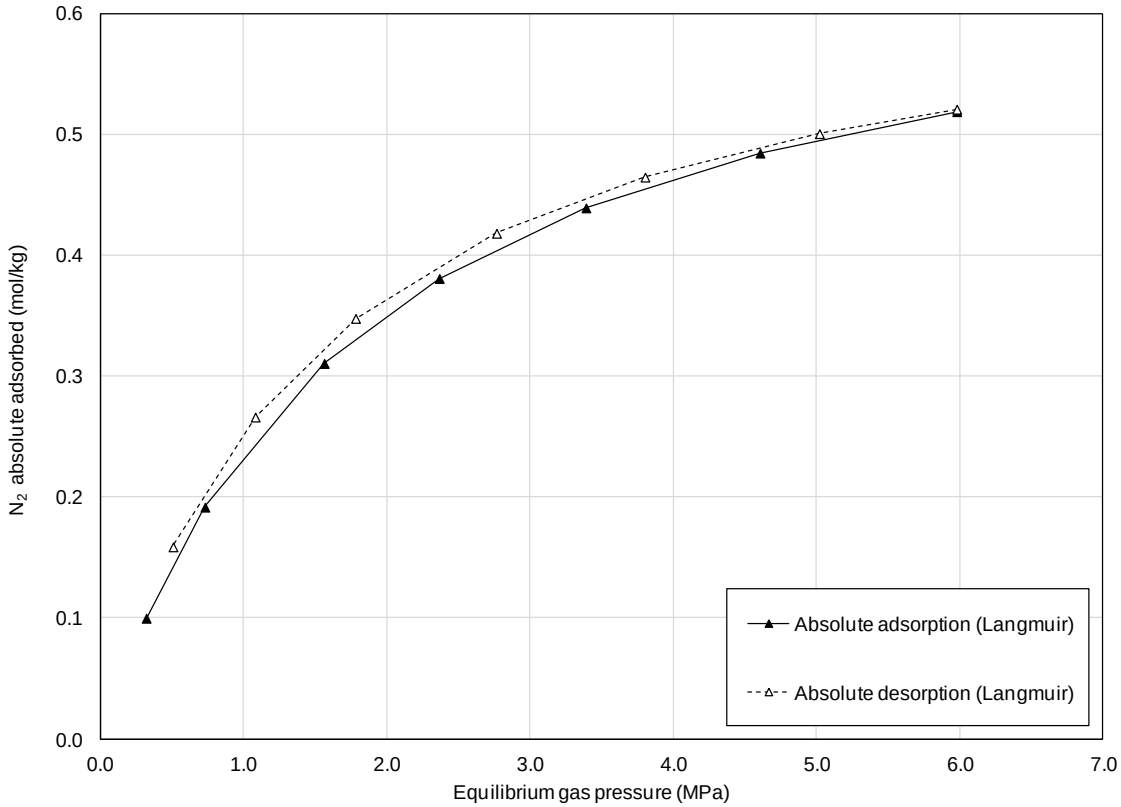

Fig. 5.7. N_2 adsorption/desorption behaviour for the coal sample at 298K.

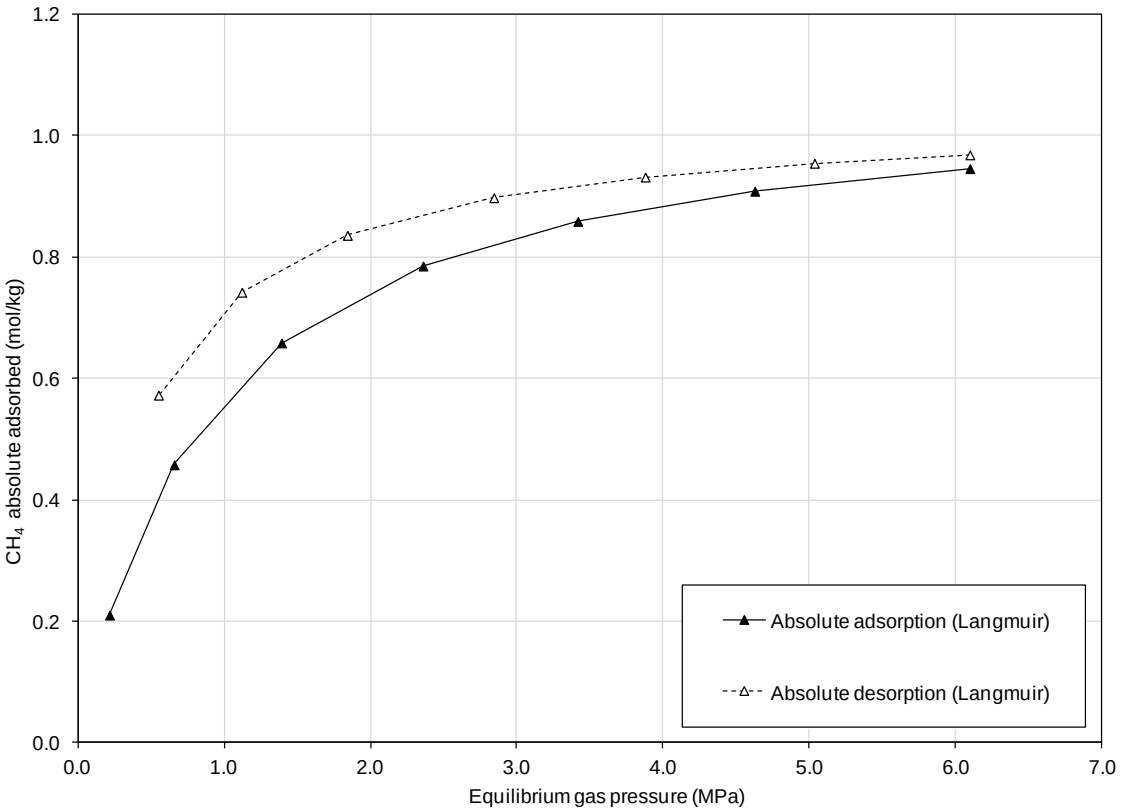

Fig. 5.8. CH_4 adsorption/desorption behaviour for the coal sample at 298K.

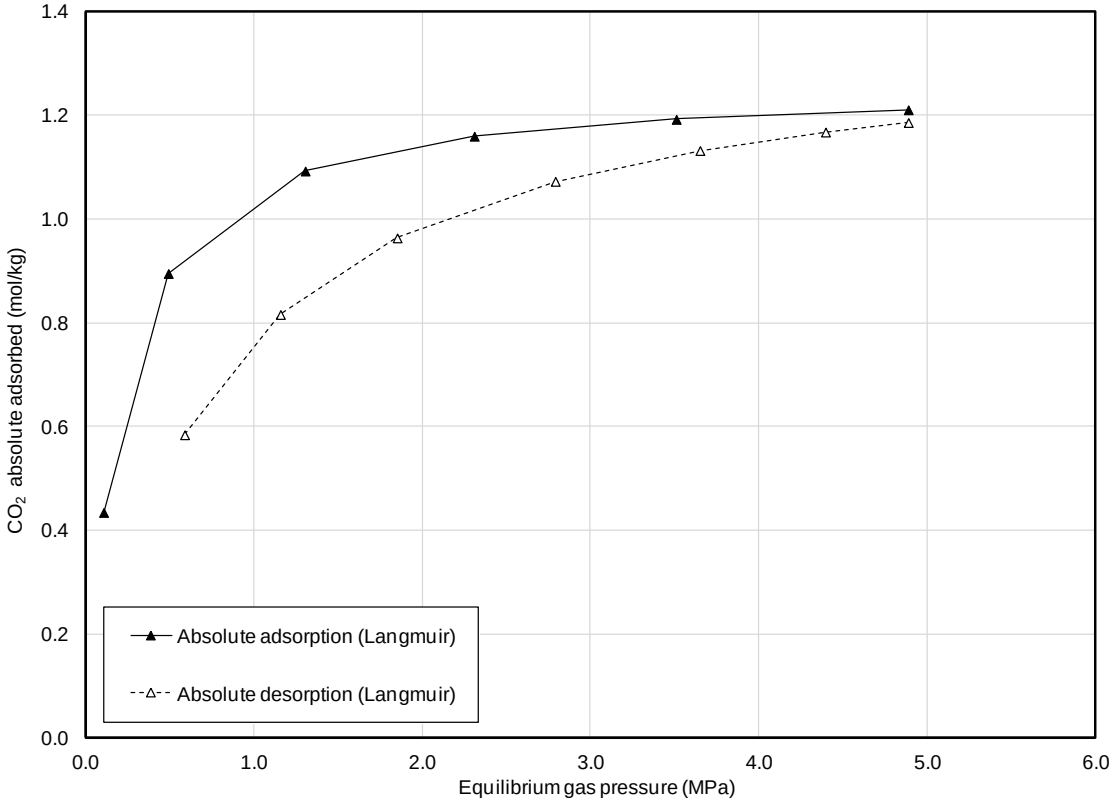

Fig. 5.9. CO_2 adsorption/desorption behaviour for the coal sample at 298K.

Table 5.2. The Langmuir parameters for gas desorption isotherms.

Gas type	Adsorbed-phase density	Langmuir parameters for desorption isotherms	
	(kg/m^3)	*P_L (MPa)*	*n_L (mol/kg)*
N_2	808	1.6	0.66
CH_4	421	0.45	1.04
CO_2	1180	0.80	1.38

As it can be seen from Figure 5.7, the desorption behaviour of N_2 is very similar to that for the adsorption behaviour. A small amount of hysteresis has been observed which remained almost constant during the pressure decrease.

In the case of the CH_4 desorption, the hysteresis effect was found to be more significant especially in low pressures (Figure 5.8). Unlike the N_2 isotherms, the CH_4 adsorption and desorption behaviour are not similar. The deviation between the adsorption and

desorption isotherms increased by pressure decrease and has reached to a maximum value of 0.2mol/kg at approximately 1MPa gas pressure.

The positive deviations of the desorption isotherms from the adsorption results can be attributed to the metastable conditions of the coal and adsorbed-gas system which prevent the release of the gas to the extent corresponding to the thermodynamically equilibrium value during desorption (Kim et al., 2011; Busch et al., 2003). Due to this effect, the absolute amount of adsorbed CH_4 in the coal during the desorption process is higher than that found during the adsorption.

The CO_2 desorption isotherm, however, exhibited a negative hysteresis from the adsorption isotherm (Figure 5.9). This implies that the adsorbed CO_2 in coal has been relatively stable during the deperessurisation of the system. Similar to the case of CH_4, the deviation of the CO_2 desorption behaviour from adsorption behaviour increased with decrease in pressure. It is noted that the negative hysteresis observed for the CO_2 desorption is in agreement with the observations reported for wet coals in subcritical region or dry coals in supercritical phase, e.g. Kim et al. (2011), He et al. (2010). From the results of the adsorption isotherms and volumetric effects during CO_2 adsorption, it can be concluded that the interaction between CO_2 and coal sample of this study has been irreversible to a great extent within the pressure ranges applied in this study (subcritical phase). He et al. (2010) has also reported an irreversible coal swelling behaviour after applying a vacuum to the system for several hours. This confirms the hysteresis effects due to the volumetric effects on coal during interaction with CO_2 even at low pressure conditions.

5.5. The adsorption kinetics

The literature review presented in Chapter 2 showed that most of the experimental investigations on gas sorption in coal have mainly focused on gas adsorption capacity measurements of coals at a range of equilibrium pressures and temperatures, while experimental investigation of gas sorption kinetics has received very little attention.

Experimental data related to the pressure decay rate (time-series) observed for adsorption tests were analysed to investigate the kinetics of coal-gas interactions. As mentioned earlier, for the N_2 and CH_4 adsorption experiments, seven steps of injection pressures were applied (0.5, 1, 2, 3, 4, 5.5, 7MPa). For the CO_2 adsorption experiment, in order to avoid gas condensation in the system, a maximum pressure of 5.5MPa has been applied, i.e. six steps of pressure injections. The gas pressure was recorded every 10 seconds.

Figures 5.10 to 5.16 present the pressure decay curves after connecting the reference cell to sample cell. The pressure spikes related to the adiabatic (Joules-Thomson) cooling of the injected gas, which can be appeared for a few seconds immediately after connecting the cells, have been removed from the results. Depending on the gas type and experimental conditions, the equilibration condition was achieved after approximately 5 to 25h, when the gas pressure remained unchanged for more than 2 hours.

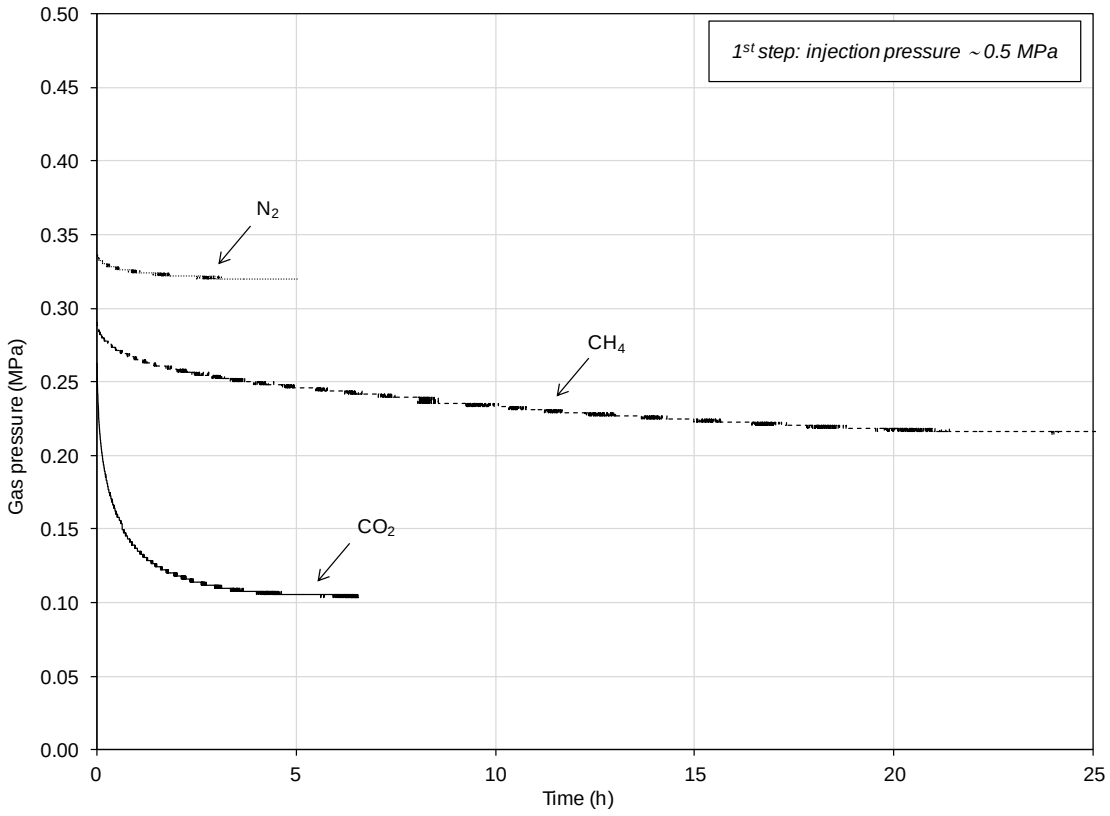

Fig. 5.10. The 1st injection pressure step: The pressure decay curves due to N_2, CH_4 and CO_2 adsorption on coal at 298K.

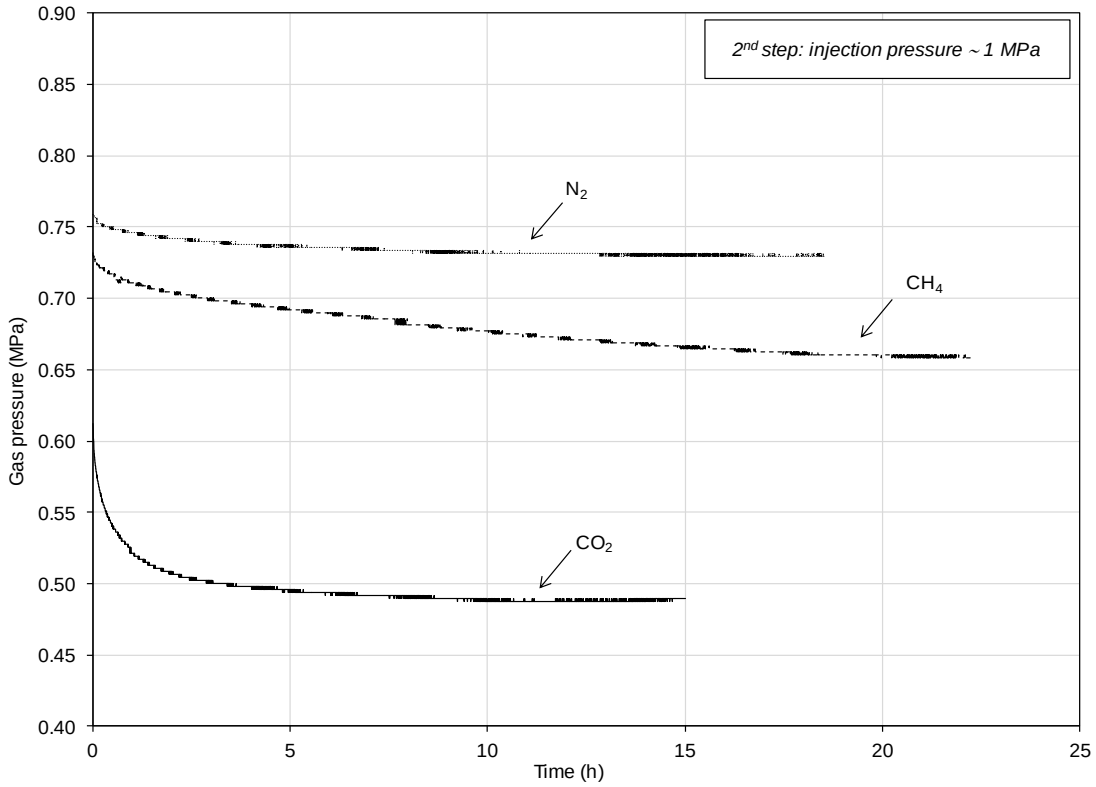

Fig. 5.11. The 2nd injection pressure step: The pressure decay curves due to N_2, CH_4 and CO_2 adsorption on coal at 298K.

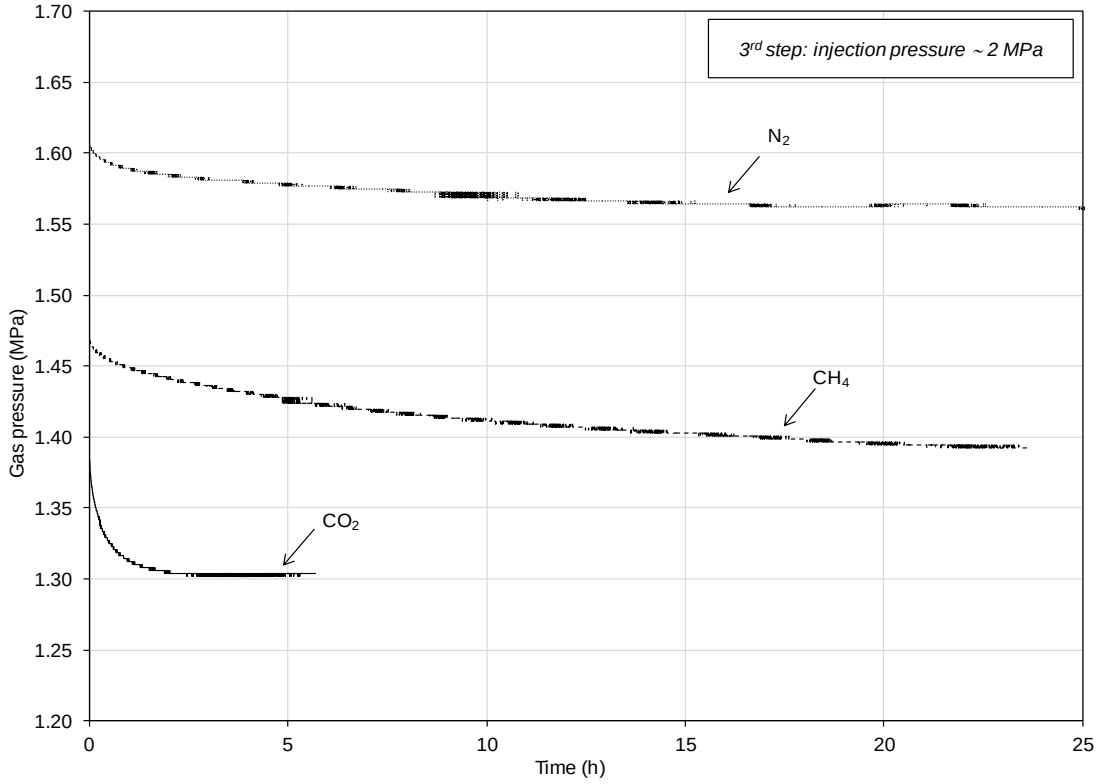

Fig. 5.12. The 3rd injection pressure step: The pressure decay curves due to N_2, CH_4 and CO_2 adsorption on coal at 298K.

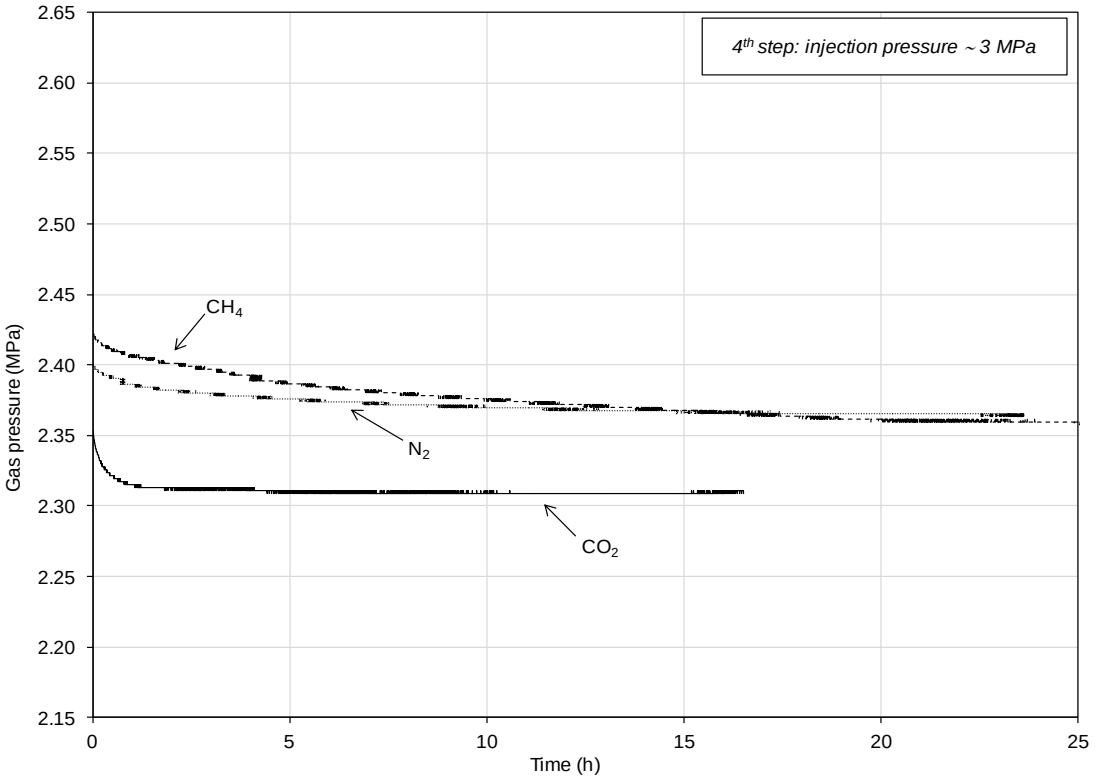

Fig. 5.13. The 4th injection pressure step: The pressure decay curves due to N_2, CH_4 and CO_2 adsorption on coal at 298K.

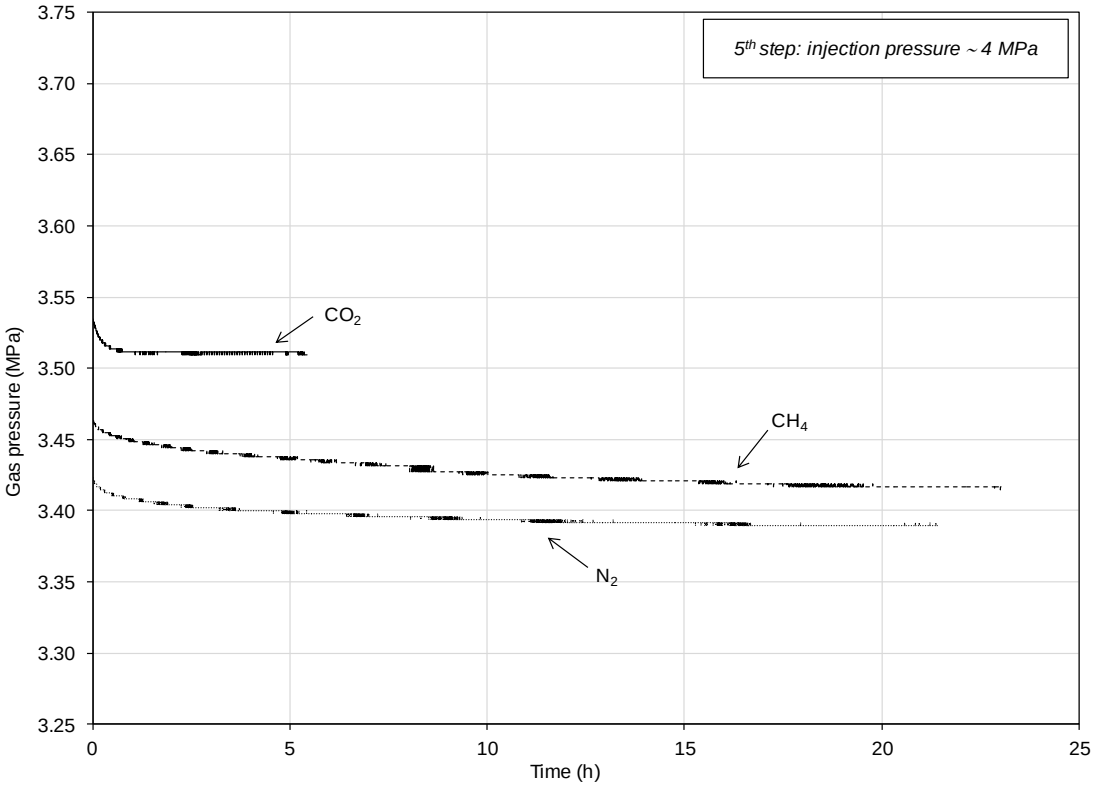

Fig. 5.14. The 5th injection pressure step: The pressure decay curves due to N_2, CH_4 and CO_2 adsorption on coal at 298K.

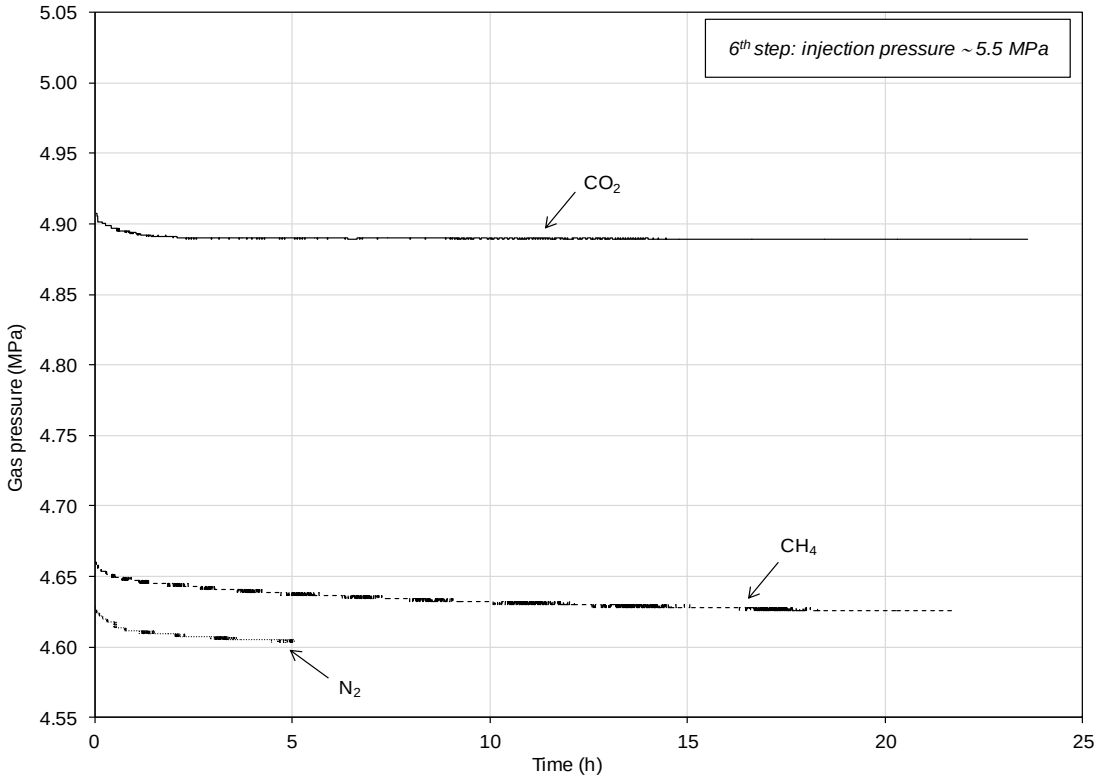

Fig. 5.15. The 6th injection pressure step: The pressure decay curves due to N_2, CH_4 and CO_2 adsorption on coal at 298K.

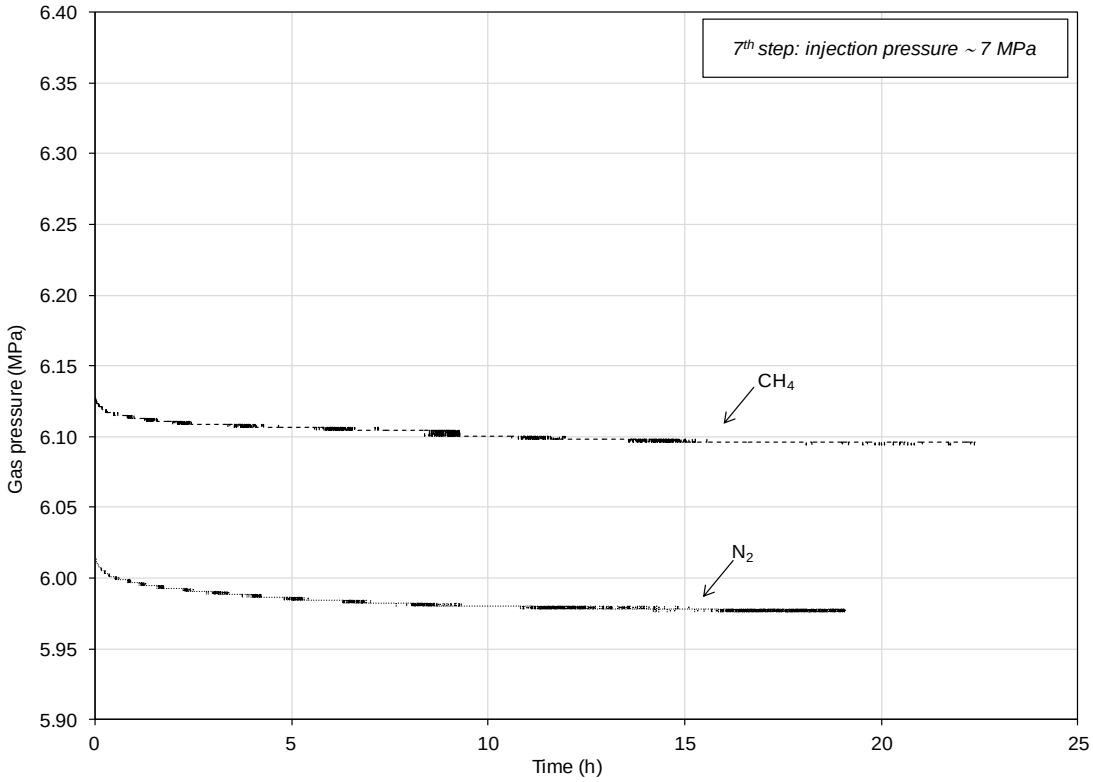

Fig. 5.16. The 7th injection pressure step: The pressure decay curves due to N_2 and CH_4 adsorption on coal at 298K.

The longest durations to reach the equilibrium state were related to the CH_4 experiment and the fastest rate to reach equilibrium was related to the CO_2 experiment.

Figures 5.10 to 5.16 provide graphical comparisons of the magnitudes of the pressure decreases for different gases during gas adsorption experiments. In order to quantitatively investigate the adsorption rate of different gas species, the normalised gas adsorption values were calculated for each time intervals based on an approach suggested by Busch et al. (2004). In this approach the normalised gas adsorption residual amount ($\overline{n}_{residual(t)}$) at each time interval is expressed as:

$$\overline{n}_{residual(t)} = \frac{n_t - n_{eq}}{n_0 - n_{eq}} \tag{5-3}$$

where, n_t is the gas adsorption amount at time *t (h)*, n_{eq} is the total gas adsorption at equilibrium and n_0 is the initial gas adsorption at the beginning of each pressure step at each stage.

Figure 5.17 to 5.19 show the plots of the residual gas adsorption versus time using the equation (5-3) for N_2, CH_4 and CO_2, respectively. In the case of N_2, the first and sixth pressure steps were eliminated from the kinetic analyses due to incompleteness of equilibrium process required.

It can be seen from the results that the average equilibration time for N_2 was approximately 15h (Figure 5.17), whereas for CH_4, the average equilibration time is at least 20h (Figure 5.18). The results related to CO_2 showed significantly shorter equilibration times, i.e. less than 3h (Figure 5.19).

The various adsorption rates observed for CO_2, CH_4 and N_2 gases in coal can be attributed to several influential factors. As mentioned earlier, the higher affinity of CO_2 to coal can accelerate its adsorption equilibration on coal. In addition, a CO_2 molecule has a linear structure and with the smallest kinetic diameter (0.33nm), compared to N_2 (0.36nm) and CH_4 (0.38nm) (Cui et al., 2004), therefore, CO_2 can access smaller pores (Cui et al., 2004; Busch et al., 2004; Narkiewicz and Mathews, 2009). The higher diffusion coefficient (Shieh and Chunh, 1999; Xu et al., 2003) and higher solubility of CO_2 (Milewska-Duda et al.,

2000; Busch and Gensterblum, 2011) have also been reported as the influential factors in its shorter equilibration time.

Although N_2 has less affinity to coal compared to CH_4, its shorter equilibration time can be attributed to its smaller kinetic diameter as well as its higher diffusion coefficient (Cui et al., 2004).

Various approaches have been suggested to parametarise the kinetics of the gas adsorption on coal. Most of the approaches proposed are based on theoretical approaches (e.g. Clarkson and Bustin, 1999; Smith and Williams, 1984; Crank, 1975).

In this study, the rate functions proposed and applied widely including the first-order and second-order rate functions are used to obtain the kinetic parameters. In addition, a third method based on a semi-empirical approach suggested by Busch et al. (2004) was also applied to assess the adsorption behaviour of different gases.

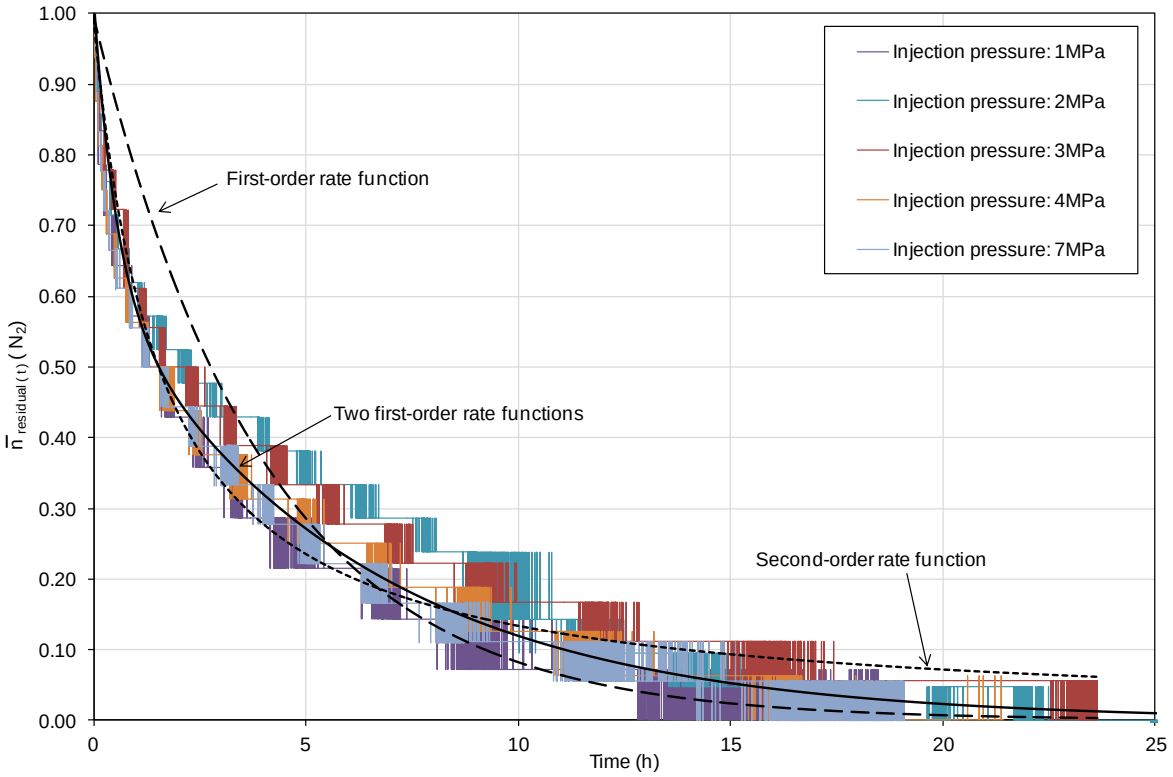

Fig. 5.17. The variations of $\bar{n}_{residual(t)}$ with time obtained from N_2 adsorption measurement experiment.

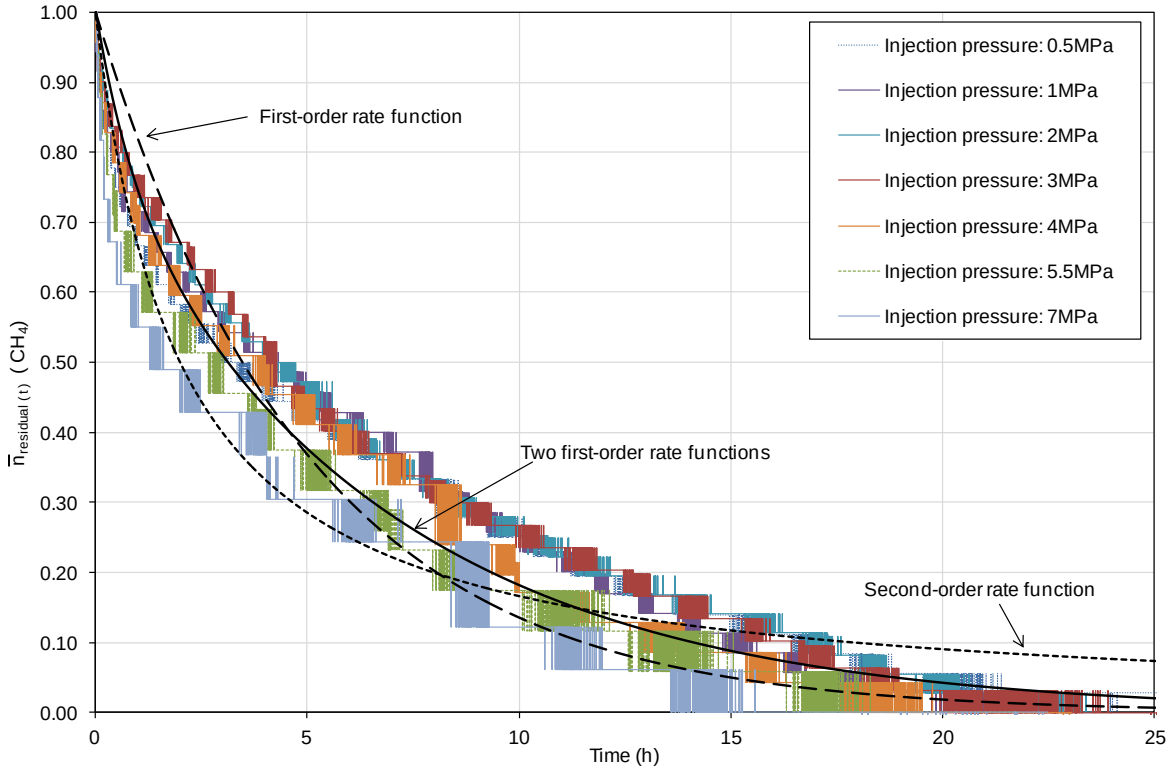

Fig. 5.18. The variations of $\bar{n}_{residual(t)}$ with time obtained from CH_4 adsorption measurement experiment.

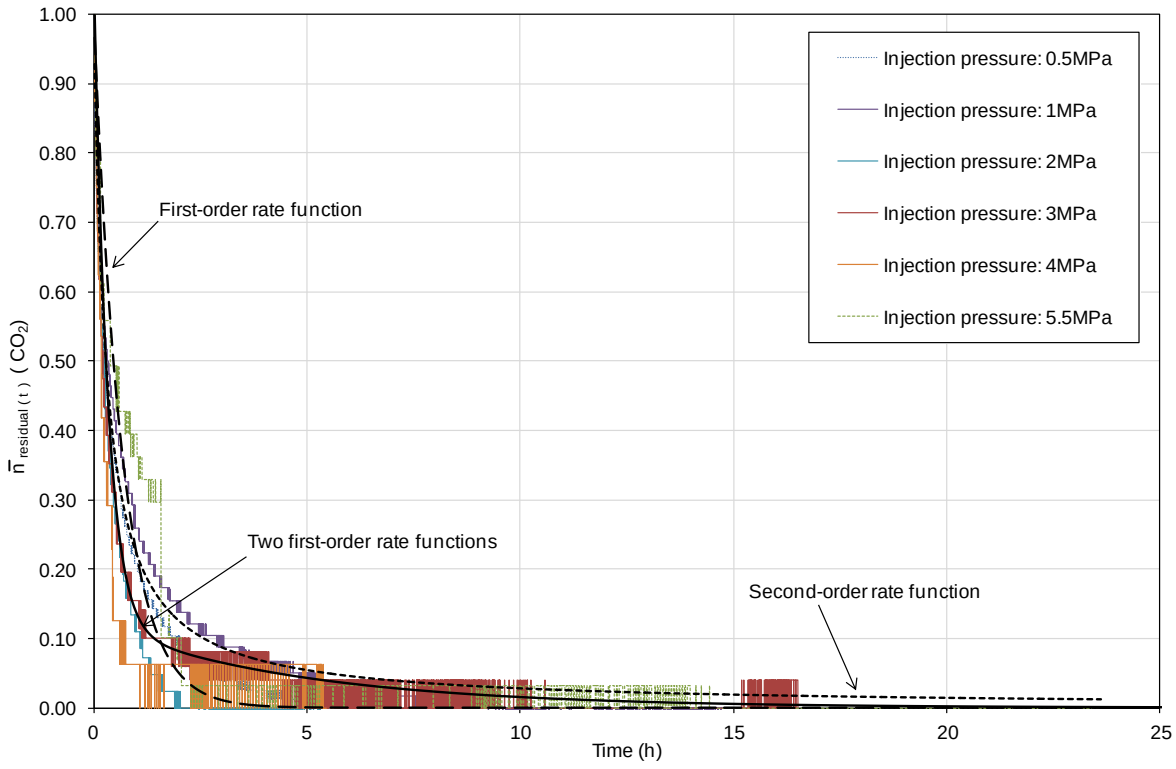

Fig. 5.19. The variations of $\bar{n}_{residual(t)}$ with time obtained from CO_2 adsorption measurement experiment.

The first-order rate function, in its integrated form, can be expressed as (Sparks, 1985):

$$\overline{n}_{residual(t)} = \overline{n}_{residual(0)} exp(-\tau t) \tag{5-4}$$

where, $\overline{n}_{residual(0)}$ is the initial residual adsorption at time zero (=1) and τ is the adsorption rate coefficient (mol/h).

Using the second-order rate function, the amount of the residual adsorption ($\overline{n}_{residual(t)}$) in its integrated form can be expressed as (Sparks, 1985):

$$\frac{1}{\overline{n}_{residual(t)}} - \frac{1}{\overline{n}_{residual(0)}} = -\tau' t \tag{5-5}$$

where, τ' is the second-order rate coefficient (mol/h).

Applying the semi-empirical approach by using two combined first-order rate functions (Busch et al., 2004), the amount of the residual adsorption can be expressed as:

$$\overline{n}_{residual(t)} = \overline{n}'_{residual(0)} exp(-\tau'' t) + \overline{n}''_{residual(0)} exp(-\tau''' t) \tag{5-6}$$

where, $\overline{n}'_{residual(0)}$ and $\overline{n}''_{residual(0)}$ are the amounts of residual gas adsorption on coal with $\overline{n}''_{residual(0)} = 1 - \overline{n}'_{residual(0)}$ and τ'' *and* τ''' are the adsorption rate coefficients (1/h).

The residual adsorption amounts were calculated separately by using the equations (5-4) to (5.6). The results of three functions have been illustrated in Figure 5.17 to 5.19. Table 5.3 summarises the values of the adsorption rate coefficients based on the approaches described in this section.

The comparison of three approaches and the experimental results (Figures 5.17 to 5.19) shows that the first and second approaches based on a single first-order and second-order rate functions provided some approximations. The first-order function (dashed lines) provided a better fit for the pressure decay curves at gas pressures near to equilibrium, whereas, the second-order function (dotted lines) provided a better fit for the pressure decay curves at the start of each pressure step. Although the first-order and

the second-order functions did not provide a perfect fit for the experimental results, they may be sufficient as an approximation for certain purposes such as making a first estimate of the transport rates in a specific coal reservoir (Busch et al., 2004).

Table 5.3. Adsorption rate coefficients of the first-order and the second-order rate functions and the equation including two first-order rate functions.

Gas type	First-order	Second-order	Two first-order	
	τ (1/h)	τ' (1/h)	τ'' (1/h)	τ''' (1/h)
N_2	0.24	0.65	1.80	0.15
CH_4	0.18	0.50	1.08	0.13
CO_2	1.29	3.50	2.52	0.20

The third approach, however, provided a better agreement with the experimental data. This indicates that the gas adsorption on coal can be described by more than a single function and requires at least the assumption of a two-step process (Siemons et al., 2003; Cui et al., 2004; Shi and Durucan, 2003). Busch et al. (2004) compared the experimental results of gas pressure decay curves with a bidisperse diffusion model and concluded that gas adsorption on coal is controlled by a combined diffusion-adsorption process which results in gas transport and adsorption in macro-pores and micro-pores occurrence at different time scales. Therefore, the structure of coal matrix or distribution of macro-pores and micro-pores is an influential factor in creating different rates of gas adsorption and diffusion at different stages of gas adsorption process. Gan et al. (1972) calculated the pore-volume distribution curve for coal from nitrogen adsorption isotherm at 77K and showed that pore volumes in coal matrix are distributed in two major diameter ranges. This characteristic of the coal matrix might explain two different time scales of gas diffusion-adsorption processes observed in this study.

The half-life value ($t_{½}$) as the characteristic parameter of the combined adsorption-diffusion processes was defined based on the first-order and the second-order rate coefficients (τ and τ'). The relationships between half-time value and first-order and second-order rate coefficients are defined as following (Sparks, 1985):

$$t_{1/2} = \frac{ln2}{\tau} \tag{5-7}$$

$$t'_{1/2} = \frac{1}{\tau' n_{residual(0)}} \tag{5-8}$$

where, $t_{½}$ and $t'_{½}$ are the half-lives of first-order and the second-order rate functions, respectively (h). The results of estimated half-life values are presented in Table 5.4.

Table 5.4. Summary of the estimated half-life values based on the first-order and the second-order rate functions.

Gas type	First-order rate function	Second-order rate function	Two first-order rate functions	
	$t_{½}$ (h)	$t'_{½}$ (h)	$t_{½}$ (h)	$t_{½}$ (h)
N_2	2.89	1.54	0.39	4.6
CH_4	3.85	2.00	0.64	5.33
CO_2	0.54	0.29	0.28	3.47

In order to assess the effect of gas pressure on the adsorption rates, the half-life values of different gas species versus their corresponding injection pressure were plotted (Figure 5.20). As expected, the half-life values for CH_4 were higher than other gases due to its smaller diffusion coefficient which led to longer equilibration times especially at lower pressure steps (more than 4 hours). For N_2, the overall half-life values were less than CH_4 but higher than CO_2. Finally, CO_2 exhibited the lowest half-life among other gases (less than 30min).

A clear increase of adsorption rate with increase in gas pressure was observed for CH_4 and N_2. A similar observation has been reported by Nandi and Walker (1975) and Busch et al. (2004) for high rank coals. For CO_2, this effect was not apparent which can be attributed to the swelling effect due to CO_2 adsorption that occurs as the pressure increases (Busch et al., 2004). These observations, however, are in contrast with the results of Cui et al. (2004) who reported a negative correlation between the gas diffusivity and gas pressure.

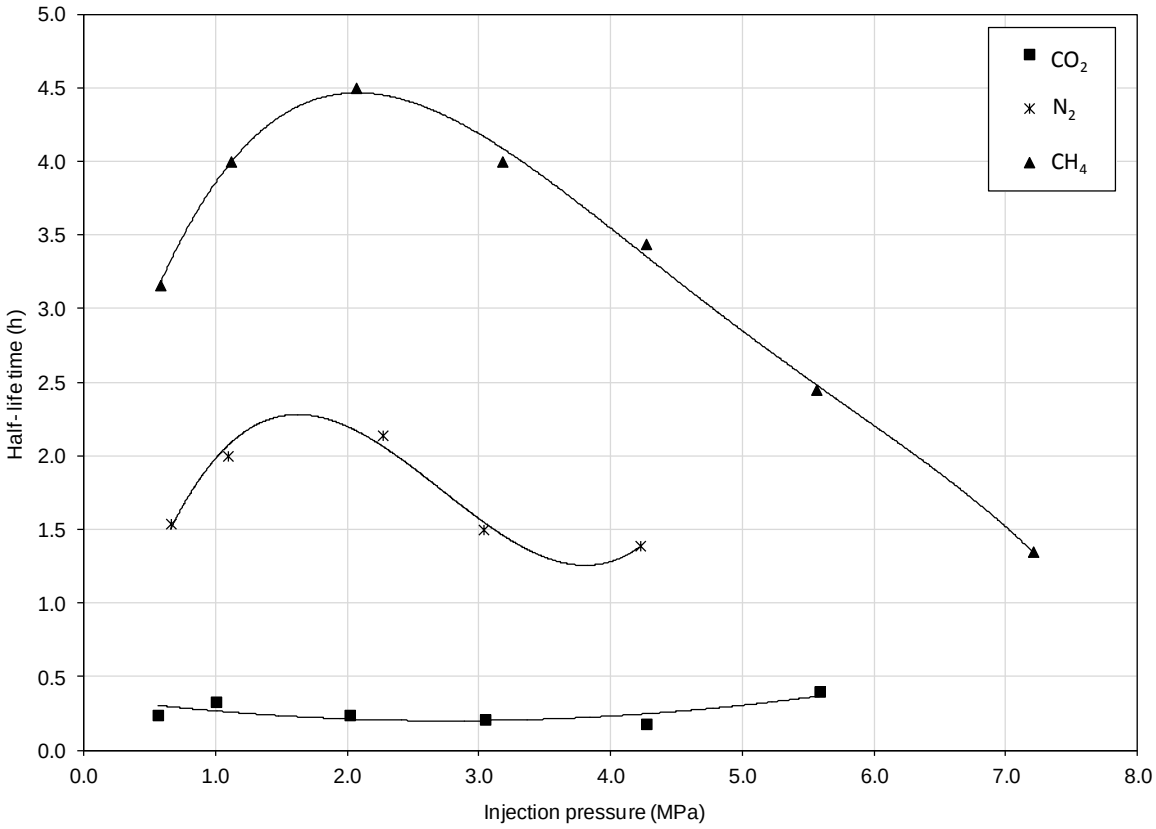

Fig. 5.20. Half-life time versus injection pressure for N_2, CH_4 and CO_2 at 298K.

5.6. Conclusions

The results of the adsorption and desorption measurements of N_2, CH_4 and CO_2 on coal sample of this study have been presented and discussed in this Chapter. The excess adsorption isotherms showed that the N_2 and CH_4 adsorption capacity increased monotonously with the increase in gas pressure. The volumetric effects of N_2 and CH_4 adsorption on coal were found to be negligible. The CO_2 excess adsorption isotherm, however, exhibited significant volumetric effects at equilibrium gas pressures greater than 3MPa. The volumetric effects were evident from the apparent decrease in gas adsorption capacity of the coal sample at higher gas pressures.

The absolute adsorption/desorption values were calculated by applying appropriate adsorbed-phase density values and accounting for the volumetric effects of gas species on coal. The results of the absolute adsorption measurements show that the coal sample

has the highest adsorption capacity to CO_2 (1.21mol/kg) in comparison with other gases studied here. However, the adsorption capacity of the coal sample decreased with changing the experimental gases from CO_2 to CH_4 (1.3 times reduction) and from CH_4 to N_2 (1.8 times reduction). On the other hand, considerable volumetric effects due to interaction of CO_2 with coal were observed which can be related to several factors such as the swelling effect of CO_2 on coal matrix and dissolution of CO_2 into the coal structure. A maximum deviation of 66% was observed between the CO_2 excess and absolute adsorption isotherms at 4.9MPa equilibrium gas pressure.

The results showed that the interaction between coal and CO_2 gas has caused a considerable volumetric effect. However, quantifying the amount of swelling from the adsorption/desorption data obtained from the unconfined powdered coal samples may result in unrealistic interpretations of the actual process. This is mainly due to the fact that both the coal structure and confining pressure are influential factors in coal matrix swelling and permeability evolution during interactions with various gases. Since the structure of the coal sample may have been altered during the powdering process, direct measurements are required for further evaluations of the coal swelling by using intact coal sample under confined conditions. Coal swelling and volumetric strain measurements using intact coal samples will be further discussed in Chapter 6.

Depending on the gas type, the results of desorption isotherm measurements exhibited various types of hysteresis. For N_2 and CH_4, positive hystereses from adsorption isotherms were observed. In the case of CO_2, negative hysteresis can be an indication of a stable condition of the adsorbed CO_2 on coal. This suggests that the processes of CO_2 sorption on coal and its consequential volumetric effects on coal matrix can be partially irreversible. Such observations, for instance, can be useful for assessing the stability of the adsorbed CO_2 during carbon sequestration process in coal reservoirs, e.g. possibility of gas release due to pressure depletions in the reservoirs. More discussions related to the fate of adsorbed CO_2 in coal and reversibility of the process will be provided in Chapter 6.

The investigation on gas adsorption kinetics showed that gas adsorption rates in coal are controlled by more than a single rate function. Due to the nature of the coal matrix and pore size distribution, gas diffusion and adsorption processes occur in two different time scales by applying two first-order rate functions. The half-life values for gas adsorption versus gas pressure showed that despite the decrease in gas diffusivity at higher pressures, gas adsorption rates increased, especially for CH_4. In the case of CO_2 however, the adsorption rate did not increase with the increase in gas pressure which may be related to the swelling effect of CO_2 on coal matrix at elevated pressures.

5.7. References

Battistutta, E., van Hemert, P., Lutynski, M., Bruining, H. and Wolf, K.H. 2010. Swelling and sorption experiments on methane, nitrogen and carbon dioxide on dry Selar Cornish coal. *International Journal of Coal Geology,* 84(1), pp. 39-48.

Busch, A. and Gensterblum, Y. 2011. CBM and CO_2-ECBM related sorption processes in coal: A review. *International Journal of Coal Geology*, 87(2), pp. 49-71.

Busch, A., Gensterblum, Y. and Krooss B.M. 2003. Methane and CO_2 sorption and desorption measurements on dry Argonne premium coals: pure components and mixtures. *International Journal of Coal Geology*, 55(2-4), pp. 205-224.

Busch, A., Gensterblum, Y., Krooss, B.M. and Littke, R. 2004. Methane and carbon dioxide adsorption-diffusion experiments on coal: upscaling and modeling. *International Journal of Coal Geology*, 60(2-4), pp. 151-168.

Clarkson, C.R. and Bustin, R.M. 1999. The effect of pore structure and gas pressure upon the transport properties of coal: a laboratory and modeling study. 2. Adsorption rate modeling. *Fuel*, 78(11), pp. 1345-1362.

Crank, J. 1975. *The Mathematics of diffusion,* 2nd ed. London: Oxford University Press.

Cui, X., Bustin, R.M. and Dipple, G. 2004. Selective transport of CO_2, CH_4 and N_2 in coals: insights from modeling of experimental gas adsorption data. *Fuel*, 83(3), pp. 293-303.

Dutta, P., Bhowmik, S. and Das, S. 2011. Methane and carbon dioxide sorption on a set of coals from India. *International Journal of Coal Geology*, 85(3-4), pp. 289-299.

Fitzgerald, J.E., Pan, Z., Sudibandriyo, M., Robinson, J.R.L., Gasem, K.A.M. and Reeves, S. 2005. Adsorption of methane, nitrogen, carbon dioxide and their mixtures on wet Tiffany coal. *Fuel*, 84(18), pp. 2351-2363.

Gan, H., Nandi, S.P. and Walker, Jr.P.L. 1972. Nature of the porosity in American coals. *Fuel,* 51(4), pp. 272-277.

Gensterblum, Y., van Hemert, P., Billemont, P., Battistutta, E., Busch, A., Krooss, B.M., De Weireld, G. and Wolf, K.H.A.A. 2010. European inter-laboratory comparison of high pressure CO_2 sorption isotherms II: Natural coals. *International Journal of Coal Geology.* 84(2), pp. 115-124.

He, J., Shi, Y., Ahn, S., Kang, J.W. and Lee, C. 2010. Adsorption and desorption of CO_2 on Korean coal under subcritical to supercritical conditions. *The Journal of Physical Chemistry*, 114(14), pp. 4854-4861.

Humayun, R. and Tomasko, D.L. 2000. High-resolution adsorption isotherms of supercritical carbon dioxide on activated carbon. *AlCHE Journal,* 46(10), pp. 2065-2075.

Kim, H.J., Shi, Y., He, J., Lee, H. and Lee, C. 2011. Adsorption characteristics of CO_2 and CH_4 on dry and wet coal from subcritical to supercritical conditions. *Chemical Engineering Journal*, 171(1), pp. 45-53.

Langmuir, I. 1918. The adsorption of gases on plane surfaces of glass, mica and platinum. *Journal of the American Chemical Society,* 40(9), pp. 1361-1403.

Larsen, J.W., Hall, P. and Wernett, P.C. 1995. Pore structure of Argonne Premium coals. *Energy and Fuel*, 9(2), pp. 324-330.

Larsen, J.W. and Wernett, P. 1988. Pore structure of Illinois No. 6 coal. *Energy and Fuel*, 2(5), pp. 719-720.

Malbrunot, P., Vidal, D. and Vermesse, J. 1997. Adsorbent helium density measurement and its effect on adsorption isotherms at high pressure. *Langmuir*, 13(3), pp. 539-544.

Milewska-Duda, J., Duda, J., Nodzenski, A. and Lakatos, J. 2000. Absorption and adsorption of methane and carbon dioxide in hard coal and active carbon. *Langmuir,* 16(12), pp. 5458-5466.

Nandi, S.P. and Walker, Jr.P.L. 1975. Activated diffusion of methane from coals at elevated pressures. *Fuel,* 54(2), pp. 81-86.

Narkiewicz, M.R. and Mathews, J.P. 2009. Visual representation of carbon dioxide adsorption in a low-volatile bituminous coal molecular model. *Energy and Fuels,* 23(1), pp. 5236-5246.

Ozdemir, E. 2004. *Chemistry of the adsorption of carbondioxide by Argonne Premium coals and a model to simulate CO_2 sequestration in coal seams*. PhD Thesis. University of Pittsburgh.

Ozdemir, E., Morsi, B.I. and Schroeder, K. 2003. Importance of volume effects to adsorption isotherms of carbon dioxide on coals. *Langmuir*, 19(23), pp. 9764-9773.

Ozdemir, E. Morsi, B.I. and Schroeder, K. 2004. CO_2 adsorption capacity of argonne premium coals. *Fuel,* 83(7-8), pp. 1085-1094.

Shieh, J.-J. and Chunh, T.S. 1999. Gas permeability, diffusivity,and solubility of poly (4-vinylpyridine) film. *Journal of Polymer Science*, 37(20), pp. 2851-2861.

Shi, J.Q. and Durucan, S. 2003. A bidisperse pore diffusion model for methane displacement desorption in coal by CO_2 injection. *Fuel,* 82(10), pp. 1219-1229.

Siemons, N. and Busch, A. 2007. Measurement and interpretation of supercritical CO_2 sorption on various coals. *International Journal of Coal Geology*, 69(4), pp. 229-242.

Siemons, N., Busch, A., Bruining, H., Krooss, B.M. and Gensterblum, Y. 2003. Assessing the kinetics and capacity of gas adsorption in coals by a combined adsorption/diffusion method. *SPE Annual Technical Conference and Exhibition,* Denver, USA, October 2003, SPE *84340.*

Smith, D.M. and Williams, F.L. 1984. Diffusion models for gas production from coals, application to methane content determination. *Fuel*, 63(2), pp. 251-255.

Sparks, D.L. 1985. Kinetics of ionic reactions in clay minerals and soils. *Advances in Agronomy*, 38(1), pp. 231-266.

Sudibandriyo, M., Pan, Z., Fitzgerald, J.E., Robinson, Jr.R.L. and Gasem, K.A.M. 2003. Adsorption of methane, nitrogen, carbon dioxide and their binary mixtures on dry activated carbon at 318.2K and pressures to 13.6MPa. *Langmuir,* 19(13), pp. 5323-5331.

Wu, Y., Liu, J., Chen, Z., Elsworth, D. and Pone, D. 2011. A dual poroelastic model for CO_2-enhanced coalbed methane recovery. *International Journal of Coal Geology,* 86(2-3), pp. 177-189.

Xu, J.W., Chng, M.L., Chung, T.S., He, C.B. and Wang, R. 2003. Permeability of polyimides derived from non-coplanar diamines and 4,40-(hexafluoroisopropylidene) diphthalic anhydride. *Polymer,* 44(16), pp. 4721-5715.

Chapter 6

Gas Flow Behaviour in Coal

6.1. Introduction

In Chapter 5, the results of the experimental investigations on adsorption/desorption behaviour of various gas species on unconfined powdered coal samples were presented and discussed. This chapter presents the results of further experimental investigations on gas transport and reactions in intact coal samples under the confined conditions. The coal permeability to different gases including helium (He), nitrogen (N_2), methane (CH_4) and carbon dioxide (CO_2) has been studied under a range of gas pressures and confining pressures. The main objectives of the study presented in this chapter are i) to investigate the gas flow and coal permeability evolutions in coal due to sorption-induced strains and variations in effective stress conditions and ii) to provide further insights into the fate of adsorbed gases in coal and possible effects of gas desorption on coal permeability evolutions.

A unique sequence of core flooding experiments was conducted using various gas species described above. The triaxial core flooding system developed and described in Chapter 3 was used to conduct the experimental studies presented here. Figure 6.1 presents the flow diagram of the sequential experimental studies performed and discussed in this chapter.

In Section 6.2, the results of the helium flooding experiment are presented. Helium has been used as a non-reactive gas to assess the initial gas transport properties of the coal sample. The absolute permeability of the coal sample to helium has been evaluated and the effect of effective stress on mechanical deformation of the coal sample is discussed.

Sections 6.3 and 6.4 present the results of gas flow and permeability measurements of the coal samples to N_2 and CO_2, respectively. For each gas species, the interactions between gas and coal in terms of their effects on gas transport properties of the coal sample are discussed. The volumetric strains of the coal sample as a result of expansions/compressions due to variations in effective stresses as well as the sorption-induced swellings/shrinkages of the coal matrix are presented.

In Section 6.5 the fate of the adsorbed CO_2 in coal has been investigated. After the CO_2 flooding experiment, N_2 and CH_4 gases were injected into the coal sample to evaluate their effects on CO_2 desorption. The reversibility of the coal matrix swelling induced by the adsorbed CO_2 was investigated by analysing the changes in coal permeability and volumetric strain. Helium flooding experiments were also performed before and after injecting N_2 and CH_4 gases to assess the effects of those gases.

Finally, the conclusions drawn from the results achieved and the effects of different gas species on transport properties of coal are provided in Section 6.6.

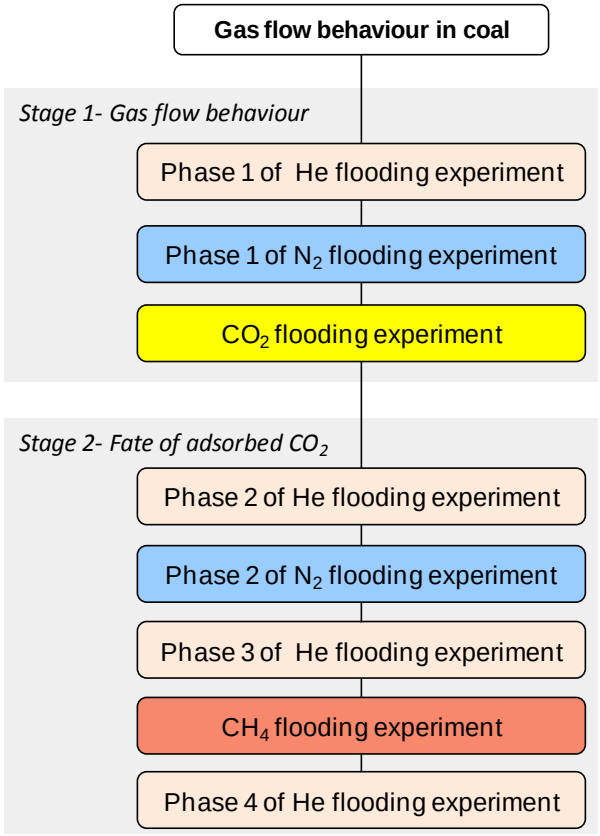

Fig. 6.1. The flow diagram of the experimental studies presented in this chapter on gas flow behaviour in coal.

6.2. He flooding experiment

The preparations of the core sample, assembling of the sample on the triaxial cell and the procedure for the experimental measurements have been provided in Chapter 4. All

experimental measurements presented in this Chapter have been conducted on the coal sample B, as described in Chapter 4. Helium was selected as the first experimental gas to be injected into the coal sample. Helium was used at this stage as the following objectives could be met:

1. Helium is a non-adsorptive gas and its interaction with coal is negligible (Chen et al., 2006). Therefore, the results of the experiments can be used to study the expansion/compression of the coal sample with no chemically included deformation in the system (Pini et al., 2009; Mazumder et al., 2006).

2. Helium has the smallest kinetic diameter among other gases, i.e. 0.26nm (Mehio et al., 2014), considered which can penetrate most of the pores that are not available to other gases (Gan et al., 1972). As a result, data produced from the helium flow measurements provide crucial information about the initial condition of the coal sample.

3. Coefficient of permeability values obtained from the helium flooding experiment, i.e. the absolute permeability of the coal sample to helium, is a useful basis for comparison of the relative permeability of a single sample to various gas species (Shen et al., 2011).

4. The results of the helium flow and permeability measurements can be used as a basis for comparing different coal samples in terms of their initial gas flow properties.

Figure 6.2 presents the results of the helium flow rate versus differential pressure obtained for a range of gas injection pressures up to 5.5MPa and confining pressures up to 6MPa at 298K.

According to the results achieved and despite a certain pressure gradient across the sample, no flow could be recorded at low pressures within the timescale allowed, i.e. 15 to 30 minutes. This effect has been attributed to “threshold phenomenon” (Chen et al.,

2006). Accordingly, a certain nonzero pressure gradient (1.7MPa/m) was required to initiate the flow.

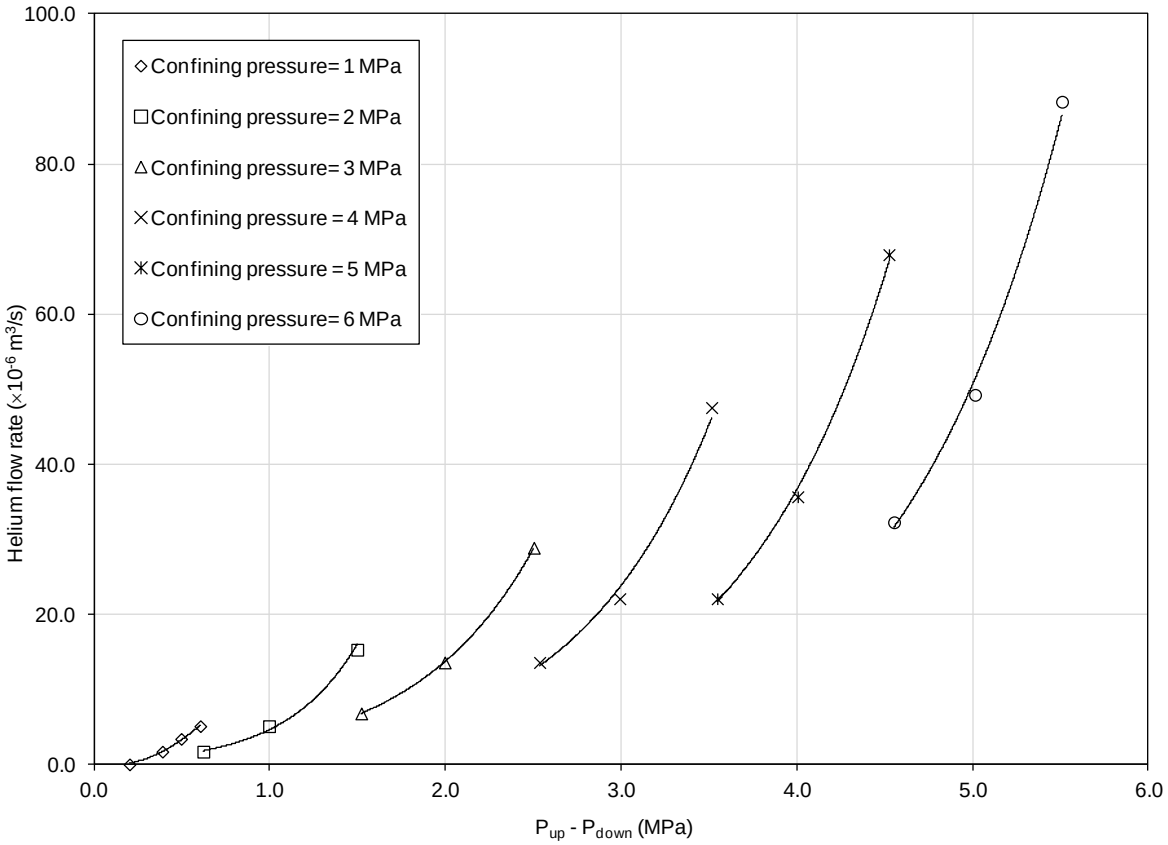

Fig. 6.2. The results of helium flow rates versus differential gas pressure between the upstream and downstream at various confining pressures (T=298K).

The overall gas flow rate was increased with increases in the gas injection pressure. A maximum value of $88\times10^{-6}m^3/s$ at approximately 5.5MPa differential gas pressure and 6MPa confining pressure has been observed. In addition, under constant gas injection pressures, a considerable decrease in the gas flow rate was observed as a result of increases in the confining pressure applied.

The results presented in Figure 6.2 exhibited a slight non-linearity between the volumetric gas flow rate and the differential pressure across the sample, especially at lower confining pressures (3MPa and less). According to Darcy's law, the relationship between gas flow rate and differential pressure is considered to be linear. The non-

linearity observed between the gas flow rate and differential pressure has also been reported by other researchers. Jasinge et al. (2011) has mentioned the possibility of a transition of the flow regime to a non-Darcian gas flow. The non-linearity in gas flow behaviour has been also reported to be attributed to the influence of changes in the effective stress applied during coal permeability measurements (Vishal et al., 2013; Jasinge et al., 2011; Perera et al., 2011). The relationship between coal permeability and effective stress is discussed in the following section. In addition, the compliance of the system due to changes in stress conditions may have also been influential on the non-linearity observed between the gas flow rates and differential gas pressure.

The linearity of the flow, however, has improved at higher pressures. This could be due to the fact that under higher confining pressures, potential changes in the stress regime have less effect on pore morphology (Jasinge et al., 2011). The gas flow rate observed in this study under constant effective stress has been assumed to be linear, therefore Darcy's Law was applied for the calculations of the gas permeability coefficients.

6.2.1. Absolute permeability of the coal

The absolute permeability of the coal sample was calculated using data from the phase 1 of helium flow measurements using Darcy's equation (equation 4-11). Figure 6.3 presents the absolute permeability of the coal sample at different gas pressures and confining pressures.

As shown in Figure 6.3, at constant confining pressure of 1MPa, the absolute permeability of the coal sample has increased considerably by the increase in gas injection pressure and reached to a maximum value of $1.35\times10^{-15}m^2$ (at differential gas pressure of 0.6MPa). The gas injection pressure was then kept constant and the confining pressure was increased to 2MPa. As a result, the coal permeability has decreased by 68%. After considerable changes observed in the first stage, the permeability variations due to increase in gas pressure or confining pressure became steadier. At constant gas injection pressures, an average permeability reduction of 54% was observed for every 1MPa

increase in confining pressure. The lowest absolute permeability, i.e. $0.19\times10^{-15}m^2$, was obtained at the confining pressure of 6MPa and differential gas pressure of 4.5MPa. Overall, an average permeability reduction of 78% was estimated during the course of this experiment.

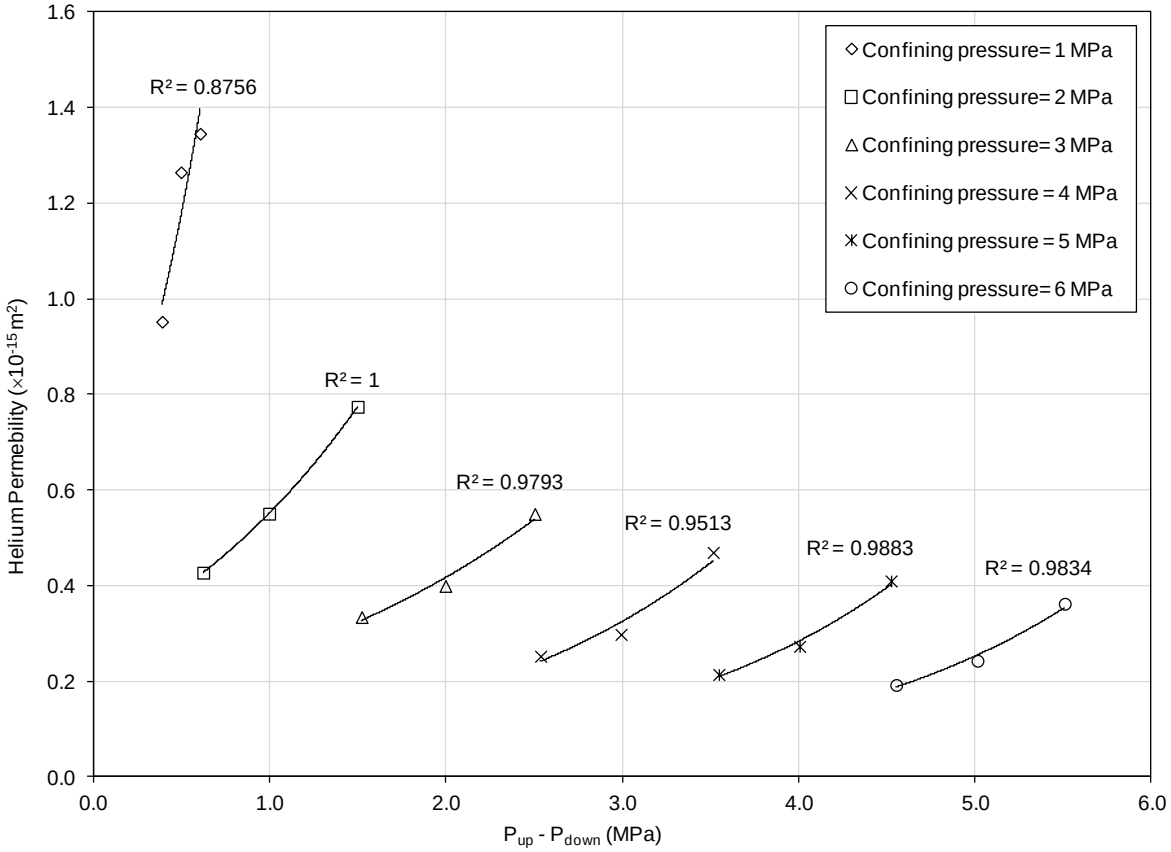

Fig. 6.3. Absolute permeability of the coal sample to helium versus differential gas pressure between upstream and downstream at various confining pressures (T=298K).

The variations in the coal permeability during gas injection experiments can be attributed to several factors. As stated earlier, helium is a non-adsorptive gas and therefore the effect of cleat volume decrease on the coal permeability induced by matrix swelling is almost negligible. Other factors that might affect the coal permeability of the coal sample are the Klinkenberg effect, especially at lower pressure range (Klinkenberg, 1941; Somerton et al., 1975; Chen et al., 2006) and the effective stress effects (Chen et al., 2011; McKee et al., 1988; Seidle and Huitt, 1995), which are discussed in details in the remainder of this section.

The Klinkenberg effect is related to the slippage of the gas molecules along the pore or fracture walls at lower gas pressures. This effect can result in higher flow rates and an apparent increase in the permeability compared to those measured for liquids (Gilman and Beckie, 2000; Klinkenberg, 1941; Pan et al., 2010; Chen et al., 2006; Somerton et al., 1975). The Klinkenberg effect, however, disappears at higher gas pressures, e.g. higher than 2MPa, as the mean free path of the gas molecules is far less than the aperture of the coal cleats (Laubach et al., 1998; Harpalani and Chen, 1997; Sometron et al., 1975). Therefore, collisions between gas molecules are more frequent than any collisions between the gas molecules and pore or fracture walls (Han et al., 2010).

The results of a study of helium flooding test on a coal sample from San Juan Basin in the US have shown that at gas pressures higher than 1.7MPa, the effect of matrix shrinkage is dominant, whereas at gas pressures lower than 1.7MPa, both gas slippage and matrix shrinkage may influence the coal permeability (Harpalani and Chen, 1997).

In addition, the methodology adopted for the experimental gas flow measurements in coal should also be considered when accounting for the Klinkenberg effect (Carles et al., 2007). The Klinkenberg effect is mostly considerable in the experimental measurements that are performed using transient method (Shen et al., 2011; Chen et al., 2011), in which the gas flow measurements are performed under unsteady-state conditions (Carles et al., 2007). Since the experimental results of this study have been obtained under the steady-state conditions, the results of the gas flow measurements and permeability coefficients are assumed to be corrected for the Klinkenberg effect (Carles et al., 2007). Therefore, the Klinkenberg effect was not considered to be a dominant factor for variations of coal permeabilities observed in this study.

The other factor, as mentioned previously, is the effect of effective stress that can be influential in coal permeability changes, especially for low permeability coals that the flow behaviour is highly dependent on the effective stress (Huy et al., 2010). The effective stress of coal subjected to a gas pressure can be expressed as (Harpalani and Chen, 1997):

$$\sigma_{eff} = P_c - \frac{P_{up} + P_{down}}{2} \tag{6-1}$$

where, σ_{eff} is the effective stress (MPa) and P_c is the confining pressure (MPa).

By plotting the experimental results of the coal permeability to helium versus the effective stress calculated using equation (6-1), a general trend of the coal permeability reduction can be observed as a result of increase in the effective stress. This behaviour has been shown in Figure 6.4.

By applying an appropriate regression to the experimental results, an empirical relation between the coal permeability to helium and effective stress was developed, given as:

$$k_{(He)} = 1.5202 exp(-0.568\,\sigma_{eff}) \tag{6-2}$$

where, $k_{(He)}$ is the permeability of the coal to helium (m^2).

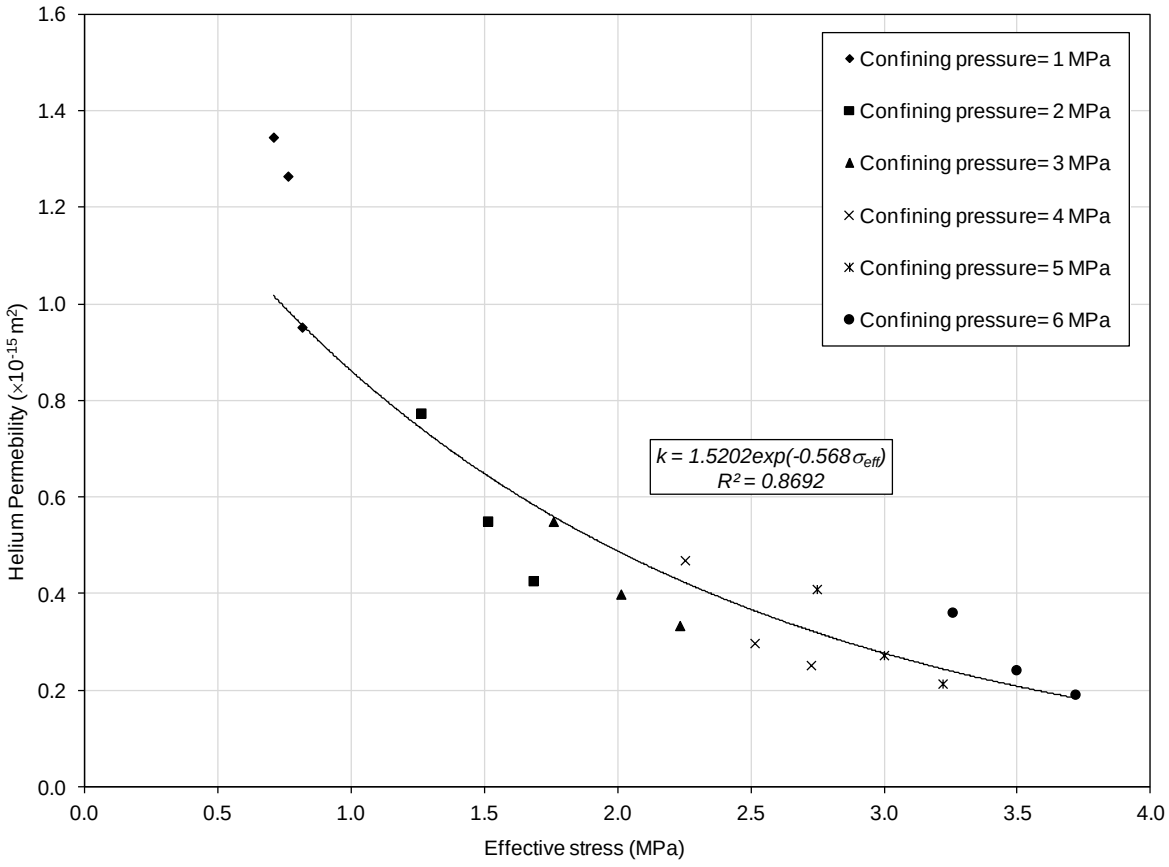

Fig. 6.4. The relationship between coal permeability to helium and effective stress (T=298K).

As the results in Figure 6.4 show, the exponential function demonstrates a relatively good fit with the experimental data. The exponential relationship between the coal permeability and effective stress has been also reported by other researchers (Jasinge et al., 2011; Vishal et al., 2013; Chen et al., 2006; McKee et al., 1988; Seidle and Huitt, 1995). It should be noted that the logarithmic and linear relationships have been also suggested in some experimental studies (Vishal et al., 2013; Seidle et al., 1992).

As shown in Figures 6.3 and 6.4, the permeability of coal to helium decreased more rapidly at lower stress conditions. This can be attributed to the immediate closure of existing microfractures under low stress conditions (Durucan and Edwards, 1986; Somerton et al., 1975). Therefore, only the second section of the curve represents the real behaviour of the coal material under stress (Durucan and Edwards, 1986).

The variations of the coal permeability with effective stress can be controlled by the compression of the pores and fracture system at higher effective stresses (Durucan and Edwards, 1986; Somerton et al., 1975), or as a result of both compression and microfracturing of the coal material (Durucan and Edwards, 1986). The compressibility of the fracture system changes as the effective stress increases (Pan et al., 2010). Therefore, at higher stress conditions, the effect of effective stress on coal permeability becomes less considerable, as observed in the results presented in Figures 6.3 and 6.4.

6.2.2. Coal volumetric strains in response to He injection

As mentioned in Chapter 4, volumetric deformation of the coal sample has been measured based on the volume of the displaced silicone oil. It should be mentioned that due to the high compressibility of the silicone oil at lower pressures (less than 1MPa), the results of the volumetric strains under 1MPa confining pressure are not included in the results which are presented here. In addition, the volumetric strains presented here are comparative values and noncumulative.

Figure 6.5 presents the results of the volumetric expansion of the coal sample due to the increase in gas pressure under the constant confining pressures. As the results in Figure

6.5 show, at a constant confining pressure, the increase in pore pressure resulted in the decrease of the effective stress and consequently expansion of the coal sample. Overall, every 0.5MPa increase in the mean gas pressure has induced an expansion of approximately 0.07% in the coal sample (under constant confining pressures).

Figure 6.6 presents the volumetric compressions of the coal sample due to increase in the confining pressure at constant gas pore pressures. The results showed that the coal sample exhibited an average compression rate of 1.9% for every 1MPa increment in confining pressure applied.

The total volumetric compression of the coal sample during the five cycles of loadings (applying ~5MPa confining pressure) applied was approximately 9.5%. The total expansion of the coal sample due to 2.7MPa increase in the mean gas pore pressure was estimated to be approximately 0.4%.

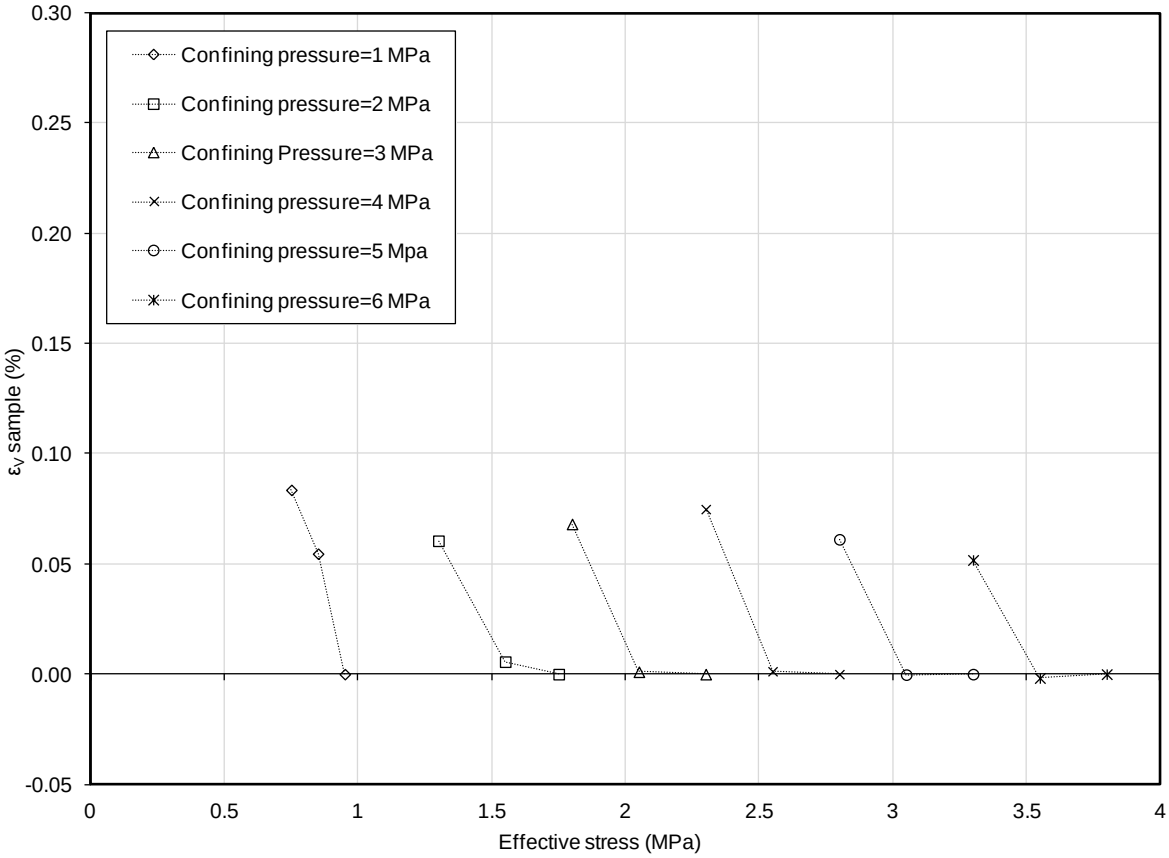

Fig. 6.5. Volumetric expansion of the coal sample versus effective stress variations due to increase in helium pressure at constant confining pressures (T=298K).

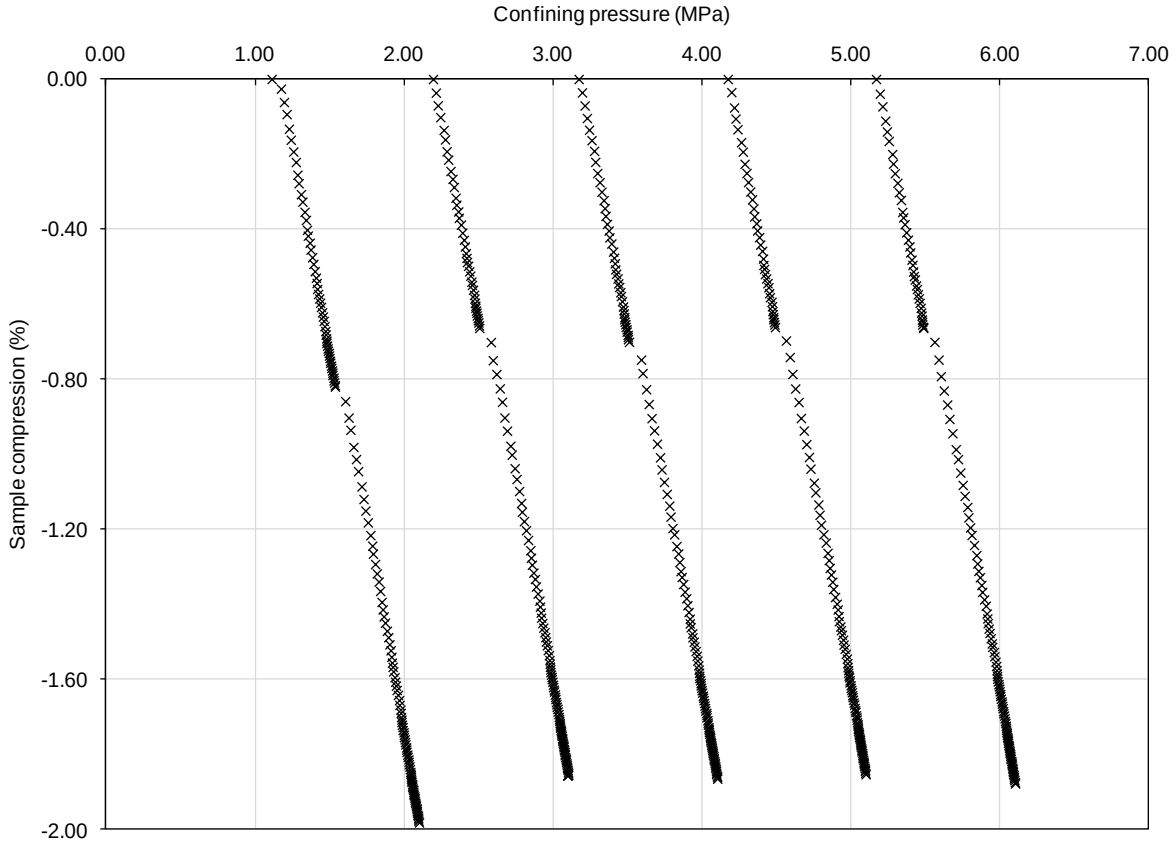

Fig. 6.6. Compression of the coal sample during helium flooding experiment due to increase in the confining pressures (T=298K).

Since helium is a non-reactive/non-adsorptive gas, the volumetric strains of the coal sample observed are purely attributed to the mechanical deformations of the coal sample due to variations in effective stress, i.e. expansion and compression in response to the internal and external forces.

6.3. N_2 flooding experiment

Similar experimental procedure that was performed for helium flow measurements was repeated for the N_2 flooding experiment. The confining pressure was set to 1MPa and the coal sample was subjected to vacuum for 24 hours. Once the sample was saturated with N_2, the gas flow measurements were performed according to the pressure steps defined in Table 4.4. The experimental results of the N_2 flow rate versus differential gas pressures at confining pressures up to 6MPa are presented in Figure 6.7.

Similar to the behaviour observed for helium, a threshold phenomenon was observed at lower gas pressures and despite a certain pressure gradient across the sample no gas flow was observed within the time scale allowed (15 to 30 minutes). A minimum pressure gradient of 1.7MPa/m was required to initiate the gas flow across the coal sample.

At constant confining pressure, the N_2 flow rate increased with the increase in gas pressure. A maximum N_2 flow rate of $7.2\times10^{-5}m^3/s$ is observed at 6MPa confining pressure when the gas pressure at upstream of the coal sample has been increased to 5.5MPa. At a constant gas injection pressure, an average gas flow reduction of approximately 65% was obtained as a result of 1MPa increase in the confining pressure.

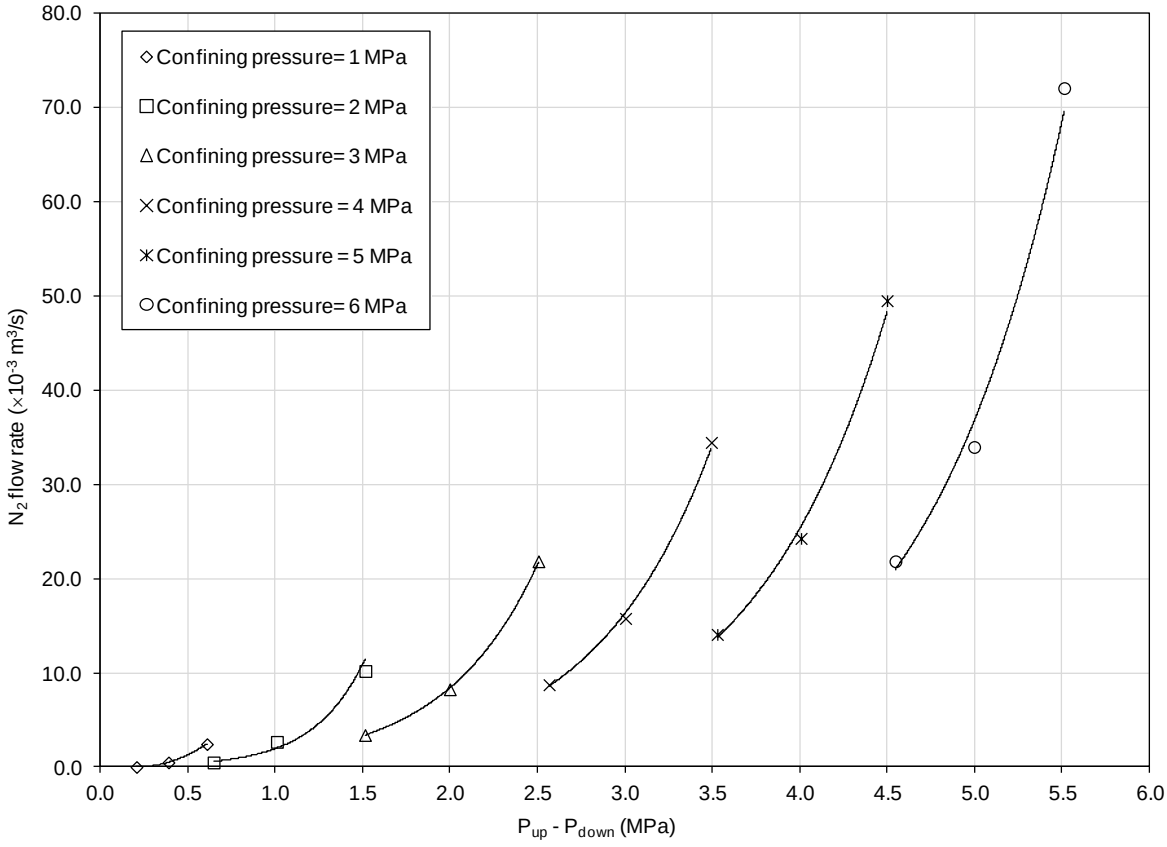

Fig. 6.7. The results of N_2 flow rates versus differential gas pressure between the upstream and downstream at various confining pressures (T=298K).

6.3.1. Permeability of the coal to N_2

The permeability coefficients of the coal sample to N_2 were calculated based on equation (4-11). The results of the N_2 permeability coefficients versus differential gas pressures up

to 5.5MPa at several confining pressures are presented in Figure 6.8. The maximum permeability coefficient of $0.55\times10^{-15}m^2$ was obtained at 0.6MPa differential gas pressure and under 1MPa confining pressure applied. The overall coal permeability decreased with increase in the confining pressure. At constant gas injection pressures, an average permeability reduction of 65% was observed as a result of every 1MPa increment of confining pressure.

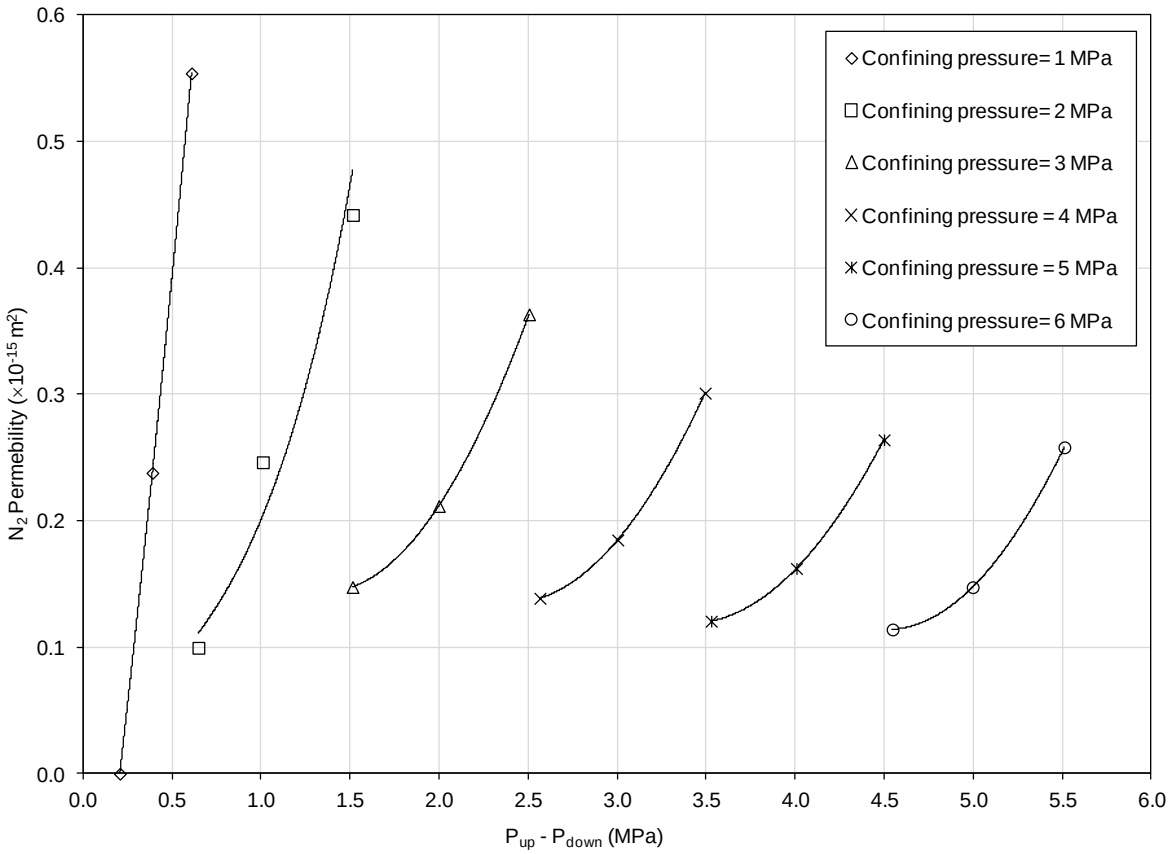

Fig. 6.8. Permeability of the coal sample to N_2 versus differential gas pressure at various confining pressures (T=298K).

Figure 6.9 presents the variations of the coal permeability to N_2 with the effective stress. Similar to the helium flooding results, overall permeability of the coal sample decreased with increase in the effective stress. An exponential relationship between the coal permeability to N_2 and the effective stress has been found as:

$$k_{(N_2)} = 0.4386exp(-0.324\,\sigma_{eff}) \tag{6-3}$$

where, $k_{(N_2)}$ is the permeability of the coal to N_2 (m^2).

As the results in Figure 6.9 show, the exponential regression between the coal permeability to N_2 and effective stress is very poor, compared to the results of helium flooding experiments, which may limit the application of the established exponential relationship, i.e. equation (6-3). Other types of regressions, e.g. logarithmic or power regressions showed slightly better fits with the highest coefficient of determination (R^2) found to be 0.46. However, in order to maintain the consistency of the results the exponential relationship has been presented here.

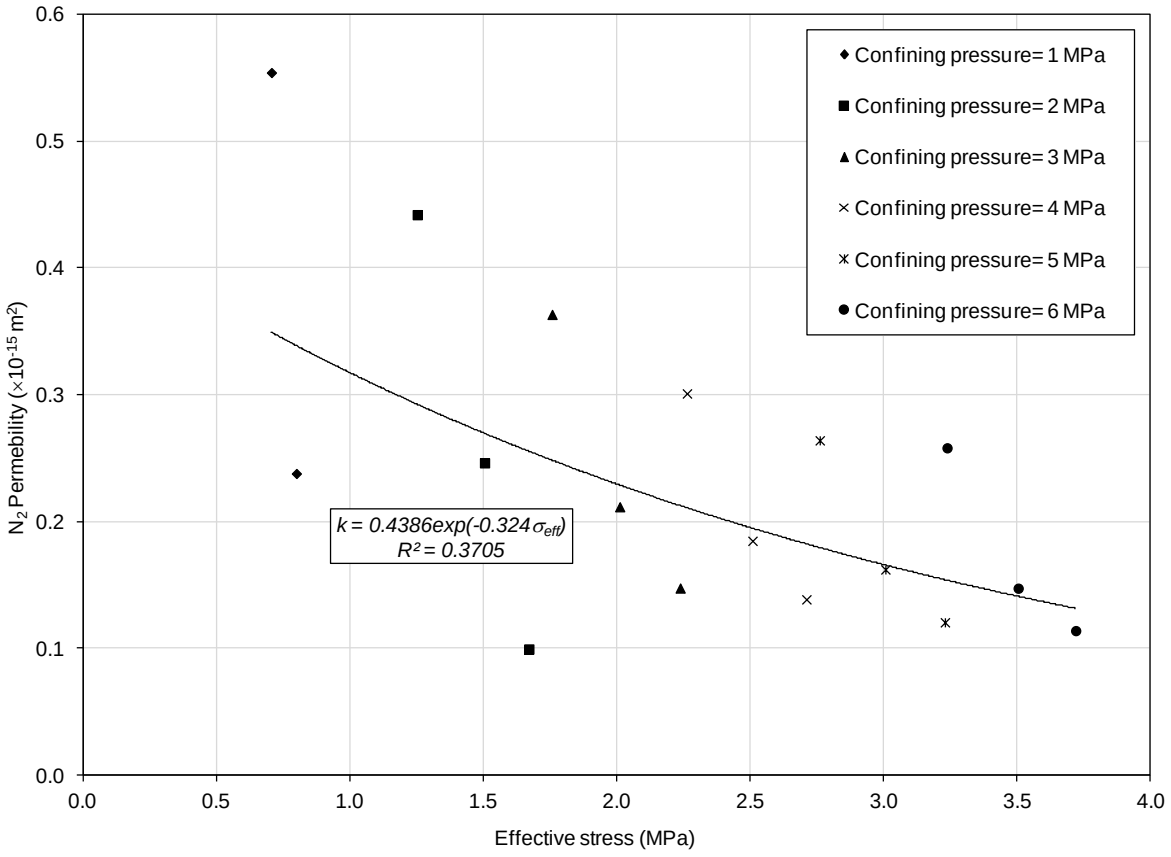

Fig. 6.9. The relationship between the coal permeability to N_2 and effective stress (T=298K).

The relative permeability values of the coal sample (k_r), i.e. $K_{(N_2)}/K_{(He)}$, were also estimated based on the results of the N_2 permeability and the absolute permeability coefficients for a range of gas pressures and confining pressures. The results are presented in Figure 6.10.

From the results it was observed that, in general, the permeability of the coal sample to N_2 was lower than those obtained for helium. The differences in permeability values of a same coal to different gas species can be attributed to several factors such as the coal matrix swelling/shrinkage due to gas adsorption/desorption processes (Mazumder et al., 2006; Pan et al., 2010), differences in kinetic diameters of different gas species (Cui et al., 2004; Gan et al., 1972) and hysteresis due to loading and unloading cycles (Somerton et al., 1975; Dabbous et al., 1974).

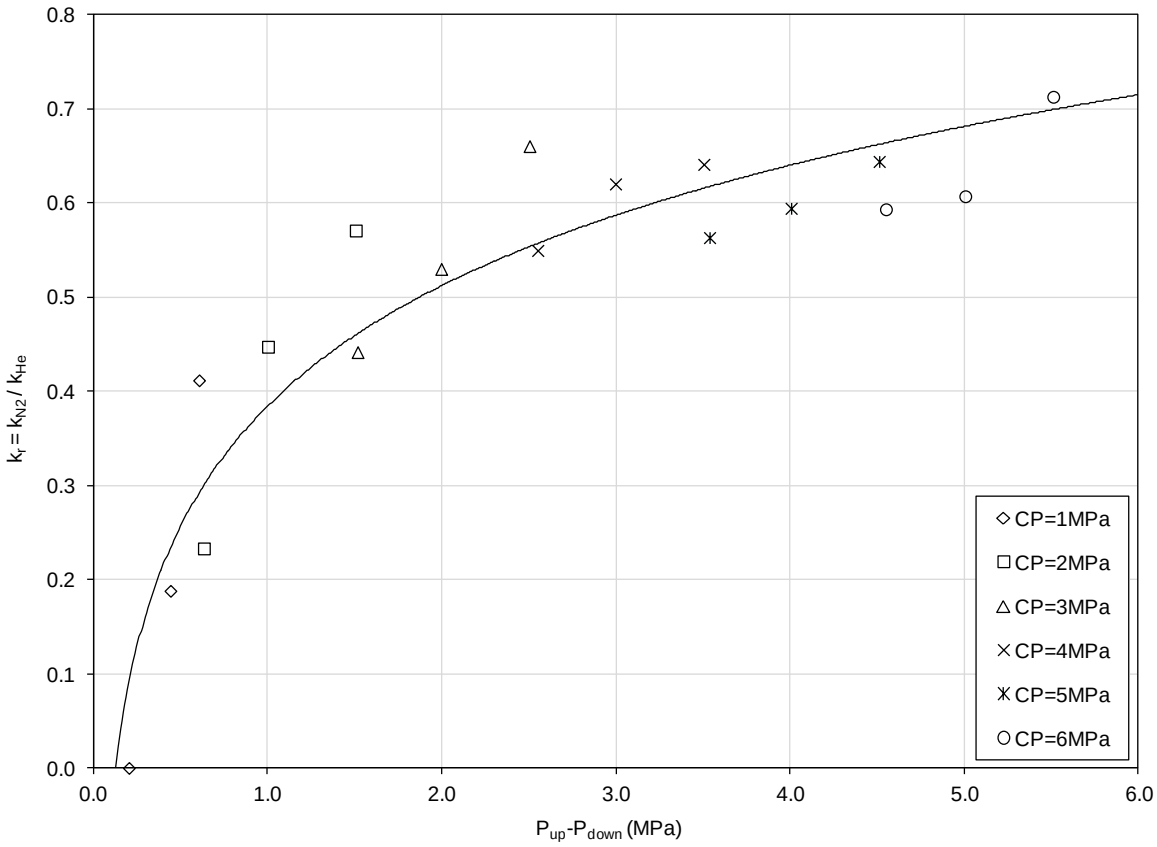

Fig. 6.10. Relative permeability (k_r) of the coal sample to N_2 versus differential gas pressure at various confining pressures (T=298K).

From the results of the N_2 adsorption/desorption measurements (Chapter 5), it was observed that N_2 adsorption capacity of the coal is smaller than the other gases. In addition, it was shown that its volumetric effect on coal is negligible. Therefore, the cleat porosity decrease due to matrix swelling and the effects on permeability of the coal sample is negligible.

The results in Figure 6.10 show that the relative permeability of the coal sample to N_2 was much lower than those for helium at lower pressures which might be related to the immediate closure of microfractures (Durucan and Edwards, 1986; Somerton et al., 1975) and larger kinetic diameter of N_2, i.e. 0.36nm (Gan et al., 1972). Due to the smallest kinetic diameter, i.e. 0.26nm (Mehio et al., 2014), helium can penetrate most of the pores that might not be accessible for N_2 molecules.

The hysteresis as a result of repeated loading and unloading cycles might have also led to the lower permeability of the coal sample to N_2 (Somerton et al., 1975; Dabbous et al., 1974). Dabbous et al. (1974) reported strong hysteresis due to different cleat compressibility at loading and unloading cycles. Although changes in fracture system and cleat aperture are largely reversible at lower stress conditions (Wang et al., 2013), higher effective stresses can result in non-reversible changes such as creating new fractures or microfractures. The relative permeability of the coal sample to N_2, however, increased with increase in gas pressure and confining pressure and reached to a maximum 70% of helium permeability at corresponding stress condition.

6.3.2. Coal volumetric strains in response to N_2 injection

The comparative and noncumulative volumetric expansions of the coal sample due to increases in N_2 pressure at constant confining pressures are presented in Figure 6.11. In order to compare the effect of N_2 on the volumetric strains of the coal sample with the behaviour observed during helium injection, the volumetric strains from the helium flooding experiment are included in this graph (dashed lines). The results show that the amounts of coal expansion due to N_2 injection into the coal are slightly higher than those obtained in the case of helium injection, especially at lower effective stress values.

As the effective stress increases, the expansion rate decreases and matches with the results of helium flooding experiment. The maximum expansion rate of 0.17% is obtained at 1MPa confining pressure when the N_2 injection pressure has been increased to

0.6MPa. At constant confining pressures, an average expansion rate of 0.08% was observed as a result of 0.5MPa increase in the gas pressure.

Figure 6.12 presents the results of the volumetric compression of the coal sample due to increases in confining pressure only. An average compression rate of 1.9% was estimated due to every 1MPa increase in the confining pressure.

The total expansion and compression of the coal sample during the N_2 flooding experiments were found to be 0.55% and 9.3% of the initial volume, respectively. As stated previously, the volumetric effects of N_2 on coal matrix due to its sorption are negligible. Therefore, it can be assumed that the volumetric deformations observed are mostly related to the mechanical deformation of the coal sample.

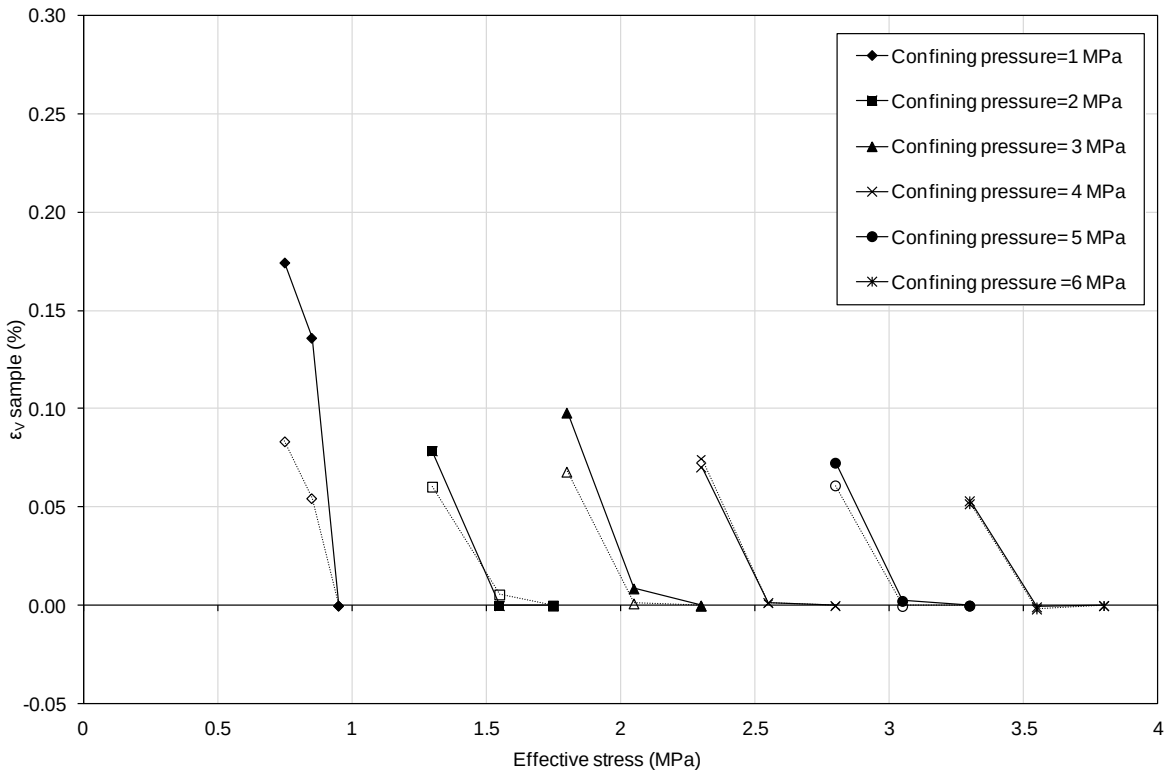

Fig. 6.11. Volumetric expansion of the coal sample versus effective stress variations due to increase in N_2 pressure at constant confining pressures (T=298K); dashed lines show the volumetric expansions of the coal sample during phase 1 of helium flooding experiment.

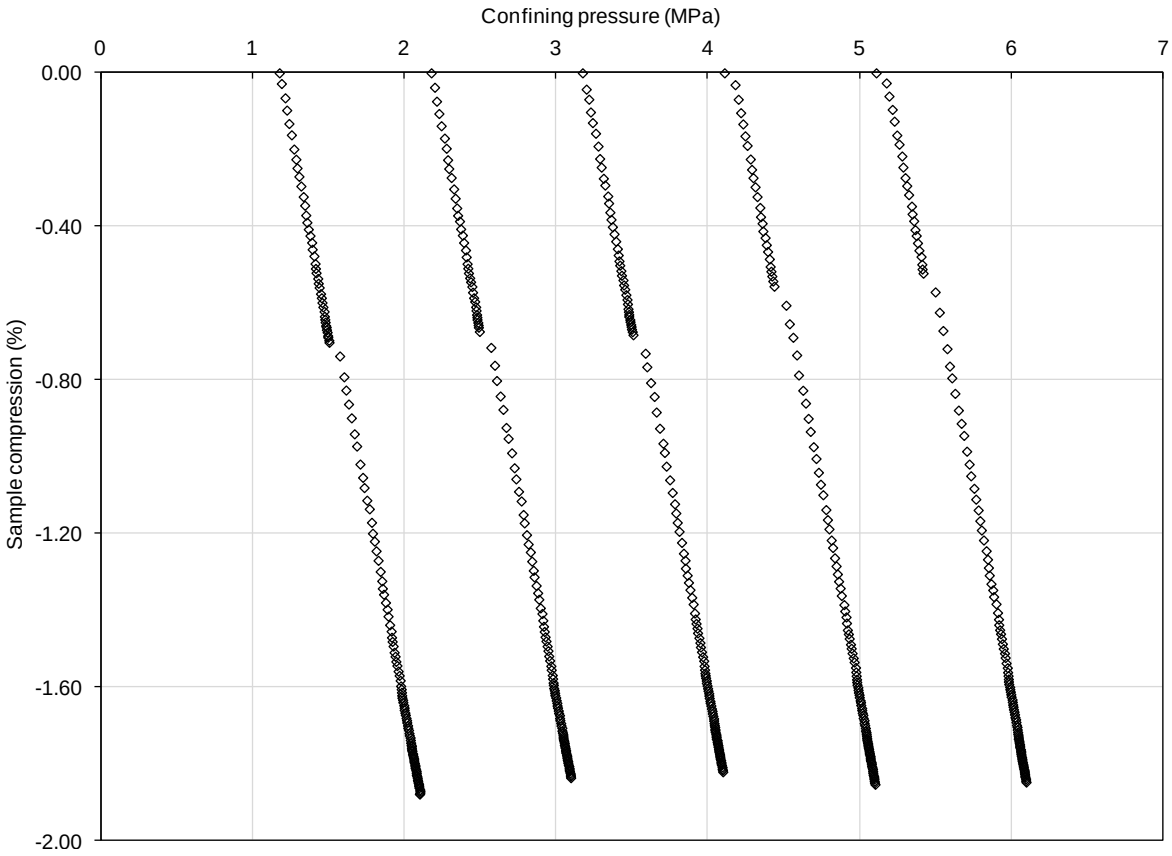

Fig. 6.12. Compression of the coal sample during N_2 flooding experiment due to increase in the confining pressures (T=298K).

The results of the volumetric strains show that the mechanical strains of the coal sample during N_2 flooding experiments are almost similar to those observed in the helium flooding experiments. Therefore, it can be suggested that the differences between permeabilities of the coal sample obtained from the He and N_2 flooding experiments are mostly related to properties of the gas species (kinetic diameter). The behaviour may be also less affected by hysteresis and changes in the coal structure related to loading and unloading applied during previous stages of the test. Although it should be mentioned that due to complex nature of coal material, it is difficult to distinguish and separately quantify the effects of different factors on gas flow and deformation behaviour of the coals. For instance, parameters such as the cleat compressibility which is often considered as a constant value in a certain coal might also change with changes in effective stress (Pan et al., 2010).

6.4. CO_2 flooding experiment

After N_2 flooding experiment, the CO_2 flooding experiment was performed on the coal sample after applying vacuum and saturating with CO_2. The pressure steps are those defined in Table 4.4. The results of the CO_2 flow rate measurements versus differential gas pressure at several confining pressures up to 6MPa are presented in Figure 6.13.

It can be seen from the results that a minimum differential gas pressure of 0.2MPa is required to initiate the flow (due to the threshold phenomenon). Similar to the previous experiments, the CO_2 flow rate increased with increase in gas pressure and reached to a maximum flow rate of $8.96\times10^{-6}m^3/s$ at 3.5MPa gas pressure and 4MPa confining pressure. However, the overall CO_2 flow rate shows a decline despite the increase in gas pressure above the 3.5MPa gas pressure.

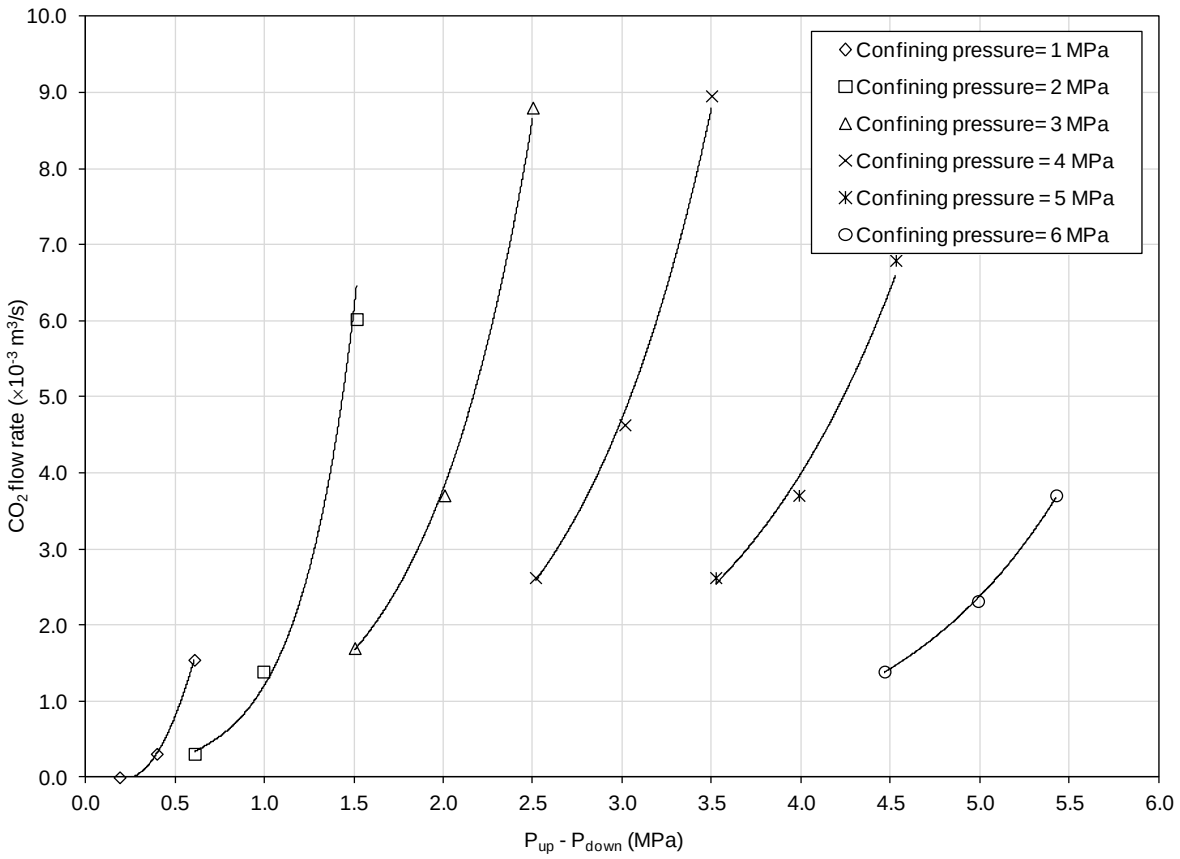

Fig. 6.13. The results of CO_2 flow rates versus differential gas pressure between the upstream and downstream at various confining pressures (T=298K).

The overall CO_2 flow rates were found to be much lower than those observed for He and N_2 gases which can be attributed to the larger kinetic diameter of CO_2 compared to helium and the hysteresis due to loading/unloading cycles, as discussed previously. In addition, the considerable reduction in gas flow rate with increase in gas pressure can be attributed to the effect of coal matrix swelling due to CO_2 adsorption which is discussed in more detail in the following section.

6.4.1. Permeability of the coal to CO_2

The CO_2 permeability of the coal sample was calculated using Darcy's equation, i.e. equation (4-11). The results of the permeability of the sample to CO_2 versus differential gas pressures at different confining pressures are presented in Figure 6.14.

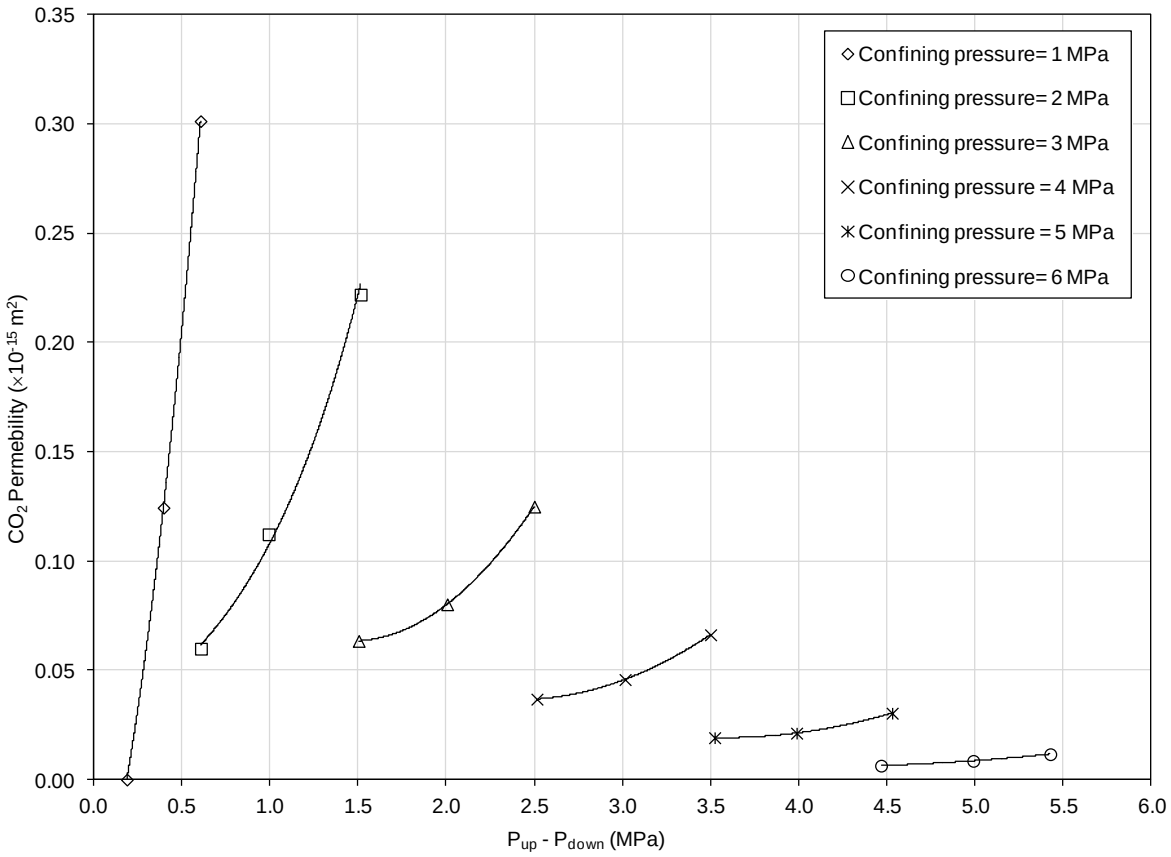

Fig. 6.14. Permeability of the coal sample to CO_2 versus differential gas pressure at various confining pressures (T=298K).

According to the results presented in Figure 6.14, at constant gas pressures every 1MPa increase in the confining pressure applied resulted in an average permeability reduction of approximately 70%. More importantly, as injection continued, the interaction between CO_2 and coal resulted in extensive coal swelling and consequently reduction of gas flow and permeability of the coal sample. At confining pressure of 6MPa, despite a 0.5MPa of increase in the gas pressure applied the coal permeability remained almost constant. The lowest permeability value of $0.01\times10^{-15}m^2$ is obtained at this stage.

The coal permeability reduction as a result of CO_2 adsorption and coal swelling has been reported elsewhere, e.g. Vishal et al. (2013), De Silva and Ranjith (2012), Jasinge et al. (2011). Vishal et al. (2013) measured the CO_2 permeability of Indian coal at 5MPa confining pressure and gas injection pressures up to 3MPa. It has been reported that the permeability of the coal reduced considerably with increase in injection pressure (Vishal et al., 2013). According to Wang et al. (2013), the overall change in the coal permeability is a function of the mechanical response, swelling or shrinkage of the matrix and the damage or fracture induced by the applied stress. The expansion of the coal matrix due to CO_2 adsorption leads to the closure of the cleats and fractures, which in turn reduces the permeability of coal (Siriwardane et al., 2009). Permeability decline despite the increase in pore pressure at constant confining pressures has been reported to be attributed to the adsorption-induced coal swelling (Pan et al., 2010).

Figure 6.15 presents the results of the coal permeability measurements versus effective stress. The coal permeability to CO_2 decreased exponentially with increase in the effective stress. The exponential relationship was found which can be given as:

$$k_{(CO_2)} = 0.6637exp(-1.146\,\sigma_{eff}) \quad (6\text{-}4)$$

where, $k_{(CO_2)}$ is the permeability of the coal to CO_2 (m^2).

The coal permeability to CO_2 decreased much faster at lower stress conditions which can be attributed to the closure of microfractures at low stresses (Durucan and Edwards, 1986; Somerton et al., 1975) as well as the swelling effect of CO_2 on coal matrix. The later effect, i.e. matrix swelling, can be more dominant at higher pressures as it was evident

from the results of CO_2 adsorption isotherms presented in Chapter 5. However, at low pressures the sharper decrease in the coal permeability compared to the He and N_2 flooding experiments can be explained by the effect of CO_2 adsorbed-phase volume on closure of the microfractures.

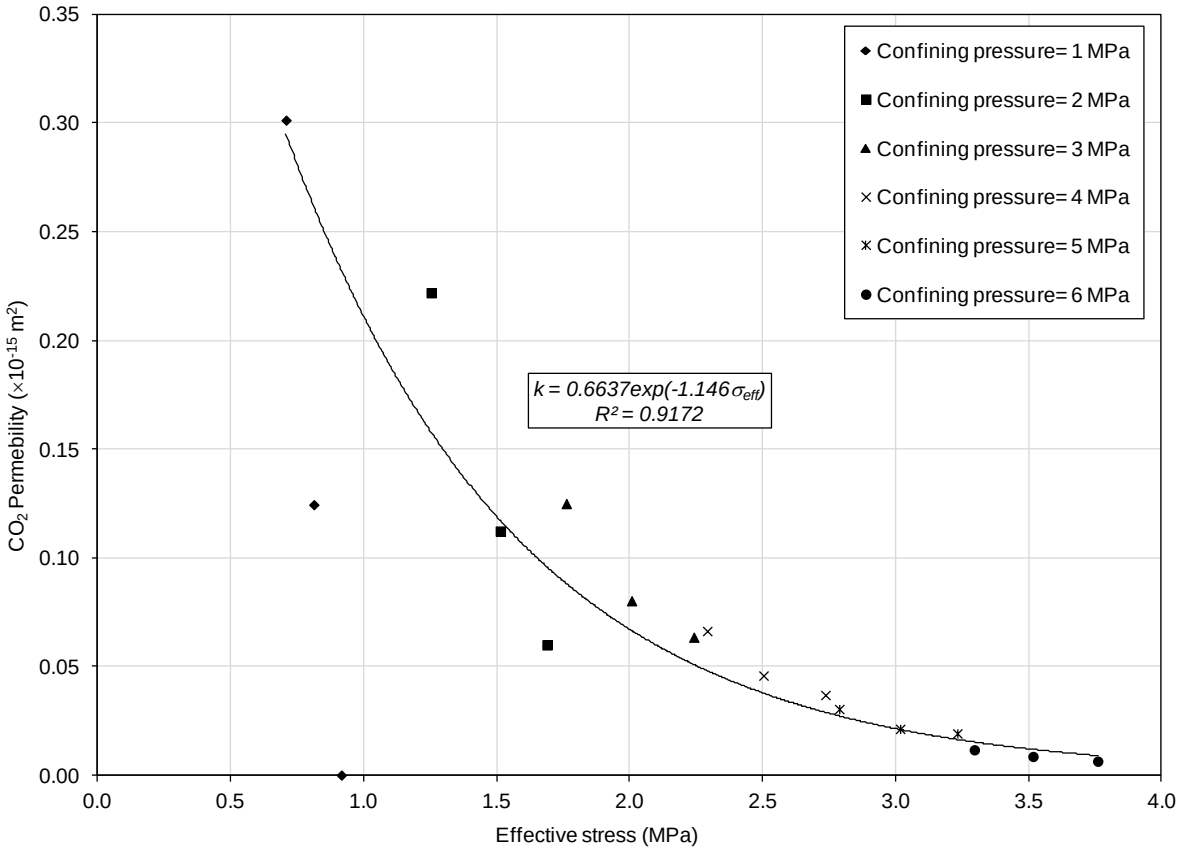

Fig. 6.15. The relationship between coal permeability to CO_2 and effective stress (T=298K).

As the experiment continued and gas pressure and confining pressure increased, the effect of the effective stress on coal permeability became less significant and the matrix swelling is likely to be the dominant factor in changes of the coal permeability. In general, the exponential relationship between the coal permeability to CO_2 and effective stress is found to be much stronger than those observed for He and N_2 (higher coefficient of determination for the case of CO_2).

The relative permeability of the coal sample to CO_2, i.e. $K_{(CO_2)}/K_{(He)}$, are presented in Figure 6.16. As the results show, the relative permeability of the coal sample to CO_2 at its highest

was less than 30% of its absolute permeability (helium permeability at corresponding pressures). Similar to the N_2 flooding experiment, this can be partly attributed to the larger kinetic diameter of CO_2 compared with He (Gan et al., 1972), as well as the hysteresis due to loading and unloading cycles (Somerton et al., 1975; Dabbous et al., 1974). However, the effect of adsorbed-phase volume on microfractures might have influenced the coal permeability even before the CO_2 flow measurements, i.e. during saturation stage. This may explain such lower permeability of the coal sample to CO_2.

The sharp decrease in the relative permeability of coal to CO_2 at higher effective stresses is related to the effect of coal matrix swelling on cleats and fracture system at higher pressures (Vishal et al., 2013; De Silva and Ranjith, 2012; Jasinge et al., 2011). The lowest relative permeability can be observed at effective stress of 5.5MPa (Figure 6.16) which was found to be 5% of its initial absolute permeability at corresponding stress conditions.

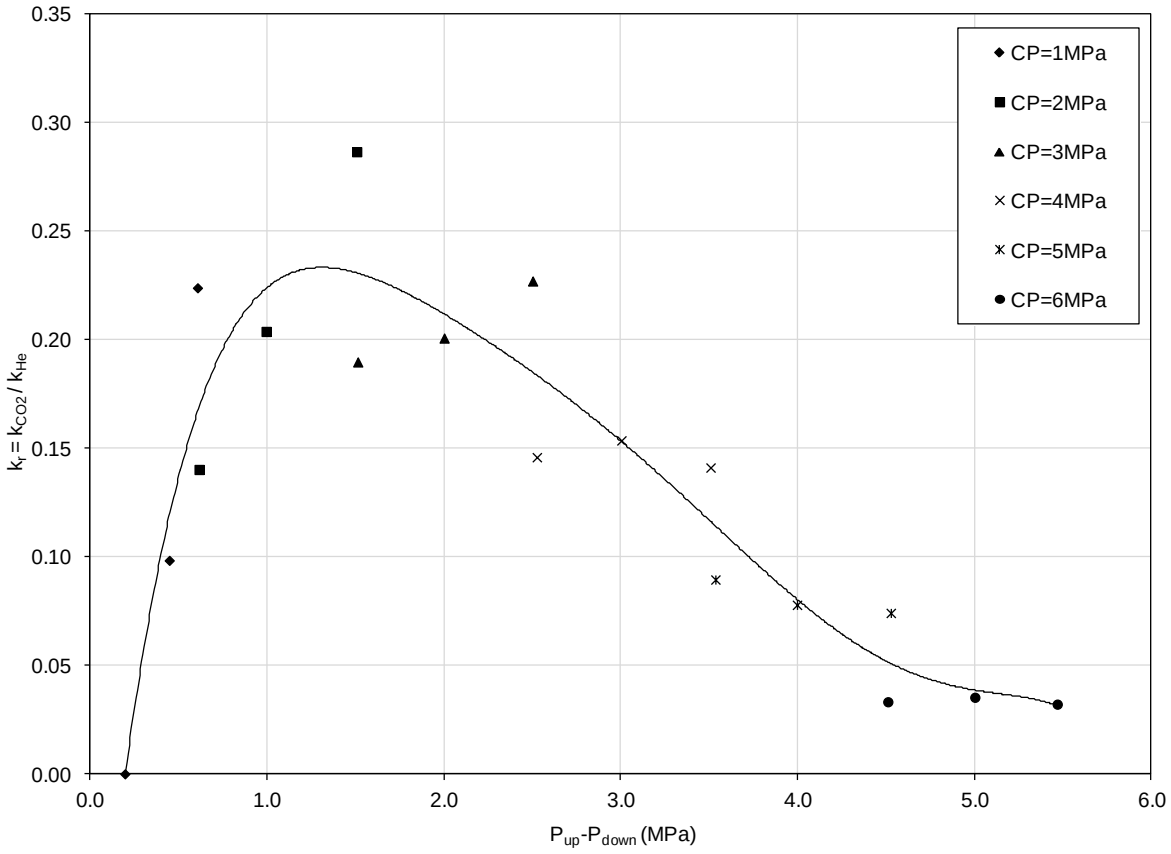

Fig. 6.16. Relative permeability (k_r) of the coal sample to CO_2 versus differential gas pressure at various confining pressures (T=298K).

6.4.2. Volumetric strains due to CO_2 injections

The volumetric deformations of the coal sample due to CO_2 injection at different confining pressures are presented in Figure 6.17 (Dashed lines represent the results of the phase 1 of helium flooding experiment). The overall volumetric expansion of the coal sample during CO_2 flooding experiment was much higher than those for other gases. For He and N_2 flooding experiments, it was observed that although the coal sample was expanded due to the increase in the pore gas pressure, the amounts of the volumetric expansion at different confining pressures were almost comparable. In the case of CO_2, however, this similarity is not observed and the amount of coal expansion increases more clearly which can be related to the swelling effect of CO_2 adsorption on coal.

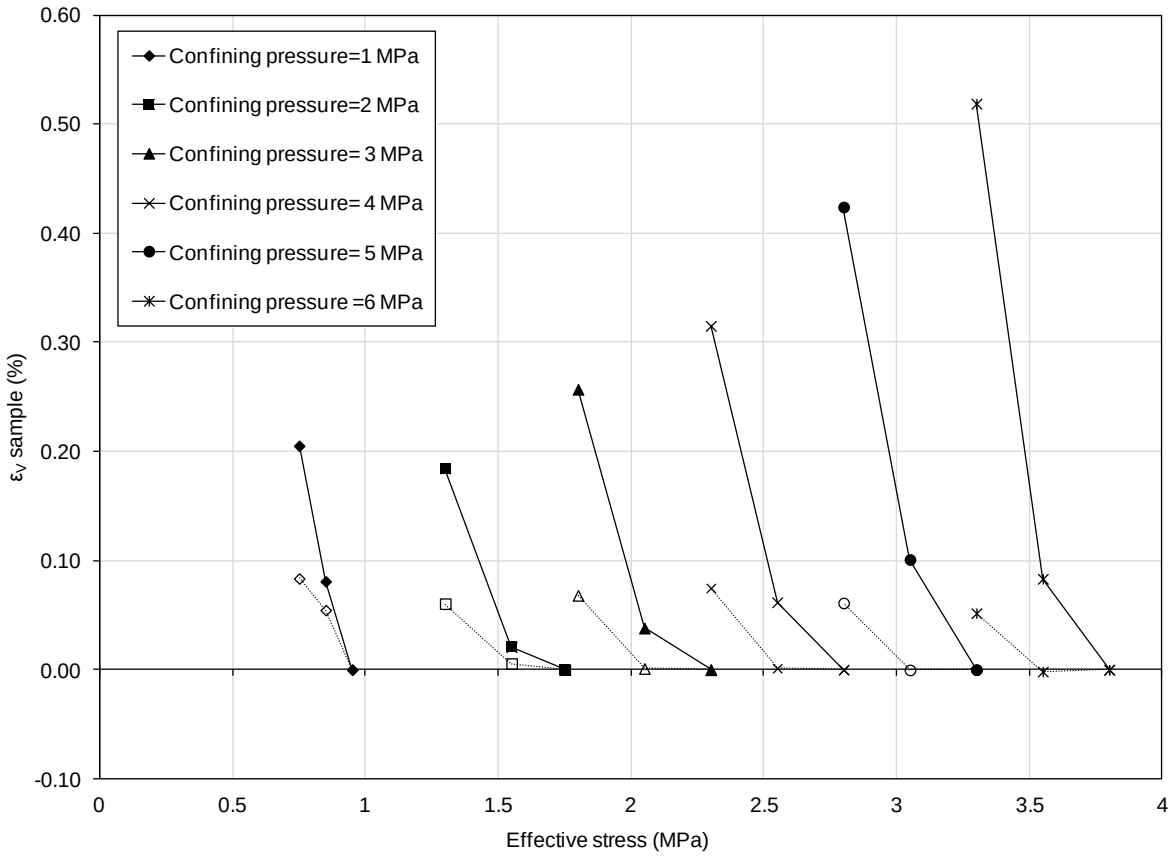

Fig. 6.17. Volumetric expansion of the coal sample versus effective stress variations due to increase in CO_2 pressure at constant confining pressures (T=298K); dashed lines show the volumetric expansions of the coal sample during phase 1 of helium flooding experiment.

The results of the volumetric compression of the coal sample due to increase in confining pressure at constant gas pressures are presented in Figure 6.18. From the results, it is observed that the average compression rate of the coal sample due to CO_2 flooding experiment is slightly lower than those obtained in N_2 flooding experiment. In addition, unlike previous experiments, the rate of the volumetric compression decreased with increase in the confining pressure.

A comparison between the results of the CO_2 and He flooding experiments shows that at 1MPa confining pressure, the increased volume of the coal sample due to 0.4MPa increase in CO_2 injection pressure is two times larger than those for the helium flooding experiment.

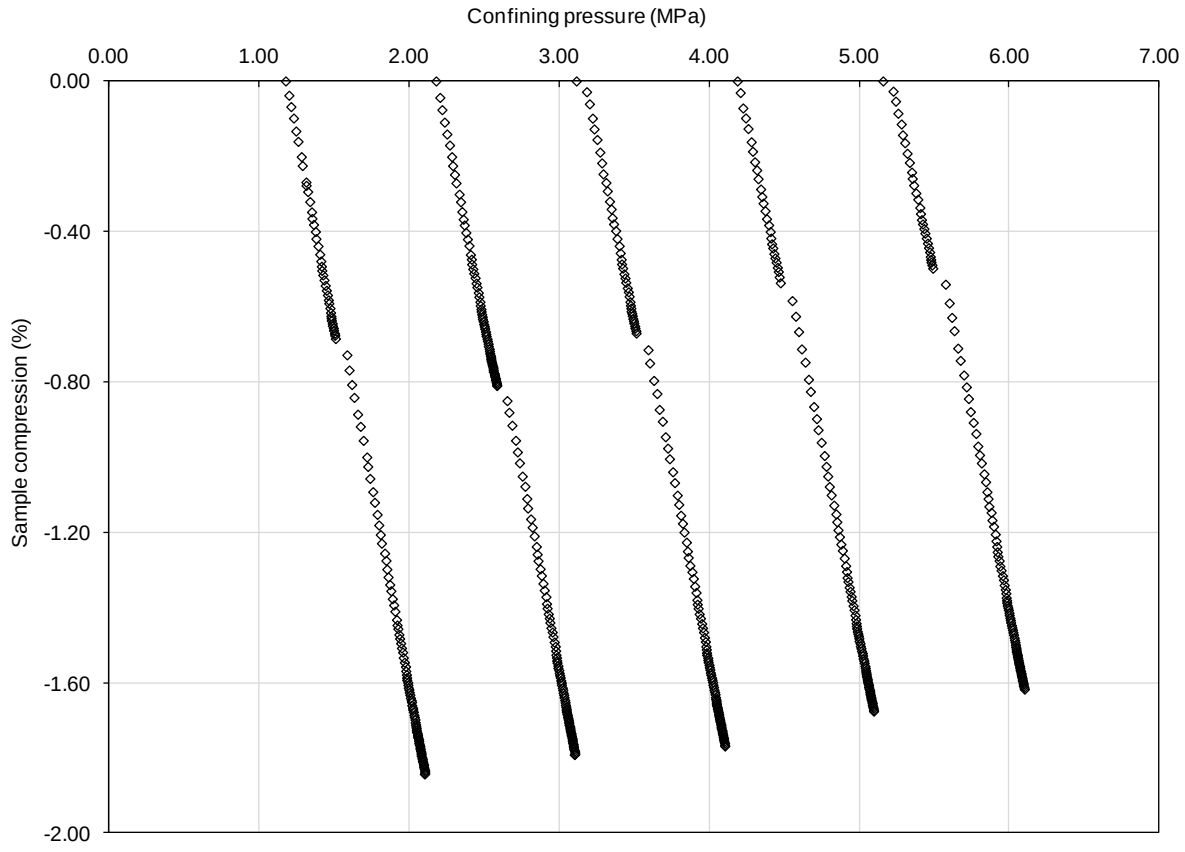

Fig. 6.18. Compression of the coal sample during CO_2 flooding experiment due to increase in the confining pressures (T=298K).

As higher injection pressure was applied, the difference between the volumetric strains observed in the He and CO_2 flooding experiments increased considerably. At the final step of the injection, the increase in the coal volume was found to be ten times more than those observed in the He flooding experiment. In general, the trend of the coal permeability variation with pore pressure was found to be opposite to that of the volumetric increase in coal. This behaviour can be attributed to the fact that coal adsorbs more CO_2 at higher injection pressures which leads to further swelling of the coal matrix.

The reduction in compression rate of the coal sample with increase in the confining pressure can be partly related to the permanent changes of the coal structure as a result of cyclic loadings and unloading. However, due to the extensive swelling of the coal sample which was observed (Figure 6.17), the actual response of the coal sample to mechanical compressions, i.e. increase in the compression rate, might have been underestimated.

Pan et al. (2010) observed that the cleat compressibility increased with increase in CO_2 pore pressure. In addition, the weakening effect due to adsorption of CO_2 in coal has been reported (Wang et al., 2011; De Silva and Ranjith, 2012; Harpalani and Mitra, 2010). Therefore, it can be suggested that the reduction in the volumetric compression of the coal sample is mostly related to the swelling effect of the coal sample and not increase in the coal strength.

The coal sample exhibited a total value of 1.9% volume increase during the CO_2 flooding experiment. The swelling effect was then quantified by subtracting the mechanical effects obtained from the phase 1 of helium flooding experiment. According to the results, the swelling effect of CO_2 in the volumetric expansion of the coal is 1.5%. It should also be mentioned that the volumetric strain measured here may have been underestimated for the matrix swelling because the cleat porosity may take part of the displacements (Vishal et al., 2013). In addition, due to the relatively short exposure of the coal sample to CO_2, the adsorption process might have not been completed and more swelling could be expected in longer exposure.

6.5. Fate of the adsorbed CO_2 in coal

In order to further assess the effect of CO_2 sorption on coal permeability evolution and more importantly to evaluate the fate of adsorbed CO_2 in coal, the coal sample was subjected to a sequence of gas flooding experiments using He, N_2 and CH_4 gases (Figure 6.1). The main objectives in conducting these experiments were to examine the extent of which the CO_2 adsorption in coal can remain in coal after a sequence of several gas flooding experiments and to evaluate the reversibility of the coal swelling due to CO_2 desorption and its effect on coal permeability evolution.

The phase 2 of helium flooding experiment was performed based on the pressure steps provided in Table 4.4. The experimental procedures were exactly similar to those performed for previous flooding experiments. The only difference here was that due to the significant reduction in coal permeability due to CO_2 adsorption-induced swelling, the vacuum process (for removing the residual/free gas) after CO_2 flooding experiment was found to be very slow. Therefore, in order to accelerate the evacuation process it was decided to purge the sample with helium.

The results of the coal permeability to helium obtained from the phase 2 of helium flooding experiment are presented in Figure 6.19. For comparison, the results of the phase 1 of helium flooding experiment (before CO_2 injections) are also included in the graph (dashed lines). It should be mentioned that the effect of the phase 1 of the N_2 flooding experiment on the coal sample was not accounted here as it was considered to be very small.

From the results it can be observed that the coal permeability has considerably decreased as a result of coal interactions with CO_2. For instance, at confining pressure of 1MPa despite a differential gas pressure of 0.3MPa existed across the sample no gas flow was observed. The coal permeability slightly increased at the differential gas pressure values higher than 0.6MPa. However, the gas flow rates and permeability values obtained from the phase 2 of helium injections, in general, were found to be very low. The overall trend

of the coal permeability remained almost steady throughout the test and did not show a considerable change with the effective stress.

An overall permeability reduction of 89% was observed at lower pressures. Although, the results of the relative permeability (presented in Figure 6.16) suggests a larger permeability reduction (nearly 95%), it can be assumed that some of the coal permeability was restored due to CO_2 desorption during vacuum process and helium saturation. At the higher gas injection pressures and confining pressures, the coal permeability increased slightly and reached to a value of approximately $0.07\times10^{-15}m^2$, i.e. 75% of the initial value. The average permeability value of the coal sample was increased by 14% during the phase 2 of helium injections.

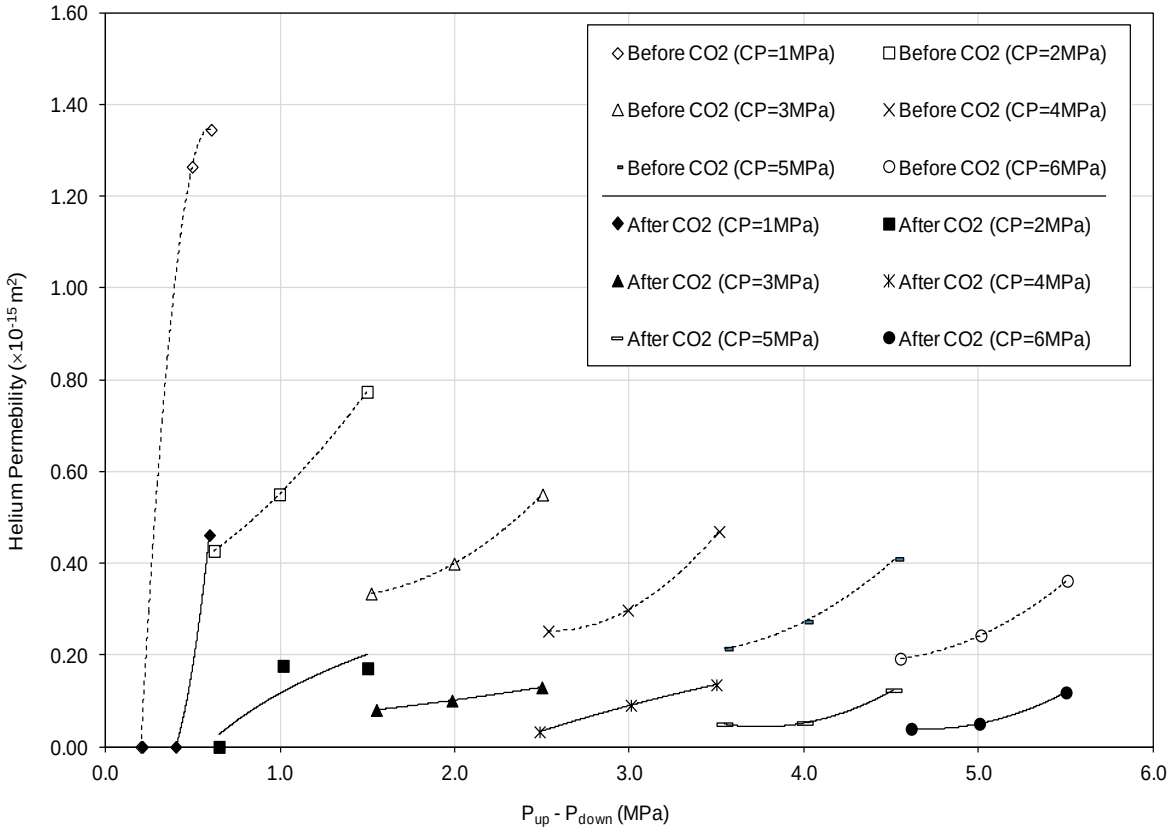

Fig. 6.19. Helium permeability of the coal sample before (dashed line) and after (solid line) CO_2 injections (T=298K).

6.5.1. The phase 2 of N_2 flooding experiment

Since helium is a non-adsorptive gas, its interaction with coal is almost negligible. Although, it might replace the free CO_2 molecules in the matrix pores and fracture system, it cannot replace the strongly adsorbed CO_2 molecules on coal surface. With N_2, however, the behaviour can be different. From the results of the N_2 adsorption/desorption isotherms presented in Chapter 5, it was observed that N_2 adsorbs to the coal to some extent. Therefore, its replacement with some of the adsorbed CO_2 might affect the coal swelling and permeability. In order to further investigate that, the coal sample was subjected to the phase 2 of N_2 injections. Accordingly, in order to evaluate the effect of the phase 2 of N_2 injections on changes in coal permeability and swelling effects of adsorbed CO_2, the phase 3 of helium flooding experiment was performed. The results are presented in Figure 6.20 along with the results of the phase 2 of helium flooding experiments (before and after the phase 2 of N_2 flooding experiment).

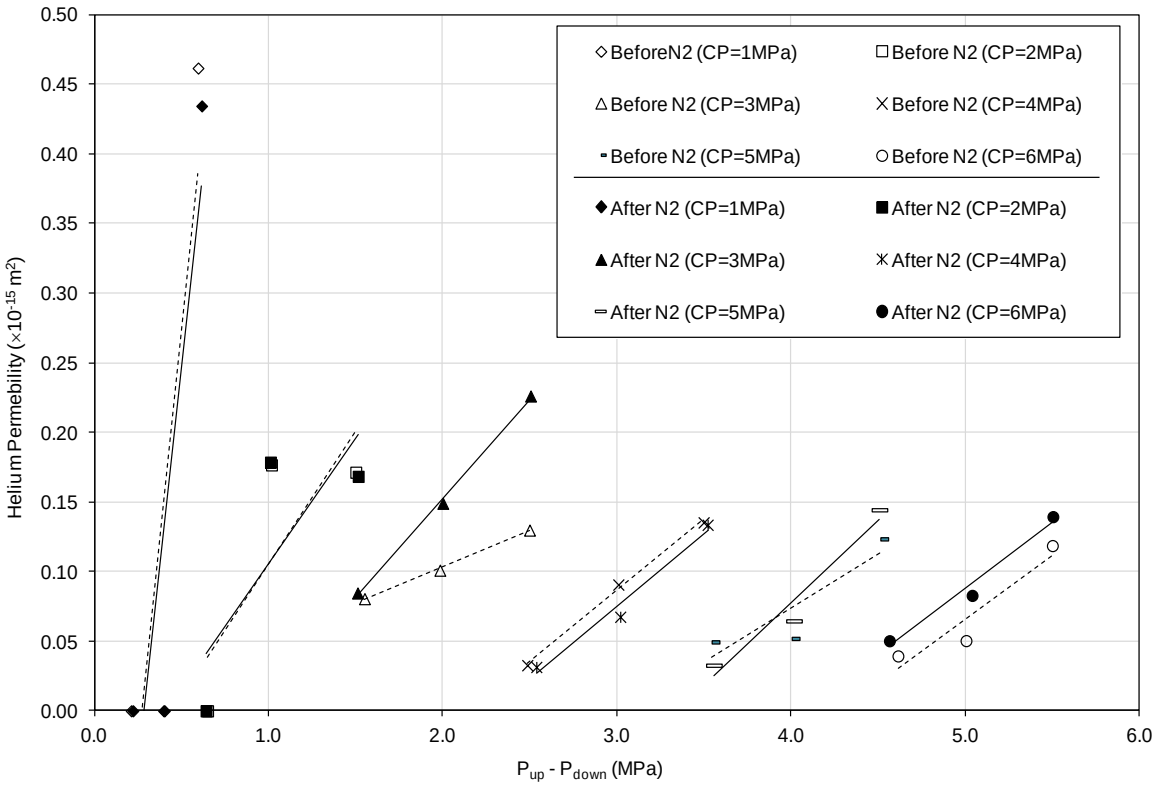

Fig. 6.20. Helium permeability of the coal sample before (dashed line) and after (solid line) the phase 2 of N_2 injections (T=298K).

According to the results, at lower confining pressures, i.e. up to 2MPa, no considerable change in the permeability of the coal sample can be observed. At higher pressures and constant confining pressures, however, the variations in coal permeability due to increase in the gas pressure did not show consistent trends. Therefore, slight increases and decreases in the coal permeability are observed. Inconsistency between the results at different confining pressures can be related to the minor differences in the experimental conditions or slight changes in the coal structure during several cycles of loading and unloading. Overall, no significant change in terms of permeability improvement is observed as the result of the phase 2 of N_2 flooding experiment.

6.5.2. CH_4 flooding experiment

From the results of adsorption isotherms presented in Chapter 5, it was found that coal has stronger affinity to CH_4 than to N_2. The volumetric effects of CH_4 on the coal matrix were also found to be negligible. In order to study the possibility of the displacement of the adsorbed CO_2 with CH_4, a CH_4 flooding experiment was performed on the coal sample.

The results of the phase 3 of helium flooding experiment were used as a representative of the initial conditions of the coal sample before the CH_4 injection. Accordingly, another helium flooding experiment was performed after the CH_4 injection in order to evaluate the effect of CH_4 injections on the permeability on the coal sample. Figure 6.21 shows the results of the coal permeability variations from the helium flooding experiments performed before and after the CH_4 injections.

As shown in Figure 6.21, at lower pressures permeability changes are small. At higher pressures, however, the coal sample exhibited higher permeability values compared to the initial conditions, i.e. before CH_4 injection. The increased permeability observed can be partly related to the decrease in the cleat compressibility due to the increase in He and CH_4 pore pressures. On average, the permeability of the coal sample was found to be increased by 1.6 times as a result of the CH_4 injection.

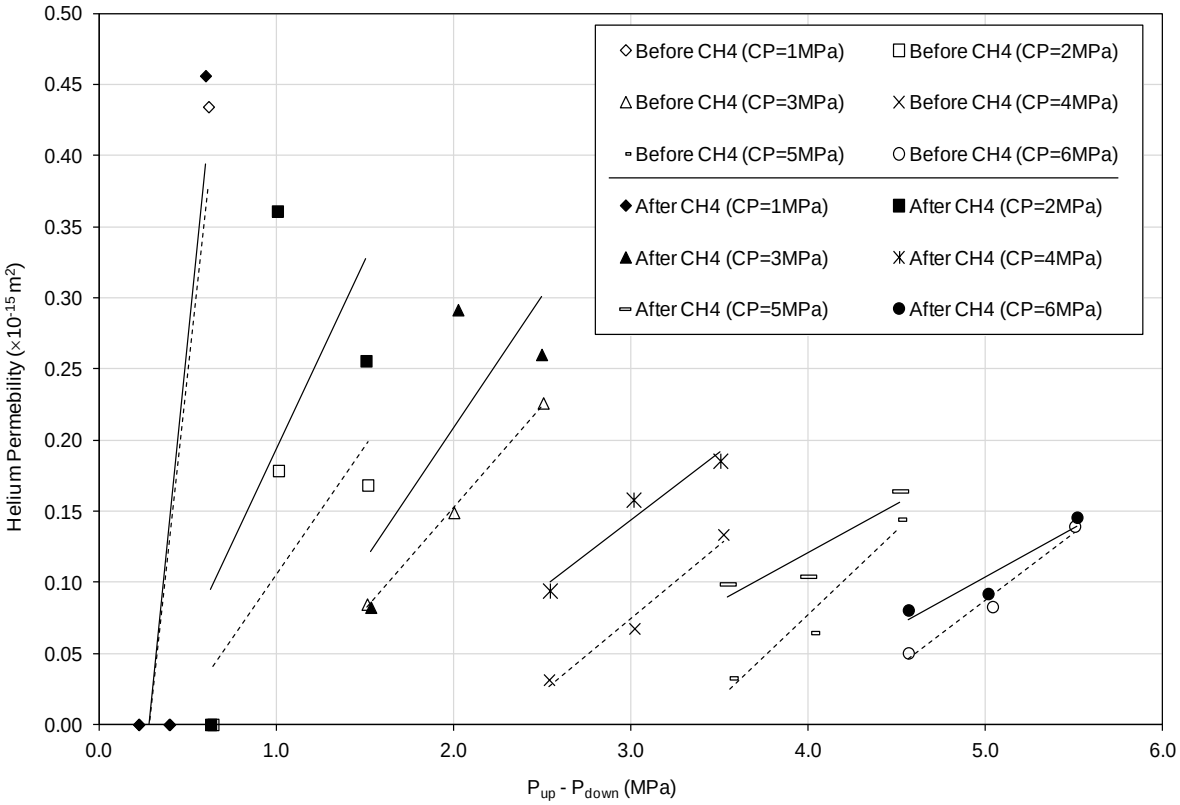

Fig. 6.21. Helium permeability of the coal sample before (dashed line) and after (solid line) CH_4 injection (T=298K).

Although, some researchers have suggested that the swelling effect is a fully reversible process, e.g. Battisttuta et al. (2010), De Silva and Ranjith (2012), for the coal sample of this study the swelling effects were found to be partially reversed during the CH_4 injection but not fully reversed. As a result, the coal permeability was also restored to some extent. Nonetheless, the time dependency of such processes should also be taken into account when interpreting the results (Fokker and van de Meer, 2004).

On the other hand, the results of this investigation showed that CO_2 can be adsorbed to the coal to a great extent and the variations of the gas composition does not lead to a significant release of adsorbed CO_2. Such data are crucial for assessing long-term stability of the injected CO_2 in coal reservoirs, in applications such as carbon sequestration process in coal seams.

6.6. Conclusions

Further insights into the interactions between coal and various gas species have been achieved through a series of core flooding experiments presented in this chapter. The experimental results of different gas species injected into the coal sample at a range of gas pressures up to 5.5MPa and confining pressures up to 6MPa were presented. The gas flow rates showed a slight non-linearity with differential gas pressures. This was found to be predominantly related to the effect of effective stress on coal permeability.

From the results, increases in gas pressure led to an increase in the coal permeability in the case of He and N_2 flow. In the case of the CO_2 flooding experiment, despite the increase in the gas pressure at higher effective stress values, the coal permeability was found to decrease considerably. Based on the results of the volumetric strain measurements and volumetric effects observed during CO_2 adsorption isotherm tests presented in Chapter 5, it can be concluded that the decrease observed in coal permeability at higher effective stresses can be related to the effect of coal matrix swelling induced by the CO_2 adsorption.

Relationships between the coal permeability of different gas species and effective stress were established from the experimental results which are based on an exponential function. Such relationships can be used to assess the behaviour of permeability evolution in coal during gas injection and reaction processes.

In general, the results of the coal permeability measurements showed a strong dependency on effective stress, especially for the CO_2 flooding experiment. A notable aspect of this investigation was to incorporate the coupled effects of the effective stress variations due to increases in gas pore pressure and confining pressure as well as the effect of coal matrix swelling on permeability evolution of the coal sample.

The volumetric deformations of the coal sample during He, N_2 and CO_2 flooding experiments were measured. The results showed that the coal sample exhibited almost similar rates of the volumetric strains during He and N_2 flooding experiment. This behaviour can be related to the mechanical expansion and compression of the coal

sample due to variations in gas pore pressure and confining pressure, respectively. The volumetric effects of He and N_2 on coal matrix (due to adsorption/desorption) have been found to be very small or negligible. In the case of CO_2, however, significant volumetric strains observed, can be related to the swelling of coal matrix induced by CO_2 adsorption on coal. The swelling effect due to adsorption of CO_2 on coal sample was found to be 1.5% volumetric increase.

The fate of the adsorbed CO_2 in coal was investigated by performing a unique sequence of flooding experiments using He, N_2 and CH_4 gases. The coal permeability was found to be reduced by 95% as a result of matrix swelling induced by CO_2 adsorption at 6MPa confining pressure. The results of the phase 2 of He and N_2 injections indicate no significant changes in the coal permeability and reversibility of the coal matrix swelling. The injection of CH_4 into the coal sample, on the other hand, resulted in relatively considerable improvement in the coal permeability of the sample. However, it was found that the initial permeability of the coal sample was not fully restored.

The results presented in this chapter provide a comprehensive set of data to be used for the development of the numerical models, i.e. permeability evolution or deformation models. The results also provide new insights into the fate of adsorbed CO_2 in coal and coal permeability evolutions during and after CO_2 injection which have not been previously reported in the literature.

6.7. References

Battistutta, E., van Hemert, P., Lutynski, M., Bruining, H. and Wolf, K.H. 2010. Swelling and sorption experiments on methane, nitrogen and carbon dioxide on dry Selar Cornish coal. *International Journal of Coal Geology,* 84(1), pp. 39-48.

Carles, P., Egermann, P., Lenormand, R. and Lombard, J. 2007. Low permeability measurements using steady-state and transient methods. *The International Symposium of the Society of Core Analysts,* Calgary, Canada. 10-14 September 2007.

Chen, Z., Huan, G. and Ma, Y. 2006. *Computational methods for multiphase flows in porous media (Computational Science and Engineering)*. Philadelphia: Society for Industrial and Applied Mathematics (SIAM).

Chen, Z., Pan, Z.J., Liu, J.S., Connell, L.D. and Elsworth, D. 2011. Effect of the effective stress coefficient and sorption-induced strain on the evolution of coal permeability: Experimental observations. *International Journal of Greenhouse Gas Control,* 5(5), pp. 1284-1293.

Cui, X., Bustin, R.M. and Dipple, G. 2004. Selective transport of CO_2, CH_4 and N_2 in coals: insights from modeling of experimental gas adsorption data. *Fuel*, 83(3), pp. 293-303.

Dabbous, M.K., Reznik, A.A., Taber, J.J. and Fulton, P.F. 1974. The permeability of coal to gas and water. *SPE Journal,* 14(6), pp. 563-572.

De Silva, P.N.K. and Ranjith, P.G. 2012. Advanced core flooding apparatus to estimate permeability and storage dynamics of CO_2 in large coal specimens. *Fuel*, 104, pp. 417-425.

Durucan, S. and Edwards, J.S. 1986. The effects of stress and fracturing on permeability of coal. *Mining Science and Technology,* 3(3), pp. 205-21.

Fokker, P.A. and van de Meer, L.G.H. 2004. The injectivity of coalbed CO_2 injection wells. *Energy,* 29(9-10), pp. 1423-1429.

Gan, H., Nandi, S.P. and Walker, Jr.P.L. 1972. Nature of the porosity in American coals. *Fuel,* 51(4), pp. 272-277.

Gilman, A. and Beckie, R. 2000. Flow of coalbed methane to a gallery. *Transport in Porous Media*, 41(1), pp. 1-16.

Han, F., Busch, A., van Wageningen, N., Yang, J., Liu, Z. and Krooss, B.M. 2010. Experimental study of gas and water transport processes in the inter-cleat (matrix) system of coal: anthracite from Qinshui Basin, China. *International Journal of Coal Geology*, 81(2), pp. 128-138.

Harpalani, S. and Chen, G. 1997. Influence of gas production induced volumetric strain on permeability of coal. *Geotechnical and Geological Engineering*, 15(4), pp. 303-25.

Harpalani, S. and Mitra, A. 2010. Impact of CO_2 injection on flow behavior of coalbed methane reservoirs. *Transport in Porous Media,* 82(1), pp.141-156.

Huy, P.Q., Sasaki, K., Sugai, Y. and Ichikawa, S. 2010. Carbon dioxide gas permeability of coal core samples and estimation of fracture aperture width. *International Journal of Coal Geology,* 83(1), pp. 1-10.

Jasinge, D., Ranjith, P.G. and Choi, S.K. 2011. Effects of effective stress changes on permeability of latrobe valley brown coal. *Fuel* 90(3), pp. 1292-1300.

Klinkenberg, L.J. 1941. The permeability of porous media to liquids and gases. *Drilling and Productions Practices*, pp.200-213.

Laubach, S.E., Marrett, R.A., Olson, J.E. and Scott, A.R. 1998. Characteristics and origins of coal cleat: A review. *International Journal of Coal Geology*, 35(1), pp. 175-207.

Mazumder, S., Karnik, A.A. and Wolf, K.H.A.A. 2006. Swelling of coal in response to CO_2 sequestration for ECBM and its effect on fracture permeability. *SPE Journal*, 11(3), pp. 390-398.

McKee, C.R., Bumb, A.C. and Koenig, R.A. 1988. Stress-dependent permeability and porosity of coal and other geologic formations. *SPE Formation Evaluation*, 3(1), pp. 81-91.

Mehio, N., Dai, S. and Jiang, D. 2014. Quantum mechanical basis for kinetic diameters of small gaseous molecules. *The Journal of Physical Chemistry A,* 118(6), pp. 1150-1154.

Pan, Z., Connell, L.D. and Camilleri, M. 2010. Laboratory characterisation of coal reservoir permeability for primary and enhanced coalbed methane recovery. *International Journal of Coal Geology,* 82(3-4), pp. 252-261.

Perera, M.S.A., Ranjith, P.G. and Choi, S.K. 2011. A review of coal properties pertinent to carbon dioxide sequestration in coal seams: with special reference to Victorian brown coals. *Environmental Earth Sciences*, 64(1), pp. 223-235.

Pini, R., Ottiger, S., Burlini, L., Storti, G. and Mazzotti, M. 2009. Role of adsorption and swelling on the dynamics of gas injection in coal. *Journal of Geophysical Research,* 114 (B4), pp. 1978-2012.

Seidle, J.R. and Huitt, L.G. 1995. Experimental measurement of coal matrix shrinkage due to gas desorption and implications for cleat permeability increases. *Proceedings of International Meeting on Petroleum Engineering*. 14-17 November, Beijing, China, *SPE 30010*.

Seidle, J.P., Jeansonne, M.W. and Erickson, D.J. 1992. Application of matchstick geometry to stress dependent permeability in coals. *SPE Rocky Mountain Regional Meeting.* 18-21 May, Casper, Wyoming*, SPE-24361*, pp. 432-444.

Shen, J., Qin Y., Wang G.X., Fu X., Wei C. and Lei B. 2011. Relative permeabilities of gas and water for different rank coals. *International Journal of Coal Geology*, 86(2-3), pp. 266-275.

Siriwardane, H., Haljasmaa, I., McLendon, R., Irdi, G., Soong, Y. and Bromhal, G. 2009. Influence of carbon dioxide on coal permeability determined by pressure transient methods. *International Journal of Coal Geology*, 77 (1–2), pp. 109-118.

Somerton, W.H., Soylemezoglu, I.M. and Dudley, R.C. 1975. Effect of stress on permeability of coal. *International Journal of Rock Mechanics and Mining Sciences & Geomechanics*, 12(5-6), pp. 129-45.

Vishal, V., Ranjith, P.G. and Singh, T.N. 2013. CO_2 permeability of Indian bituminous coals: Implications for carbon sequestration. *International Journal of Coal Geology,* 105(1), pp. 36-47.

Wang, G.G.X., Zhang, X., Wei, X., Fu, X., Jiang, B. and Qin, Y. 2011. A review on transport of coal seam gas and its impact on coalbed methane recovery. *Frontiers of Chemical Science and Engineering,* 5(2), pp. 139-161.

Wang, S., Elsworth, D. and Liu, J. 2013. Permeability evolution during progressive deformation of intact coal and implications for instability in underground coal seams. *International Journal of Rock Mechanics and Mining Sciences,* 58(1), pp. 34-45.

Chapter 7

Gas Storage and Displacement in Coal

7.1. Introduction

In this chapter, the results of a series of experimental studies on gas storage and displacement in coal using carbon dioxide (CO_2), nitrogen (N_2) and methane (CH_4) are presented. The aim of this chapter is to provide a better understanding of coal-gas interactions during gas storage and recovery processes. The experimental work has been carried out to study the gas storage and displacement processes in coal. Nitrogen and carbon dioxide have been used to evaluate the competitive displacement of methane with those gases. Two core flooding experiments have been performed in which nitrogen and carbon dioxide were injected into a methane saturated coal sample. The displacement process and gas breakthrough was monitored and analysed. Figure 7.1 presents a summary of the experimental studies which are presented and discussed in this chapter.

In Section 7.2, the initial conditions of the coal sample in terms of gas transport properties are presented. The helium (He) flooding experiment performed is described and the absolute permeability of the coal sample to helium estimated at several gas injection pressures and confining pressures is explained. The permeability of the coal sample to methane estimated by performing a methane flooding experiment is then presented.

Section 7.3 and 7.4 present the results of the Nitrogen and carbon dioxide storage and displacement experiments, respectively. Both experiments were conducted on a same sample of coal (coal sample B) which was first saturated with methane at 5MPa gas pressure and 6MPa confining pressure prior to each test. Nitrogen or carbon dioxide was injected into the coal sample at a constant pressure of 5MPa at upstream while the downstream was kept at atmospheric pressure (0.1MPa) during the experiments. The composition of the outflow gas was analysed during the test to evaluate the breakthrough time and displacement process.

The results of the methane recovery as a by-product during each experiment are presented in Section 7.5. The rate of the methane production was calculated based on the amount of injected nitrogen or carbon dioxide.

The amount of carbon dioxide taken by the coal sample was calculated from the results of the carbon dioxide experiment. The results are presented in Section 7.6.

Finally, concluding remarks related to the results of experimental investigations presented in this chapter are provided in Section 7.7.

Further investigation into the behaviour of coal during gas injection, storage and displacement will be pursued in Chapter 8 based on a series of numerical simulations of the experimental studies presented in this chapter.

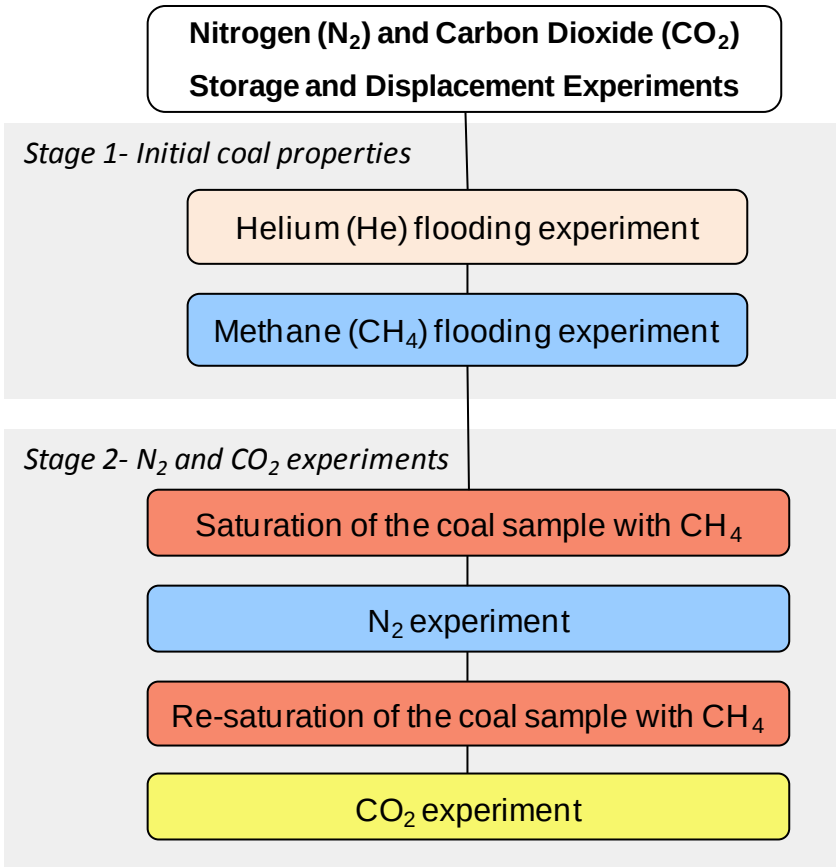

Fig. 7.1. The experimental studies carried out in relation to gas storage and displacement processes in coal which are presented in this chapter.

7.2. Initial properties of the coal sample

As mentioned in Chapter 4, the coal sample B has been used for the experimental investigations presented in this Chapter. A brief description of the initial properties of the coal sample B has been provided in Table 4.1. The experimental procedures for the sample preparation, assembling the sample on the triaxial cell and the core flooding experiment have been also described in Chapter 4 in detail. Since a different coal sample was used for the experiments presented in this chapter, the initial gas transport properties, i.e. gas flow and absolute permeability to helium have been obtained prior to performing the gas storage and displacement experiments using nitrogen (N_2) and carbon dioxide (CO_2). Although both coal samples A and B were prepared from a same block of coal, the properties can differ to some extent due to heterogeneous nature of coal material (Karacan, 2003).

The experimental programmes to assess the initial gas transport properties of the coal sample are as following:

- First, a core flooding experiment with helium was performed. The absolute permeability of the coal sample to helium (He) was estimated for a range of gas injection pressures up to 5.5MPa and at several confining pressures up to 6MPa.
- A methane (CH_4) flooding experiment was subsequently performed to evaluate the permeability of the coal sample to CH_4 under similar stress conditions which were applied for the gas storage and displacement experiments, i.e. N_2 and CO_2 experiments.

The results of both He and CH_4 flooding experiments are presented in the following sections.

7.2.1. He flooding experiment

The coal sample B was assembled on the triaxial cell and a confining pressure of 1MPa was applied to the sample. The coal sample was then subjected to vacuum for 24 hours

before it was saturated with helium. This was carried out according to the procedure provided in Chapter 4. The gas pressure and confining pressure were gradually increased to values up to 3.5MPa and 4MPa, respectively. The pressure steps defined for the helium flooding experiments on coal sample B are summarised in Table 7.1.

In order to evaluate the effects of confining pressure on gas flow properties of the coal sample, the confining pressure was first increased stepwise up to 6MPa while the gas injection pressure was kept constant at 3.5MPa. To assess the effect of pore pressure changes on the gas flow and permeability of the coal sample, the gas pressure was then increased gradually to 5.5MPa while the confining pressure was kept constant (6MPa).

Table 7.1. The experimental pressure steps for helium flooding experiment on coal sample B.

Confining pressure (MPa)	Upstream gas pressure (MPa)
4.0	3.5
4.5	3.5
5.0	3.5
5.5	3.5
6.0	3.5
6.0	4.0
6.0	4.5
6.0	5.0
6.0	5.5

Figure 7.2 presents the results of the helium flow rates measured during the helium flooding experiment on coal sample B at a range of mean pore pressures and effective stresses applied. The mean pore pressure in Figure (7.2) represents the average gas pressure at the upstream and downstream of the coal sample, i.e. $(P_{up}+P_{down})/2$. The gas pore pressure was first kept constant at approximately 1.8MPa and the confining pressure was increased stepwise. This caused an increase in the effective stress and a decrease in gas flow rate. After the step four, the confining pressure was kept constant and the gas pressure was gradually increased. At this stage, the decreases in the effective stress and the increases in the gas flow rate were observed.

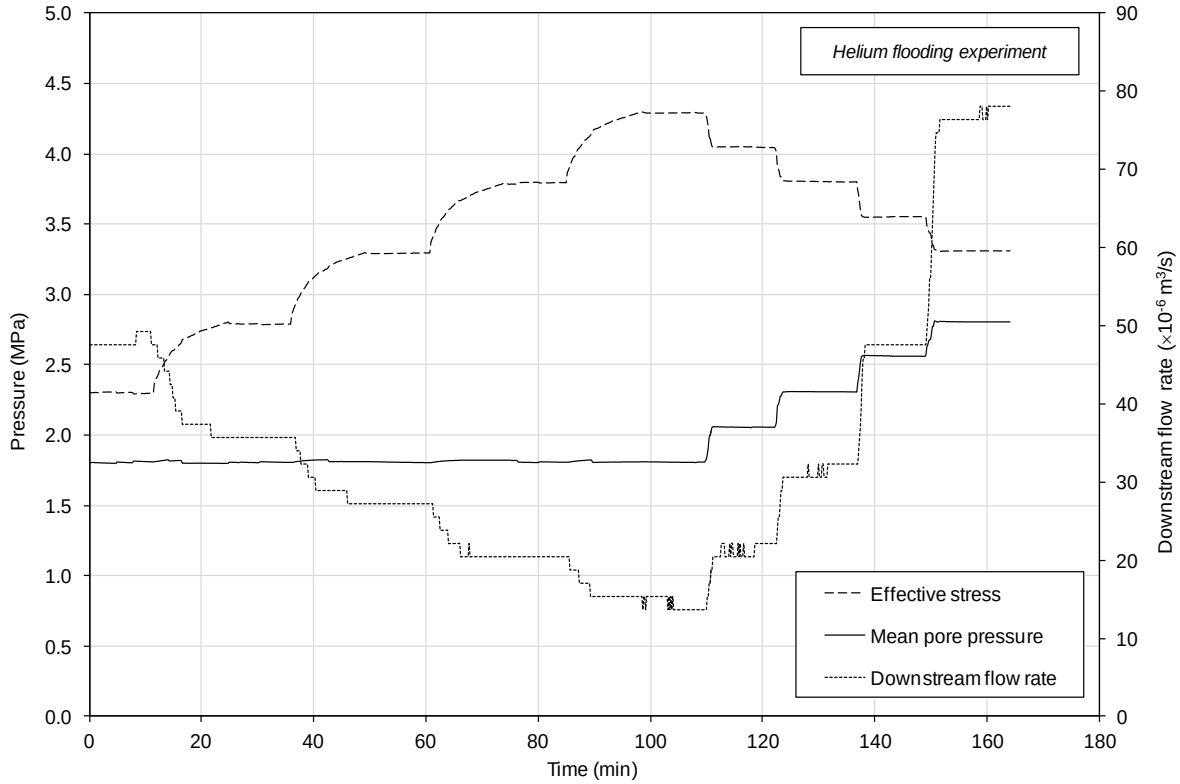

Fig. 7.2. Variations of gas flow rates during helium flooding experiment on coal sample B (at 298K).

At each pressure step, once the steady-state condition was observed, the absolute permeability of the coal sample to helium was estimated based on Darcy's law (equation 4-11). The results of the absolute permeability of the coal sample B to helium are presented in Figure 7.3.

It can be observed from the results presented in Figure 7.3 that the variations in the confining pressure and gas pressure have had slightly different effects on the permeability evolution of the coal sample. The coal permeability decreased gradually with increase in the confining pressure, whereas the variations in the pore pressure at constant confining pressure resulted in greater changes in the coal permeability. The decrease in the coal permeability due to increase in the confining pressure can be attributed to the closure of the internal fractures/microfractures under larger confining stress values applied. The increase in the coal permeability due to increase in the gas pore pressure can only be attributed to the expansion of the macroporosity at larger gas pore pressure (Vishal et al., 2013).

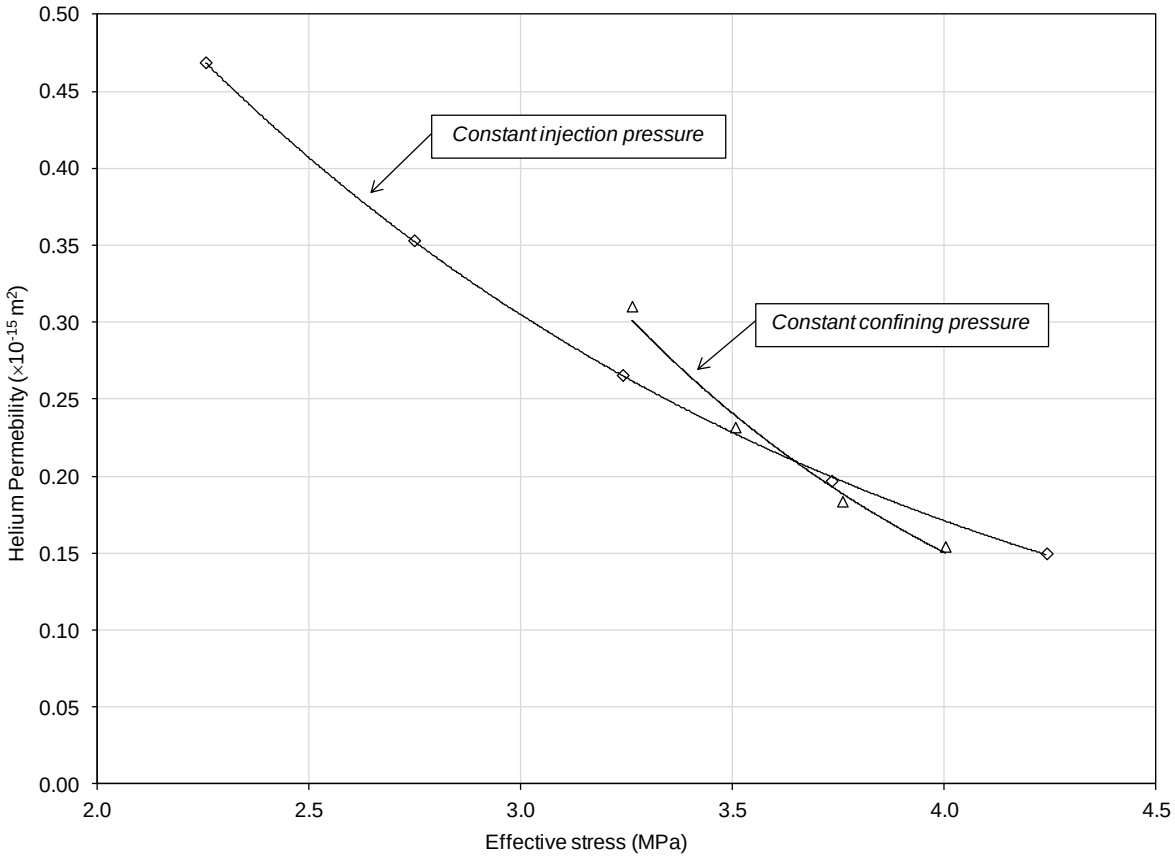

Fig. 7.3. Variations of the coal permeability to helium with effective stress under constant injection pressure and constant confining pressure (at 298K).

A comparison between the results of the helium permeability of the coal sample B and those for coal sample A (presented in Chapter 6, Figure 6.4) shows that the permeability values for both samples under similar gas pressures and stress conditions are almost similar. Since the helium flooding experiment on coal sample B (Figure 7.3) was performed only at higher pressure values, the sharp decrease in the coal permeability due to any closure of the microfractures at lower pressures was not observed here. Therefore, the results presented in Figure 7.3 represent a more realistic behaviour of the coal in response to variations in the stress values (Durucan and Edwards, 1986).

7.2.2. CH_4 flooding experiment

The permeability of the coal to CH_4 was evaluated by performing a CH_4 flooding experiment. As stated previously, the CH_4 permeability was primarily performed to assess

the gas flow ranges in the coal sample that might be observed during the gas storage and displacement experiments, i.e. N_2 and CO_2 experiments. However, in order to minimise the effect of hysteresis on the coal sample during loading and unloading cycles, e.g. Somerton et al. (1975), the CH_4 flow measurements were only performed at a few pressure steps close to the pressure values applied for the N_2 and CO_2 experiments.

After the helium flooding experiment, helium was removed from the coal sample by applying vacuum to the downstream of the sample while the confining pressure was kept constant at 6MPa. The sample was then saturated with CH_4 at 5MPa injection pressure according to the procedure described in Chapter 4. The permeability of the coal to CH_4 was then calculated based on equation (4-11) and the gas flow rates measured at every steady-state condition for a range of injection pressures, i.e. 3.5, 4.5 and 5.5MPa. The results of the coal permeability to CH_4 versus effective stress are presented in Figure 7.4.

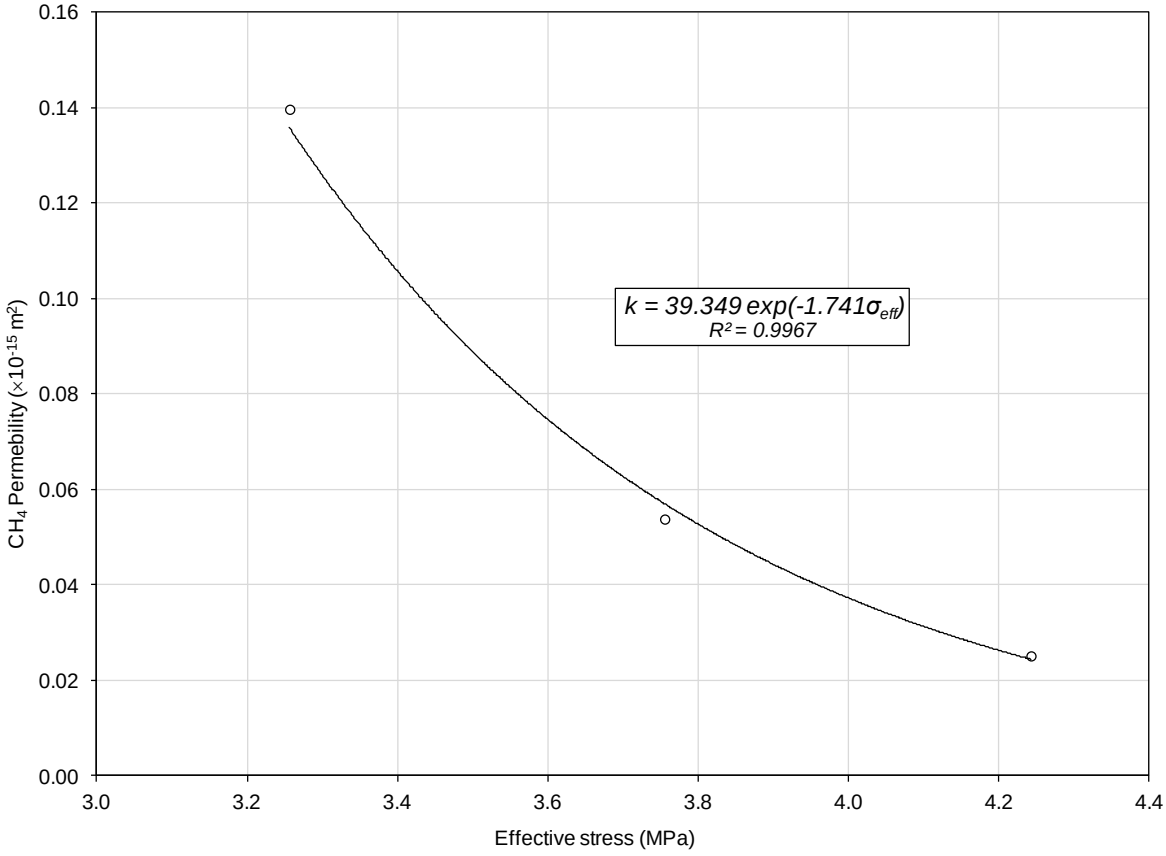

Fig. 7.4. The relationship between permeability of the coal sample B to CH_4 and effective stress (T=298K).

The results in Figure 7.4 present the behaviour of the coal sample in terms of the CH_4 permeability variations with effective stress. The coal permeability to CH_4 was found to be between $0.03\times10^{-15}m^2$ and $0.14\times10^{-15}m^2$ under the applied stresses.

Once the evaluation of the initial properties of the coal sample was completed, the coal sample was then re-saturated with CH_4 at injection pressure of 5MPa and confining pressure of 6MPa. The N_2 and CO_2 experiments were then performed accordingly. The results of the N_2 and CO_2 experiments are presented in the following sections.

7.3. N_2 experiment

Since the sample of coal has been used for both N_2 and CO_2 experiments, it was decided to perform the N_2 experiment first before introducing the highly reactive CO_2 gas to the coal sample. From the results of the gas sorption and flow behaviour in coal (presented in previous chapters), it was evident that the interactions between coal and N_2 are much less than those observed for CO_2. Therefore, the effects of N_2 on the coal structure are minimal, whereas with CO_2, the coal matrix can experience a significant change due to the adsorption-induced swelling which may change the coal flow properties. Figure 7.5 presents a schematic diagram of the experimental conditions applied for the N_2 experiment.

The coal sample was first saturated with CH_4 at 5MPa injection gas pressure and at constant confining pressure of 6MPa. It should be mentioned that during CH_4 saturation process, a slight pressure gradient across the sample was observed after closing the valves. The gas pore pressure, however, was equalised at the final stage of the gas saturation process and before N_2 injection. Once the coal sample was saturated, the upstream valve was closed and the experimental gas was changed to N_2. N_2 was injected at upstream of the coal sample at 5MPa injection pressure while the downstream valve was opened to the atmospheric pressure, i.e. 0.1MPa. The composition of the outflow gas was analysed during the experiment by the gas analyser described in Chapter 3.

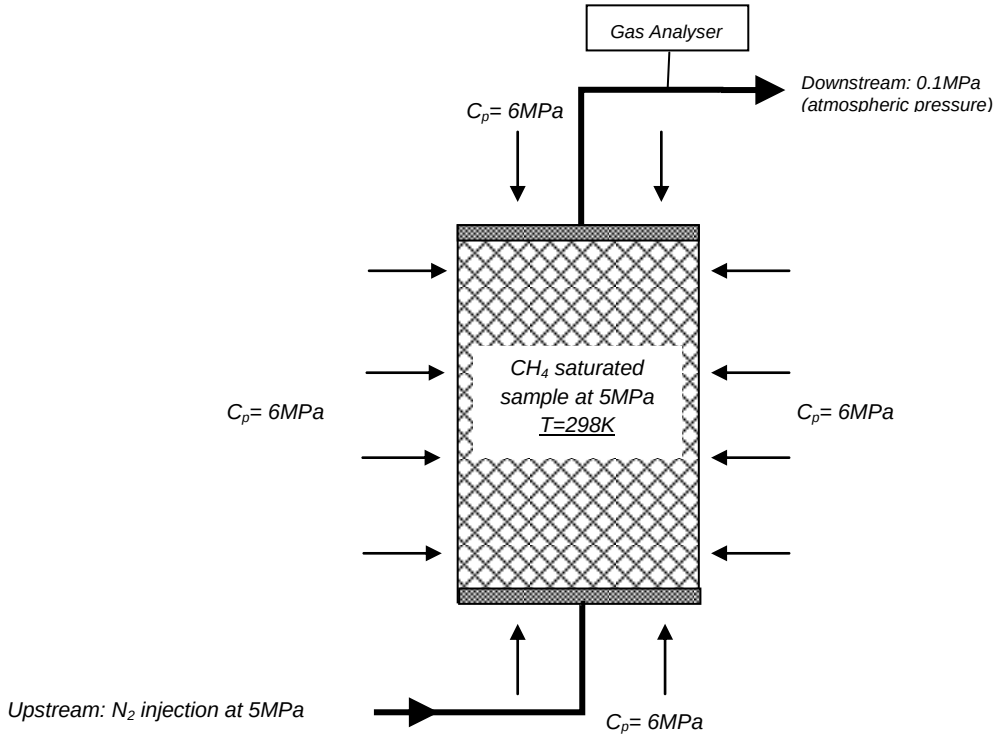

Fig. 7.5. Schematic diagram of the experimental conditions applied for the N_2 experiment, C_p is the confining pressure.

The results of the gas displacement process during N_2 experiment are presented in Figure 7.6. The results present the variation of the gas composition in the outflow with time.

It can be seen from the results that an early breakthrough of the injected N_2 has occurred shortly after the injection (4min). The definition of the breakthrough time of the injected gas varies in the literature. For instance, Onur Balan (2008) defined the breakthrough as the time at which the molar composition of the injection gas in the production gas (outflow) is higher than 10%. A more common definition for the breakthrough in work related to gas storage and recovery processes has been described as the time at which 1% of the total gas injected is recovered (van Hemert et al., 2012; Mazumder and Wolf, 2008; Ross, 2007). In this study, the latter definition, i.e. 1%, has been considered as gas breakthrough time.

It should be mentioned that with regards to the experimental conditions defined in Figure 7.5, i.e. relatively high injection pressure under low effective stress, the early

breakthrough observed in the N_2 experiment and relatively fast displacement of CH_4 are primarily related to the displacement of the free gas exist within the coal cleats/microfractures rather than the free gas in the coal matrix. Therefore, the breakthrough time reported in the literature might vary greatly ranging from several minutes to several days depending on the coal type, permeability, gas injection pressure and effective stresses (e.g. Connell et al., 2011; Shi et al., 2008; Yu et al., 2008).

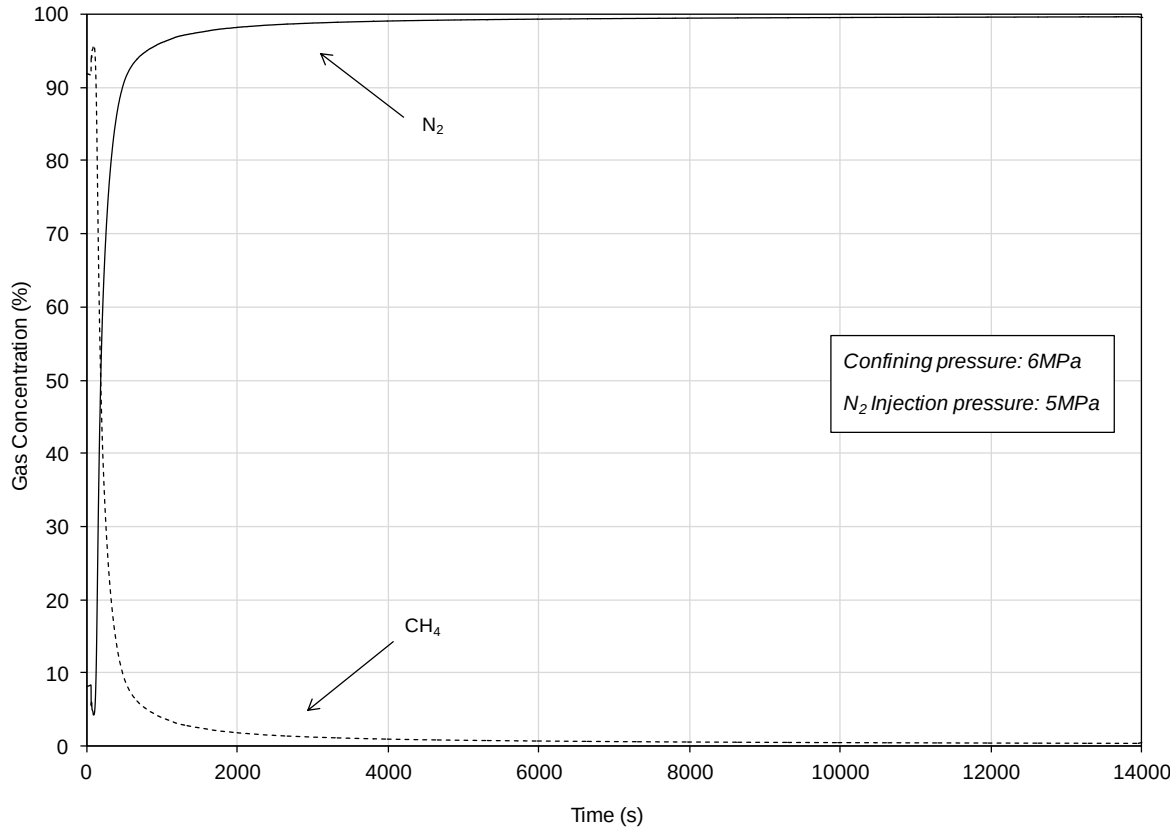

Fig. 7.6. The composition of the production gas with time during the N_2 experiment (T=298K).

The results presented in Figure 7.6 show that within the first half an hour of the experiment more than 95% of CH_4 was displaced with N_2. As stated earlier, at this stage, it can be assumed that most of the free CH_4 in coal cleats and microfractures have been displaced by N_2. As the experiment continued, the fraction of CH_4 in the production gas became very small (less than 0.5%), however, it remained steady and continuous. This can be related to the slow diffusion of N_2 and CH_4 in the coal matrix, (e.g. Cui et al., 2004)

which is a dominant process at this stage of the experiment. As a result, the diffusion of N_2 into the coal matrix gradually reduces the partial pressure of CH_4 in the coal matrix and eventually leads to CH_4 desorption.

7.4. CO_2 experiment

After the N_2 experiment, the residual gas was removed from the coal sample by applying vacuum. The coal sample was then re-saturated with CH_4 in order to perform the CO_2 experiment. The CH_4 saturation process was carried out at 5MPa gas pressure and 6MPa confining pressure, according to the procedure described in Chapter 4. Figure 7.7 presents a schematic diagram of the experimental conditions applied for the CO_2 experiment. After saturating the coal sample with CH_4, the gas on the upstream side was changed to CO_2 and the downstream valve was opened to atmosphere. The composition of the outflow gas was monitored continuously and the test was continued until CH_4 was displaced with CO_2.

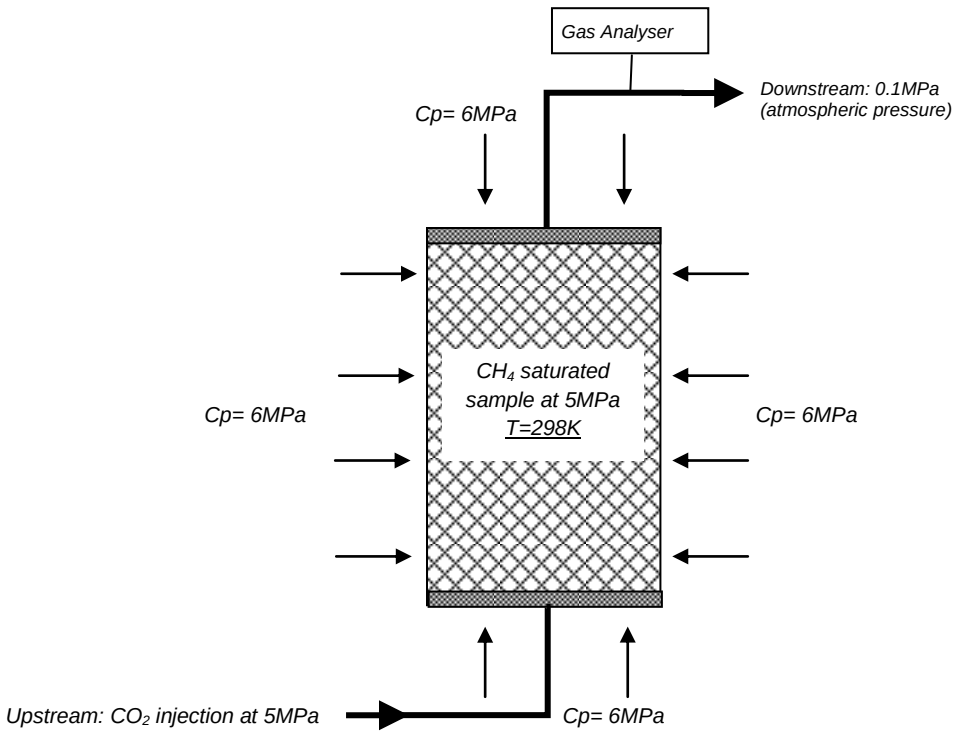

Fig. 7.7. Schematic diagram of the experimental conditions applied for the CO_2 experiment, C_p is the confining pressure.

The experimental results of the gas displacement process during the CO_2 experiment are presented in Figure 7.8. The variations of the gas composition in the production gas with time as a result of CH_4 displacement with CO_2 are presented in this Figure. The small spikes on the graph are related to minor fluctuations in the injection pressure generated as a result of simultaneous operation of the gas booster.

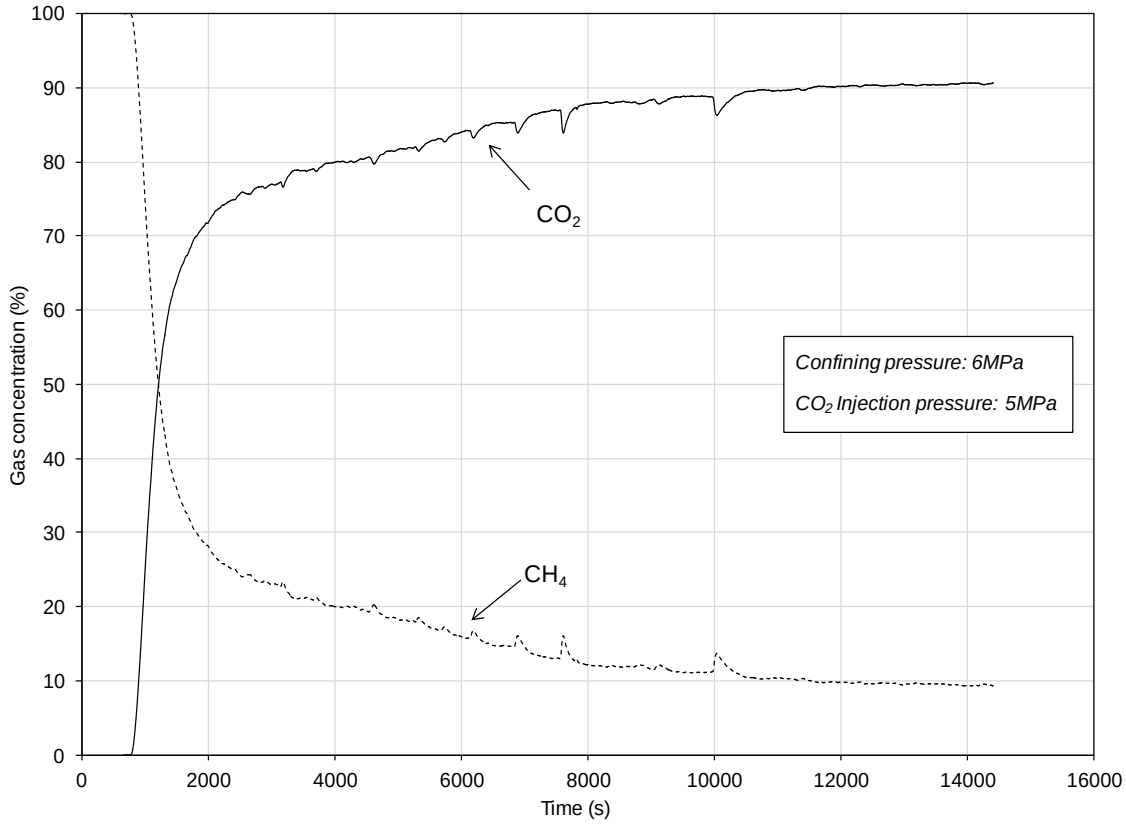

Fig. 7.8. The composition of the production gas with time during the CO_2 experiment (T=298K).

From the results presented it is apparent that the breakthrough time of CO_2 is longer than that for the N_2 experiment (8min). The breakthrough time for the CO_2 experiment is almost two times slower than the N_2 experiment. This can be attributed to a combination of gas diffusion process in the coal and the effects of coal matrix swelling induced by the CO_2 adsorption.

With its relatively smaller kinetic diameter, CO_2 molecules can penetrate into the micropores which may be inaccessible or less accessible to CH_4 and N_2 molecules that

have larger kinetic diameters. This can result in one or two order of magnitude higher diffusivity of CO_2 in the coal matrix compared with N_2 and CH_4 (e.g. Cui et al., 2004). Hence, a higher diffusion of CO_2 than that for CH_4 and N_2 may limit its breakthrough in the production gas by diffusing faster into the coal matrix. Further discussion related to this will be provided in Chapter 8, where the theoretical relationship for the mass exchange between fracture and matrix are presented. Moreover, the effect of the coal swelling induced by CO_2 adsorption can also result in slower rate of gas flow in the cleat and consequently increases the time of the breakthrough. This is also evident in the results of CO_2 flooding experiment presented in Chapter 6.

The results of the gas storage and displacement experiments show that, the overall rate of CO_2 displacement with CH_4 is much slower compared to N_2. For the N_2 experiment, more than 95% of CH_4 has been displaced in less than 30min by N_2, whereas for the CO_2 experiment the fraction of the displaced CH_4 has just reached to 90% after 3 hours of continuous CO_2 injection. As stated earlier, the combined effects of gas diffusion process and coal swelling can be the factors controlling the slower gas displacement rates observed during CO_2 process. Whereas, in the N_2 process, the slower rate of N_2 diffusion into the coal matrix leads to a rapid breakthrough.

7.5. CH_4 recovery

In order to evaluate the amount of CH_4 recovery as a by-product during the N_2 and CO_2 experiments, data related to gas flow rate at downstream of the coal sample and the composition of the outflow gas have been analysed. For the N_2 and CO_2 experiments, the steady-state gas flow rates at the downstream of the sample were recorded using the mass flow meter (as described in Chapter 4). The values of the steady-state gas flow rates for the N_2 experiment at the upstream and downstream of the coal sample were found to be approximately 30 and 28g/h, respectively.

For the CO_2 experiment, the upstream and downstream flow rates were found to be approximately 4 and 3m/h, respectively. The upstream and downstream flow rates were

then converted to mole per second (mol/s) in order to estimate the amount of injected and recovered gases, respectively. The amount of recovered CH_4 was then calculated for each test by accounting for CH_4 fraction in the outflow gas obtained. The ratio of CH_4 recovery was estimated as:

$$Ratio of\ CH_4\ recovery = \frac{CH_4\ recovered}{N_2\ or\ CO_2\ injected} \tag{7-1}$$

Figure 7.9 shows the ratio of CH_4 recovery for both experiments by accounting for the amount of injected N_2 or CO_2 with time, based on equation (7-1).

The results show that the CO_2 injection leads to a higher ratio of CH_4 recovery throughout the experiment (1.5 to 9 times higher than that obtained by N_2 injection). This is mainly related to the higher amounts of N_2 injected under similar experimental conditions, i.e. gas injection pressure and confining pressure.

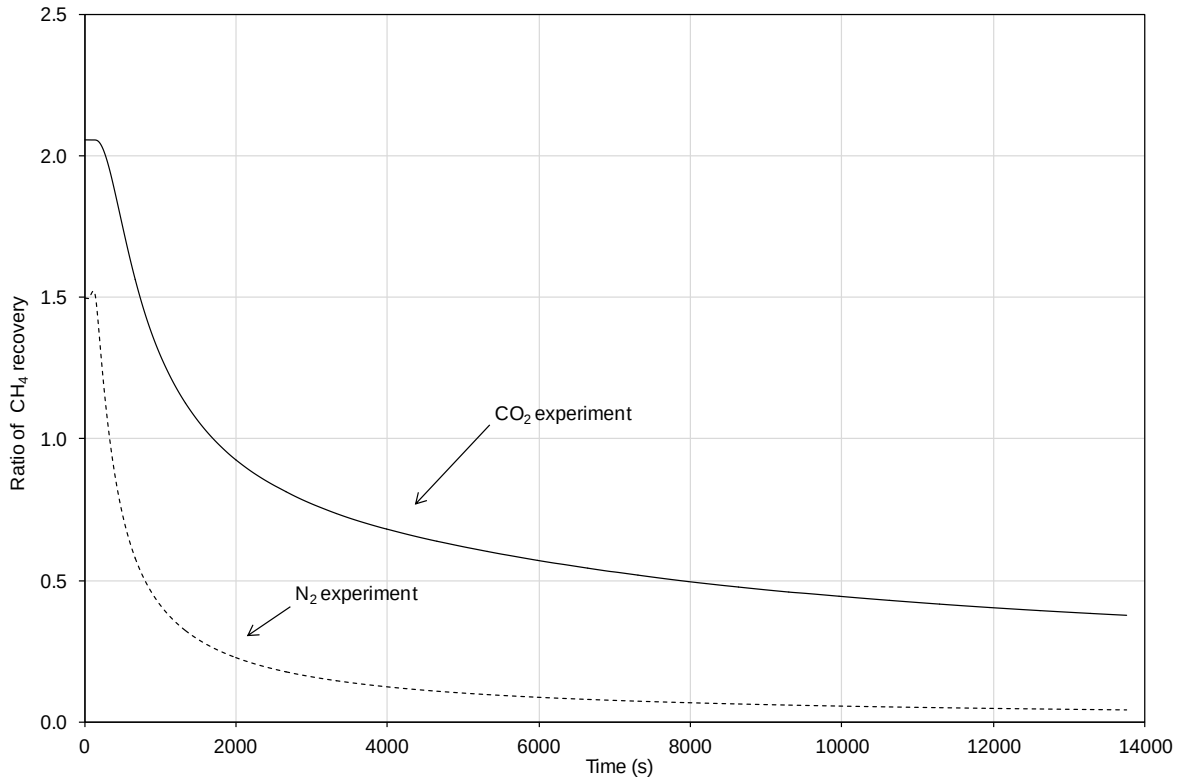

Fig. 7.9. The ratio of CH_4 recovery with time during the N_2 and CO_2 experiments.

The amount of the CH_4 recovery for both experiments decreased sharply in the first hour of the experiments. This behaviour can be related to faster displacement of CH_4 in the coal cleats with N_2 or CO_2, as observed in the results of gas adsorption kinetics which were presented in Chapter 5. The rate of CH_4 recovery, however, remained almost steady for the N_2 experiment after the first hour, whereas for the CO_2 experiment, it decreased gradually over time. This behaviour can be attributed to the effect of coal matrix swelling on gas permeability and flow as described previously.

7.6. CO_2 storage in coal

It this section, the extent of the CO_2 storage in coal has been evaluated by comparing the results of CO_2 and N_2 experiments. Based on the experimental data of gas flow rates at upstream and downstream as well as the composition of the outflow gas, the amounts of N_2 and CO_2 injected, recovered and stored in the coal sample were calculated.

It should be mentioned that the gas storage here implies the total amount of gas adsorbed to the coal matrix as well as the free gas stored in cleats/microfractures and matrix pore volumes. Figures 7.10 and 7.11 present the cumulative amounts of gas injected, recovered and stored in the coal sample during N_2 and CO_2 experiments, respectively.

The results presented in Figures 7.10 and 7.11 show that for the same duration of the experiment and under similar experimental conditions, the total amount of injected N_2 was 12 times higher than that for CO_2 injection. This observation is in agreement with the results of core flooding experiments presented in Chapter 6, where similar order of magnitude was observed between the N_2 and CO_2 flow rates under the same experimental conditions.

In addition, the results show that 90% of the total injected N_2 is in the production gas, whereas in the case of the CO_2 experiment, only 60% of the total injected CO_2 is in the production gas. Therefore 40% of the injected CO_2 has been retained in the coal sample.

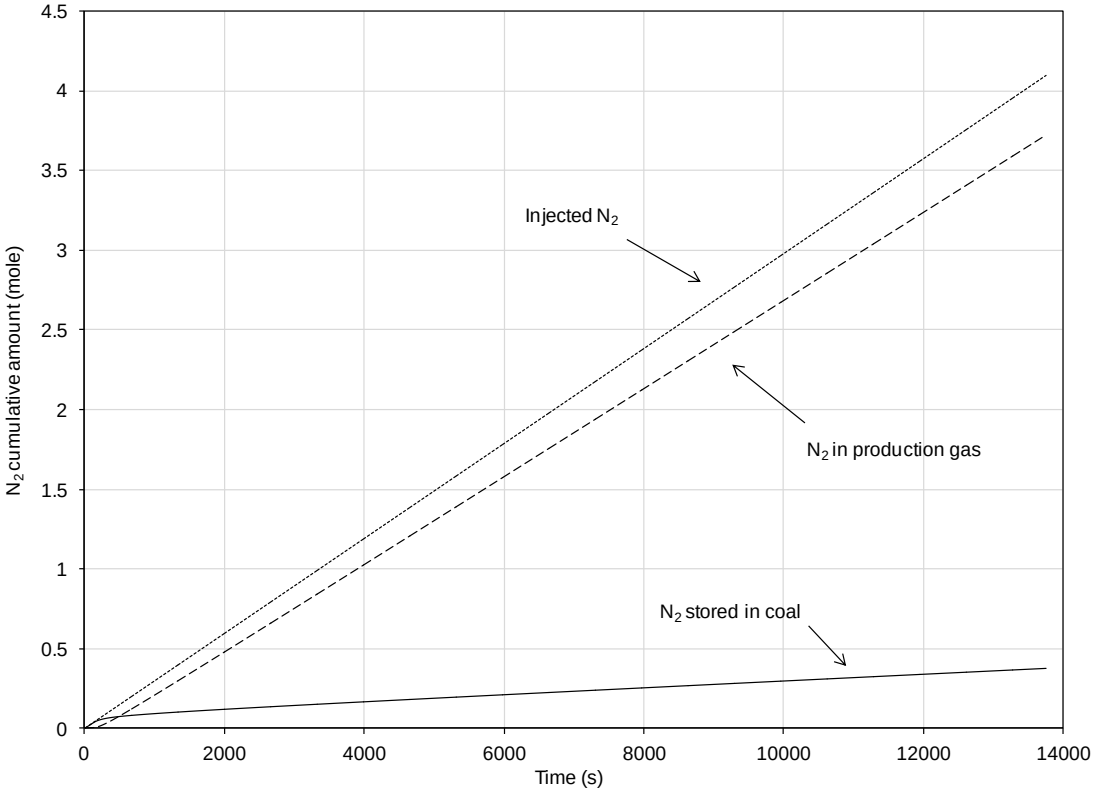

Fig. 7.10. Cumulative amounts of N_2 injected, recovered and stored with time during the N_2 experiment.

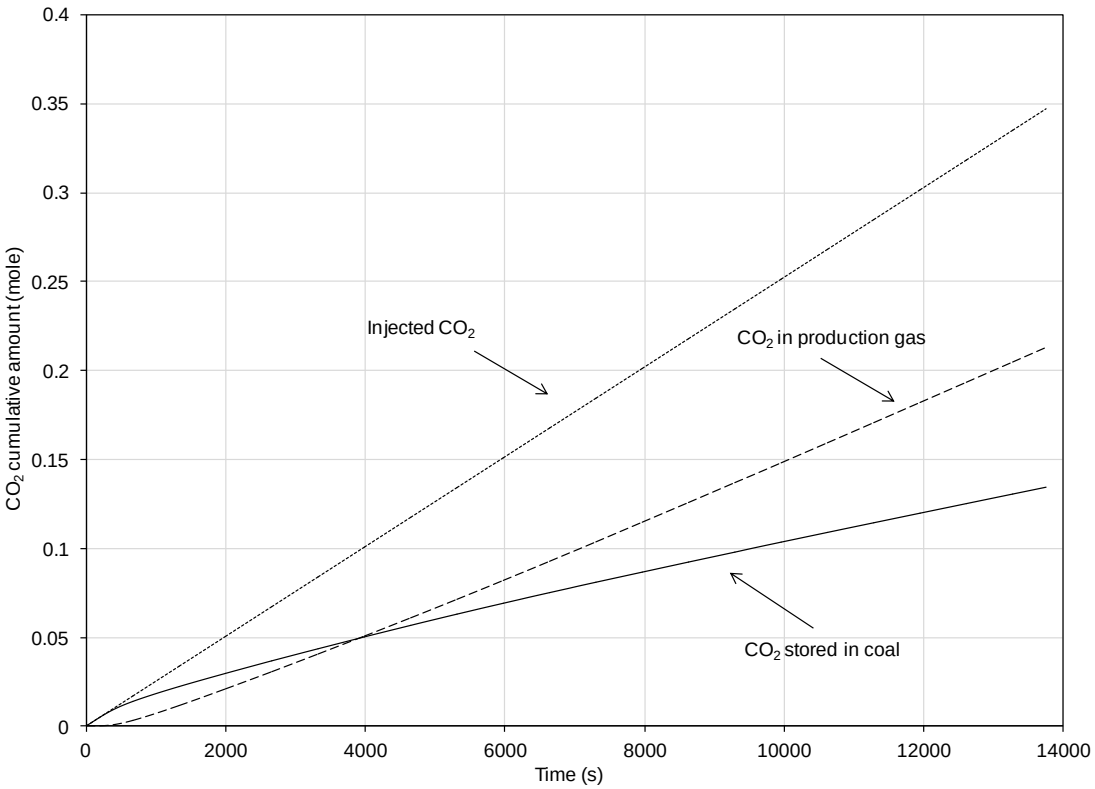

Fig. 7.11. Cumulative amounts of CO_2 injected, recovered and stored with time during the CO_2 experiments.

A comparison between the amounts of CO_2 stored in coal during the CO_2 experiment with the results of CO_2 absolute adsorption on powdered coal (presented in Chapter 5) also shows that only 20% of the adsorption capacity of the powdered coal sample was utilised in the CO_2 experiment. This can be related to several factors:

- Much shorter duration of the CO_2 experiment (~4h) as compared with the duration of the gas adsorption isotherm measurements (~24h). The equilibrium state may have not been achieved in the CO_2 experiment compared to the adsorption isotherm test.

- The different capacity of adsorption due to the differences in the sample size, i.e. the powdered coal used in the adsorption measurement test and the intact core sample used in the gas storage and displacement experiments.

- The coal swelling induced by gas adsorption may result in reduction of coal permeability under the confined conditions, as also observed in the results of CO_2 flooding experiment presented in Chapter 6.

- The effect of effective stresses on the coal permeability during N_2 and CO_2 experiment, i.e. compression of the coal sample.

The result show that for every moles of CO_2 stored in the coal sample an equivalent amount of CH_4 was recovered. Higher ratios have also been reported in the literature, i.e. ratio of 2 to 1 (Tsotsis et al., 2004). However, considering the differences in the experimental conditions and the factors mentioned above, it can be suggested that the CO_2 experiment conducted provided further understanding in terms of CO_2 storage in coal, gas breakthrough time and the rate of gas displacement and CH_4 recovery.

7.7. Conclusions

Experimental results presented in this chapter were part of the investigation conducted to gain a further understanding of coal-gas interactions during N_2 and CO_2 storage and

displacement processes. Before conducting the N_2 and CO_2 experiments, the absolute permeability of the coal sample to helium was measured. The results were compared to those measured for the coal sample used in Chapter 6 (Sample A). The results showed that the permeability values for both samples under similar gas pressures and stress conditions are almost similar.

The effects of confining pressure and gas pore pressure on the coal permeability were investigated. The results indicate that the variation of coal permeability in response to changes in the confining pressure and gas pore pressure varies slightly which can be attributed to the different mechanisms involved in those processes.

The coal permeability to CH_4 and its variations with the effective stress has been investigated. A relationship between CH_4 permeability of the coal sample B and the effective stress has been obtained which is based on exponential relationship.

The gas storage and displacement experiments were conducted on the CH_4 saturated coal sample. N_2 and CO_2 were injected at the upstream of the sample and the outflow gas was monitored until breakthrough was observed. Both experiments were assessed and compared in terms of breakthrough time, gas displacement rate, CH_4 recovery and gas storage.

The results showed that the N_2 breakthrough (1% in production gas) was almost spontaneously whereas for the case of CO_2 the breakthrough time was delayed by two orders of magnitude. Similarly, the gas displacement rate observed in both experiments varied greatly which was mostly related to differences between diffusivity of N_2 and CO_2 as well as higher affinity of coal to CO_2. The later effect also resulted in storage of 40% of injected CO_2 in coal.

The rate of CH_4 recovery was estimated based on the amount of injected gas. The results showed that with respect to injected gas, the amount of CH_4 recovered during CO_2 experiment was higher than those for N_2 experiment by at least two orders of magnitude.

The results of the N_2 experiment showed that the early N_2 breakthrough and higher rate of N_2 production may lead to additional challenges in order to separate N_2 from CH_4 and thus affects the efficiency of the method. For the case of CO_2, the total CH_4 recovery, displacement ratio, breakthrough and CO_2 storage are more favourable. In general, the displacement ratio, CO_2 breakthrough time and CO_2 storage are important parameters affecting the success of carbon sequestration application. However, the swelling effect of CO_2 on coal permeability and injectivity should also be taken into account as observed in the experimental tests presented.

The notable aspect of the experimental investigation presented in this chapter is the sequence of the experiments performed on the coal sample in order to assess its initial gas transport properties as well as to better understand the mechanisms involved in gas storage, displacement and recovery. To the knowledge of the author, such sequence of experiments has not been reported previously in the published works.

In addition, the results of this investigation will provide a validation benchmark for the numerical simulations. Such validation exercise will be presented in the following chapter. In addition, through a series of numerical investigation presented in Chapter 8, further insight into the behaviour of coal during gas injection and recovery will be provided.

7.8. References

Connell, L.D., Sander, R., Pan, Z., Camilleri, M. and Heryanto, D. 2011. History matching of enhanced coal bed methane laboratory core flood tests. *International Journal of Coal Geology*, 87(2), 128-138.

Cui, X., Bustin, R.M. and Dipple, G. 2004. Selective transport of CO_2, CH_4 and N_2 in coals: insights from modeling of experimental gas adsorption data. *Fuel*, 83(3), pp. 293-303.

Durucan, S. and Edwards, J.S. 1986. The effects of stress and fracturing on permeability of coal. *Mining Science and Technology,* 3(3), pp. 205-216.

Karacan, C.Ö. 2003. Heterogeneous sorption and swelling in a confined and stressed coal during CO_2 injection. *Energy and Fuels,* 17(6), pp. 1595-1608.

Mazumder, S. and Wolf, K. 2008. Differential swelling and permability change of coal in response to CO_2 injection for ECBM. *International Journal of Coal Geology*, 74(2), pp. 123-138.

Onur Balan, H. 2008. *Modeling the effects of variable coal properties on methane production during enhanced coalbed methane recovery*. MSc Thesis, Middle East Technical University.

Ross, H.E. 2007. *Carbon dioxide sequestration and enhanced coalbed methane recovery in unmineable coalbeds of the Powder River Basin, Wyoming.* PhD Thesis, Stanford University.

Shi, J., Mazumder, S., Wolf, K. and Durucan, S. 2008. Competitive methane desorption by supercritical CO_2 injection in coal. *Transport in Porous Media*, 75(1), pp. 35-54.

Somerton, W.H., Soylemezoglu, I.M. and Dudley, R.C. 1975. Effect of stress on permeability of coal. *International Journal of Rock Mechanics and Mining Sciences & Geomechanics*, 12(5-6), pp. 129-45.

Tsotsis, T.T., Patel, H., Najafi, B.F., Racherla, D., Knackstedt, M.A. and Sahimi, M. 2004. Overview of laboratory and modelling studies of carbon dioxide sequestration in coal beds. *Industrial and Engineering Chemistry Research,* 43(12), pp. 2887-2901.

van Hemert, P., Wolf, K. and Rudolph, E.S.J. 2012. Output gas stream composition from methane saturated coal during injection of nitrogen, carbon dioxide, a nitrogen-carbon dioxide mixture and a hydrogen-carbon dioxide mixture. *International Journal of Coal Geology,* 89(1), pp. 108-113.

Vishal, V., Ranjith, P.G. and Singh, T.N. 2013. CO_2 permeability of Indian bituminous coals: Implications for carbon sequestration. *International Journal of Coal Geology,* 105(1), pp. 36-47.

Yu, H., Zhou, L., Guo, W., Cheng, J. and Hu, Q. 2008. Predictions of the adsorption equilibrium of methane/carbon dioxide binary gas on coals using Langmuir and ideal adsorbed solution theory under feed gas conditions. *International Journal of Coal Geology*, 73(2), pp. 115-129.

Chapter 8

Further Insight into the Permeability Evolution during Gas Flow and Displacement in Coal

8.1. Introduction

In chapter 6 the results of a series of core flooding experiments were presented in which the permeability of a coal sample to different gas species was studied. Chapter 7 also presented the results of a series of experiments in which the storage and displacement of gases in coal were investigated. Together the mentioned chapters have provided experimental observations of the transport behaviour of gases in coal for a broad range of gas pressures and confining stress conditions. This chapter aims to provide further insight into the transport properties of coal, permeability evolution and major mechanisms that control the behaviour of coal during gas storage and displacement processes. The theoretical approach was found to be beneficial for better understanding of the material behaviour that were not possible to be explored through the experimental investigations presented in previous chapters.

This chapter presents the results of a series of modelling investigations on permeability evolution in coal due to gas injection, storage and displacement by adopting a theoretical approach and numerical model which considers the effective physical and chemical mechanisms controlling the gas transport behaviour in coal. Together with the experimental results presented in previous chapters, the outcome will be used:

1. To explore the new aspects of the porosity and permeability evolution in coal for a range of gas pressure and stress conditions related to the core flooding experiments presented in chapter 6.

2. To investigate the material behaviour and the evolution of transport properties of the coal sample during gas storage and displacement tests presented in chapter 7.

3. To better understand the major mechanisms and micro-scale processes which control the reactive transport of gases in coal by comparison between the predicted results and the experimental data.

4. To identify the areas where lack of experimental data exists by assessing the material parameters required for the numerical simulations. This may provide new platform for further research developments of the experimental studies.

The theoretical model used to describe the permeability evolution and the numerical model to simulate the reactive transport of gases in coal is base on the work developed and presented by Hosking (2014). As stated in Chapter 2, Hosking (2014) has developed a numerical model to simulate transport of gases in fractured rock based on a coupled THCM formulation i.e. COMPASS. The model has been developed to study the physical, chemical and mechanical processes related to carbon dioxide sequestration in coal. A summary of the theoretical formulations of the model developed by Hosking (2014) is provided in Appendix A. In addition, Hosking (2014) has developed a model for gas permeability evolution in coal which has been adopted and used in the investigations presented in this chapter. The model verification and validation tests have been carried out by Hosking (2014).

In Section 8.2, the permeability evolution model developed by Hosking (2014) is briefly described. In this model, the effects of the deformation of the coal porosity and permeability due to effective stress and gas sorption-induced strain have been considered. The model has been used to predict the variation of the coal sample to nitrogen (N_2), methane (CH_4) and carbon dioxide (CO_2) studied in chapter 6 for a range of gas pressure and confining stress conditions. Predicted results from the permeability model are then compared with the experimental results.

In Section 8.3, an application of the numerical model developed by Hosking (2014) to simulate the gas storage and displacement tests presented in chapter 7 is presented. The permeability model tested in section 8.2 has been used to describe the transport properties of the coal sample. The simulation conditions are defined based on the conditions applied for the gas storage and displacement experiments, i.e. nitrogen (N_2) and carbon dioxide (CO_2) experiments, presented in Chapter 7. The initial and boundary conditions applied are described and the material parameters required for the simulations are presented. The results of the gas storage and displacement simulations

for nitrogen (N_2) and carbon dioxide (CO_2) are then presented and compared with those obtained from the experiments. The material behaviour during the interactions with different gas species and displacement processes are discussed.

The conclusions based on the results presented in this chapter are presented in Section 8.4.

8.2. Permeability evolution model

As stated previously, one objective of this chapter is to obtain a better understanding of the permeability evolution during gas storage and displacement tests a result of variations in effective stress and sorption-induced strain. In order to achieve this, the porosity and permeability model developed by Hosking (2014) has been adopted to assess the material behaviour for a range of gas pressures and stress conditions applied during the experimental tests described in Chapter 6.

The permeability evolution model developed by Hosking (2014) is first described. It should be mentioned that in this work, only the final forms of the governing equations related to the fracture and matrix porosity and permeability behaviour are presented. Details of the development of the model can be found in Hosking (2014). Predicted results of the model for permeability variation in coal are then compared with the experimental results of different gas species which were presented in Chapter 6.

8.2.1. Permeability model- background

The porosity and permeability evolution with effective stress, gas pressure and matrix swelling/shrinkage have been evaluated using a theoretical approach described by (Hosking, 2014). The model has been adopted based on a similar approach of Levine (1996) and Robertson and Christiansen (2008), in which changes in fracture width due to various controlling mechanisms are coupled with the changes in the fracture permeability. In the model described by Hosking (2014), the fracture network is defined in

the same manner as by Robertson and Christiansen (2008), i.e. a collection of uniformly-sized cubic matrix blocks. However, instead of neglecting the matrix pore volume, it is considered to be a collection of cubic sub-matrix blocks, as shown in Figure 8.1.

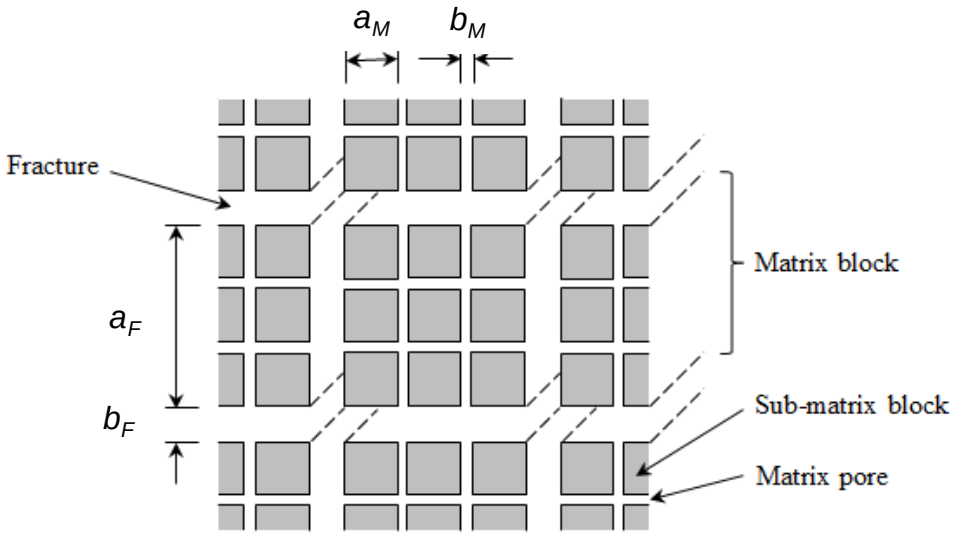

Fig. 8.1. Schematic of the concept used to develop the porosity, permeability model (Hosking, 2014).

The geometry of the system is defined by the fracture width (b_F), the matrix block width (a_F), an arbitrary matrix pore width (b_M) and sub-matrix block dimension (a_M). The general assumptions considered for the development of the model are (Hosking, 2014):

1) Coal is a dual poroelastic medium, i.e. a porous medium that deforms elastically.

2) The fracture and matrix properties are homogeneous and isotropic.

3) The absolute permeability depends only on the gas flow and reactions. The effect of water saturation is considered via relative phase permeabilities.

4) Strains are infinitesimal or very small compared to the length scale.

5) Matrix pores are much stiffer than the fractures.

6) Changes in porosity and permeability are assumed to depend mainly on the changes in b_F , b_M and not a_F , a_M .

In this model, changes in the porosity and permeability of the fracture are attributed to i) the pore compressibility, ii) the matrix block compressibility and iii) the sorption induced matrix block strain. The matrix pores have been assumed to be much stiffer than the fractures. This allows the pore compressibility to be neglected in the matrix deformation equations. As a result, changes in the porosity and permeability of the matrix are attributed to i) matrix block compressibility and ii) sorption induced strain. The compression of the matrix blocks can cause an increase in the fracture porosity and a decrease in the matrix porosity, whilst sorption induced strains result in a variation in the porosity of both continua.

The final forms of the fracture porosity and permeability equations are given as (Hosking, 2014):

$$n_F = n_{F0} - \frac{n_{F0}c_{f0}}{\alpha_f}\left(1 - e^{\alpha_f \sum_{j=1}^{n_g}(Z_F RTc_{gF}^j - Z_{F0}RTc_{gF0}^j)}\right) + 3\sum_{j=1}^{n_g}\left[\frac{(1-2v)}{E}\left(Z_F RTc_{gF}^j - Z_{F0}RTc_{gF0}^j\right) - \left(\varepsilon_s^j - \varepsilon_{s0}^j\right)\right] \tag{8.1}$$

$$k_F = k_{F0}\left\{1 - \underbrace{\frac{c_{f0}}{\alpha_f}\left(1 - e^{\alpha_f \sum_{j=1}^{n_g}(Z_F RTc_{gF}^j - Z_{F0}RTc_{gF0}^j)}\right)}_{\text{Fracture compressibility}} + \frac{3}{n_{F0}}\sum_{j=1}^{n_g}\left[\underbrace{\frac{(1-2v)}{E}\left(Z_F RTc_{gF}^j - Z_{F0}RTc_{gF0}^j\right)}_{\text{Matrix block compressibility}} - \underbrace{\left(\varepsilon_s^j - \varepsilon_{s0}^j\right)}_{\text{Sorption induced matrix block strain}}\right]\right\}^3 \tag{8.2}$$

where, n_{F0} is the initial fracture porosity, c_{f0} is the initial fracture compressibility, α_f is the rate of fracture compressibility change, v is the Poisson's ratio, E is the Young's modulus and ε_s^j is the sorption induced strain for the j^{th} pore gas component in the matrix continuum, ε_{s0}^j is the initial sorption induced strain for the j^{th} pore gas component in the matrix continuum, k_F *is t*he absolute permeability in the fracture and k_{F0} is the initial absolute permeability in the fracture continuum.

The fracture compressibility, c_f , is expressed as (Hosking, 2014):

$$c_f = -\frac{c_{f0}}{\alpha_f (P_{gF} - P_{gF0})}\left[1 - e^{\alpha_f (P_{gF} - P_{F0})}\right] \tag{8.3}$$

and the Langmuir strain isotherm in its multicomponent form (ε_s^j) is given as (Levine, 1996; Hosking, 2014):

$$\varepsilon_S^j = \frac{\varepsilon_L^j b_L^j Z_M RTc_{gM}^j}{1 + Z_M RT\sum_{k=1}^{n_g} b_L^k c_{gM}^k} \tag{8.4}$$

where, ε_L^j and b_L^j are the Langmuir strain and inverse Langmuir pressure constants for the j^{th} component, respectively.

The final forms of the matrix porosity and permeability equations are given as (Hosking, 2014):

$$n_M = n_{M0} - 3\sum_{j=1}^{n_g}\left[\frac{(1-2v)}{E}\left(Z_F RTc_{gF}^j - Z_{F0} RTc_{gF0}^j\right) + \left(\varepsilon_s^j - \varepsilon_{s0}^j\right)\right] \tag{8.5}$$

$$k_M = k_{M0}\left\{1 - \frac{3}{n_{M0}}\sum_{j=1}^{n_g}\left[\underbrace{\frac{(1-2v)}{E}\left(Z_F RTc_{gF}^j - Z_{F0} RTc_{gF0}^j\right)}_{\text{Matrix block compressibility}} + \underbrace{\left(\varepsilon_s^j - \varepsilon_{s0}^j\right)}_{\text{Sorption induced matrix block strain}}\right]\right\}^3 \tag{8.6}$$

where, n_{M0} is the initial matrix porosity, k_M is the absolute permeability in the matrix continuum and k_{M0} is the initial absolute permeability in the matrix continuum. The subscripts *F* and *M* in equations (8-1) to (8-6) represent the conditions in fracture and matrix continua, respectively.

In this model, the gas pressures have been converted into the equivalent gas concentrations using the real gas law, given as (Hosking, 2014):

$$c_g^i = \frac{P_g}{ZRT} \tag{8.7}$$

where, c_g^i is the gas concentration (mol/m^3), P_g is the gas pressure (MPa), T is the temperature (K), R is the universal gas constant (J/mol.K) and Z is the compressibility factor obtained using the Peng and Robinson (1976) equation of state.

8.2.2. Variation of the coal permeability to N_2, CH_4 and CO_2

In this section, the porosity and permeability model is adopted and examined by comparing the predicted results with the experimental results of the coal permeability measurements presented in Chapter 6. The experimental results are related to the coal permeability to N_2, CH_4 and CO_2 at confining pressures of 4, 5 and 6MPa. Table 8.1 presents a summary of the experimental conditions including the injection pressures used at each confining pressure in the core flooding experiments with N_2, CH_4 and CO_2, presented in Chapter 6.

Table 8.1. Summary of the injection pressures used at each confining pressure in the core flooding experiments with N_2, CH_4 and CO_2.

Confining pressure (MPa)	**Injection pressure steps (MPa)**		
	Step 1	Step 2	Step 3
4.0	2.5	3.0	3.5
5.0	3.5	4.0	4.5
6.0	4.5	5.0	5.5

Since the coal matrix permeability is typically 8 to 9 orders of magnitude less than that in the fracture network (Seidle, 2011), the contribution of the matrix permeability to the bulk permeability has been neglected (Hosking, 2014). Therefore the changes in bulk permeability, k_F, was predicted using only the fracture permeability equation, i.e. equation (8-2). The input parameters used in equation (8-2) are summerised in Table 8.2. Some of the material parameters have been obtained from the experimental results of this study presented in previous chapters and some have been obtained from the literature as presented by Hosking (2014). The material parameters presented in Table 8.2 are briefly described, as follows:

Table 8.2. Material parameters and initial conditions for the permeability evolution model.

Material parameters				**Source/Reference**
Initial Fracture porosity, n_{F0} (-)	0.0025			Hosking (2014)
Compressibility change rate, α_f (MPa^{-1})	4.41×10^{-13}			Hosking (2014)
Poisson ratio, v (-)	0.34			Robertson and Christiansen (2008); Shi and Durucan (2004)
Young's modulus, E (MPa)	2710			
Adsorption parameters				
	N_2	CH_4	CO_2	
Average Langmuir pressure, P_L^i (MPa)	1.73	0.68	0.5	This study
Inverse Langmuir pressure, b_L^j (MPa^{-1})	0.58	1.47	2	This study
Langmuir linear strain constant, ε_L^j (-)	0.0025	0.003	0.008	Hosking, 2014
Initial conditions				
C.P. 4MPa				
	N_2	CH_4	CO_2	
Initial fracture permeability, k_{F0} (m^2)	1.85×10^{-16}	4.43×10^{-17}	4.58×10^{-17}	This study
Initial fracture compressibility, c_{f0} (MPa^{-1})	6.53×10^{-13}	6.53×10^{-13}	6.53×10^{-13}	Robertson and Christiansen (2008)
Initial gas pressure, P_{g0} (MPa)	2.13	2.09	2.05	This study
C.P. 5MPa				
	N_2	CH_4	CO_2	
Initial fracture permeability, k_{F0} (m^2)	1.62×10^{-16}	4.32×10^{-17}	2.13×10^{-17}	This study
Initial fracture compressibility, c_{f0} (MPa^{-1})	4.35×10^{-13}	4.35×10^{-13}	4.35×10^{-13}	Robertson and Christiansen (2008)
Initial gas pressure, P_{g0} (MPa)	2.89	2.87	2.85	This study
C.P. 6MPa				
	N_2	CH_4	CO_2	
Initial fracture permeability, k_{F0} (m^2)	1.48×10^{-16}	3.88×10^{-17}	8.57×10^{-18}	This study
Initial fracture compressibility, c_{f0} (MPa^{-1})	3.05×10^{-13}	3.05×10^{-13}	3.05×10^{-13}	Robertson and Christiansen (2008)
Initial gas pressure, P_{g0} (MPa)	3.69	3.72	3.78	This study

1) The initial fracture porosity

In this model, the initial bulk porosity (n_B) is considered to be 0.025 (Hosking, 2014). The fracture porosity has been then calculated using equation (8-1). It should be mentioned that the total porosity value considered by Hosking (2014) is in agreement with the lower porosity range defined for the coal sample of this study presented in Chapter 4, i.e. total porosity of 2.5 to 6% (Figure 4.5).

2) The initial fracture compressibility and compressibility change rate

The values have been defined based on the ranges suggested by Robertson and Christiansen (2008).

3) Poisson's ratio and Young's modulus

These parameters have been defined based on the values reported by Robertson and Christiansen (2008) and Shi and Durucan (2004).

4) Langmuir constants

The Langmuir pressures used in the permeability model (equation 8-4) were calculated based on an average of the adsorption and desorption isotherms presented in Chapter 5 (average of P_L values presented in Tables 5.1 and 5.2). This was mainly because of the hysteresis observed between the adsorption and desorption behaviour of the coal reported in Chapter 5.

5) The initial fracture permeability

The initial fracture permeability values were obtained from the experimental results presented in Chapter 6. The permeability value for the second gas injection pressure step at each confining pressure has been considered as initial fracture permeability.

The results of the coal permeability evolution due to interaction with N_2, CH_4, and CO_2 gases for a range of gas injection pressures and confining pressures are presented in Figures 8.2, 8.3, and 8.4, respectively. The results of the experiments are also included for comparison.

The results of the model show that at each constant confining pressure, the coal permeability increases with increase in gas pressure for N_2, CH_4 and CO_2. At higher confining pressures, the increase in the coal permeability with increase in gas pressure is less significant. This behaviour was also observed in the experimental results of permeability variations with effective stress presented in Chapter 6, i.e. Figures 6.4 and 6.9 and 6.15.

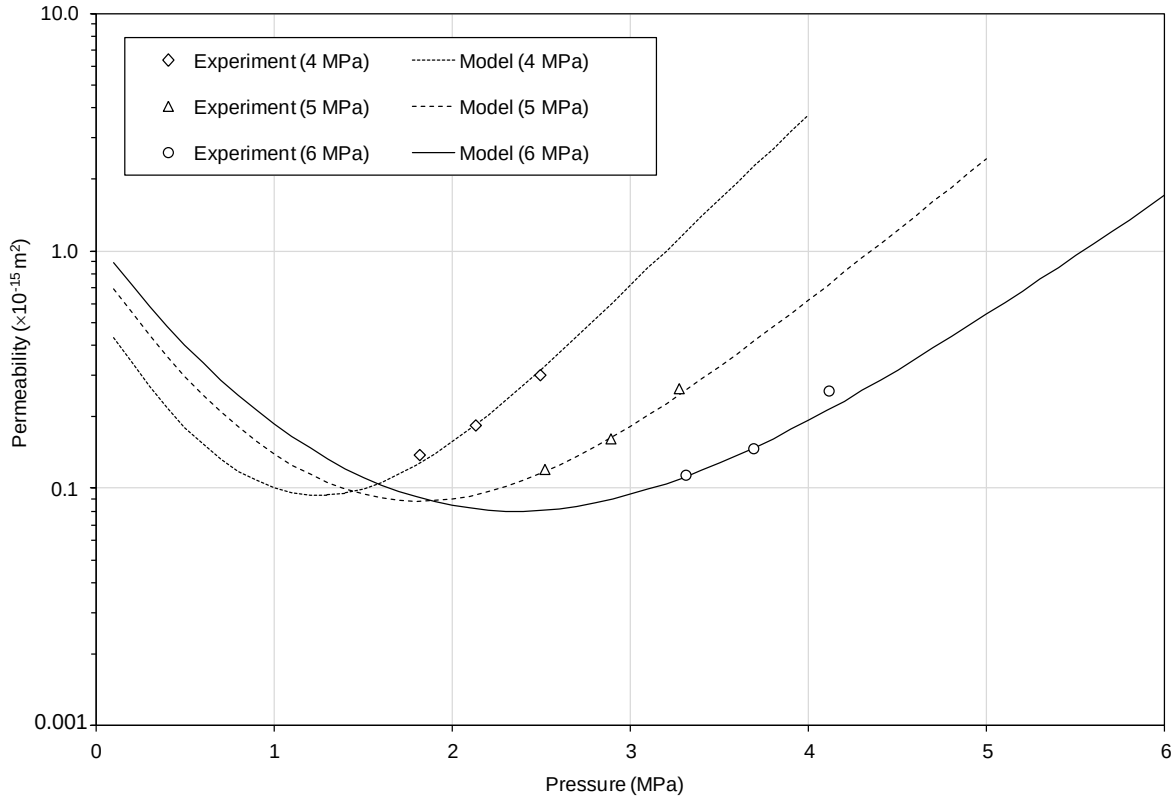

Fig. 8.2. Variation of coal permeability to N_2 with pressure from the experimental results and theoretical model.

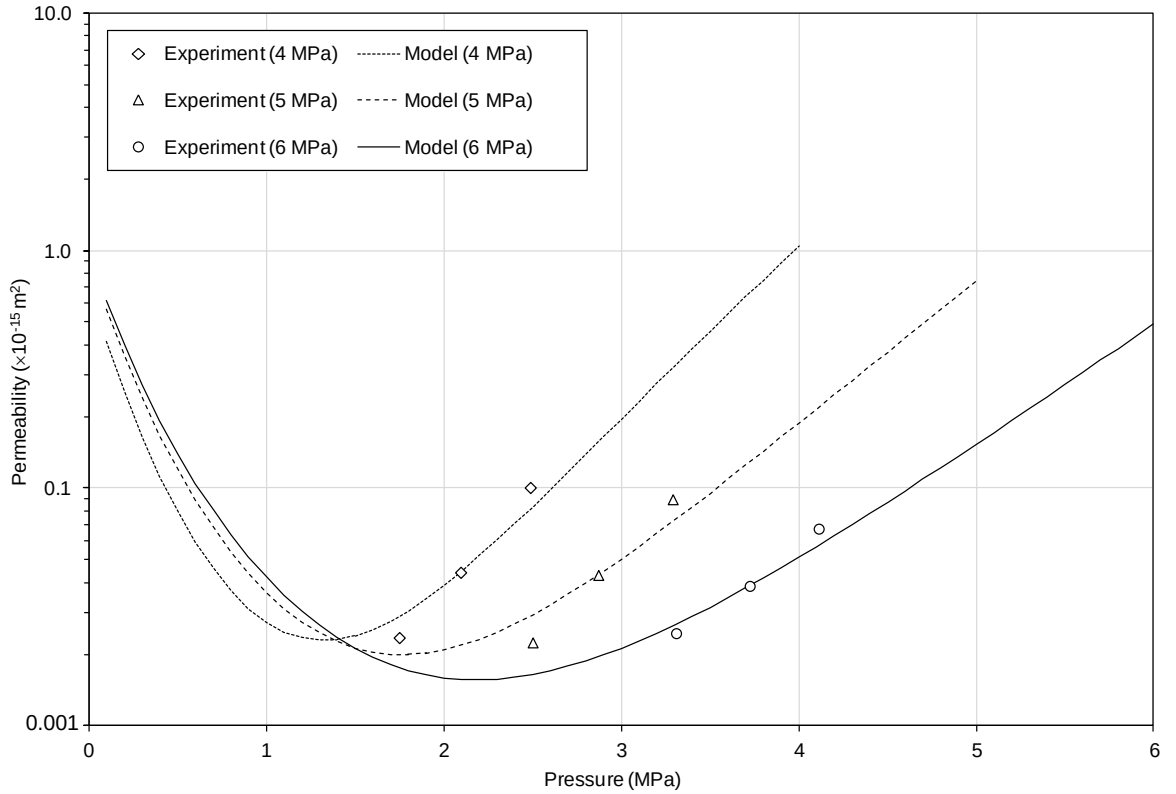

Fig. 8.3. Variation of permeability to CH_4 with pressure from the experimental results and theoretical model.

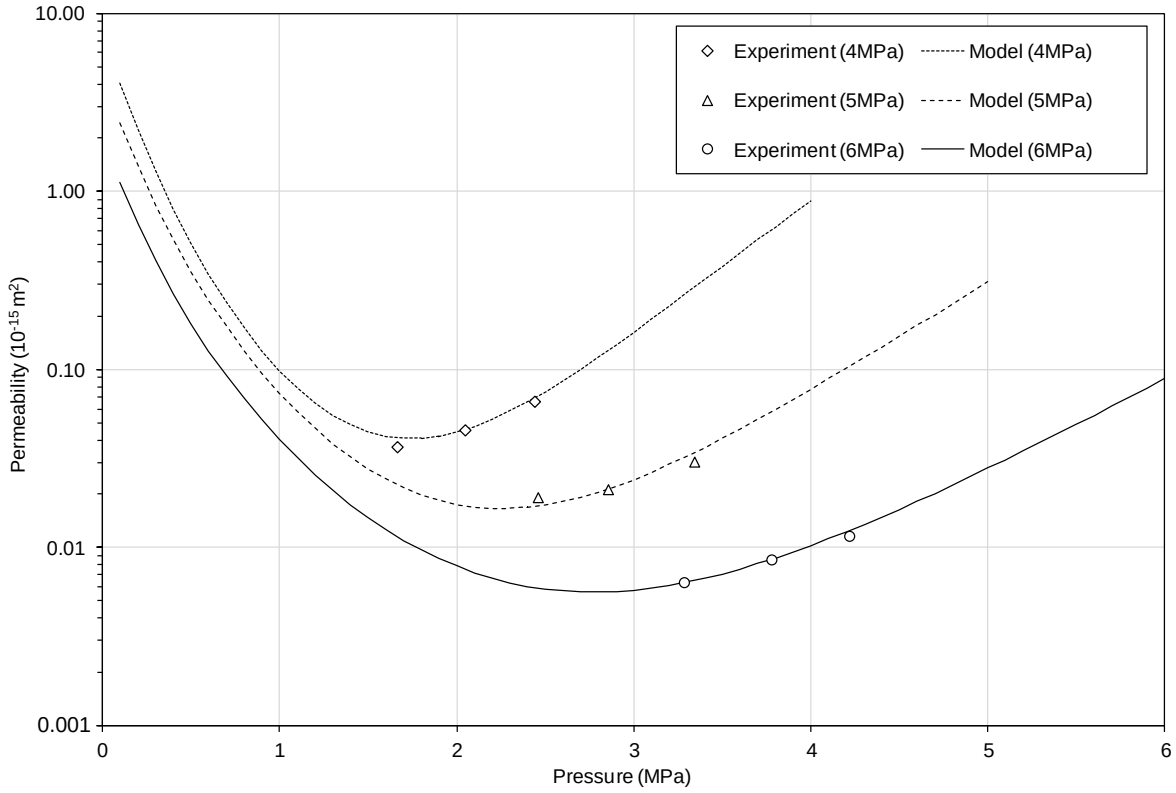

Fig. 8.4. Variation of permeability to CO_2 with pressure from the experimental results and theoretical model.

The coal permeability increases at lower injection pressures can be attributed to desorption of the gas from the coal which results in the matrix shrinkage in accordance to the mechanisms described in coal permeability evolution model. This is more significant for the case of CO_2, as shown in Figure 8.4.

As stated previously, changes in coal permeability due to the fracture compressibility, matrix block compressibility and sorption induced matrix block swelling have been included in the permeability model. The compressibility of the fracture and matrix is a physico-mechanical process which depends only on the effective stress. The permeability evolution observed for the cases of N_2 and CH_4 in Figures 8.2 and 8.3, respectively, can be mainly related to the physico-mechanical processes mentioned above. This has been also observed from the results of the core flooding experiments presented in Chapter 6, where the volumetric effects of those gases on coal due to gas sorption was negligible.

The sorption-induced swelling, however, is a chemo-mechanical process and depends on the type of gas. As observed from the results of the gas adsorption in coal presented in Chapter 5, coal has a greater affinity to adsorb CO_2 compared with other gases studied, i.e. CH_4 and N_2. The experimental results also indicated that the sorption induced swelling effect of CO_2 on the coal matrix is more significant than those for other gases. Therefore, as shown in Figure 8.4, the permeability to CO_2 is on average 7 times lower than the N_2 permeability across the range of effective stress values considered. Unlike other gases, the coal permeability to CO_2 does not increase significantly due to the effect of sorption induced matrix block swelling based on the model.

A comparison between the results predicted by the model and the experimental data shows that the adopted model is capable of predicting the permeability variations in coal for the range of gas pressures and confining pressures considered. Therefore, it can be used for the simulations of the N_2 and CO_2 storage and displacement processes in coal. The results of the simulations are presented and discussed in the following section.

8.3. Permeability model application in gas storage/displacement experiments

In this section, the application of the permeability model described in Section 8.2 in numerical simulation of the gas storage and displacement tests in coal described in Chapter 7 is presented. First, the initial and boundary conditions defined for the simulations of N_2 and CO_2 storage and displacement processes in coal are described. The initial and boundary conditions are mainly based on the conditions considered for the N_2 and CO_2 storage and displacement experiments presented in Chapter 7. The additional material parameters required for the simulations are also described. Finally, the results of the N_2 and CO_2 storage in coal and their displacement with CH_4 are presented and discussed.

In the formulation of the gas transport in coal, the coal system is described via a dual continuum system, i.e. a dual porosity, dual permeability approach (Hosking, 2014). This

approach has been selected as the structure of coal exhibits a non-uniform porosity system which contains a dispersed fracture network and blocks of rock matrix. Geochemical reactions are also included via sink/source terms in the governing equations. Non-ideal gas mixture behaviour at high pressure has been also considered in the formulation which is relevant to applications such as the geological sequestration of carbon dioxide (CO_2) in coal. The model has been developed under a coupled thermal, hydraulic, chemical, gas and mechanical formulation. However, for the current application the following assumptions/limitations have been considered:

- Thermal effects are not considered and the processes are simulated under the assumption of isothermal conditions.
- Gas dissolution in liquid phase is not considered as it is assumed that the majority of gas is either free gas or adsorbed gas in the solid phase.
- In this formulation, the deformation behaviour has not been explicitly expressed. The effects of the coal deformation, however, have been included on the flow variables using appropriate relationships describing the permeability and porosity evolution with gas pressure and composition, as presented in Section 8.2.

The formulation has been developed based on the principle of mass conservation for the i^{th} gas component in a dual porosity medium, expressed as (Hosking, 2014):

$$\frac{\partial(\theta_{g\alpha} c^i_{g\alpha} \delta V_\alpha)}{\partial t} = \underbrace{-\delta V_\alpha \nabla \cdot \mathbf{J}^i_{g\alpha}}_{\text{Transport}} \underbrace{-\delta V_\alpha \lambda \Gamma^i_g}_{\substack{\text{Mass exchange} \\ \text{between fracture} \\ \text{and matrix}}} \underbrace{-\delta V_\alpha R^i_{g\alpha}}_{\text{Reaction}} \tag{8.8}$$

where, $\theta_{g\alpha}$ is the volumetric gas content in continua α ($\alpha=F$ for the fracture continuum, and $\alpha=M$ for the matrix continuum), $c^i_{g\alpha}$ is the gas concentration of the i^{th} component, δV_α is the incremental volume, , t is time, $\mathbf{J}^i_{g\alpha}$ is the total flux of the gas component i^{th}, λ is the parameter defining the conditions between fracture and matrix continua and $\Gamma^i_{g\alpha}$ is the sink/source term representing the mass exchange of the gas component i

between the fracture and matrix continua. ∇ is the gradient operator and $R^i_{g\alpha}$ represents the sink/source term accounting for geochemical reactions, e.g. gas adsorption and desorption.

The transport term ($\mathbf{J}^i_{g\alpha}$) in equation (8-8) includes both advective and diffusive transport mechanisms. The advective transport of the gas is considered as the gradients of the bulk gas pressure using Darcy's Law and the diffusive transport can be considered via a combination of the diffusion processes such as the ordinary diffusion, the Knudsen diffusion and configurational diffusion (Hosking, 2014).

The mass exchange term ($\Gamma^i_{g\alpha}$) in equation (8-8) can include the components due to advection and diffusion. The first order mass exchange coefficient for gas advection is defined based on the geometry of the matrix blocks, the typical thickness of a matrix block or fracture spacing and mean gas conductivity and gas densities in fracture and matrix. The diffusive flux of multicomponent pore gas exchange is assumed to be an ordinary diffusion process (Hosking, 2014).

The reaction term ($R^i_{g\alpha}$) in equation (8-8) considers the amount of gas lost/gained due to adsorption/desorption reactions with the solid phase which has been only considered in the matrix continuum (Hosking, 2014).

The details related to the theoretical formulation have been provided in Appendix A and further details can be found in Hosking (2014). The formulation has been incorporated in a numerical model, COMPASS by Hosking (2014). The background of the COMPASS model has been presented in Chapter 2.

8.3.1. Initial and boundary conditions

The system considered is a two dimensional domain with 0.12m long and 0.07m width which was discretised into 100 equally sized 4-noded quadrilateral elements. The gas flow is assumed to be one dimensional. The total duration of the simulations is 90min with

time steps of 10s. The system is considered to be dry and remained isothermal at 298K similar to the conditions of the experiment. A summary of the initial and boundary conditions used in the simulations of the N_2 and CO_2 storage and displacement processes are presented in Figures 8.5 and 8.6, respectively.

The coal was considered to be initially saturated with methane (CH_4) at a pressure of 5MPa. In both simulation scenarios, the gas was injected at a constant pressure of 5MPa. In Figures 8.5 and 8.6, the specified gas pressures have been expressed in terms of the gas concentrations as a variable of the model calculated based on the Equation of State introduced by Peng and Robinson (1976).

The gas abstraction boundary condition was fixed at atmospheric pressure, i.e. $P_g = 0.1MPa$, for the multicomponent mixture. The initial adsorbed phase concentration of CH_4 was assumed to be at equilibrium with the free gas phase at 5MPa gas pressure and was obtained from the CH_4 adsorption isotherm presented in Chapter 5, i.e. Figure 5.5.

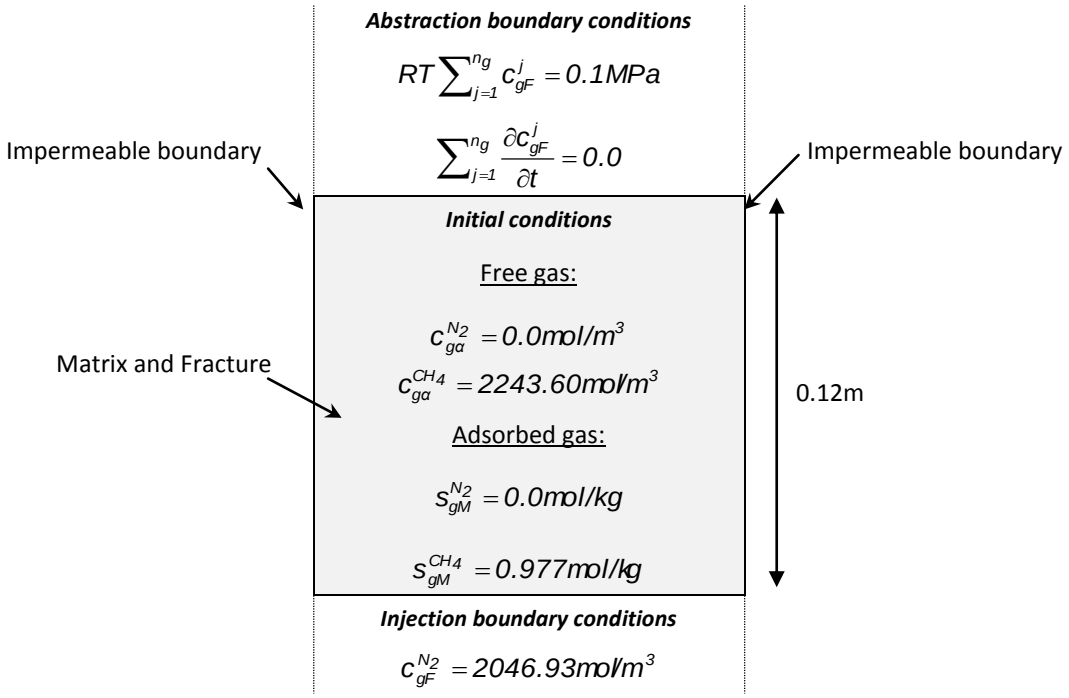

Figure 8.5. Schematic of the initial and boundary conditions used for N_2 storage and displacement simulation.

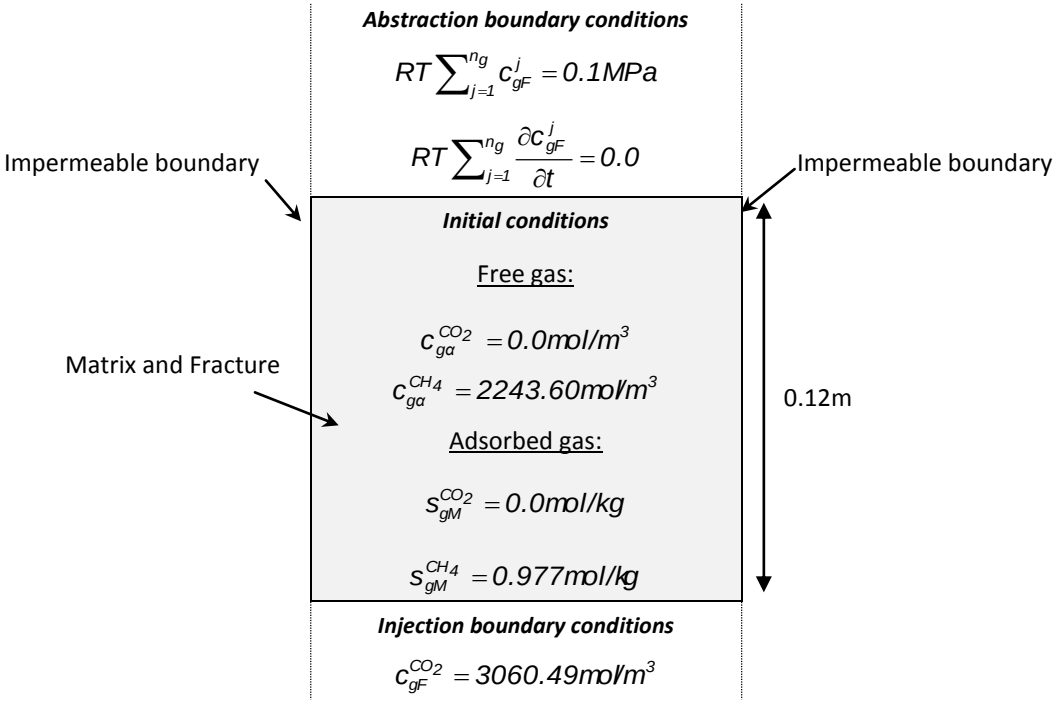

Figure 8.6. Schematic of the initial and boundary conditions used for CO_2 storage and displacement simulation.

8.3.2. Additional material parameters

The material parameters required for the prediction of the permeability evolutions in coal have been presented in Table 8.2. The additional material parameters required for the simulations of N_2 and CO_2 storage and displacement processes are presented in Table 8.3. As stated previously, in the absence of experimental data, the material parameters were adopted from the literature survey or via the history matching (Hosking, 2014).

Based on the recommendation by Seidle (2011), the initial local permeability in the matrix pore region, i.e. k_{M0}^{L}, has been considered to be eight orders of magnitude less than the fracture permeability. The sorption parameters have been obtained from the results of gas adsorption/desorption measurements on coal presented in Chapter 5, i.e. Tables 5.1, 5.2 and 5.3.

Table 8.3. Additional material parameters required for the simulations (Hosking, 2014).

Material parameter	**value**		
Matrix block width, l (m)	0.010		
Initial bulk porosity, n_{B0} (-)	0.025		
Volumetric weighting factor, w_f (-)	0.005		
	Fracture	Matrix	
Initial local porosity, $n^L_{\alpha 0}$ (-)	0.5	-	
Initial bulk porosity, $n_{\alpha 0}$ (-)	0.0025	0.0225	
Initial local permeability, $k^L_{\alpha 0}$ (m^2)	4.50×10^{-16}	4.50×10^{-24}	
Initial bulk permeability, $K_{\alpha 0}$ (m^2)	2.25×10^{-18}	4.48×10^{-24}	
	N_2	CH_4	CO_2
Diffusion coefficient (free), D^i_g, (m^2/s)	2.04×10^{-5}	2.23×10^{-5}	1.10×10^{-5}

8.3.3. Simulations results and discussions

Based on the initial and boundary conditions described in Section 8.3.1 and the material parameters presented in Tables 8.2 and 8.3, the N_2 and CO_2 storage and displacement processes have been simulated using the double porosity, double permeability formulations developed by Hosking (2014). The results of the simulations for N_2 and CO_2 are presented and discussed in the following sections.

8.3.3.1. N_2 simulation

Figure 8.7 presents the simulated results of the N_2 storage and displacement in coal. The experimental results have been also included in the graph for comparison. As it can be seen from the results, the predicted results are overall in good agreement with the experimental data.

The slight differences between the results can be attributed to the following factors:

1. The sorption capacities used in the simulations were obtained based on the experimental results on powdered coal samples (Chapter 5). Therefore, additional

surface area in powdered samples may have been exposed to the gas (Pone et al., 2009).

2. The sorption rates used in the simulations were based on the results on unconfined samples (Chapter 5), therefore application of the sorption rates to the confined conditions of the intact coal sample may involve some limitations. The application of a confining pressure may further reduce the sorption capacity and sorption rate by reducing the aperture of nanopores (Lwin, 2011).

It is therefore likely that the sorption capacities and rates used in the simulations were slightly larger than the actual values.

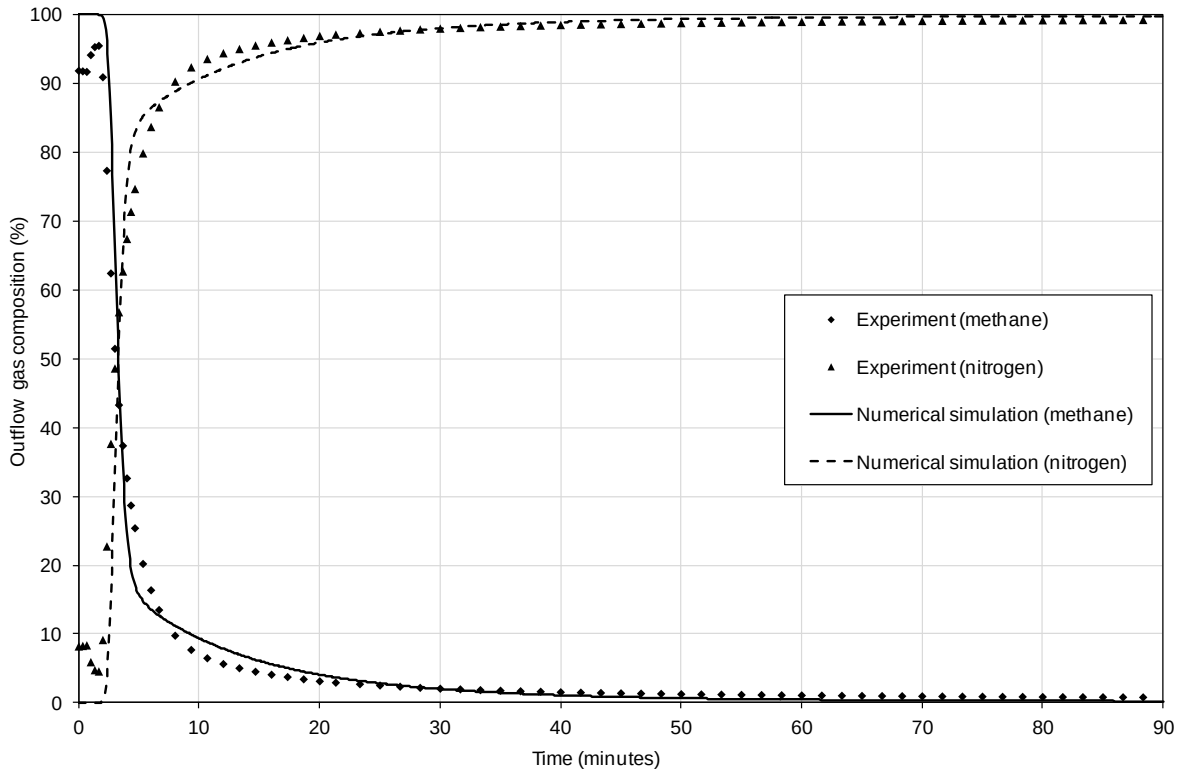

Fig. 8.7. Comparison of the gas outflow with time obtained from the simulations of N_2 storage and displacement in coal. The experimental results are also presented for comparison.

8.3.3.2. CO_2 simulation

The simulated results of CO_2 storage and displacement in coal are presented in Figure 8.8. As it can be seen from the results, for the case of CO_2, the predicted results showed much

faster gas displacement rate compared to the experimental data. This could be partly explained by the factors mentioned above, i.e. application of sorption parameters related to unconfined powdered coal samples in the simulations.

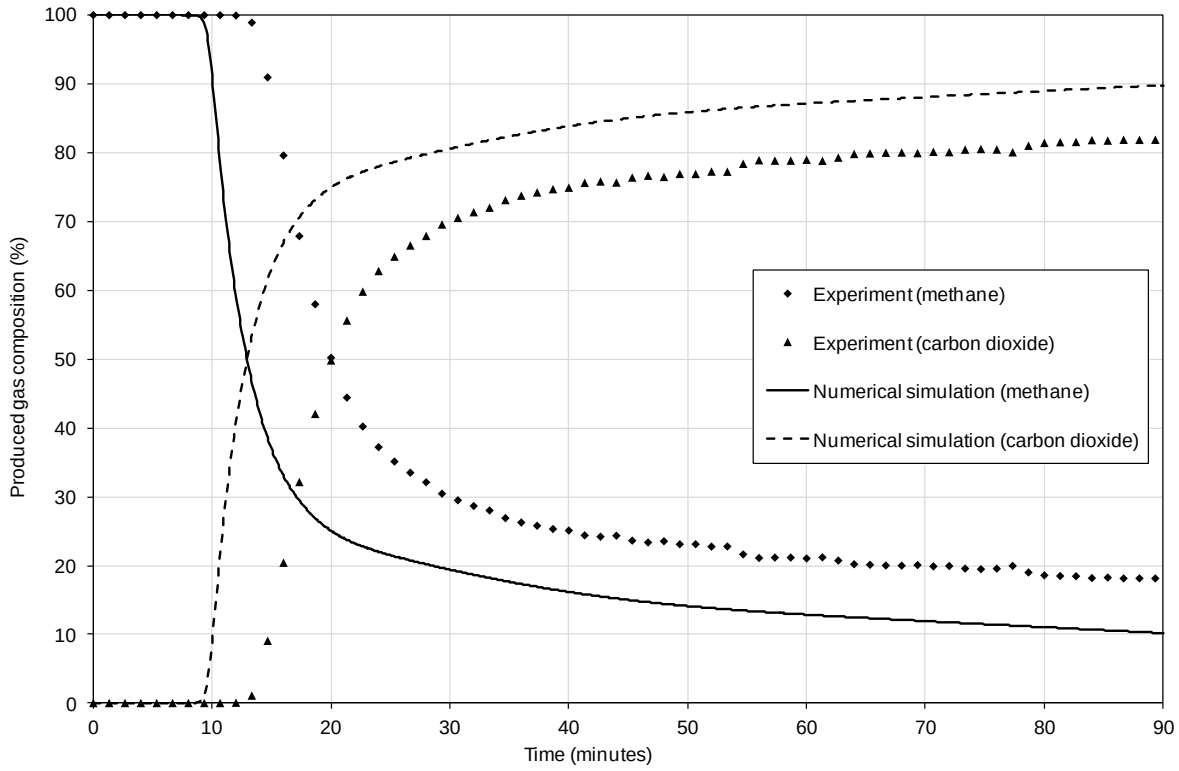

Fig. 8.8. Comparison of the gas outflow with time obtained from the simulations of CO_2 storage and displacement in coal. The experimental results are also presented for comparison.

For the case of CO_2 simulation, faster displacement rate was more noticeable, since CO_2 has a higher tendency to displace adsorbed CH_4 compared to N_2. However, the differences observed here are larger than to be explained with only one or two factors.

Further examination of the simulated results showed that the agreement between the predicted results and the experimental data improves if the initial local fracture permeability defined in Table 8.2 is reduced to a third of the value used for the N_2 simulation, i.e. $3.0\times10^{-16}m^2$. The predicted results using the reduced permeability value are presented in Figure 8.9.

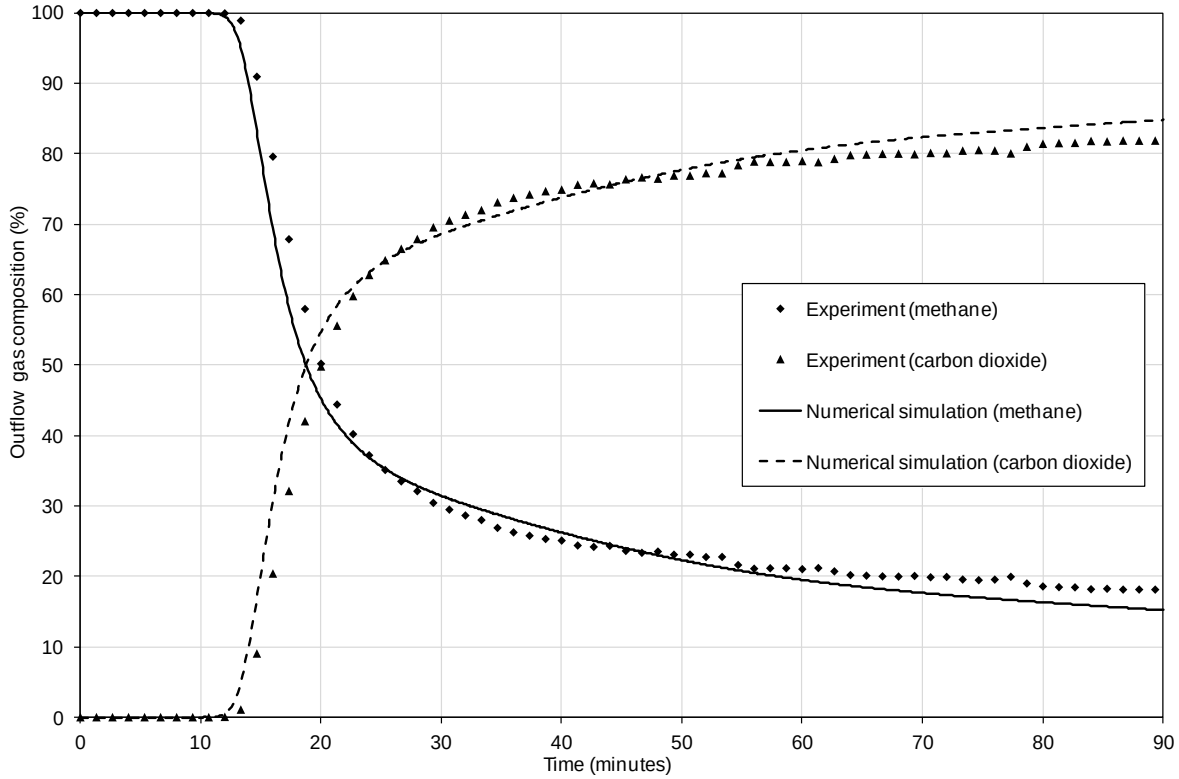

Fig. 8.9. Comparison of the gas outflow with time obtained from the simulations of CO_2 storage and displacement process, after reducing the initial local fracture permeability to a third of its initial value. The experimental results have been also shown for comparison.

The reduction of the initial fracture permeability can be explained by a number of influential factors, as follows:

1. **The uncertainty in the experimental data**

The required reduction of the initial coal permeability to CO_2 can be related to the permeability hysteresis as a result of cyclic loading during the experimental measurements. The hysteresis effect due to the effective stress variations on the coal permeability has been also observed in the results of the gas flow and permeability measurements presented in Chapter 6. From the experimental results of helium and N_2 flooding experiments it was observed that the relative permeability of the coal sample to N_2 was reduced by at least 30% of its absolute permeability to helium. Although, this was to some extent related to the molecular size of gas species, it was also observed that the hysteresis effect as a result of cyclic loadings and variation in effective stress may have reduced the coal permeability. Therefore, similar process might have occurred for the

coal sample B on which the experiments have been performed. Although from the results presented in Chapter 7, the confining pressure was kept constant during and after both N_2 and CO_2 experiments, the changes in the gas pore pressure could result in changes in the effective stress and therefore might have had some impact on coal permeability and imposing hysteresis to the coal sample.

2. The rates of sorption-induced strain

From the discussion presented in Chapter 7, it was concluded that the delayed breakthrough of CO_2 can be related to a combination of gas diffusivity and coal matrix swelling induced by CO_2 adsorption. The latter effect can lead to a progressive reduction in the fracture permeability and can be a controlling factor for the delayed breakthrough of CO_2. Therefore, another factor related to lower permeability required for the simulation can be related to the slower sorption strain rates that have been used in the numerical simulations. The slower sorption strains in the numerical simulation can potentially be related to:

- The rate of mass exchange between the fracture and matrix.
- The application of an equilibrium approach for the sorption induced strain.

The mechanisms that control the fracture-matrix mass exchange can be influential in uncertainties associated with sorption strain rates. In the adopted formulation (Appendix A), the mass exchange coefficient has been treated as a constant value. Whereas, it has been postulated in the literature, i.e. Gerke and van Genuchten (1993a; 1993b), that this assumption can be valid only at long duration after the pressure front has reached the centre of the matrix blocks. Therefore, implementation of a transient mass exchange coefficient could have possibly increased the rate of sorption strains in the CO_2 simulation. Consequently, the need for lowering the initial permeability could be prevented.

On the other side, by referring to the permeability evolution model presented in Section 8.2, the sorption strains have been implemented in the code based on the equilibrium

sorption strain approach (extended Langmuir strain), therefore the kinetic of the adsorbed concentrations (the CO_2 injection boundary condition) has not been applied in the matrix continuum which has resulted in slower rate of sorption strain development. The sorption strain may have developed faster if it was calculated using a kinetically controlled adsorption. This is because the CO_2 injection boundary condition could then have been applied in the matrix continuum without inducing unrealistic instantaneous sorption strains. The rate of sorption strain development would then have been directly related to the rate of CO_2 adsorption. The faster rate of CO_2 adsorption has been observed from the results of adsorption kinetics presented in Chapter 5.

Implementing the above changes would require a good understanding of the relationship between the adsorbed amount and sorption strain at non-equilibrium conditions. In order to extend this concept for non-equilibrium conditions, sufficient sorption strain kinetics data would be required which is beyond the scope of the present work.

8.4. Conclusions

The results of a series of modelling studied related to coal permeability evolution due to effective stresses and sorption-induced strain were presented and compared with the experimental results from previous chapters. The effects of deformation on the permeability evolution of coal were explored based on the mechanisms included in the permeability model such as the effects of fracture compressibility, matrix block compressibility and sorption induced matrix block swelling.

A comparison between the predicted results from the adopted theoretical approach and the experimental data shows that for N_2 and CH_4 gases, the permeability evolution of the coal sample has been mainly controlled by the physico-mechanical processes, i.e. compressibility of the factures and matrix blocks due to variations in effective stress. For the case of CO_2, however, the permeability evolution of the coal sample studied has been mainly controlled by chemo-mechanical processes, i.e. sorption-induced strain.

A series of numerical simulations of the N_2 and CO_2 storage and displacement were performed considering the initial and boundary conditions applied in the experimental studies presented in Chapter 7. The major mechanisms controlling the advection and diffusion flow of gases in coal were considered based on the adopted permeability model.

In the N_2 simulation, good correlation between the theoretical approach and the experimental data was observed. The gas displacement rate after the initial breakthrough of the injected gas was found to be slightly faster than that observed in the experiments. This was attributed to the fact that the sorption capacities and sorption rates used in the simulations were based on the experimental results of the unconfined and powdered coal samples. Therefore, it is expected that those values were larger than the values for a confined intact coal sample. Therefore, the rate of the gas adsorption and desorption capacity might have been overestimated for the confined intact coal resulting in a faster displacement rate for the simulated results.

For the CO_2 simulation, the differences between the simulated results and the experimental data were found to be larger than those observed in the N_2 simulation. Further investigation showed that the discrepancies between the predicted results and experimental data decreases to a great extent if a lower initial fracture permeability value is applied to the CO_2 simulation.

A number of experimental and computational factors have been discussed in relation to the lower initial permeability required for the case of CO_2 simulation which can be summarised, as follows:

- The uncertainties in the experimental results, i.e. the effect of hysteresis during the loading/unloading cycles.
- The uncertainties related to the computational factors such as the influence of the mass exchange process which has been currently considered as a constant value rather than a transient coefficient.

- Application of the equilibrium sorption strain approach which found to be an influential factor. This can be prevented by obtaining and applying the kinetics of sorption-induced strain to simulations of gas displacement process in coal.

The results of this chapter have highlighted the importance of the chemically controlled processes in relation to coal permeability evolution as a result of coal-gas interactions during CO_2 injection.

The results also underline the need for further laboratory investigations on kinetics of sorption-induced strains on intact coal samples under the confined conditions. Such data can be used for further validation and improvement of the numerical models and therefore would lead to obtain more realistic results from the numerical models without the need of modifying the initial properties.

8.5. References

Gerke, H.H. and van Genuchten, M.T. 1993a. A dual-porosity model for simulating the preferential movement of water and solutes in structured porous media. *Water Resources Research*, 29(2), pp. 305-319.

Gerke, H.H. and van Genuchten, M.T. 1993b. Evaluation of a first-order water transfer term for variably saturated dual-porosity flow models, *Water Resources Reseach*, 29(4), pp. 1225-1238.

Hosking, L. 2014. *Reactive transport modelling of high pressure gas flow in coal*. PhD Thesis. Cardiff University.

Levine, J.R. 1996. Model study of the influence of matrix shrinkage on absolute permeability of coal bed reservoirs. In: Gayer, R. and Harris, I. eds. *Coalbed Methane and Coal Geology*, *Geological Society Special Publication* No. 109, London, pp. 197-212.

Lwin, M.J. 2011. The effect of different gases on the ultrasonic response of coal. *Geophysics*, 76(5), pp. 155-163.

Peng, D-Y. and Robinson, D.B. 1976. A new two-constant equation of state. *Industrial and Engineering Chemistry Fundamentals*, 15(1), pp. 59-64.

Pone, J.D.N., Halleck, P.M. and Mathews, J.P. 2009. Sorption capacity and sorption kinetic measurements of CO_2 and CH_4 in confined and unconfined bituminous coal. *Energy and Fuels*, 23(9), pp. 4688-4695.

Robertson, E.P. and Christiansen, R.L. 2008. A permeability model for coal and other fractured, sorptive-elastic media. *Society of Petroleum Engineers Journal*, 13(3), pp. 314-324.

Seidle, J. 2011. *Fundamentals of coalbed methane reservoir engineering*. PennWell Corporation, Tulsa, Oklahoma, USA.

Shi, J-Q. and Durucan, S. 2004. Drawdown induced changes in permeability of coalbeds: A new interpretation of the reservoir response to primary recovery. *Transport in Porous Media*, 56(1), pp. 1-16.

Chapter 9

Conclusions and Suggestions for Further Research

9.1. Introduction

The specific conclusions pertinent to each chapter have been presented at the end of each chapter. This chapter aims to synthesise those conclusions and relate them to the objectives of this study. Recalling from chapter 1, the fundamental objectives of this study can be summarised as: i) developing a laboratory facility to investigate the processes of gas transport and reactions in coal at high pressure conditions, ii) investigating the sorption behaviour of various gas species in coal for a broad range of gas pressures and under isothermal conditions, iii) studying the effect of effective stress and sorption-induced strain on coal permeability evolution and gas storage and displacement in coal via a series of laboratory experiments and the theoretical modeling approaches, iv) assessing and quantify the volumetric deformations of the coal due to interactions with reactive gases such as carbon dioxide and v) obtaining permeability and sorption properties of coal samples from South Wales coalfield. In addition, key contributions and advancements made by this research will be highlighted throughout this chapter. The suggestions for further research are also provided in Section 9.8.

9.2. Laboratory development

An experimental facility has been developed to investigate the sorption behaviour and reactive transport of gases in coal under high pressure conditions. The facility comprises three main sections, as follows:

- A manometric sorption apparatus.
- A triaxial core flooding system.
- The ancillary system including the gas supply unit and gas analysing unit.

The manometric sorption apparatus is capable of measuring adsorption/desorption isotherms of various gas species on powdered and intact samples at gas injection pressures up to 20MPa and temperatures up to 338K. The triaxial core flooding system is

capable of replicating the ground conditions in terms of pore pressure and confining pressure for depths up to 2000m. Using the bespoke triaxial core flooding system, the gas flow behaviour, the permeability of the sample to various gas species and sorption-induced swelling/shrinkage of the sample can be studied under a broad range of effective stress conditions, i.e. gas pore pressures and confining pressures up to 20MPa.

The literature review in Chapter 2 highlighted that only a limited number of experimental apparatuses exist for the investigation of coal-gas interactions at high pressure conditions. In addition, the majority of the experimental apparatuses have been specifically developed to investigate a certain area, e.g. gas sorption in coal, gas transport in coal or swelling/shrinkage of coal. The facility developed as part of this research offers a more detailed and comprehensive set of experimental tools for the investigations of coal-gas interactions.

The broad range of sample sizes (from powdered sample to large intact core samples with up to 0.7m diameter) that can be accommodated within the apparatus and the broad range of gas pressures (up to 20MPa) that can be applied, provide an advanced experimental platform to expand the knowledge of gas transport and reactions in coal.

The features of the facilities developed enable a simultaneous run of the experiments using both units, i.e. the gas sorption apparatus and the triaxial core flooding system. This is considered to be an important advantage due to the long-term nature of the experiments.

A high level of accuracy and resolution of the data-set has been obtained and presented in this thesis by designing and adopting appropriate measuring/monitoring devices, e.g. the pressure transducers with 0.002MPa (2kPa) resolution and 0.15% accuracy, mass flow meters with flow rates of 3×10^{-7} to 23×10^{-7} m^3/s (20-1000 mLn/min) and accuracy of 0.5%. This also highlights the significance of the detailed and thorough analyses performed and presented in Chapter 3 to define and optimise the specifications of the measurement devices.

9.3. Gas sorption behaviour in coal

Prior to the gas sorption measurements, a thorough coal characterisation test was performed on the coal samples collected from South Wales coalfield (6-ft seam) including the Ultimate analysis (moisture content, ash content, volatile matter, fixed carbon content) and Proximate analysis (sulphur and carbon contents). The results showed that the coal samples of this study were high rank coals with 86% carbon content. The average bulk density and porosity of the coal samples were estimated to be 1496kg/m^3 and 2.5-6%, respectively.

Excess and absolute adsorption/desorption isotherms were measured on powdered coal samples using N_2, CH_4 and CO_2 for gas equilibrium pressures up to 7MPa. The volumetric effects due to N_2 and CH_4 adsorption on coal were found to be negligible, whereas CO_2 adsorption in coal exhibited considerable volumetric effects with a maximum deviation of 66% between the excess and absolute adsorption isotherms at 4.9MPa equilibrium gas pressure. This was found to be related to the swelling effect of CO_2 on the coal matrix. A considerable decrease in the adsorption capacity of the coal sample was observed when the experimental gases were changed from CO_2 to CH_4 (1.3 times reduction) and from CH_4 to N_2 (1.8 times reduction).

Positive hystereses between the adsorption and desorption isotherms were observed for N_2 and CH_4. In the case of CO_2, negative hystereses observed were indication of stable conditions of the adsorbed CO_2 in coal under the conditions applied. Such observations are of value for assessing the stability of the adsorbed CO_2 during carbon sequestration process in coal reservoirs, e.g. possibility of gas release due to pressure depletion in the reservoirs.

In this study and in order to address the kinetics of gas adsorption in coal a large set of experimental data was analysed. The results revealed that the rate of gas adsorption on coal may vary during different stages of gas adsorption process on coal. For instance, the rate of CO_2 adsorption on coal during the first stage (first two hours) of adsorption process was found to be 12 times higher than the adsorption rate related to the second

stage. This is mainly due to the nature of the coal matrix and its pore size distribution (macro-pores and micro-pores) in which the gas diffusion and adsorption processes can occur at more than one time scale.

9.4. Gas flow behaviour in coal

A series of core flooding experiments were conducted on the coal samples using He, N_2, CO_2 and CH_4 gases. In these experiments, the coupled effects of effective stress variations (due to increases in gas pore pressure and confining pressure) and the effect of coal matrix swelling on permeability of the coal samples were studied in more details. The outcomes were also used to establish a set of relationships between coal permeability and effective stress for various gas species. Such relationships are of importance when it comes to assessing the behaviour of permeability evolution in coal during the gas injection process. The established relationships are also of value for developing the numerical models.

The results of gas flow and permeability measurements in coal showed that under the constant confining pressure the permeability of the coal to He and N_2 increases with increase in gas pressure. In the case of the CO_2, however, despite the increase in gas pressure at higher effective stress values, the permeability of the coal was found to decrease considerably. At 6MPa confining pressure, the permeability of the coal sample was found to be reduced by 95% which was related to the effect of coal matrix swelling induced by the CO_2 adsorption on the fracture porosity.

The sorption-induced volumetric effects of He and N_2 on coal matrix were found to be negligible. In the case of CO_2, however, the significant volumetric strain observed (1.5%) was attributed to the swelling of the coal matrix induced by CO_2 adsorption.

A set of experiments were also undertaken to evaluate the fate of adsorbed CO_2 in coal. To the knowledge of the author, such set of experimental data is new and this aspect has not been previously studied in such detail. A sequential series of He, N_2 and CH_4 flooding

experiments were performed. The results of He and N_2 injections did not show significant improvements in the permeability of the coal sample and reversibility of the coal matrix swelling. Nevertheless, the injection of CH_4 into the coal sample resulted in relatively considerable increase (1.6 times) in the permeability of the coal sample possibly due to the stronger affinity of CH_4 to coal compared with He and N_2. The initial permeability of the coal sample however was not fully restored. The outcome of this investigation has also provided a new insight into the fate of adsorbed CO_2 in terms of its stability in coal which has previously not being observed or reported in literature.

9.5. Gas storage and displacement processes in coal

A series of gas storage and displacement experiments were conducted on a CH_4-saturated coal sample to address the mechanisms involved in gas storage and displacement processes. Prior to those tests, the initial gas transport properties of the coal sample, i.e. its absolute permeability to He and CH_4 was evaluated. To the author's knowledge, such a sequence of experiments has not previously been reported in the literature.

N_2 and CO_2 were injected into the coal sample and the outflow gas was monitored until the breakthrough (1% of N_2 or CO_2 in production gas) was observed. The results showed that the N_2 breakthrough was almost spontaneous whereas the CO_2 breakthrough time was delayed by two orders of magnitude. Accordingly, at the early stages of gas injection, the ratio of CH_4 recovered in the production gas was 1.5 times higher in the CO_2 experiment as compared with the N_2 experiment. Similarly, the gas displacement rate observed in both experiments varied greatly which was mostly related to differences between diffusivity of N_2 and CO_2 as well as higher affinity of coal to CO_2. The latter effect resulted in the storage of 40% of injected CO_2 in coal. The results also showed that with respect to the amount of injected gas, the amount of CH_4 recovered during the CO_2 experiment was at least two times higher than those during the N_2 experiment.

The gas storage and displacement experiments performed within the scope of this study have provided a high resolution validation exercise for the development of the numerical

models. From the literature review presented in Chapter 2, it can be postulated that the number of validation exercises available in the literature at this level of accuracy and comprehensiveness are limited. In addition, the focus of the majority of the reported experimental studies has been either on gas flow and permeability evaluation in coal or on gas storage/recovery in coal. The work presented in this thesis has provided a comprehensive set of data including all the areas mentioned above.

9.6. Permeability evolution during gas flow and displacement in coal

A theoretical approach specifically developed for the modelling of reactive gas transport in dual porosity media such as coal by Hosking (2014) was adopted to obtain further insights into the processes involved in gas flow and displacement in coal. The primary focus of this work was to evaluate the permeability evolution of the coal sample during gas injection and displacement by considering the effect of mechanisms such as the fracture compressibility, the matrix block compressibility and the sorption induced matrix block strain on coal permeability.

The results of the simulations were compared with those from the experimental tests, including the results obtained from the helium flooding experiments. From the results it was underlined that for N_2 and CH_4 gases, the permeability evolution of the coal sample has been mainly controlled by the physico-mechanical processes, i.e. compressibility of the factures and matrix blocks due to variations in the effective stress. For the case of CO_2, however, the permeability evolution of the coal sample studied has been mainly controlled by chemo-mechanical processes, i.e. sorption-induced strain.

A series of numerical simulations of the N_2 and CO_2 storage and displacement were performed considering the initial and boundary conditions applied in the experimental studies presented in Chapter 7. The results of N_2 simulation were found to be in good agreement with the experimental data, whereas for the case of CO_2 simulation, higher discrepancy between the predicted results and experimental data was observed. The outcome also underlined a series of effective factors which can be considered to improve

the accuracy of the predicted results. Apart from the computational factors, a few experimental factors such as the lack of experimental data related to the kinetics of sorption-induced strain has been identified which will be described in more details in the section dedicated to suggestions for future research later in this chapter.

9.7. Overall conclusions

In terms of overall conclusions that can be drawn from the research performed, the following observations are presented:

- A state-of-the-art laboratory facility has been developed and used within the scope of this study which is capable of producing results and data with high level of resolution for a broad range of sample sizes from powdered coal to large intact coals up to 0.1m diameters and high pressure gas injections up to 20MPa. The two analysing units, i.e. the manometric gas sorption apparatus and triaxial core flooding system, enable the study of various aspects of coal-gas interactions by replicating a broad range of ground conditions for depths up to 2000m (gas pressure and confining pressures up to 20MPa and temperatures up to 338K).

- This thesis has provided a detailed and comprehensive set of data, including coal characterisation data, gas sorption and transport properties of the coal samples from South Wales coalfield. Such data-set at this level of accuracy and comprehensiveness is believed to be produced for the first time for the South Wales coals.

- The results of gas sorption behaviour in coal have provided important information related to the sorption properties of coal to various gas species up to 7MPa gas injection pressure, with the highest adsorption capacity related to CO_2 (1.21mol/kg). The outcomes can be considered as an essential information for further interpretation of the results of reactive gas transport in coal.

- The study on gas adsorption kinetics in coal has provided a notable insight into the controlling mechanisms of the rate of adsorption during gas adsorption process on

coal. The rate of gas adsorption on coal was found to be varied during different stages of gas adsorption process which was mainly due to different rates of gas diffusion and adsorption in coal macro-pores and micro-pores.

- The study of gas transport behaviour in coal has provided valuable information about the effects of gas adsorption/desorption on coal permeability under a range of effective stresses. The effect of N_2 and CH_4 on permeability evolution of the coal sample was found to be negligible, whereas the absolute permeability of the coal sample was found to be reduced by 95% as a result of the coal matrix swelling induced by CO_2 adsorption.

- A novel approach in the development of the laboratory testing programme was used to study the fate of adsorbed CO_2 in coal and permeability evolution due to CO_2 desorption by performing a sequential He, N_2 and CH_4 core flooding experiments. The initial permeability of the coal sample was partially restored, i.e. by an average of 20%, during subsequent CH_4 flooding experiment. This approach has also provided a new insight into the stability of the injected CO_2 into coal which can be of value for assessing the long-term stability of the injected and stored CO_2 in coal reservoirs.

- The results of N_2 and CO_2 storage and displacement experiments showed the efficiency of CO_2 injection into coal in terms of the total CH_4 recovery, gas displacement ratio, breakthrough time and amount of gas storage. Nevertheless, the swelling effect of CO_2 on the coal permeability was found to be considerable (i.e. 95% permeability reduction at 5.5MPa gas pressure and 6MPa confining pressure) which needs to be taken into account in the applications of carbon sequestration in coal.

- The results of N_2 and CO_2 storage and displacement experiments have also provided a detailed set of data that can be used as validation benchmark for numerical model developments. The results of this work are among the limited works reported in the literature, however it can be postulated that compared to other works, the results presented in this thesis include more comprehensive information and parameters required for the validation of the numerical models.

- The importance of the chemically controlled processes, e.g. CO_2 sorption-induced strain, in relation to coal permeability evolution during CO_2 injection has been highlighted. The results of the numerical simulations have also led to the identification of the influential factors in gas storage and displacement processes in coal such as the kinetically controlled sorption-induced strain and the transient rate of mass exchange between fracture and matrix.

9.8. Suggestions for further research

The research findings presented in this thesis have highlighted a number of potential areas for future research works. The following suggestions for future developments have been identified.

- Although the primary objective of developing the laboratory facility was to investigate the interactions between coal and gases, its potentials for other applications should not be disregarded. The current facility offers a broad range of experimental investigations on various materials including different types of rocks and soils.

- The gas pressure applied in this study was up to 7MPa. It is therefore suggested that the interactions can be further studied at higher gas pressure conditions. This can improve the understanding of coal interactions with supercritical CO_2. Similarly, the effect of temperature and moisture content can be considered in future works.

- From the literature review presented in Chapter 2 it has been underlined that very little information exists related to the gas transport and sorption properties of coals from South Wales coalfield. Accordingly, a broader range of coal samples/ranks are suggested to be experimentally studied. This is especially important for identifying the target coal seams for the purpose of carbon sequestration.

- Due to the time constrains, the gas sorption measurements have been conducted on powdered coal samples. Since the coal structure can be influential in gas transport and

sorption properties of coal, direct measurements are suggested for further evaluations of the gas sorption properties of coal and sorption kinetics by using intact coal sample.

- The literature review conducted in this study has also highlighted that most of the experimental works related to gas sorption behaviour in coals are related to the equilibrium conditions. Therefore, more work is required for understanding the kinetics of gas sorption in coal.

- Long term experiments are required to evaluate the fate of CO_2 in coal and permeability evolution during and after implementation of carbon sequestration in coal.

- The experimental data related to gas storage and displacement processes in coal is limited, especially at high pressure conditions. Production of such data is very important for understanding the mentioned processes as well as providing validation exercises for the numerical models.

- The results of numerical simulations underline the need for further laboratory investigations on kinetics of gas sorption strains on intact coal samples under the confined conditions. Such data can be used for further validation and improvement of the numerical models.

- In order to assess the validity of the porosity and permeability relationships, it is important to perform core flooding experiment beyond the pressure range performed in this work.

9.9. References

Hosking, L. 2014. *Reactive transport modelling of high pressure gas flow in coal*. PhD Thesis. Cardiff University.

Appendix A

Theoretical formulation of gas transport and reactions

The theoretical formulation presented in this appendix has been developed and incorporated in a numerical model, COMPASS, by Hosking (2014). The background of the COMPASS model was presented in Chapter 2. The governing equations of thermal, hydraulic, chemical/gas and mechanical behaviour in a single porosity system of unsaturated soils have been presented by Thomas and He (1998), Cleall (1998), Seetharam (2003), Sedighi (2011) and Masum (2012). In order to investigate the transport and reactions of multicomponent gas in fractured rock (e.g. coal), Hosking (2014) extended the work of Sedighi (2011) and Masum (2012) by introducing a dual continuum system for high pressure reactive flow in fractured rock.

The principle of conservation of mass for the i^{th} gas component in a dual porosity medium can be expressed mathematically as (Hosking, 2014):

$$\frac{\partial(\theta_{g\alpha} c^i_{g\alpha} \delta V_\alpha)}{\partial t} = \underbrace{-\delta V_\alpha \nabla \cdot \mathbf{J}^i_{g\alpha}}_{\text{Transport}} \underbrace{- \delta V_\alpha \lambda \Gamma^i_g}_{\substack{\text{Mass exchange} \\ \text{between fracture} \\ \text{and matrix}}} \underbrace{- \delta V_\alpha R^i_{g\alpha}}_{\text{Reaction}} \tag{A-1}$$

where, $\theta_{g\alpha}$ is the volumetric gas content in continua α ($\alpha=F$ for fracture continuum, and $\alpha=M$ for matrix continuum), $c^i_{g\alpha}$ is the gas concentration, δV_α is the incremental volume, , t is the time, $\mathbf{J}^i_{g\alpha}$ is the total flux of gas component i , $\Gamma^i_{g\alpha}$ is the sink/source term for mass exchange of gas component i between the fracture and matrix continua, ∇ is the gradient operator and $R^i_{g\alpha}$ represents the sink/source term accounting for geochemical reactions.

To comply with the principle of mass conservation between the two continua, the parameter λ is defined as (Hosking, 2014):

$$\begin{aligned} \lambda &= 1 \quad if \quad \alpha = F \\ \lambda &= -1 \quad if \quad \alpha = M \end{aligned} \tag{A-2}$$

where, F denotes the fracture network and M denotes the matrix blocks.

The sink/source term ($R^i_{g\alpha}$) can therefore be expressed as:

$$R^i_{g\alpha} = \rho_s \frac{\partial s^i_{g\alpha}}{\partial t} \tag{A-3}$$

where, ρ_s is the density of the solid phase (i.e. coal), $s^i_{g\alpha}$ is the amount of gas lost/gained due to adsorption/desorption reactions with the solid phase.

The volumetric gas content ($\theta_{g\alpha}$) of the fracture network and matrix blocks can be expressed in terms of the degree of gas saturation and the porosity in each continuum, given as:

$$\theta_{g\alpha} = n_\alpha S_{g\alpha} \tag{A-4}$$

where, n_α is the porosity and $S_{g\alpha}$ is the degree of gas saturation.

In equation (A-4), the fracture porosity (n_F) and the matrix porosity (n_M) are the fraction of the bulk porosity (n_B) associated with the fracture network and the matrix blocks, respectively, which are given as (Hosking, 2014):

$$n_F = w_f n^L_F \tag{A-5}$$

$$n_M = n_B - w_f n^L_F \tag{A-6}$$

where, n^L_F is the local fracture porosity given by the volume of the pores in the fractured zone divided by the total volume of the fractured zone (V^P_F / V^T_F). w_f is the volumetric weighting factor, defined as:

$$w_f = \frac{V_F^T}{V_B} \tag{A-7}$$

where, V_B is the bulk volume of the rock.

By substituting equation (A-3) into equation (A-1) and by rearranging the parameters, equation (A-1) can be expressed for a dry system as:

$$\frac{\partial(n_\alpha c_{g\alpha}^i)}{\partial t} + \rho_s \frac{\partial s_{g\alpha}^i}{\partial t} = -\nabla \cdot J_{g\alpha}^i - \lambda \Gamma_g^i \tag{A-8}$$

The key gas properties related to the formulation are as follows (Hosking 2014):

1) Real gas bulk compressibility

The real gas compressibility behaviour was considered using an equation of state (EoS) proposed by Peng and Robinson (1976).

2) Bulk gas viscosity

Gas mixture viscosity has been included using the semi-empirical model proposed by Chung et al. (1988). The relationship is based on the kinetic gas theory in combination with empirical density-dependent functions to include the behaviour of dense gas mixtures, giving (Hosking, 2014):

$$\mu_{g\alpha} = 0.1[f(\mu_{g\alpha}^0) + \mu_{g\alpha}^D] \tag{A-9}$$

where, $\mu_{g\alpha}^0$ is a function of the gas mixture viscosity at low pressure. The factor 0.1 has been applied to convert the output viscosity into units of Pa.s. $\mu_{g\alpha}^D$ is a further adjustment for dense gases.

3) Gas diffusion coefficient

In the formulation, an empirical model suggested by Reid et al., (1977) has been adopted for the gas diffusion coefficient (Hosking, 2014):

$$D^i_{g\alpha} = \frac{D^{0i}_g \rho^0_g}{\rho_{g\alpha}} \tag{A-10}$$

where, D^{0i}_g is a reference value for the diffusion coefficient obtained experimentally at a certain temperature at a low gas density of ρ^0_g, and $D^i_{g\alpha}$ is the diffusion coefficient at the same temperature but at a higher gas density of $\rho_{g\alpha}$.

A.1. Gas transport mechanisms

The total flux of the i^{th} pore gas component ($\mathbf{J}^i_{g\alpha}$) in equation (A-1) includes contributions from advective and diffusive transport mechanisms:

$$\mathbf{J}^i_{g\alpha} = \mathbf{J}^i_{gAdv\alpha} + \mathbf{J}^i_{gDif\alpha} \tag{A-11}$$

where, $\mathbf{J}^i_{gAdv\alpha}$ and $\mathbf{J}^i_{gDif\alpha}$ are the advective and diffusive components of flux, respectively.

Advective transport of the pore gas is described by gradients of the bulk gas pressure using Darcy's Law:

$$\mathbf{J}^i_{gAdv\alpha} = -\frac{c^i_{g\alpha} k_{g\alpha} Z_\alpha RT}{\rho_{g\alpha} g} \sum_{j=1}^{n_g} \nabla c^j_{g\alpha} - c^j_{g\alpha} k_{g\alpha} \nabla z \tag{A-12}$$

where, $k_{g\alpha}$ is the unsaturated gas conductivity, g is the gravitational acceleration and z is the elevation.

In equation (A-12), the pore gas pressure is expressed in terms of the sum of the partial pressures of the individual gas components based on the real gas law, as follows:

$$P_{g\alpha} = Z_\alpha RT \sum_{j=1}^{n_g} c^j_{g\alpha} \tag{A-13}$$

where, R is the universal gas constant and Z_α is the gas compressibility factor.

The gas diffusive flux in equation (A-11) involves a combination of the diffusion processes, including the ordinary diffusion, the Knudsen diffusion and configurational diffusion.

Ordinary diffusion describes the tendency of the species contained in a gas mixture to diffuse due to concentration gradients (Fick, 1855). Knudsen diffusion takes place in very tight pores with dimensions that are similar in magnitude or smaller than the molecular mean free path length (Wu et al., 1998) and is therefore ignored in the fracture continuum. Configurational diffusion can become important in very tight pores with dimensions approaching those of a single molecule (Webb, 2006) and is therefore ignored in the fracture continuum.

The final forms of the total diffusion fluxes for fracture and matrix continua including the mentioned diffusion processes are then given as (Hosking, 2014):

$$\mathbf{J}^{i}_{gDifF} = -n_F \tau_{gF} D^{i}_{gF} \nabla c^{i}_{gF} \tag{A-14}$$

$$\mathbf{J}^{i}_{gDifM} = -n_M (\tau_M \delta_{iM} D^{i}_{gM} + D^{i}_{KM}) \nabla c^{i}_{gM} \tag{A-15}$$

where, $\tau_{g\alpha}$ is the gas tortuosity factor, $\delta_{i\alpha}$ is the constrictivity factor for specifying species to account for configurational diffusion, $D^{i}_{g\alpha}$ is the free diffusion coefficient and $D^{i}_{K\alpha}$ is the Knudsen diffusion coefficient.

A detailed derivation of the total flux equations for the fracture and matrix can be found in Hosking (2014). It should be mentioned that dispersion is not considered here since it is assumed to be negligible in comparison to diffusion. This is because the gas diffusivity is high, with diffusion coefficients being around four orders of magnitude greater than those of solutes (Cussler, 1997).

A.2. Mass exchange term

The mass exchange term for pore gas presented here includes the components due to advection and diffusion. The resulting mass exchange term for the i^{th} pore gas component has been expressed as (Hosking, 2014):

$$\Gamma^{i}_{g} = \sigma_{gAdv} (P_{gF} - P_{gM}) + \sigma^{i}_{gDif} (c^{i}_{gF} - c^{i}_{gM}) \tag{A-16}$$

where, σ_{gAdv} is the first order mass exchange coefficient for gas advection and σ^{i}_{gDif} is the first order mass exchange coefficient for gas diffusion of the i^{th} component.

The mass exchange coefficient for gas advection is given as (Hosking, 2014):

$$\sigma_{gAdv} = \frac{\beta}{l^2}\left(\frac{K_g^A}{\rho_g^A g}\right) \tag{A-17}$$

where, β is the factor related to the geometry of the matrix blocks, l is the typical thickness of a matrix block or fracture spacing, K_g^A and ρ_g^A are the arithmetic means of the gas conductivities and gas densities in the fracture and matrix continua, respectively, which are given as (Hosking, 2014):

$$K_g^A = \frac{K_{gF} + K_{gM}}{2} \tag{A-18}$$

$$\rho_g^A = \frac{\rho_{gF} + \rho_{gM}}{2} \tag{A-19}$$

It is assumed that the diffusive flux of multicomponent pore gas exchange is an ordinary diffusion process. The mass exchange coefficient for gas diffusion is then given by (Hosking, 2014):

$$\sigma^{i}_{gDif} = \frac{\beta D^{i}_{geM}}{l^2} \tag{A-20}$$

where, D^{i}_{geM} is the effective diffusion coefficient which considers the pore structure of the porous medium.

Substitution of equations (A-17) to (A-20) into equation (A-16) and replacing the pore gas pressures using equation (A-11) yields:

$$\Gamma^{i}_{g} = \frac{\beta}{l^2}\left(\frac{K_g^A}{\rho_g^A g}\right)\sum_{j=1}^{n_g}(Z_F RTc^{j}_{gF} - Z_M RTc^{j}_{gM}) + \frac{\beta D^{i}_{geM}}{l^2}(c^{i}_{gF} - c^{i}_{gM}) \tag{A-21}$$

A.3. Sink/source term for adsorption/desorption

Adsorption/desorption reactions are inherently dependent on the available surface area of the solid phase over which the interactions with the gas can occur. In dual porosity media the majority of this interface exists in the porous matrix blocks. For example, micropores in the matrix blocks of coal account for approximately 95% of the total internal surface area (Shi and Durucan, 2005). In addition, sorption can be treated as an equilibrium or kinetic reaction in the matrix continuum. This formulation considers sorption as a kinetic reaction, which yields a first-order kinetics equation for the i^{th} gas component of the form (Hosking, 2014):

$$\frac{ds_{gM}^{i}}{dt} = \tau_r^i (s_{g\infty M}^{i} - s_{gM}^{i}) \tag{A-22}$$

where, τ_r^i is the sorption rate and $s_{g\infty M}^{i}$ is the adsorbed concentration at equilibrium with the free gas pressure in the matrix continuum.

As stated earlier, sorption has been only considered in the matrix continuum, therefore:

$$s_{gF}^{i} = 0 \tag{A-23}$$

For absolute amount of adsorbed gas, the extended Langmuir isotherm is used and the equilibrium adsorbed concentration for the i^{th} gas component is given as (Ruthven, 1984; Hosking, 2014):

$$s_{g\infty M}^{i} = \frac{n_L^i b_L^i Z_M R T c_{gM}^{i}}{1 + Z_M R T \sum_{j=1}^{n_g} b_L^j c_{gM}^{j}} \tag{A-24}$$

where, n_L^i and b_L^i are the Langmuir capacity and inverse of the Langmuir pressure, respectively.

Substituting the total pore gas flux $\mathbf{J}_{g\alpha}^{i}$ from equations (A-12) to (A-15), λ from equation (A-2), and Γ_g^i from equation (A-21) into the right hand side of equation (A-1), whilst taking account of equation (A-23), gives the governing equations for multicomponent

pore gas transport in a dual porosity dual permeability system, presented in the following section.

A.4. Summary of the governing equations and numerical solutions

The governing equations for multicomponent pore gas transport can be represented in a simplified form for the i^{th} component as:

1) Gas transport in the Fracture:

$$C_{c_g c_g F}\frac{\partial c_{gF}^{i}}{\partial t} = \nabla\cdot\left[\sum_{j=1}^{n_g} K_{c_g c_g F}\nabla c_{gF}^{j}\right] + J_{c_g F} + Q_{c_g F}^{ex} \tag{A-25}$$

where, in equation (A-25):

$$C_{c_g c_g F} = n_F \tag{A-26}$$

$$K_{c_g c_g F} = \frac{c_{gF}^{i} k_{gF} Z_F R T}{\rho_{gF} g} + \delta_{ij} n_F \tau_{gF} D_{gF}^{i} \tag{A-27}$$

$$\mathbf{J}_{c_g F} = \nabla\cdot(c_{gF}^{i} k_{gF}\nabla z) \tag{A-28}$$

$$Q_{c_g F}^{ex} = -\frac{\beta}{l^2}\left(\frac{K_g^A}{\rho_g^A g}\right)\sum_{j=1}^{n_g}(Z_F R T c_{gF}^{j} - Z_M R T c_{gM}^{j}) - \frac{\beta D_{geM}^{i}}{l^2}(c_{gF}^{i} - c_{gM}^{i}) \tag{A-29}$$

2) Gas transport and reactions in the Matrix:

$$C_{c_g c_g M}\frac{\partial c_{gM}^{i}}{\partial t} + C_{c_g s_g M}\frac{\partial s_{gM}^{i}}{\partial t} = \nabla\cdot\left[\sum_{j=1}^{n_g} K_{c_g c_g M}\nabla c_{gM}^{j}\right] + \mathbf{J}_{c_g M} + Q_{c_g M}^{ex} \tag{A-30}$$

where, in equation (A-30):

$$C_{c_g c_g M} = n_M \tag{A-31}$$

$$C_{c_g s_g M} = \rho_s \tag{A-32}$$

$$K_{c_g c_g M} = \frac{c_{gM}^{i} k_{gM} Z_M R T}{\rho_{gM} g} + \delta_{ij} n_M(\tau_M \delta_{iM} D_{gM}^{i} + D_{KM}^{i}) \tag{A-33}$$

$$\mathbf{J}_{c_gM} = \nabla \cdot (c_{gM}^i k_{gM} \nabla z) \tag{A-34}$$

$$Q_{c_gM}^{ex} = \frac{\beta}{l^2}\left(\frac{K_g^A}{\rho_g^A g}\right)\sum_{j=1}^{n_g}(Z_F RTc_{gF}^j - Z_M RTc_{gM}^j) + \frac{\beta D_{geM}^i}{l^2}(c_{gF}^i - c_{gM}^i) \tag{A-35}$$

COMPASS model employs numerical solutions including the finite element method (FEM) to spatially discretise the system of equations and the finite difference method (FDM) for temporal discretisation (Thomas and He, 1998). Detail of the numerical solution developed in COMPASS has been explained in the cited works in Section A.2 and is not covered here.

A.3. References

Chung, T-H., Ajlan, M., Lee, L.L. and Starling, K.E. 1988. Generalized multiparameter correlation for nonpolar and polar fluid transport properties. *Industrial and Engineering Chemistry Research*, 27(4), pp. 671-679.

Cleall, P.J. 1998. *An investigation of the thermo/hydraulic/mechanical nehaviour of unsaturated soils, including expansive clays*. PhD Thesis, Cardiff University.

Cussler, E.L. 1997. *Diffusion: mass transfer in fluid systems*. 2nd Ed. Cambridge: Cambridge University Press.

Fick, A. 1855. Ueber diffusion. *Poggendorff's Annalen der Physik und Chemie*, 94(170), pp. 59-86.

Hosking, L. 2014. *Reactive transport modelling of high pressure gas flow in coal*. PhD Thesis. Cardiff University.

Masum, S. 2012. *Modelling of reactive gas transport in unsaturated soil – a coupled thermo-hydro-chemical-mechanical approach.* PhD Thesis, Cardiff University.

Peng, D-Y. and Robinson, D.B. 1976. A new two-constant equation of state. *Industrial and Engineering Chemistry Fundamentals*, 15(1), pp. 59-64.

Reid, R.C., Prausnitz, J.M. and Sherwood, T.K. 1977. *The properties of gases and liquids*. 3rd Edition. McGraw-Hill, New York.

Ruthven, D.M. 1984. *Principles of adsorption and adsorption processes*. Wiley, New York.

Sedighi, M. 2011. *An investigation of hydro-geochemical processes in coupled thermal, hydraulic, chemical and mechanical behaviour of unsaturated soils.* PhD Thesis, Cardiff University.

Seetharam, S.C. 2003. *An investigation of the thermro/hydro/chemical/mechanical behaviour of unsaturated soils.* PhD Thesis, Cardiff University.

Shi, J-Q. and Durucan, S. 2005. Gas storage and flow in coalbed reservoirs: Implementation of a bidisperse pore model for gas diffusion in a coal matrix. *SPE Reservoir Evaluation and Engineering,* 8(2), pp. 169-175.

Thomas, H.R. and He, Y. 1998. Modelling the behaviour of unsaturated soil using an elasto-plastic constitutive relationship. *Géotechnique,* 48(5), pp. 589-603.

Webb, S.W. 2006. Gas transport mechanisms. In: Ho, C.K. and Webb, S.W. eds. *Gas transport in porous media.* The Netherlands, Dordrecht: Springer, pp. 273-278.

Wu, Y-S., Pruess, K. and Persoff, P. 1998. Gas flow in porous media with Klinkenberg effects. *Transport in Porous Media*, 32(1), pp. 117-137.